



301 Mission St Perimeter Pile Upgrade

Calculations

Vol 3 – Design for Lateral Load

301 Mission Street
San Francisco, CA

29 November 2018

SGH Project 147041.10



SIMPSON GUMPERTZ & HEGER



Engineering of Structures
and Building Enclosures

PREPARED FOR:

Millennium Tower Association
301 Mission Street
Level B-1
San Francisco, CA 94103

PREPARED BY:

Simpson Gumpertz & Heger Inc.
100 Pine Street, Suite 1600
San Francisco, CA 94111
Tel: 415.495.3700
Fax: 415.495.3550

TABLE OF CONTENTS

1.	SEISMIC HAZARD	1
1.1	Response Spectra	1
1.2	Ground Motions	2
2.	ANALYTICAL MODEL: ETABS	3
2.1	Model Description	3
2.1.1	Geometry	3
2.1.2	Gravity Loads	7
2.1.3	Stiffness Modifiers	8
2.1.4	P-Delta	8
2.1.5	Modal Response	8
2.2	Loading	11
2.2.1	Wind	11
2.2.2	Seismic	14
2.2.3	Load Combinations	18
2.3	Response	19
2.3.1	Story Forces	19
2.3.2	Base Reactions	20
2.4	Capacity Calculations	21
2.4.1	Shear Walls	21
2.4.2	Moment Frames	27
2.5	DCRs	31
2.5.1	Shear Walls	32
2.5.2	Moment Frames	41
3.	ANALYTICAL MODEL: XTRACT	50
3.1	Description and Screenshots	50
3.1.1	Existing Pile Geometry	50
3.1.2	Existing Pile Concrete Material Properties	55
3.1.3	Existing Pile Steel Material Properties	58
3.1.4	Existing Pile Cross Section “PileTop”	61
3.1.5	Existing Pile Cross Section “OneAndHalfFeet”	62
3.1.6	Existing Pile Cross Section “SevenFeet”	63
3.1.7	Existing Pile Cross Section “SeventeenFeet”	64
3.1.8	Proposed Pile Geometry and Material Properties	65
3.2	Moment-Curvature Analysis	70
4.	ANALYTICAL MODEL: LPILE	74
4.1	Group Effect Factor	74
4.2	Summary of Recommended Input Parameters from All Parties	76
4.3	Soil Spring Results	80
5.	ANALYTICAL MODEL: SAP2000	85
5.1	Description and Screenshots	85
5.2	Individual Pile Pushover Results	98

5.3	Combination of Pushover Results to Obtain Composite Foundation Backbones	103
5.4	Existing Pile Backbone Modifications	107
5.4.1	Correction for Pile Head Rotations	107
5.4.2	Correction for Tower Overturning Moment	107
6.	ANALYTICAL MODEL: PERFORM 3D	114
6.1	Substructure Analysis Model Modifications	114
6.1.1	Podium Structure Model	115
6.1.2	Basement Wall Lateral Resistance	131
6.1.3	Cumulative Lateral Foundation Backbones	144
6.2	Analysis Load Cases	151
6.2.1	Superstructure Analysis Series	153
6.2.2	Substructure Analysis Series	153
6.3	Superstructure Analysis Results	154
6.3.1	Shear Walls	154
6.3.2	Perimeter Moment Frames	181
6.3.3	Outrigger Beam Rotations	183
6.4	Substructure Analysis Results	184
6.4.1	Grillage Inelastic Beam Rotations	184
6.4.2	Foundation Lateral Displacements	185
7.	ANALYTICAL MODEL: SAFE V16	188
7.1	SAFEV16 Model Description	188
7.2	Wind Loading	188
7.3	Seismic Loading	189
7.4	Analysis Results	195
7.5	Shear Calculations	195
7.6	Flexural Calculations	205
7.6.1	SAFE Model using ENGEO Pile Springs	205
7.6.2	SAFE Model using Egan Team Pile Springs	229

1. SEISMIC HAZARD

1.1 Response Spectra

For our linear evaluation of the building for the design earthquake we used a response spectrum calculated in accordance with ASCE 7-10, shown in Figure 1-1. We also considered a service-level earthquake response spectrum shown in Figure 1-2 and provided in the 30 November 2018 report, *Geotechnical Evaluation for the Perimeter Pile Upgrade* by John Egan, Slate Geotechnical Consultants, Inc. and Shannon & Wilson, Inc. Our application of these response spectra to our analysis models is further described in Section 2.2.2.

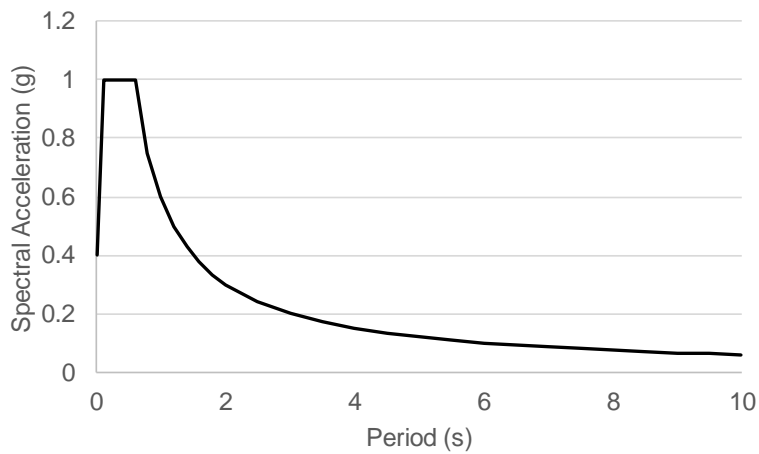


Figure 1-1 – ASCE 7-10 Design-Level Earthquake Response Spectrum

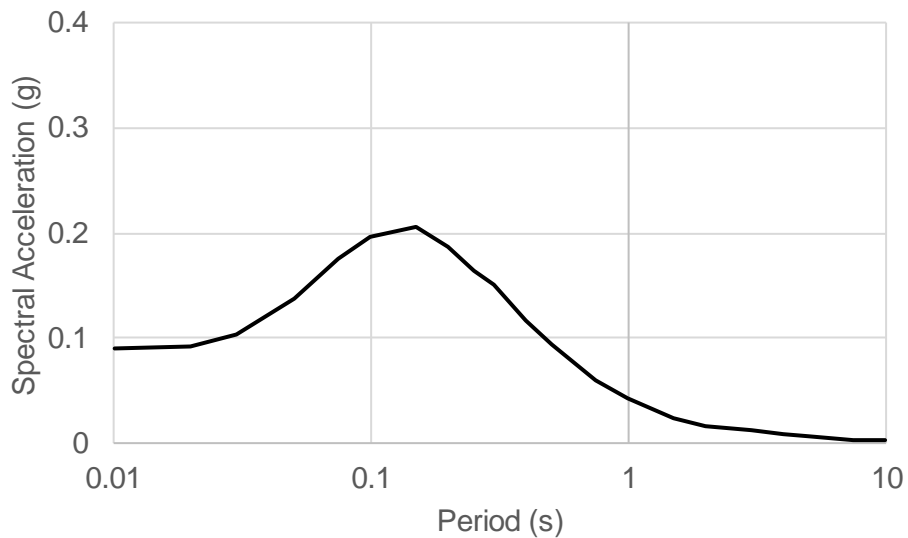


Figure 1-2 – Service-Level Earthquake Response Spectrum

1.2 Ground Motions

In our nonlinear evaluation of the structure for MCE we used 11 ground motion records and a site-specific hazard spectrum computed by ENGEEO, as described in their Sept 2018 geotechnical memorandum. John Egan, Slate Geotechnical Consultants, Inc., and Shannon & Wilson, Inc. spectrally matched these ground motions to the site-specific ENGEEO hazard spectrum and rotated the accelerations to fault-normal (FN) and fault-parallel (FP) directions, as described in their 30 November 2018 geotechnical report.

Our time history analysis uses the spectrally matched and rotated ground motion records provided by John Egan, Slate Geotechnical Consultants, Inc., and Shannon & Wilson, Inc., shown in Figure 1-3. Fault-normal motions are labeled FN; fault-parallel motions are labeled FP. Our application of these ground motions to our analysis models is further described in Section 6.2.

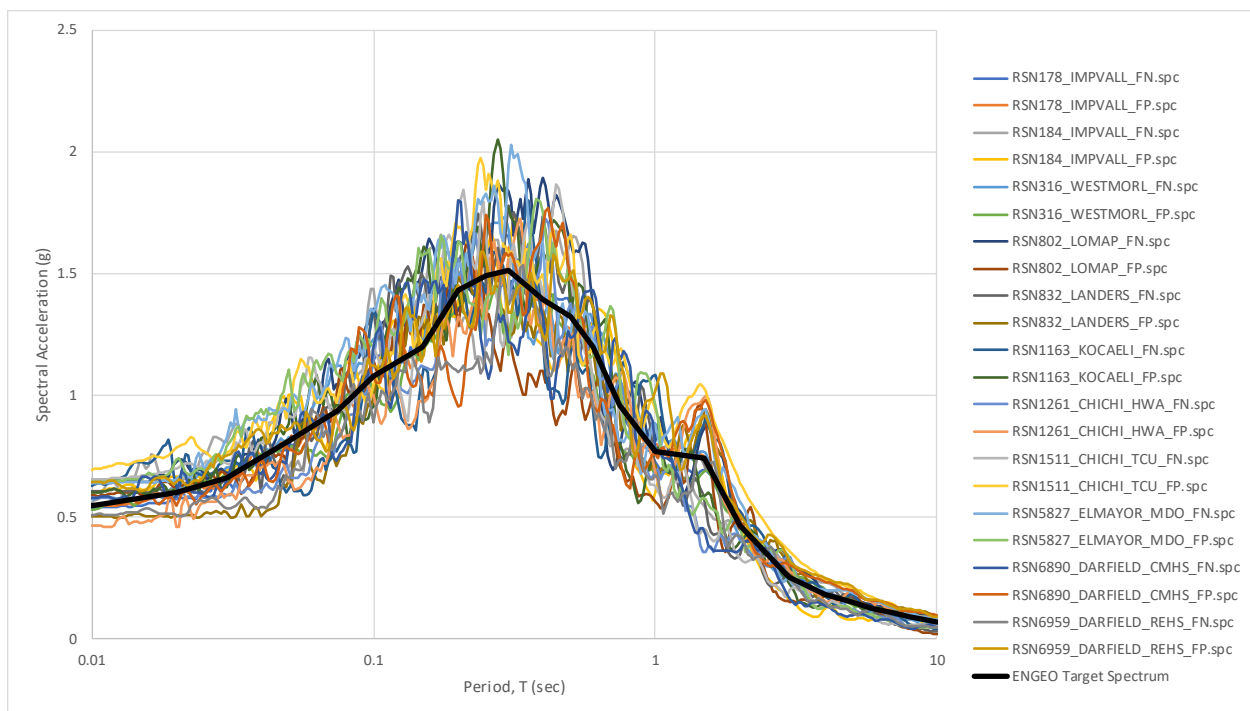


Figure 1-3 – Spectrally Matched Rotated Target Spectrum

2. ANALYTICAL MODEL: ETABS

We used an ETABS analytical model to evaluate the compliance of the tower superstructure using the new building requirements of the 2016 San Francisco Building code. We calculated wind and seismic loading in accordance with ASCE 7-10 and applied the loading to the analytical model. We compared the demands generated against calculated design capacities to determine the DCR of each structural element of the building.

2.1 Model Description

2.1.1 Geometry

We modeled the superstructure of the tower using ETABS 2016 Version 16.2.1. We modified the ETABS model originally developed by DeSimone Consulting Engineers during original building design to be consistent with the geometry and material properties shown on the structural drawings.

Figure 2-1 shows the ETABS model, which includes the shear walls, moment frame columns and beams, outriggers, and diaphragms. We modeled shear walls, outriggers, and diaphragms with shell elements. We modeled beams and columns with frame elements. Figure 2-2 shows a typical floor plan. Figure 2-3 and Figure 2-4 show elevation views of the shear walls and moment frames, colored by section property. We modeled the foundation separately, as described in subsequent sections, applying base reactions from the superstructure model. In this model, we restrained translation (pinned) the base of walls and restrained translation and rotation (fixed) the base of columns.

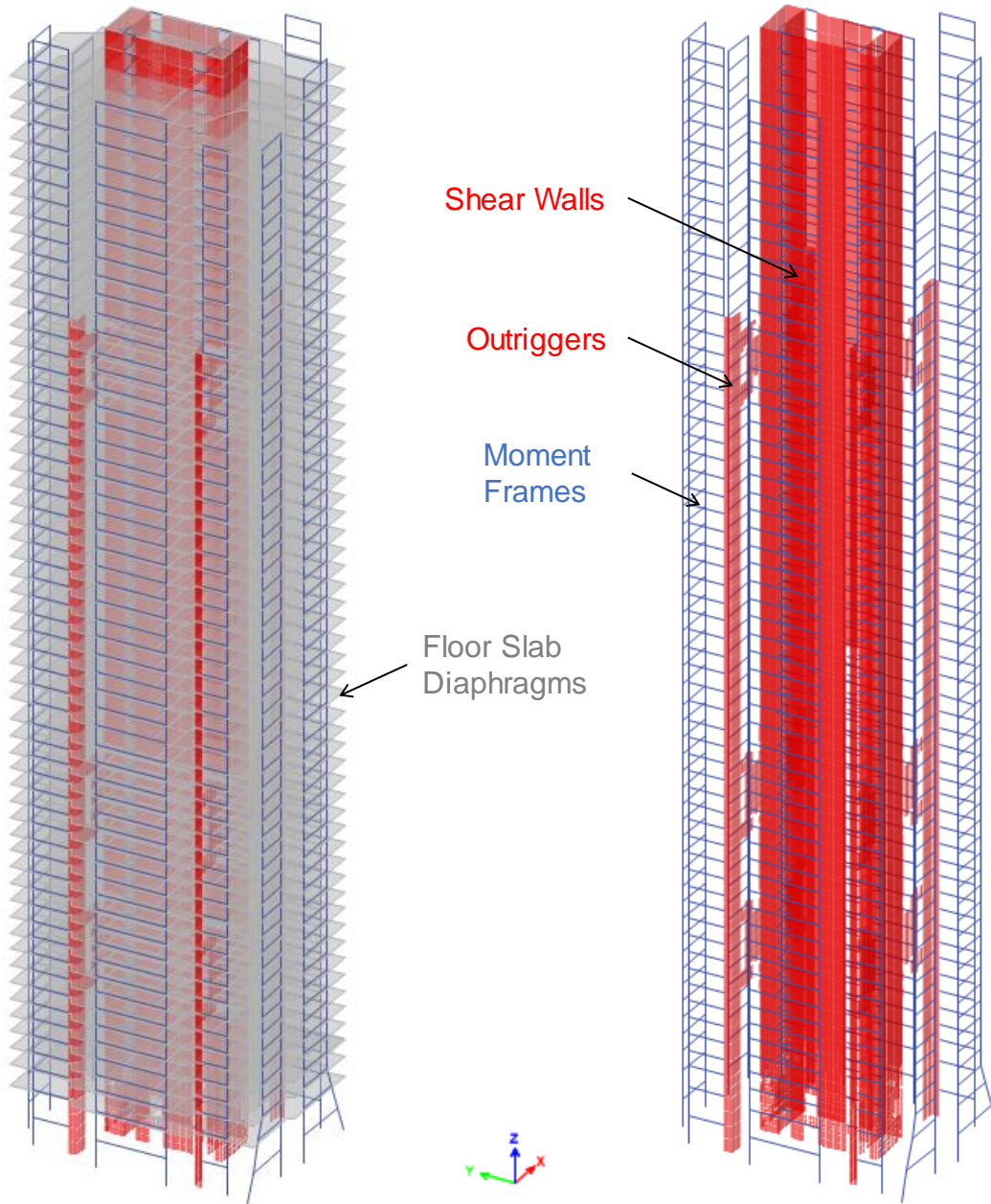


Figure 2-1 - Isometric View of ETABS Model, With and Without Floor Slabs Shown

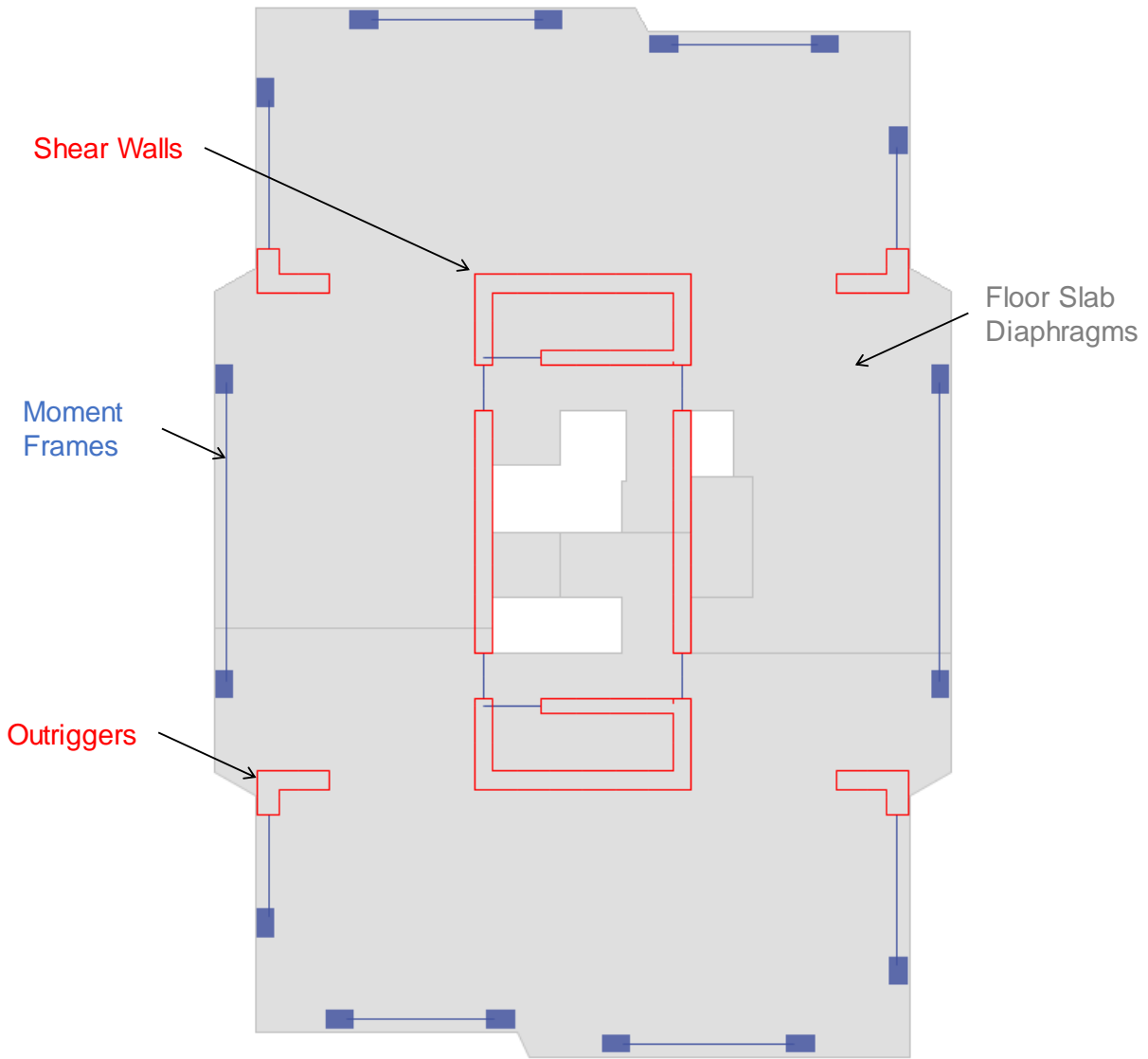


Figure 2-2 - Plan View of ETABS Model, Typical Floor

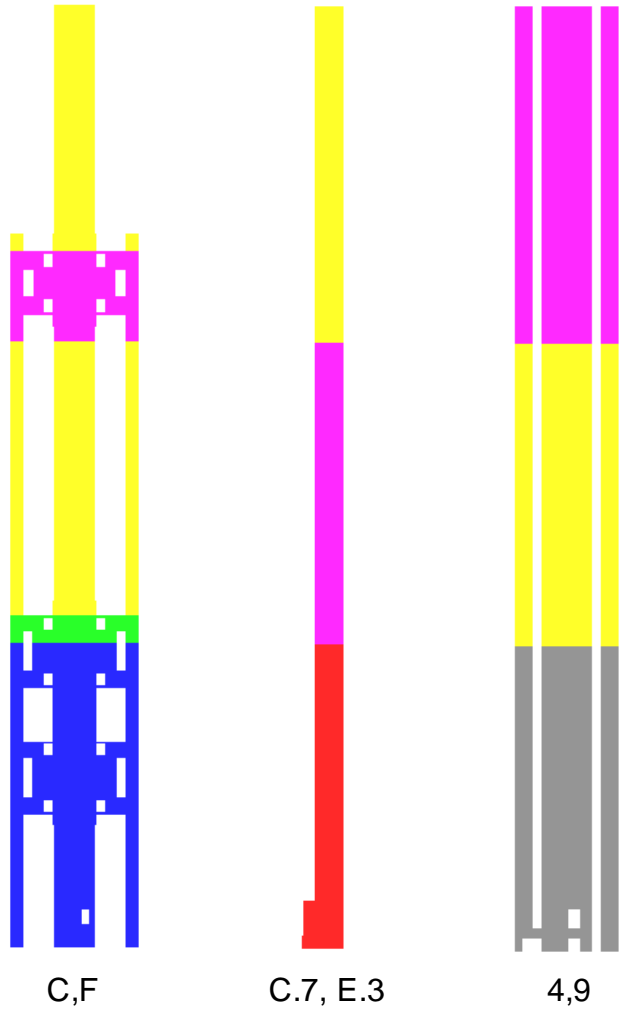


Figure 2-3 - Elevation Views of ETABs Model, Shear Walls

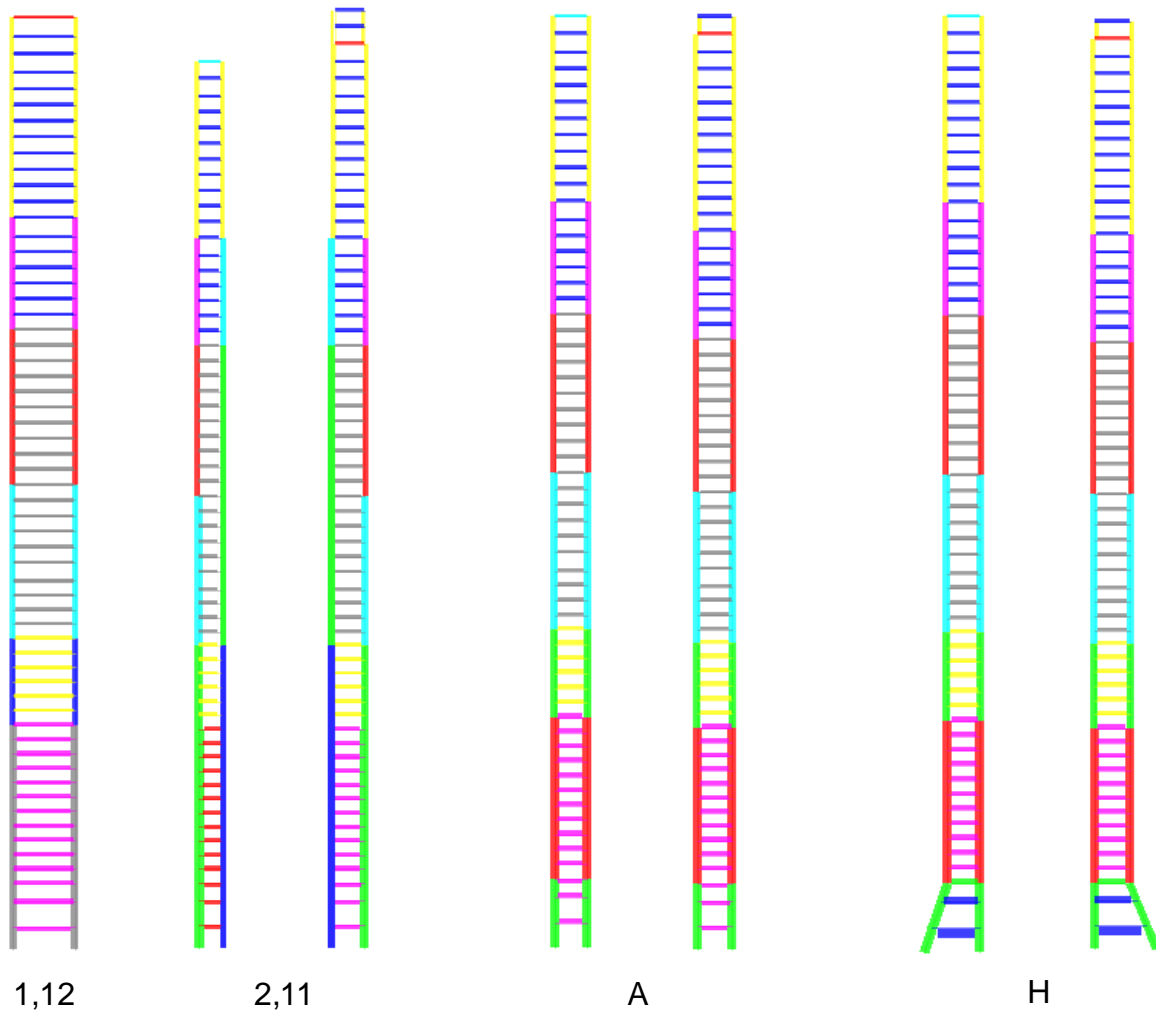


Figure 2-4 - Elevation Views of ETABs Model, Moment Frames

2.1.2 Gravity Loads

The self-weight of the structural elements is calculated directly by the program using a steel and concrete unit weights of 490 and 150 pcf, respectively. We applied distributed floor loads for super-imposed dead loads and live load as shown in Table 2-1. We applied perimeter line loads at each floor based on the story height and a curtain wall mass of 15 psf.

Table 2-1 – Floor Gravity Loads

Level	Use	SDL (psf)					LL (psf)
		Floor Finish	CMEP	Partitions	Concrete Pads	Total	
59	Mechanical	30	15	10	12	67	75
58-2	Residential	7	5	10	0	22	40
1	Lobby	25	10	25	0	60	100
0	Mechanical	0	10	10	20	40	75

2.1.3 Stiffness Modifiers

We modified the effective stiffness of structural concrete elements in accordance with PEER TBI v2 recommendations, as shown in Table 2-2.

Table 2-2 - Property Modifiers used in ETABS model

Component	Stiffness Modifier		
	Axial / In-Plane	Flexure / Out-of-Plane	Shear
Walls	0.75	0.25	1
Slabs	0.8	0.25	1
Beams	1	0.5	1
Columns	1	0.7	1
Link	1	0.14	1

2.1.4 P-Delta

We included p-delta effects in accordance with ASCE 7-10 Section 12.8.7 using the iterative method for a load combination of 1.2D+0.5L.

2.1.5 Modal Response

We used ritz vector analysis in ETABS to compute the first 50 modes of the structure. The first three modes are plotted in Figure 2-5. The period, lateral displacement, and cumulative modal mass participation for all modes are shown in Table 2-3.

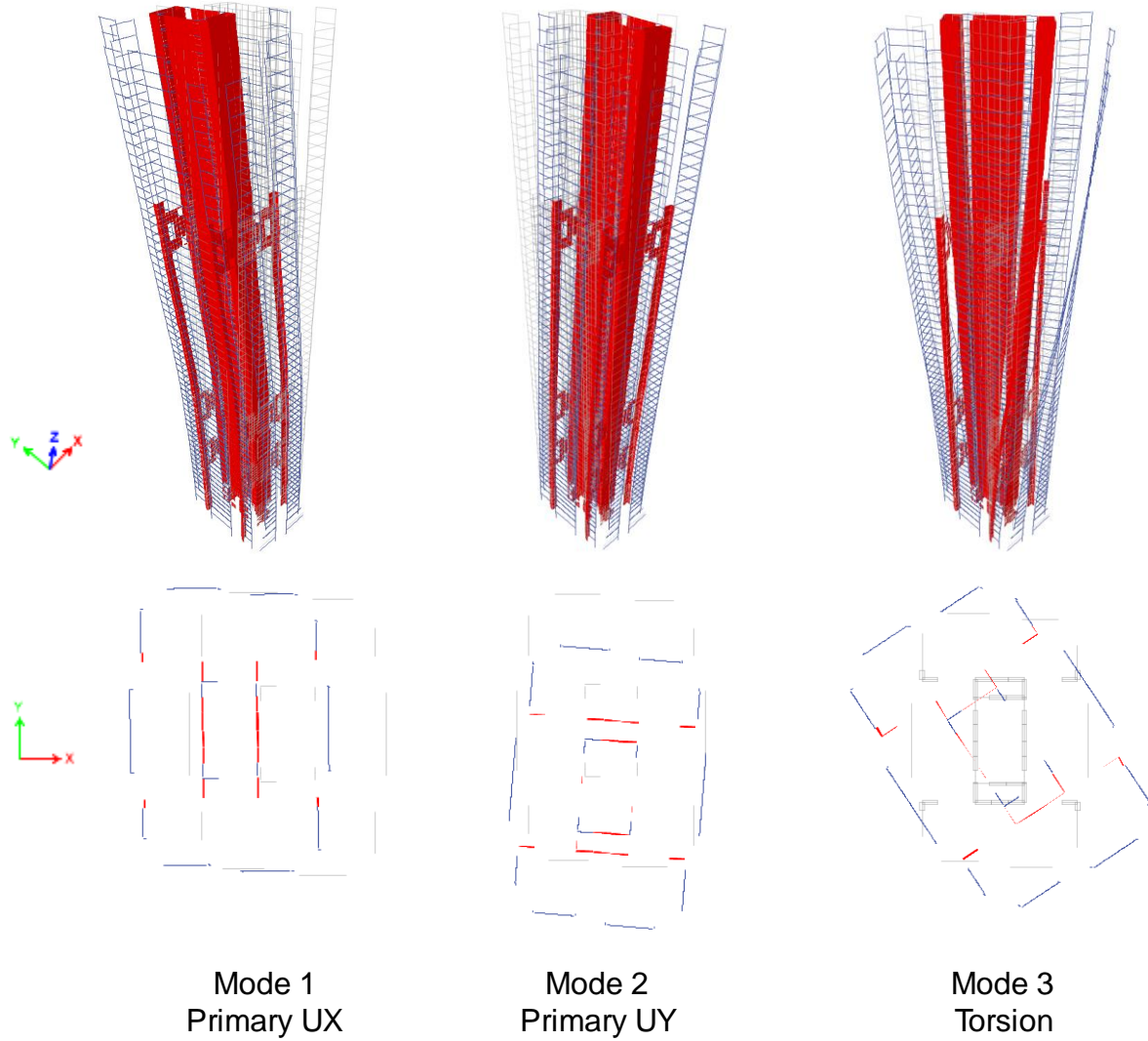


Figure 2-5 – First Three Modes

Table 2-3 – Modal Periods and Mass Participation

Mode	T (s)	Modal Mass Participating Ratio					
		UX	UY	RZ	Sum UX	Sum UY	Sum RZ
1	5.02	0.60	0.00	0.00	0.597	0.003	0.000
2	3.78	0.00	0.65	0.02	0.599	0.652	0.024
3	2.81	0.00	0.02	0.71	0.599	0.668	0.737
4	1.16	0.21	0.00	0.00	0.806	0.669	0.737
5	1.08	0.00	0.18	0.00	0.807	0.851	0.740
6	0.89	0.00	0.01	0.13	0.807	0.864	0.870
7	0.69	0.10	0.00	0.00	0.904	0.864	0.870
8	0.55	0.00	0.02	0.02	0.904	0.888	0.893
9	0.50	0.00	0.03	0.02	0.904	0.921	0.914
10	0.37	0.00	0.01	0.02	0.905	0.927	0.938
11	0.36	0.03	0.00	0.00	0.934	0.927	0.939
12	0.32	0.00	0.02	0.01	0.934	0.949	0.945
13	0.28	0.00	0.00	0.01	0.934	0.949	0.954
14	0.27	0.01	0.00	0.00	0.943	0.949	0.956
15	0.26	0.00	0.00	0.00	0.947	0.949	0.960
16	0.26	0.01	0.00	0.00	0.956	0.949	0.960
17	0.23	0.00	0.01	0.00	0.956	0.964	0.961
18	0.21	0.00	0.00	0.01	0.956	0.964	0.967
19	0.19	0.01	0.00	0.00	0.963	0.964	0.967
20	0.18	0.00	0.01	0.00	0.963	0.974	0.967
21	0.17	0.00	0.00	0.01	0.963	0.974	0.973
22	0.16	0.00	0.00	0.00	0.963	0.974	0.973
23	0.16	0.00	0.00	0.00	0.963	0.975	0.973
24	0.15	0.00	0.00	0.00	0.963	0.978	0.975
25	0.15	0.00	0.00	0.00	0.963	0.979	0.977
26	0.15	0.00	0.00	0.00	0.964	0.979	0.977
27	0.14	0.00	0.00	0.00	0.967	0.980	0.977
28	0.14	0.00	0.00	0.01	0.967	0.980	0.982
29	0.13	0.00	0.00	0.00	0.967	0.980	0.984
30	0.13	0.00	0.00	0.00	0.967	0.981	0.985
31	0.12	0.00	0.00	0.00	0.967	0.984	0.985
32	0.11	0.01	0.00	0.00	0.972	0.984	0.985
33	0.11	0.00	0.00	0.00	0.972	0.986	0.985
34	0.10	0.01	0.00	0.00	0.983	0.986	0.985
35	0.10	0.00	0.00	0.00	0.983	0.988	0.986
36	0.09	0.00	0.00	0.00	0.984	0.989	0.987
37	0.09	0.00	0.00	0.00	0.985	0.989	0.987
38	0.08	0.00	0.00	0.00	0.985	0.990	0.987
39	0.08	0.00	0.00	0.00	0.987	0.991	0.987
40	0.07	0.00	0.00	0.00	0.988	0.992	0.987
41	0.07	0.00	0.00	0.00	0.989	0.993	0.987
42	0.06	0.00	0.00	0.00	0.991	0.993	0.987
43	0.06	0.00	0.00	0.00	0.991	0.994	0.987
44	0.05	0.00	0.00	0.00	0.994	0.994	0.987
45	0.04	0.00	0.00	0.00	0.994	0.996	0.987
46	0.04	0.00	0.00	0.00	0.996	0.996	0.987
47	0.03	0.00	0.00	0.00	0.996	0.999	0.987
48	0.03	0.00	0.00	0.00	0.998	0.999	0.987
49	0.02	0.00	0.00	0.00	0.998	1.000	0.987
50	0.02	0.00	0.00	0.00	1.000	1.000	0.987

2.2 Loading

2.2.1 Wind

The original design of the tower used wind loads based on wind tunnel testing performed by RWDI in accordance with ASCE 7-02. We calculated wind loads on the tower's lateral force resisting system following the Directional Procedure for buildings of all heights described in Chapter 27 of ASCE 7-10. We scaled the wind tunnel test loads to account for the differences between ASCE 7-02 and ASCE 7-10. We considered an envelope of the scaled wind tunnel test loads and 80% of the ASCE 7-10 loads, in accordance with ASCE 7-10 Section 31.4.3.

2.2.1.1 ASCE 7-10 Wind Loads

We calculated wind loads in accordance with ASCE 7-10 using the parameters listed in Table 2-4. We considered an envelope of combined directional wind loads in accordance with ASCE 7-10 Figure 27.4-8. Resulting wind pressures and forces are shown in Figure 2-6. The ASCE 7-10 loads are greater than the equivalent demands in accordance with ASCE 7-16, as ASCE 7-16 includes a reduced wind speed of 92 mph.

Table 2-4 – ASCE 7-10 Wind Load Parameters

Parameter	Value
Building Width (E-W)	103 ft
Building Width (N-S)	146 ft
Building Height	628 ft
Risk Category	II
Wind Speed (V)	110 mph
Exposure Category	D
Topographic Factor (Kzt)	1.0
Directional Factor (Kd)	0.85
Enclosure Type	Enclosed
Damping Ratio	1.5%
Gust Factors	1.05 (E-W), 0.99 (N-S)
Internal Pressure Coefficient (GCpi)	+/- 0.18

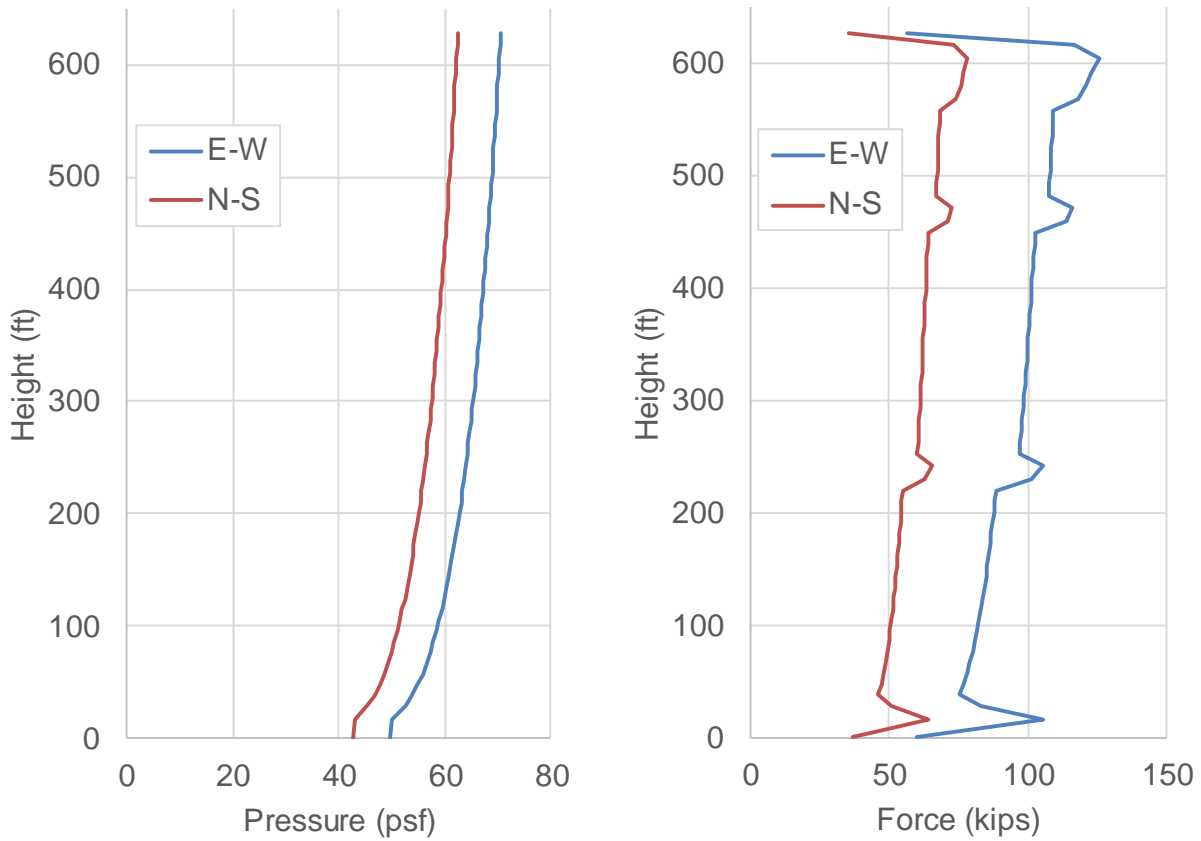


Figure 2-6 – ASCE 7-10 Wind Loads

2.2.1.2 Wind Tunnel Loads

A wind tunnel study was performed by RWDI Inc. for the original design of the tower in accordance with ASCE 7-02. We reviewed the final report from the study dated 9 Aug 2005, included here as Appendix A. The study considered both the preexisting condition of the surrounding urban landscape as well as the expected environment after completion of surrounding high-rise developments. The expected environment included an 800 ft tall structure representing Salesforce tower. The expected environment did not include the 450 ft tall structure now present at 350 Mission to the northwest, but it did include the 475 ft tall structure at 45 Fremont immediately beyond.

We modified the results of the RWDI wind study using scale factors that convert the wind pressures from ASCE 7-02 to ASCE 7-10 demand levels. ASCE 7-02 specifies wind speeds at the service level while ASCE 7-10 specifies wind speeds at the strength level. The test is specific to the geometric properties of the building and the surrounding landscape and does not depend on wind speed. The test inherently captures the effect of the gust factor. The difference in wind speeds from ASCE 7-02 to ASCE 7-10 leads to an increase in the gust factor of 12%. We scaled the original wind tunnel test loads by a factor of 1.79 to align with ASCE 7-10, comprised of 1.12 for the gust factor and 1.6 for LRFD load factors. We considered all load combinations recommended in the original wind tunnel test report.

2.2.1.3 Comparison of Wind Loads

We enveloped the scaled wind tunnel test loads and 80% of the ASCE 7-10 loads, in accordance with ASCE 7-10 Section 31.4.3. Figure 2-7 shows story forces due to the scaled wind tunnel test loads and 80% of the ASCE 7-10 loads.

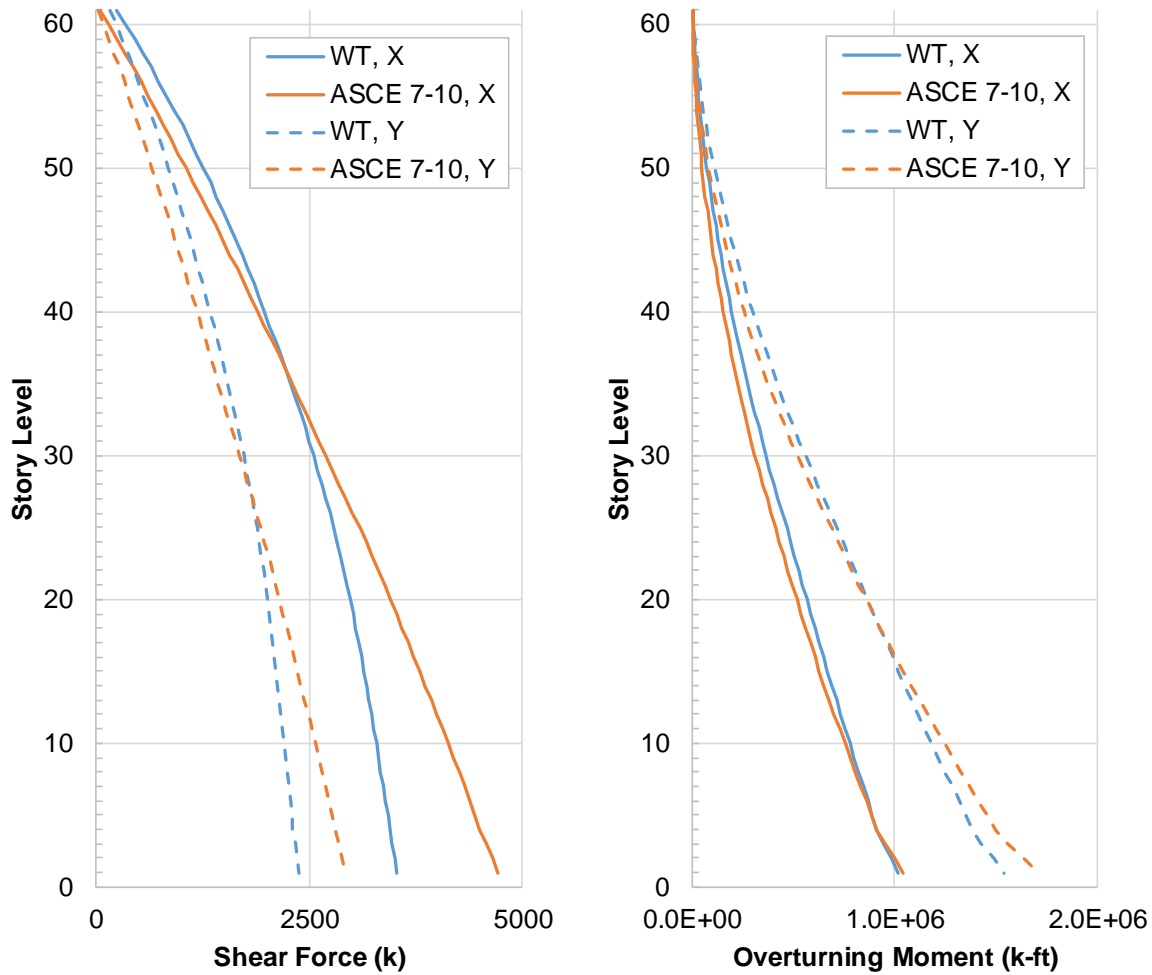


Figure 2-7 – Story Forces due to Wind Loads

2.2.2 Seismic

We calculated seismic forces following the Equivalent Lateral Force (ELF) Procedure described in ASCE 7-10 Section 12.8. We calculated seismic loads on the tower’s lateral force resisting system following the Modal Response Spectrum Analysis Procedure described in ASCE 7-10 Section 12.9. We scaled the response spectrum results to 85% of the ELF base shear in accordance with ASCE 7-10 Section 12.9.4. We also performed response spectrum analysis using a service-level earthquake provided by Slate Geotechnical Consultants, Inc. and Shannon & Wilson, Inc.

2.2.2.1 ASCE 7-10 Equivalent Lateral Forces

We obtained the response parameters shown in Table 2-5 from USGS design maps and the original design calculations by DeSimone. The equivalent lateral forces calculated in accordance with ASCE 7-10 Section 12.8 are shown in Figure 2-8.

Table 2-5 – Seismic Response Parameters

Parameter	Value
Risk Category	II
Importance Factor (I_e)	1.0
Site Class	D
Seismic Design Category	D
Spectral Acceleration	$S_s = 1.5, S_1 = 0.6$
Spectral Response Coefficients	$S_{DS} = 1.0, S_{D1} = 0.6$
Response Modification Factor (R)	7

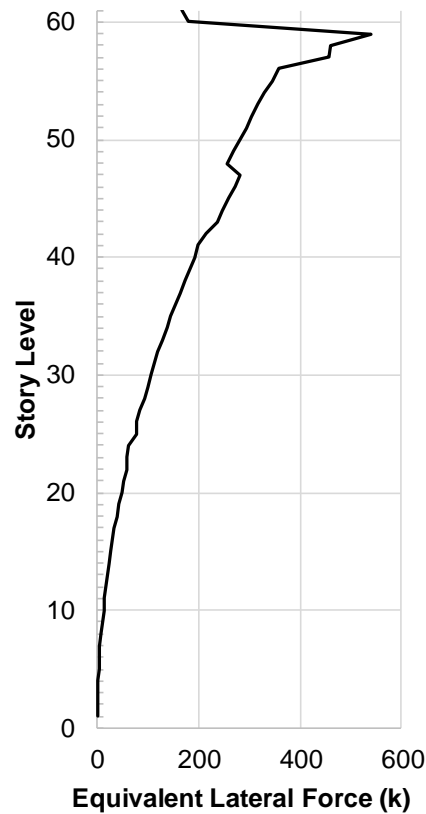


Figure 2-8 – ASCE 7-10 Equivalent Lateral Force by Story

2.2.2.2 ASCE 7-10 Design-Level Earthquake Response Spectrum

The response spectrum corresponding to the parameters shown in Table 5 is shown in Figure 2-9.

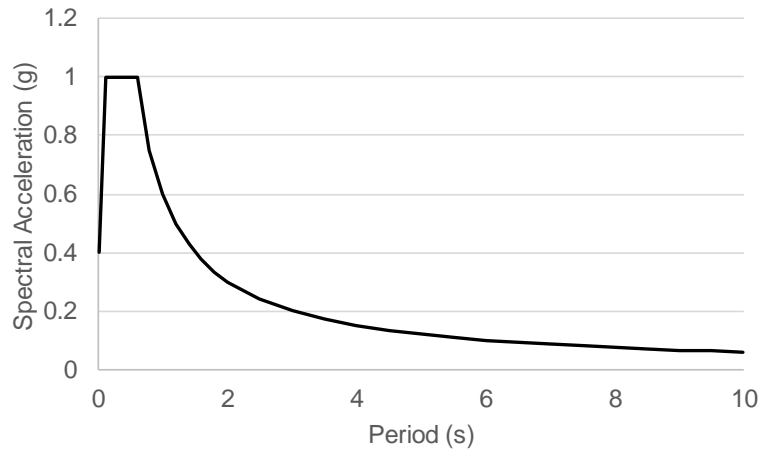


Figure 2-9 – ASCE 7-10 Design-Level Earthquake Response Spectrum

Figure 2-10 shows scaling of the design-level earthquake (DE) response spectrum forces based on the equivalent lateral forces. The effective R-factors are 4.11 and 3.74 in the X and Y directions, respectively.

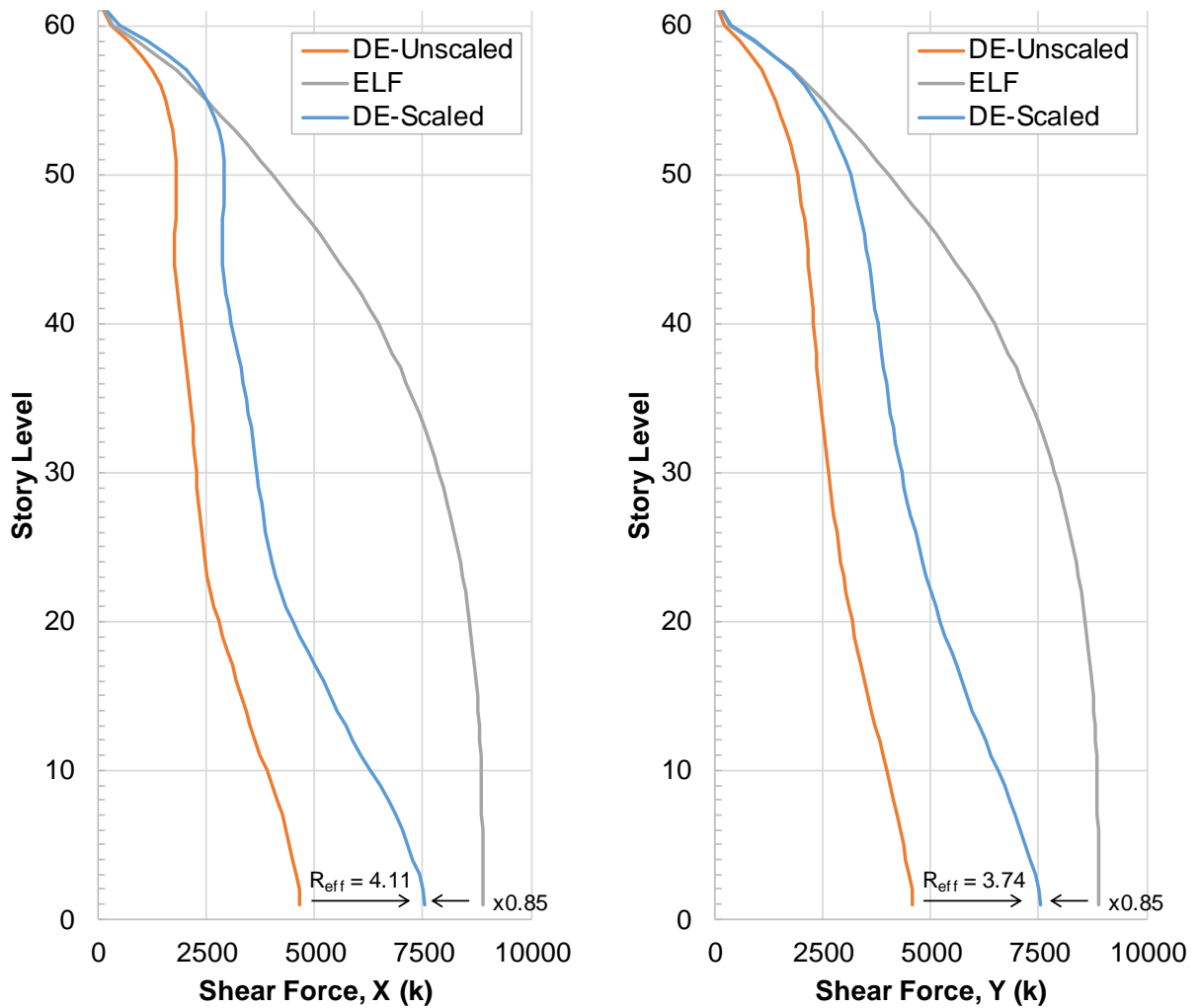


Figure 2-10 – Scaling of ASCE 7-10 Design-Level Earthquake Response

2.2.2.3 Service-Level Earthquake Response Spectrum

Slate Geotechnical Consultants, Inc. and Shannon & Wilson, Inc. provided a service-level earthquake (SE) response spectrum, representing a seismic event with a 43-year return period, as shown in Figure 2-11.

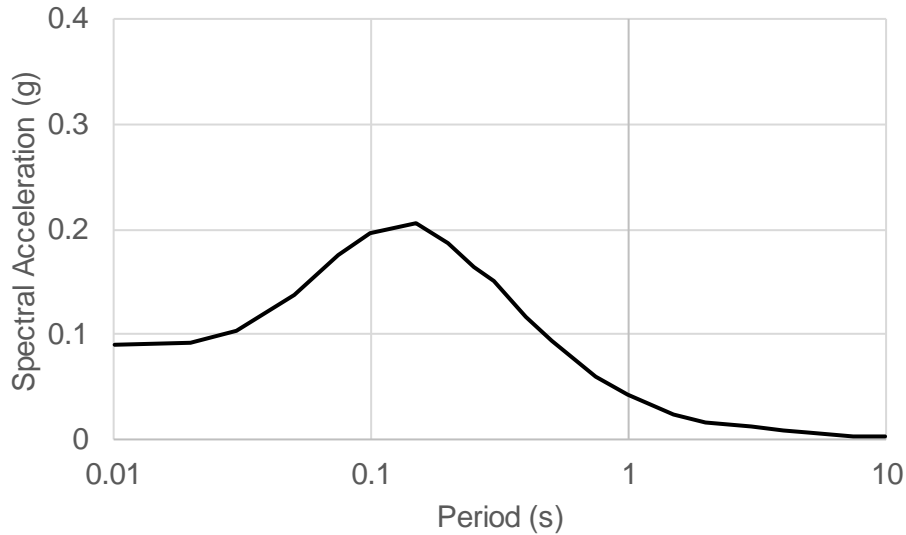


Figure 2-11 – Service-Level Earthquake Response Spectrum

2.2.2.4 Application to Analysis Model

We created the load cases shown in Table 2-6. We combined seismic response in orthogonal directions in accordance with ASCE 7-10 Section 12.5.

Table 2-6 – Seismic Response Spectrum Load Cases

Load Case Name	Response Spectrum	Acceleration (g)	
		X	Y
ASCE 7-10 RS X	ASCE 7-10	±1	±0.3
ASCE 7-10 RS Y	ASCE 7-10	±0.3	±1
Service RS X	SLE	±1	±0.3
Service RS Y	SLE	±0.3	±1

We combined the effect of different modes using the complete quadratic combination (CQC) method in accordance with ASCE 7-10 Section 12.9.3. We used a constant modal damping of 5% and considered a diaphragm center of mass eccentricity of 5%.

2.2.3 Load Combinations

We considered the load combinations shown in Table 2-7, in accordance with ASCE 7-10 Section 2.3.2. We calculated the live load factor in accordance with Exception 1 in Section 2.3.2

and live load reduction in Section 4.7.2. The seismic dead load factor includes contribution of vertical seismic effects. Results are presented for the controlling wind and seismic load cases.

Table 2-7 – Controlling Load Combinations

Load	Combination
Dead	1.4D
Live	1.2D + 1.6L
Wind	1.2D + 1.0W + 0.5L
Seismic	1.4D + 1.0E + 0.5L
Wind Uplift	0.9D + 1.0W
Seismic Uplift	0.7D + 1.0E

2.3 Response

2.3.1 Story Forces

Figure 2-12 compares shear force and overturning moment due to design and service-level earthquakes and enveloped wind loads.

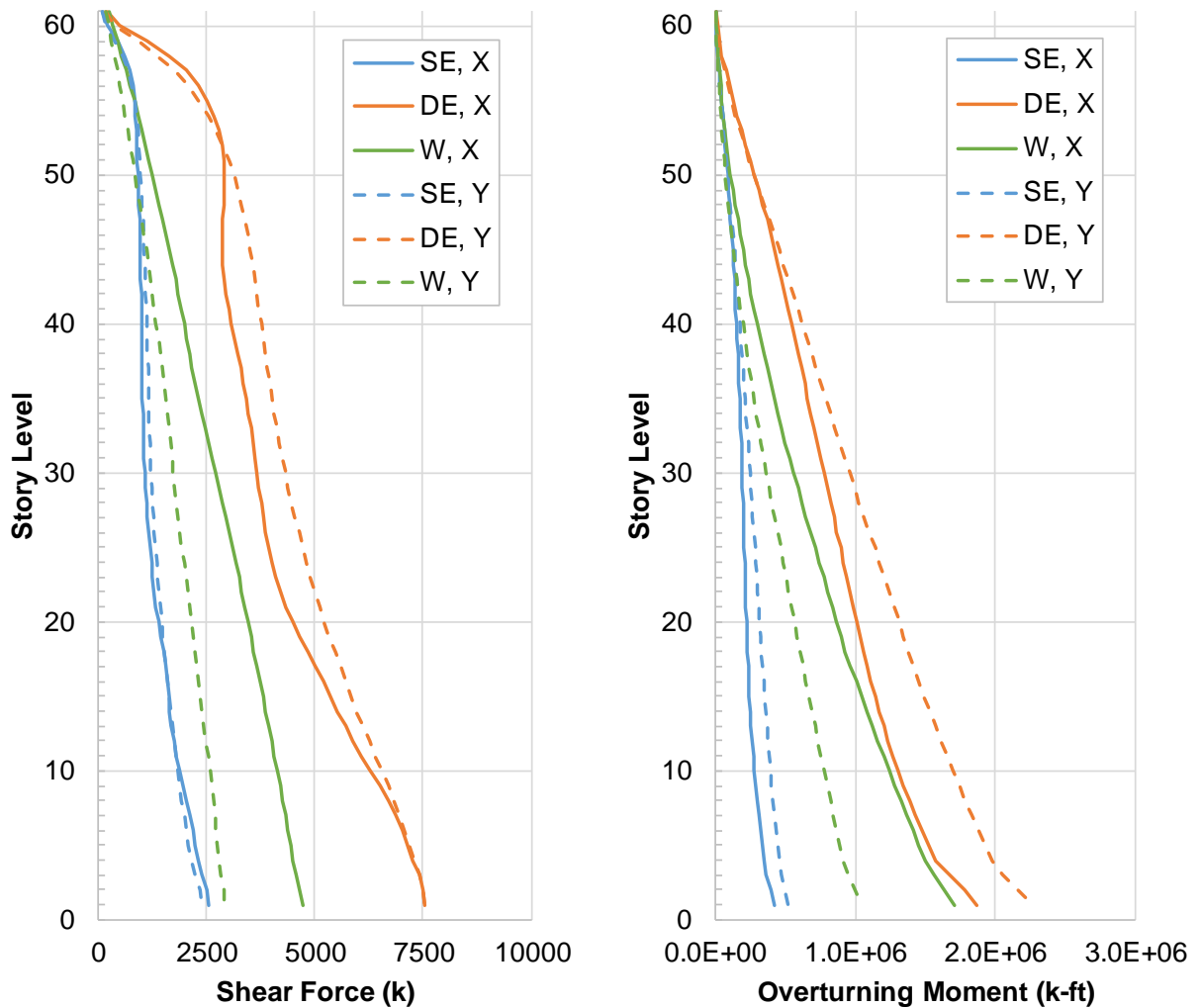


Figure 2-12 – Comparison of Story Forces

2.3.2 Base Reactions

Table 2-8 shows controlling base shear and overturning moment due to wind and seismic loads. Reactions due to design-level earthquake response spectrum analysis are reduced by the response modification factor (R), then scaled up to match 85% of the base shear generated by equivalent lateral force analysis, in accordance with ASCE 7-10 Section 12.9.4.1. Reactions due to wind and service-level earthquake demands are not modified.

Table 2-8 – Base Reactions due to Current Code Loads

Load	F_x (k)	F_y (k)	M_x (k-ft)	M_y (k-ft)
Wind	4,709	2,922	1,042,999	1,709,852
Seismic, Design-Level	7,545	7,545	2,267,288	1,869,226
Seismic, Service-Level	2,542	2,383	520,450	419,301

Note: M_x refers to moment about the X-axis, caused by Y-direction forces.

2.4 Capacity Calculations

We calculated design capacities in accordance with ACI 318-14 and AISC 360-10 provisions using nominal material properties.

2.4.1 Shear Walls

2.4.1.1 Wall In-Plane Shear

Figure 2-13 shows shear wall pier locations on a typical plan view. Table 2-9 shows in-plane shear capacities of the piers. A detailed sample capacity calculation is provided for Pier 3 at the ground level.

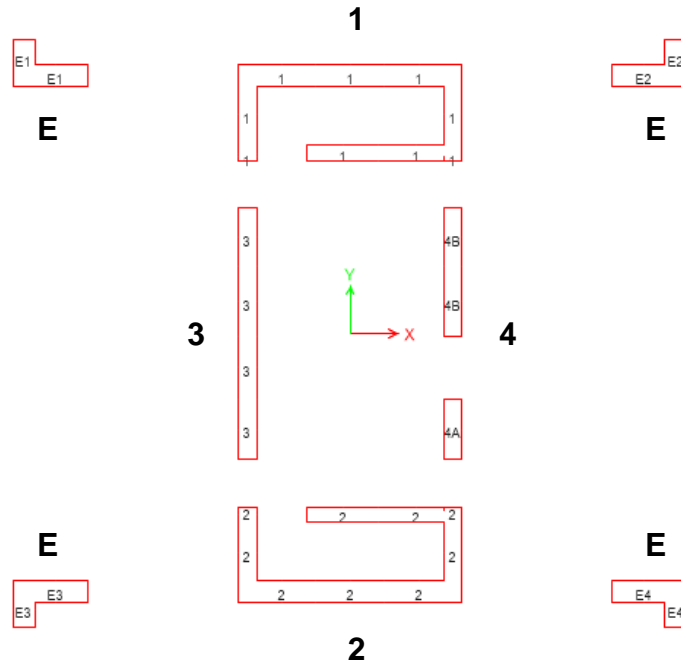


Figure 2-13 – Pier Labels on Typical Plan

Table 2-9 –Wall Pier Shear Capacities (psi)

Top Story	Pier Label				
	1	2	3	4	E
61	313	313	275	275	707
56	313	313	275	275	707
52	313	313	275	275	707
48	313	313	275	275	707
44	313	313	275	425	610
40	322	322	359	434	619
36	322	322	359	434	619
32	322	322	359	529	619
28	322	322	434	430	619
24	322	322	434	430	619
20	338	338	450	446	634
16	338	338	600	446	634
12	338	338	743	446	634
8	338	338	743	446	634
4	520	520	743	743	634
1	520	520	743	743	634

Calculate In-Plane Shear Capacity of Pier 3 at Base

Concrete compressive strength	$f_c := 10\text{ksi}$	Shear wall schedule, S3-2.21
Steel yield strength	$f_y := 60\text{ksi}$	Shear wall schedule, S3-2.21
Wall thickness	$t_w := 30\text{in}$	Shear wall schedule, S3-2.21
Horizontal bars (#9)	$A_s := 0.79\text{in}^2$	Shear wall schedule, S3-2.21
Horizontal bar spacing	$s := 4\text{in}$	Shear wall schedule, S3-2.21
Horizontal reinforcing ratio	$\rho := \frac{2 \cdot A_s}{t_w \cdot s} = 0.013$	
Concrete shear capacity	$v_c := 2 \cdot \sqrt{\frac{f_c}{\text{psi}}} \text{psi} = 200 \text{psi}$	
Reinforcement shear capacity	$v_s := \rho \cdot f_y = 790 \text{psi}$	
Shear resistance factor	$\phi_v := 0.75$	
Shear capacity	$\phi v_n := \phi_v \cdot (v_c + v_s) = 743 \text{psi}$	

2.4.1.2 Wall Axial-Flexure Interaction

We calculated P-M interaction capacities of the shear wall piers using spColumn v6.00. Figure 2-14 shows a sample interaction diagram for Pier 3 at the ground level.

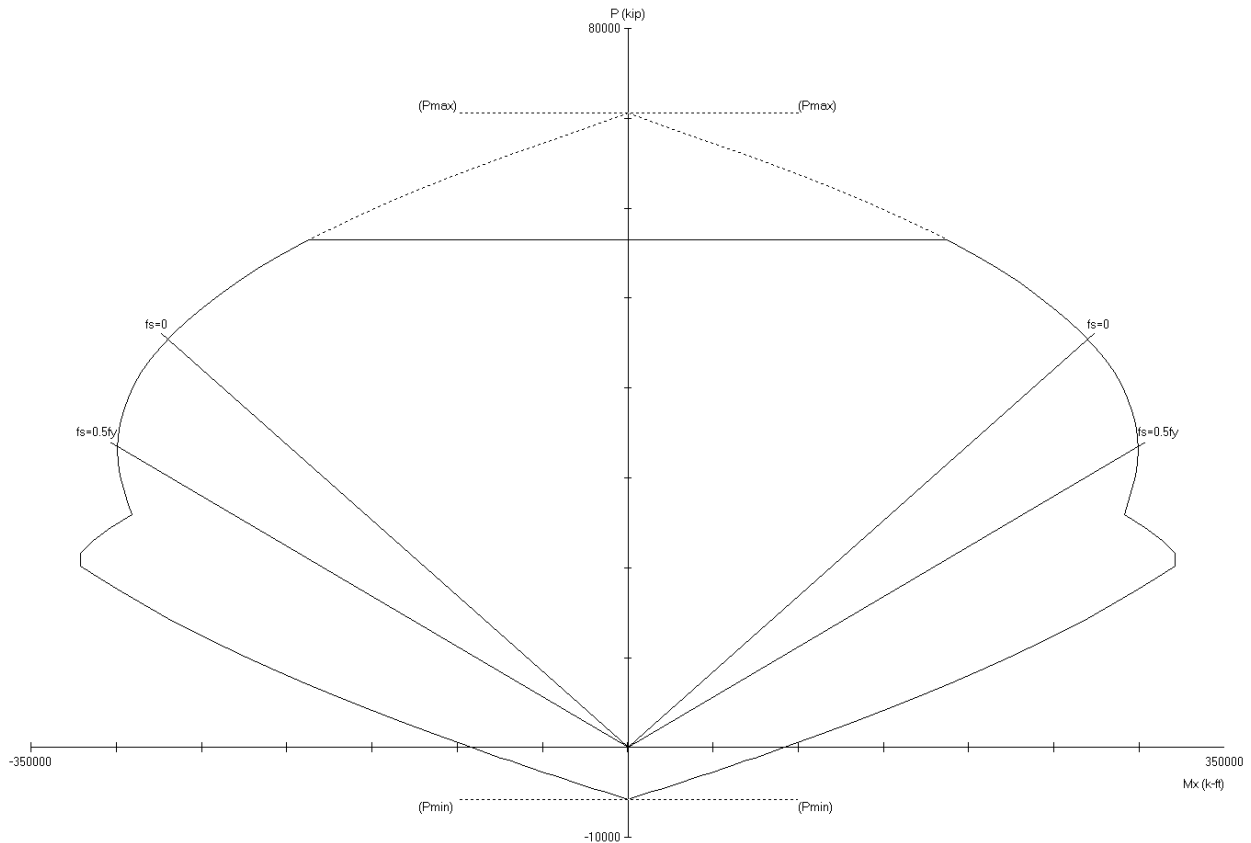


Figure 2-14 – Sample Wall PM Interaction Diagram for Pier 3 at Base

2.4.1.3 Steel Coupling Beams

Steel coupling beams transfer load between adjacent shear walls. We calculated the capacity of these beams based on the steel section capacity alone, conservatively neglecting the effect of the concrete encasement and embedded end length. The moment capacity of the coupling beams controls the behavior, rather than the shear capacity, per AISC 341-10 Section H4.5b. The capacities of the steel coupling beams are shown in Table 2-10. A detailed sample capacity calculation is provided for the W14x233 beams.

Table 2-10 – Coupling Beam Capacities

Coupling Beam Section	V (k)	M (k-ft)
W14x233	514	1,635
W14x311	723	2,260

Calculate Moment Capacity of W14x233 Coupling Beam

Steel yield stress	$f_y := 50\text{ksi}$
Plastic section modulus	$Z := 436\text{in}^3$
Flexural resistance factor	$\phi_b := 0.9$
Plastic moment capacity	$\phi M_p := \phi_b \cdot f_y \cdot Z = 1635\text{kip}\cdot\text{ft}$

2.4.1.4 Outrigger Coupling Beams

The outrigger beams transfer load from the central shear walls to the outrigger columns. The behavior of these beams is controlled by the diagonally-reinforced coupling beam sections at the openings adjacent to the outrigger columns. These coupling beams were originally designed to act as structural fuses, yielding first under high demands.

Table 2-11 shows the coupling beam shear capacities. A detailed sample capacity calculation is provided for the coupling beam at Story 12.

Table 2-11 – Outrigger Coupling Beam Shear Capacities

Story	Shear Capacity (k)
8	4,162
12	2,372
17	3,389
21	2,685
42	2,673
45	2,005

Calculate Shear Capacity of Outrigger Coupling Beam at Story 12

Coupling Beam Geometry

Length (L_c) =	72 in	
Height (h) =	136 in	
Width (b_w) =	36 in	
CLR Cover H =	1.5 in	1.5 in Minimum
CLR Cover V =	1.5 in	1.5 in Minimum
CCT =	4.0 in	

Coupling Beam Properties

Concrete Strength (f_c) =	10,000 psi
Rebar Strength (f_y) =	75,000 psi

Not all horizontal rebar shown for clarity

Coupling Beam Forces

$V_{U,Analysis}$ =	2,969 kips
$M_{U,L}$ =	100 kip-ft
$M_{U,R}$ =	100 kip-ft
V_U =	2,969 kips
M_U =	100 kip-in

Requirement of Coupling Beam

L_c/h =	0.53	May require Diagonal Reinforcement
		ACI 318-11 sec. 21.9.7.1 & 21.9.7.2
$4\sqrt{f_c}A_{cw}$ =	1,958	Diagonal Reinforcement Required
		ACI 318-11 sec. 21.9.7.2

Shear Strength $\phi V_n = \phi(2A_{vd}f_y \sin \alpha \leq 10\sqrt{f_c}A_{cw})$ (eq. 21-9)

ϕ =	0.85
α =	1.02 radians
	58.4 degrees
$A_{vd,required}$ =	27.3 total in ²

Diagonal Longitudinal Reinforcement

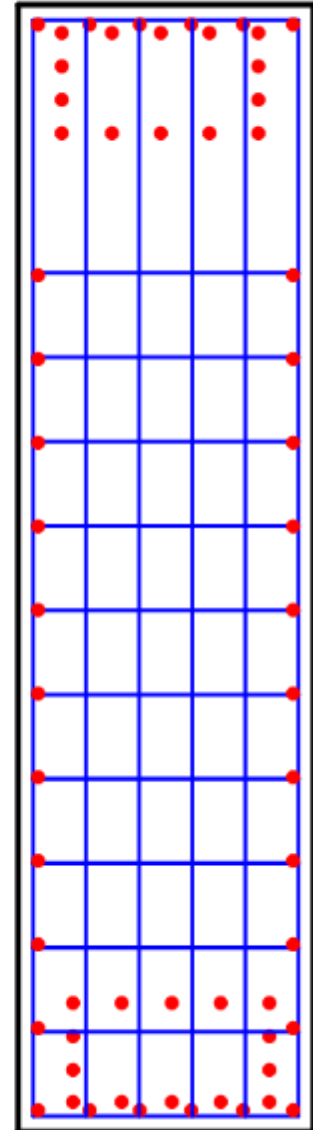
$n_{columns}$ =	5 bars	Max. n = 5
$s_{diag,h}$ =	6 in	Min. n = 2 (2 top and 2 bottom)
n_{add} =	0 bars	OK
$s_{diag,v}$ =	4 in	0 = no fill or 1 = fill
$n_{add,rows}$ =	2 rows	OK
CCD =	0.00 in	Add Spacing
Bar Size	#11	
$d_{diagonal}$ =	1.41 in	2790.62166
$A_{diagonal}$ =	1.56 in ² /bar	3411.20321
Total n_{bars} =	14	
A_{vd} =	21.8 in ²	Wt_{vd} = 3405 lbs
V_n =	2790.6 kips	$P_{DIAGONAL} \% = 0.89\%$
ϕV_n =	2372.0 kips	ACI 318-11 sec. 21.9.7.4 (a)
DCR =	1.25	NO

Full Section Transverse Reinforcement (Vertical)

n_{legs} =	6	Min. n = 2 (1left & 1right)
s_{diag} =	5 in	Max. s = 8
Bar Size	#5	
$d_{diagonal}$ =	0.6 in	
$A_{diagonal}$ =	0.31 in ² /bar	

Full Section Transverse Reinforcement (Horizontal)

n_{legs} =	14	Min. n = 2 (1left & 1right)
s_{diag} =	5 in	Max. s = 8
Bar Size	#5	
$d_{diagonal}$ =	0.6 in	
$A_{diagonal}$ =	0.31 in ² /bar	$Wt_{transv} = 1777$ lbs



2.4.2 Moment Frames

2.4.2.1 Columns

We calculated P-M interaction capacities of the column sections using spColumn v6.00. Figure 2-15 shows column locations and types on a typical plan. Figure 2-16 shows a sample interaction diagram for Column A (Story 14-20).

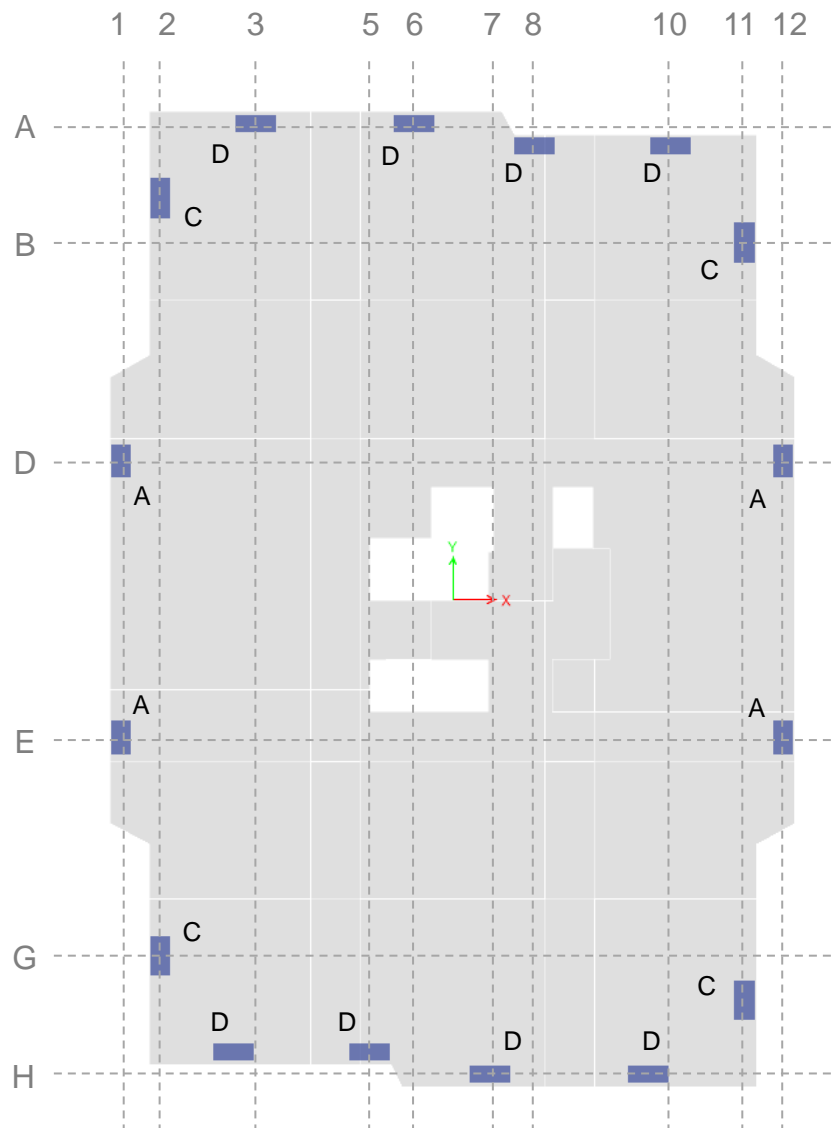


Figure 2-15 – Column Labels

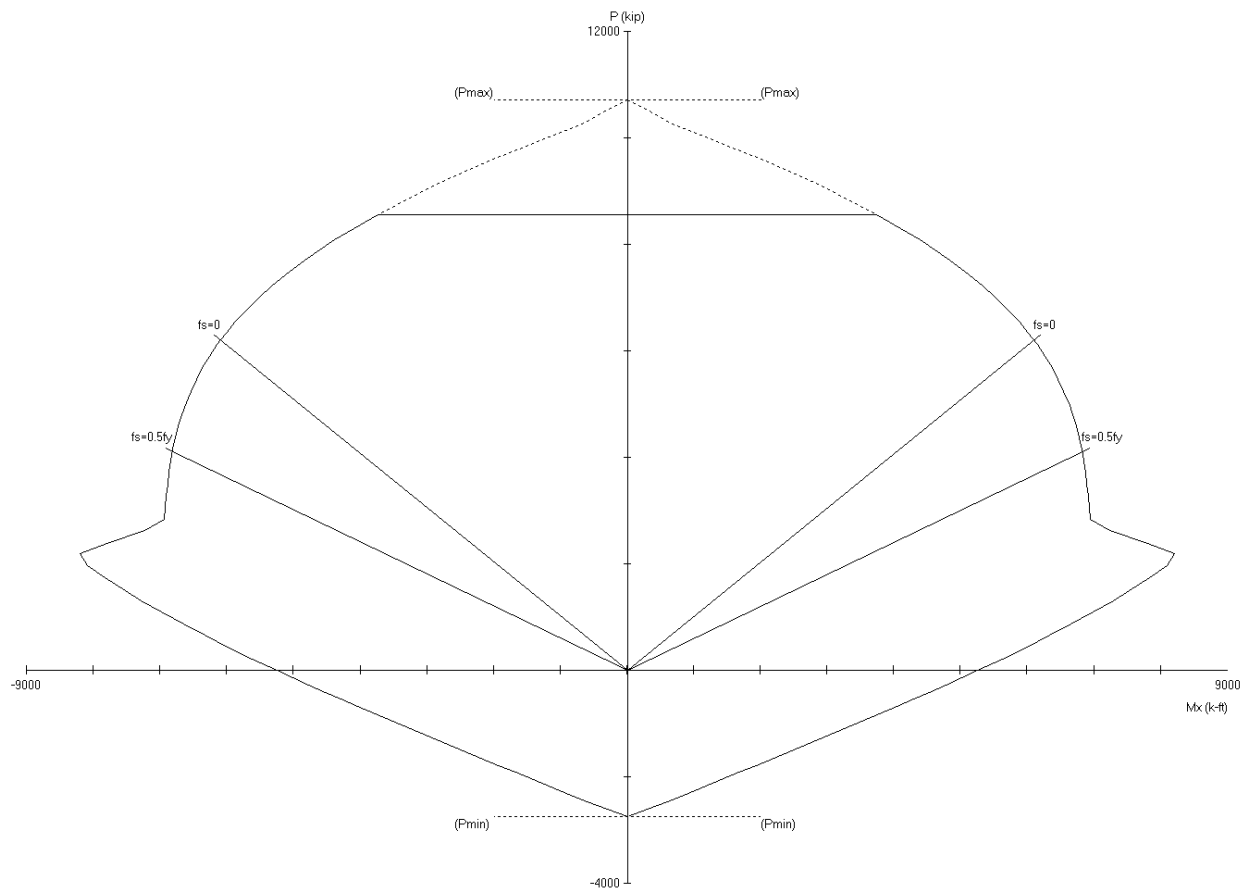


Figure 2-16 – Sample Column PM Interaction Diagram for Column A (Story 14-20)

Table 2-12 shows column shear capacities. A detailed sample capacity calculation is provided for Column A (Story 14-20).

Table 2-12 – Column Shear Capacities

Story	A		C		D	
	V1 (k)	V2 (k)	V1 (k)	V2 (k)	V1 (k)	V2 (k)
B1-4	1,273	1,070	1,547	1,214	1,538	1,214
4-14	1,278	1,070	1,547	1,214	1,242	1,159
14-20	922	914	1,033	1,025	1,021	1,025
20-30	898	892	1,006	1,001	995	1,001
30-40	794	694	794	694	779	694
40-47	611	567	611	567	590	567
47-Top	449	448	449	448	449	448

Calculate Shear Capacity of Column A (Story 14-20)

Concrete compressive strength	$f_c := 10\text{ksi}$	Column schedule, S3-2.01
Steel yield strength	$f_y := 60\text{ksi}$	Column schedule, S3-2.01
Column dimensions	$b := 30\text{in}$	Column schedule, S3-2.01
	$h := 54\text{in}$	Column schedule, S3-2.01
	$d := 49.97\text{in}$	
Transverse reinforcement (#5)	$A_s := 0.31\text{in}^2$	Column schedule, S3-2.01
Number of legs	$n := 4$	
Tie spacing	$s := 4\text{in}$	Column schedule, S3-2.01
Concrete shear capacity	$V_c := 2 \cdot \sqrt{\frac{f_c}{\text{psi}}} \cdot \text{psi} \cdot b \cdot d = 299.82 \cdot \text{kip}$	
Reinforcement shear capacity	$V_s := f_y \cdot n \cdot A_s \cdot \frac{d}{s} = 929.442 \cdot \text{kip}$	
Shear resistance factor	$\phi_v := 0.75$	
Shear capacity	$\phi V_n := \phi_v \cdot (V_c + V_s) = 922 \cdot \text{kip}$	

2.4.2.2 Beams

Figure 2-17 shows beam locations and types on a typical plan. Table 2-13 shows beam shear and moment capacities. A detailed sample capacity calculation is provided for Beam B1 (Story 14-20).

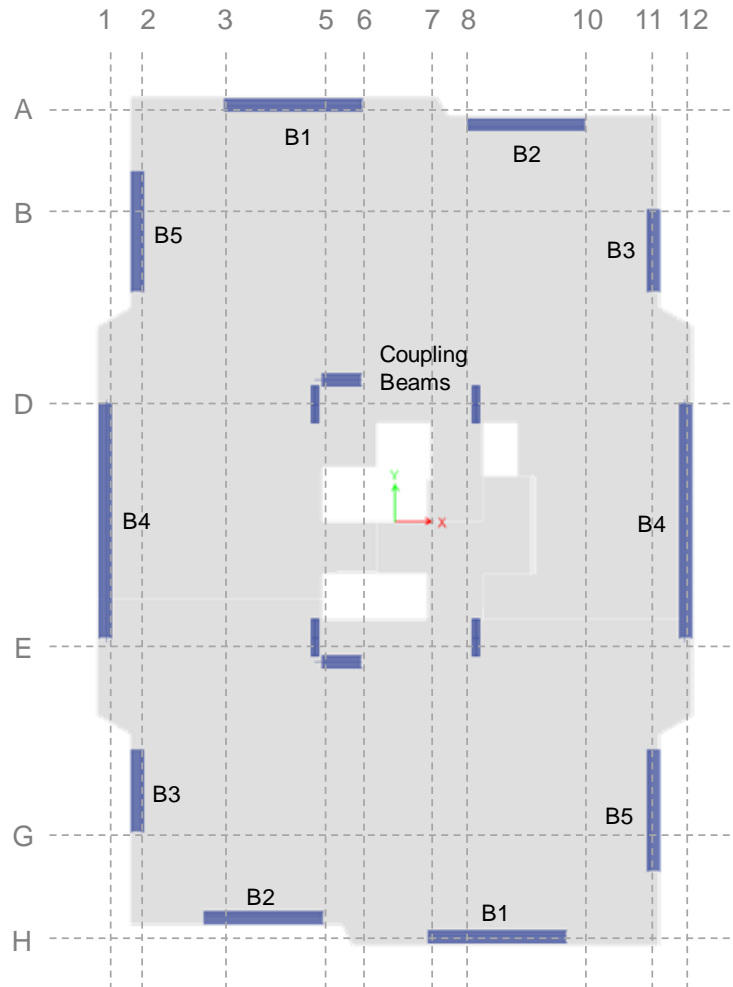


Figure 2-17 – Beam Labels

Table 2-13 – Beam Capacities

Story	B1		B2		B3		B4		B5	
	M (k-ft)	V (k)								
B1-4	2807	605	2798	717	2627	738	1161	340	2807	552
4-14	2807	605	2798	717	2627	738	1161	340	2807	552
14-20	2467	489	2457	635	2078	635	1026	302	1984	396
20-30	2071	384	2062	468	1756	544	883	253	1425	335
30-40	1764	334	1756	468	1756	544	883	253	1425	335
40-47	1311	305	1009	305	1058	351	810	229	1058	306
47-Top	1311	305	1009	305	810	306	844	238	810	306

Calculate Moment Capacity of Beam B1 (Story 14-20)

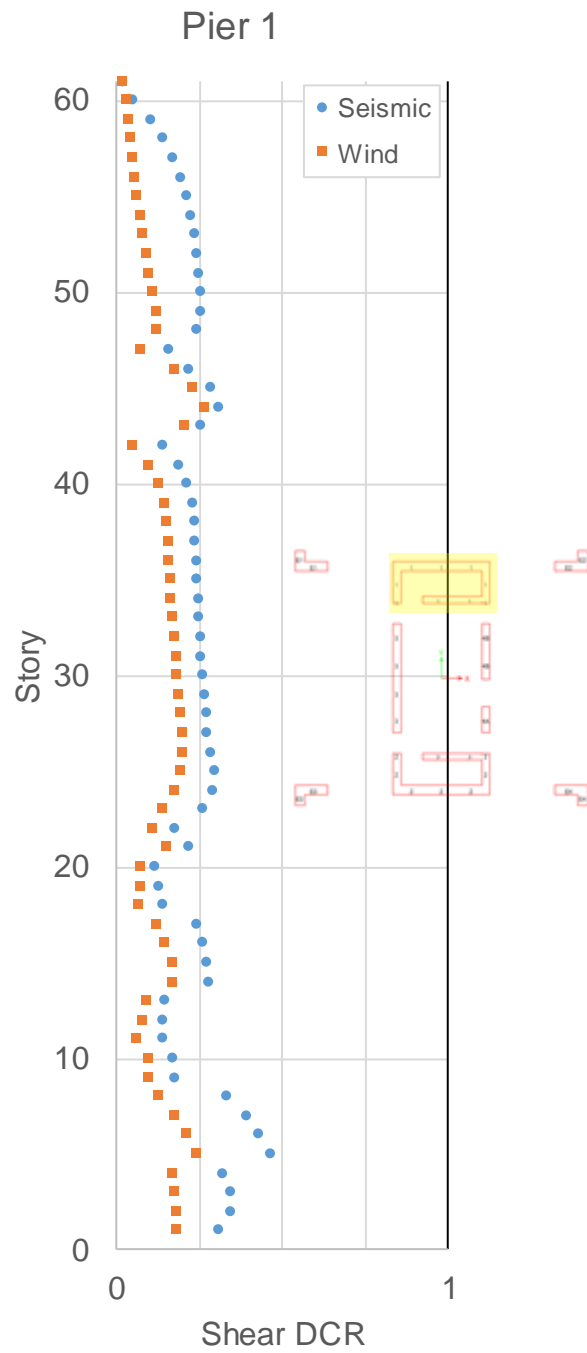
Concrete compressive strength	$f_c := 10\text{ksi}$	Column schedule, S3-2.01
Steel yield strength	$f_y := 75\text{ksi}$	Beam schedule, S3-2.71
Column dimensions	$b := 24\text{in}$	Beam schedule, S3-2.71
	$h := 34\text{in}$	Beam schedule, S3-2.71
	$d := 31.365\text{in}$	
Area of reinforcement (one side)	$A_s := 12 \cdot 1.27\text{in}^2 = 15.24\text{in}^2$	Beam schedule, S3-2.71
Flexural resistance factor	$\phi_b := 0.9$	
Depth of compression block	$a := \frac{A_s \cdot f_y}{0.85 \cdot f_c \cdot b} = 5.603\text{in}$	
Moment capacity	$\phi M_n := \phi_b \cdot A_s \cdot f_y \cdot \left(d - \frac{a}{2} \right)$	
	$\phi M_n = 2467\text{kip}\cdot\text{ft}$	

2.5 DCRs

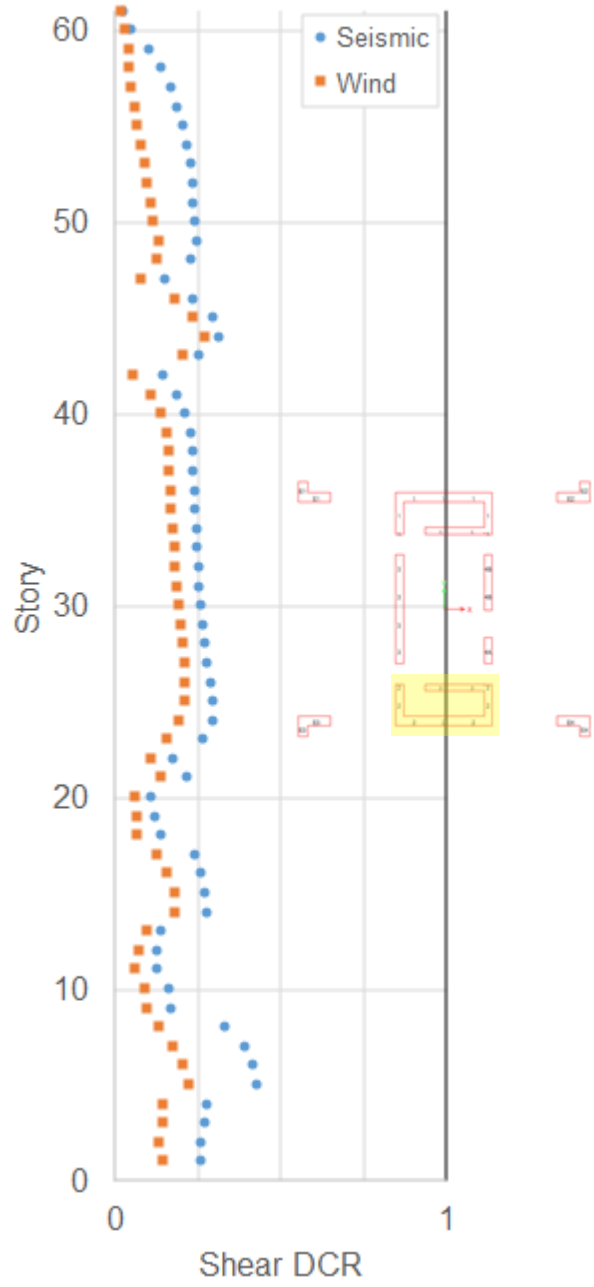
The following sections detail demand-to-capacity ratios for each structural element under controlling seismic and wind loading. All elements have DCR less than 1.0, indicating capacity greater than demand, except select outrigger coupling beams and moment frame beams. These exceedances are relatively small in magnitude and are limited to only a few elements. Overall, the structure remains in conformance with the code.

2.5.1 Shear Walls

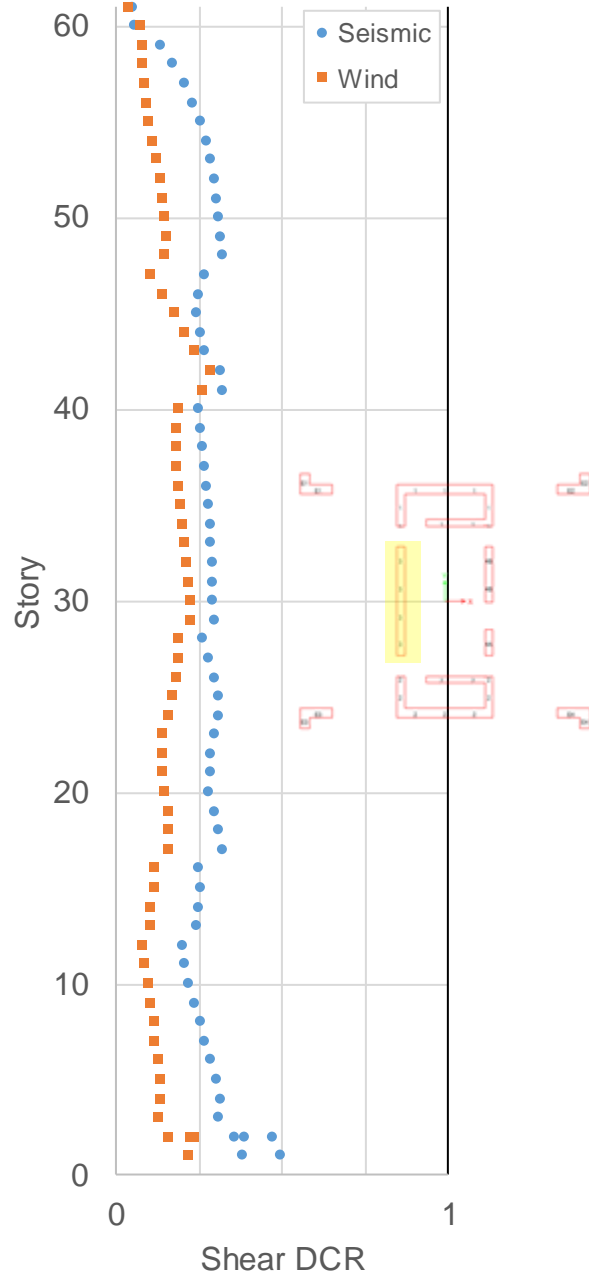
2.5.1.1 Wall In-Plane Shear



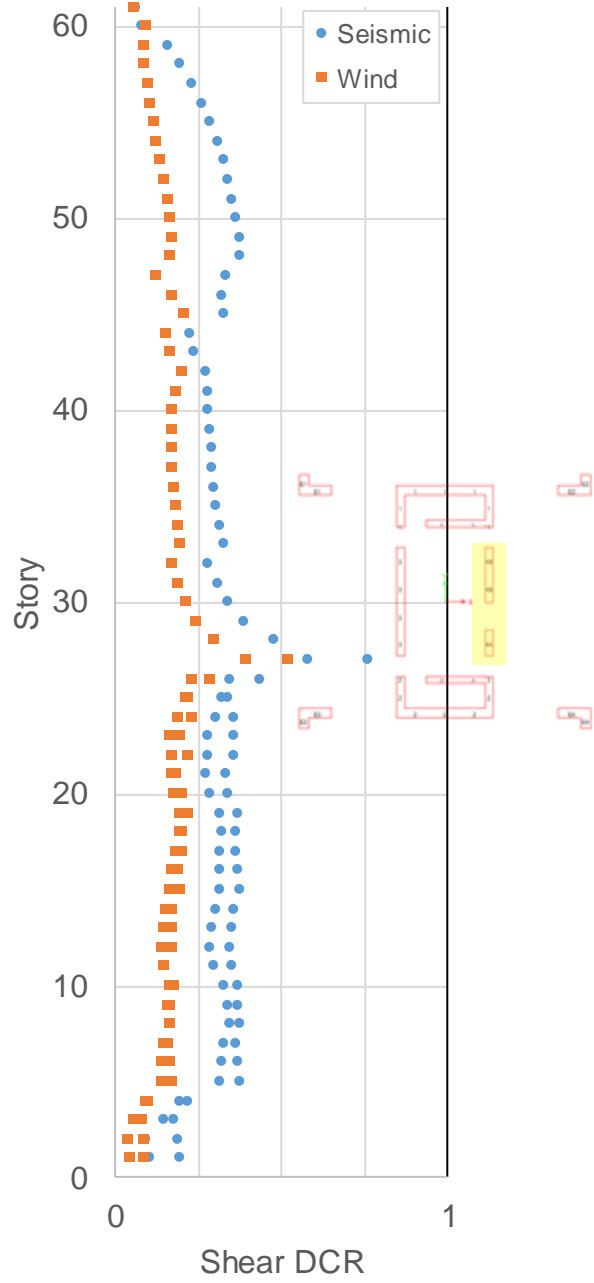
Pier 2



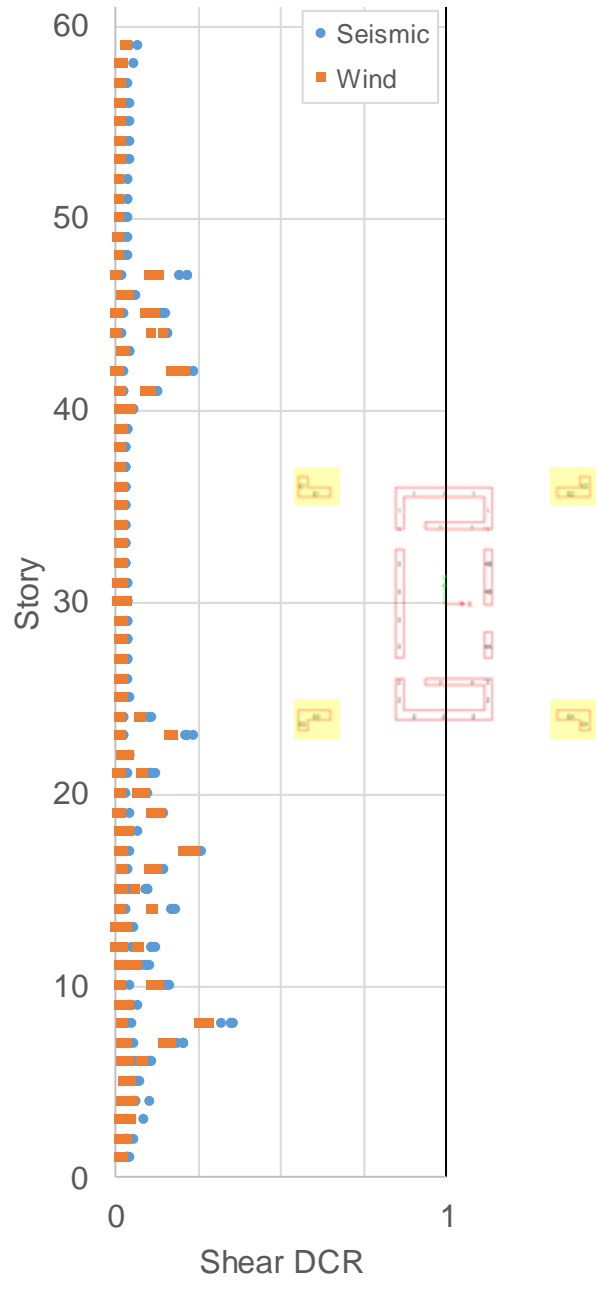
Pier 3



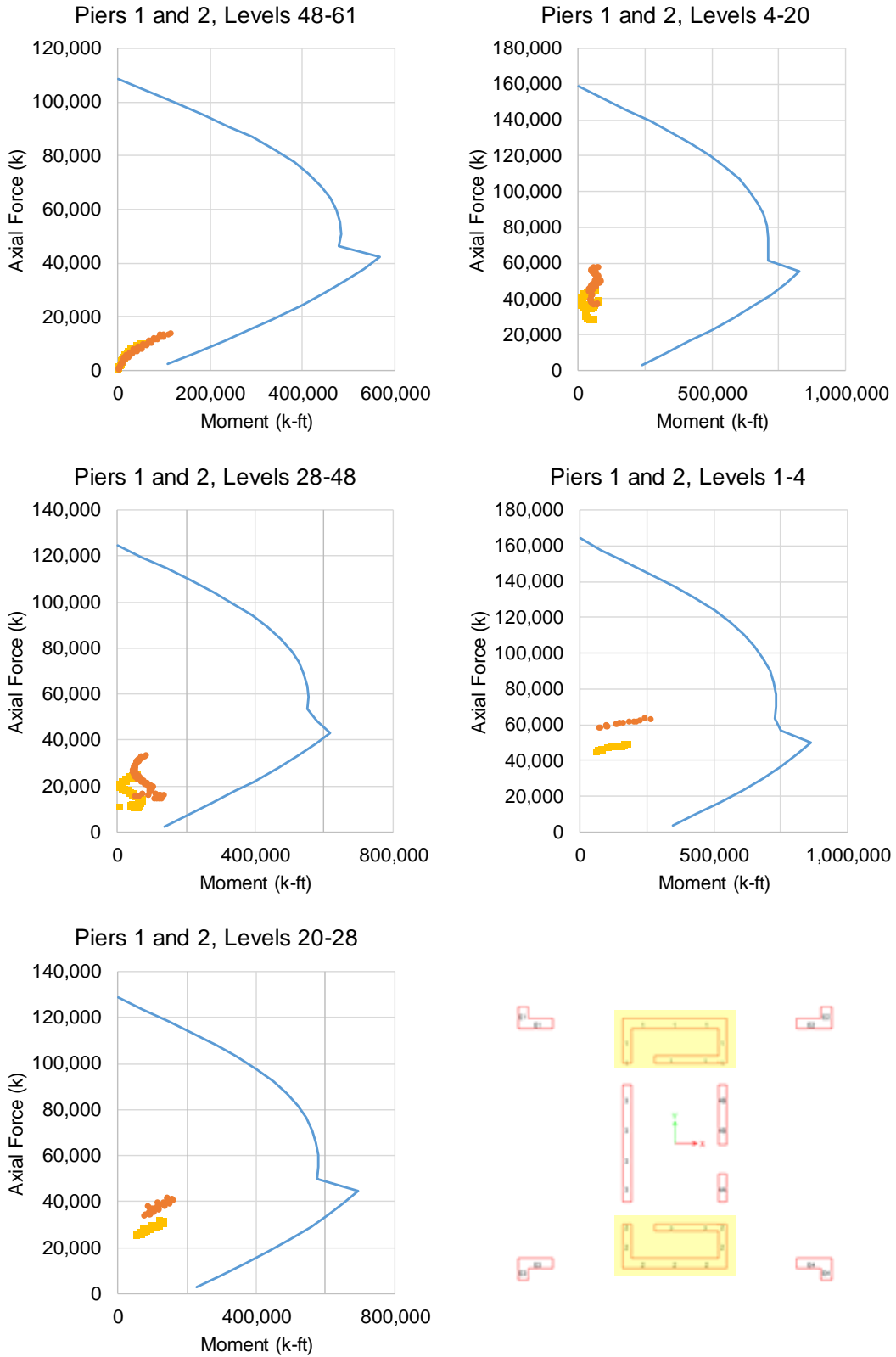
Pier 4

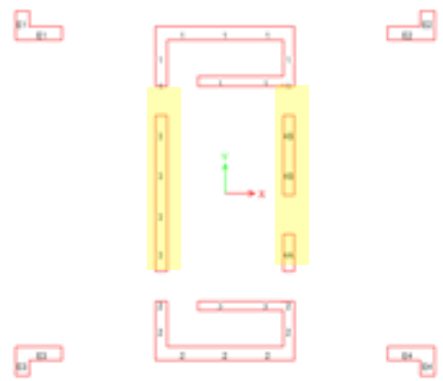
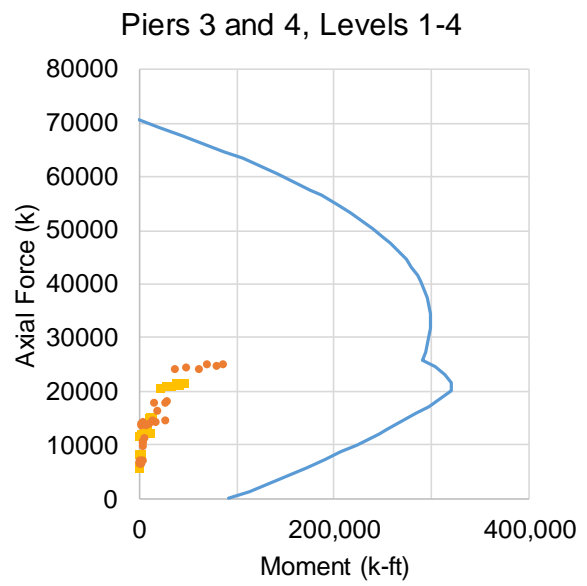
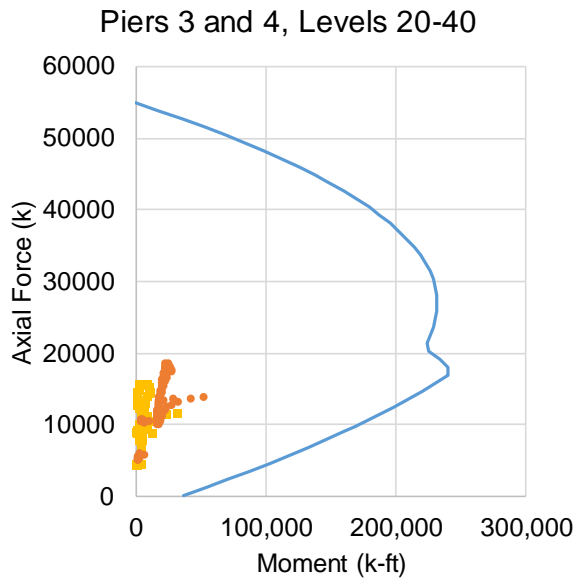
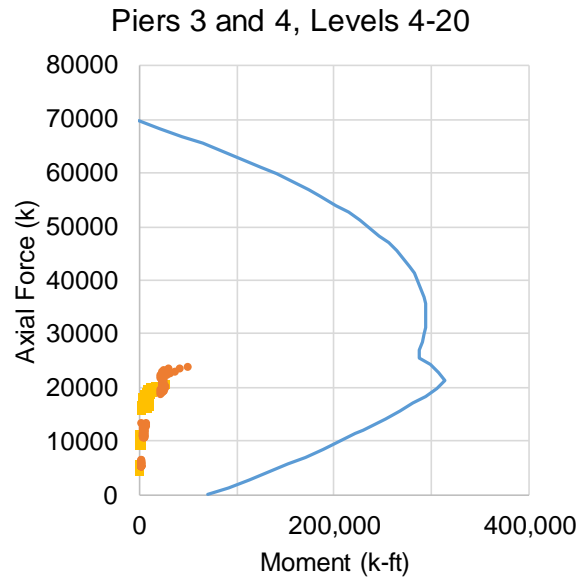
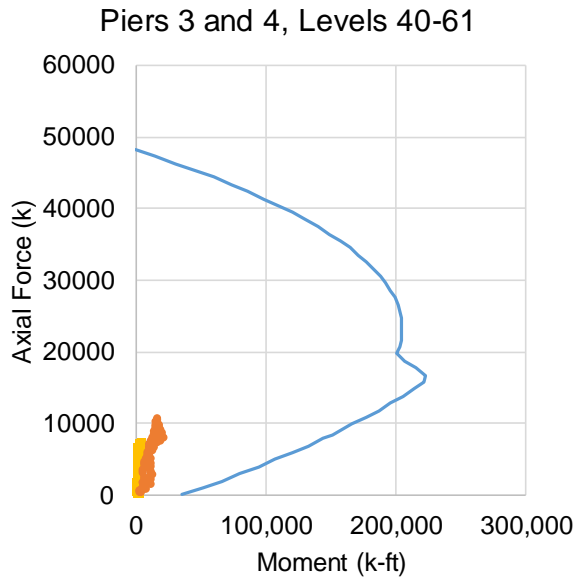


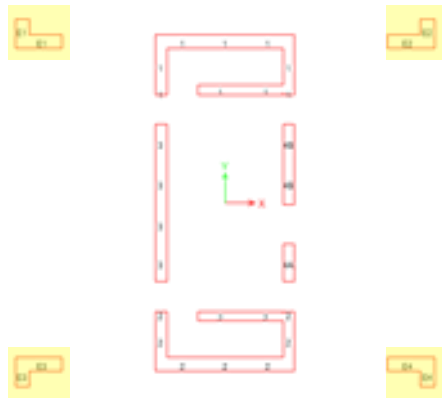
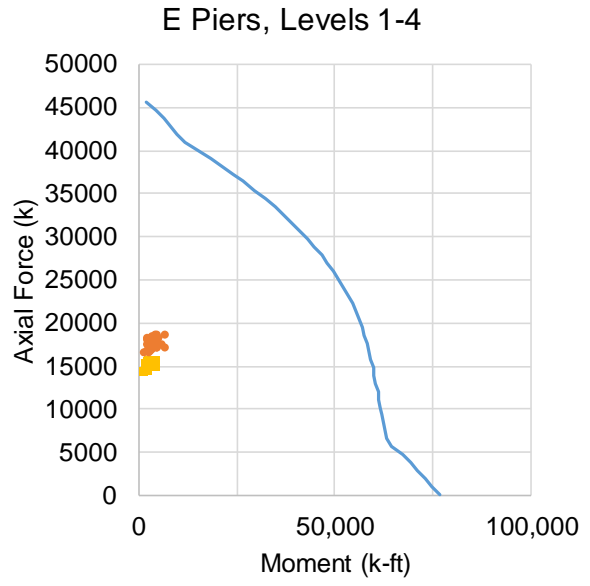
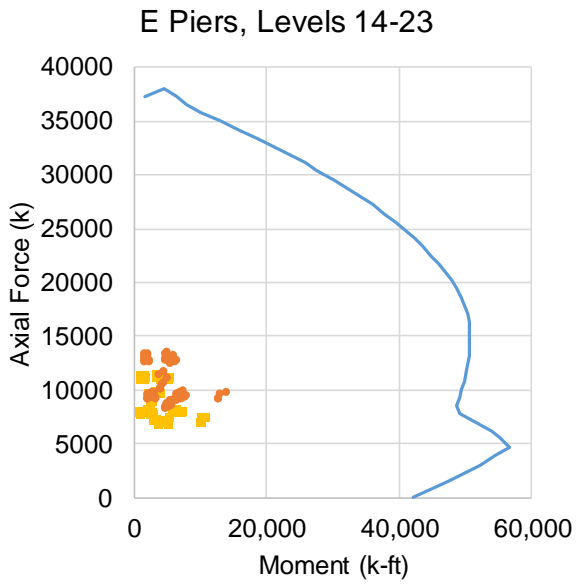
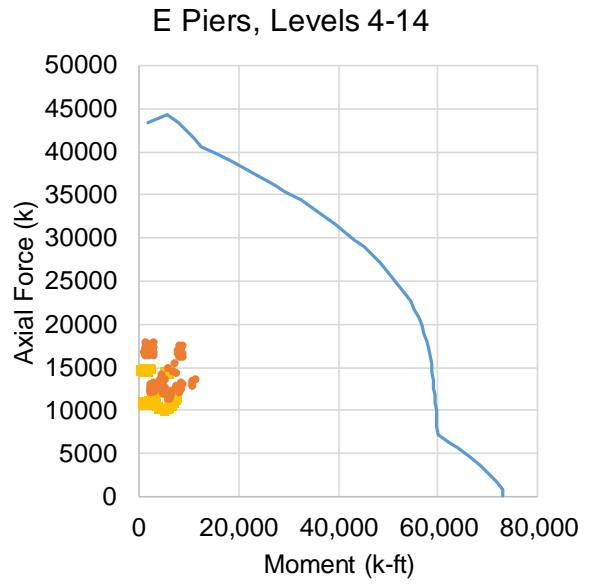
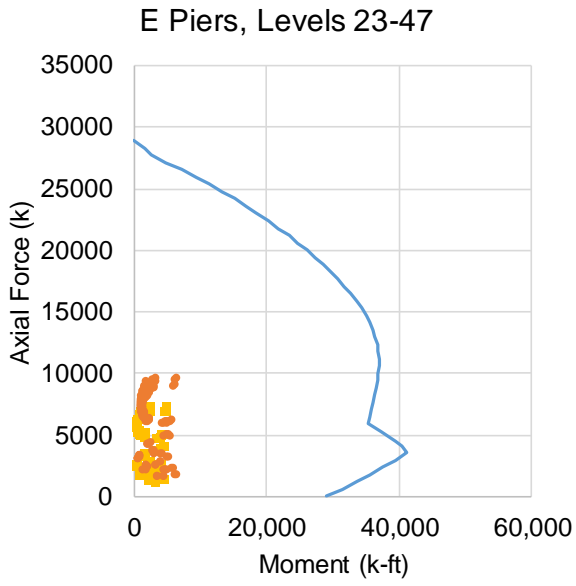
Pier E



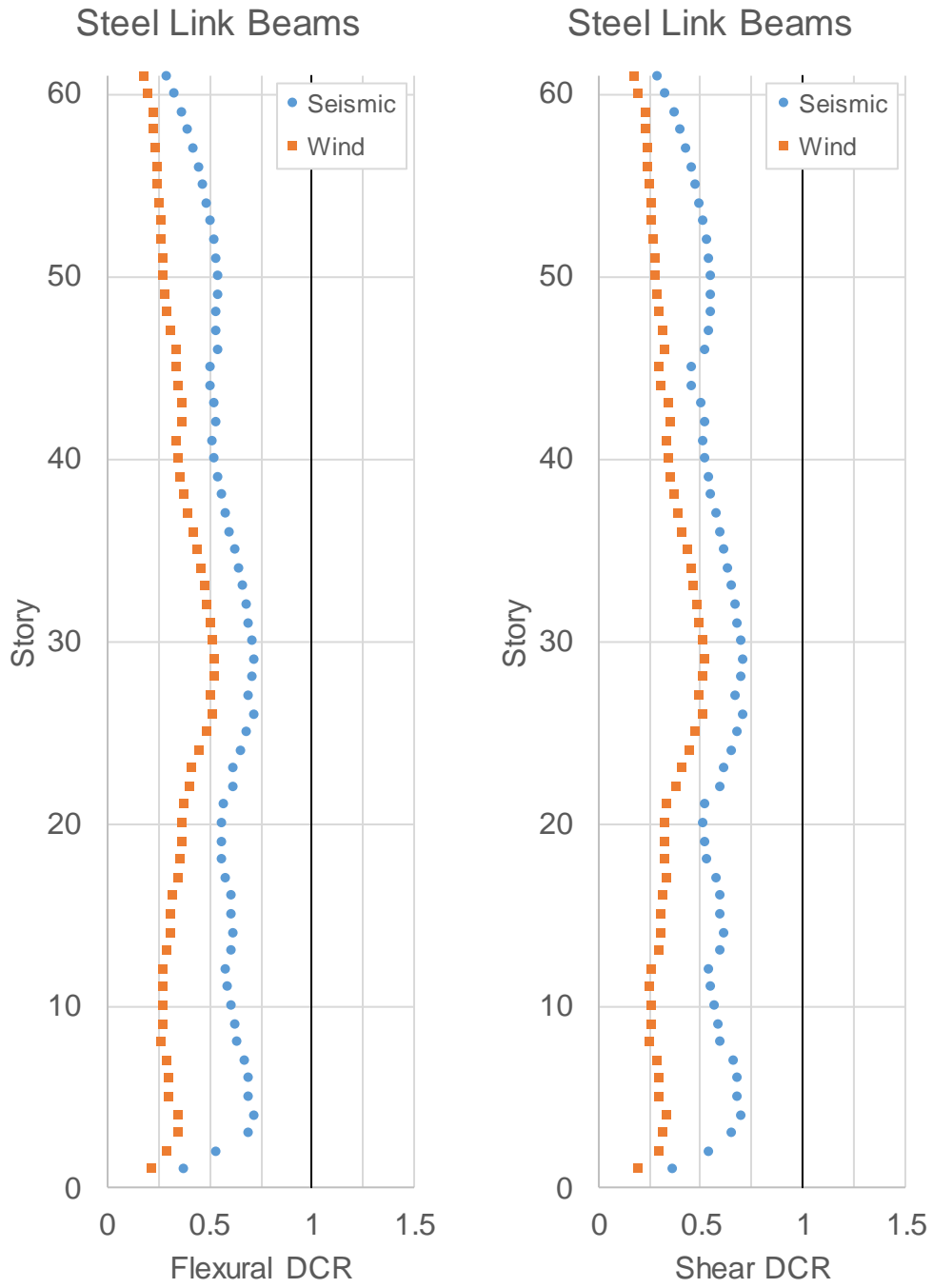
2.5.1.2 Wall Axial-Flexure Interaction (PM)







2.5.1.3 Steel Coupling Beams

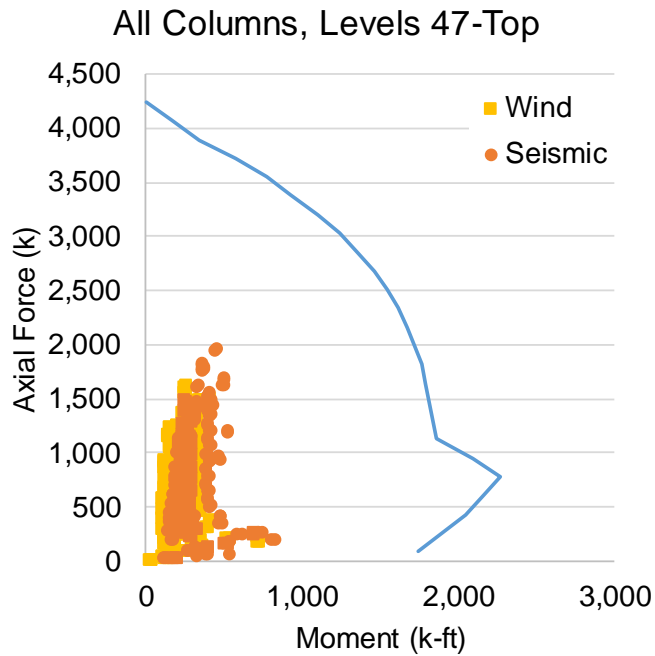


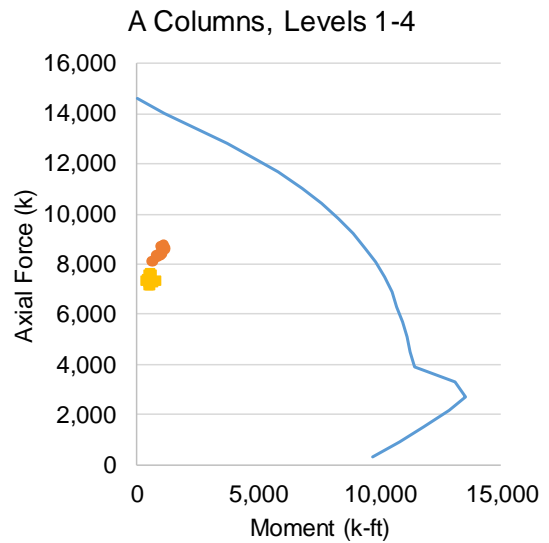
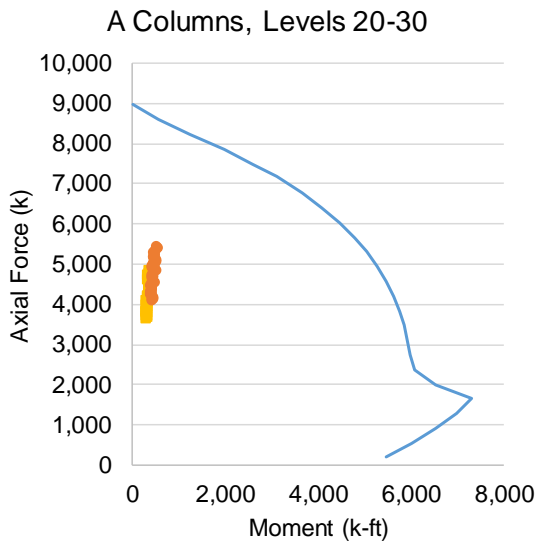
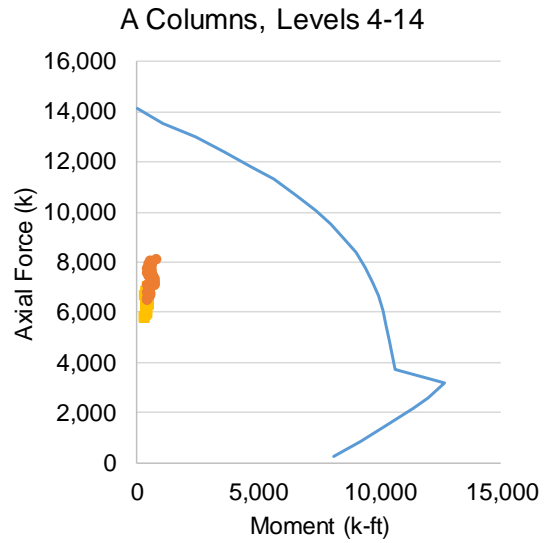
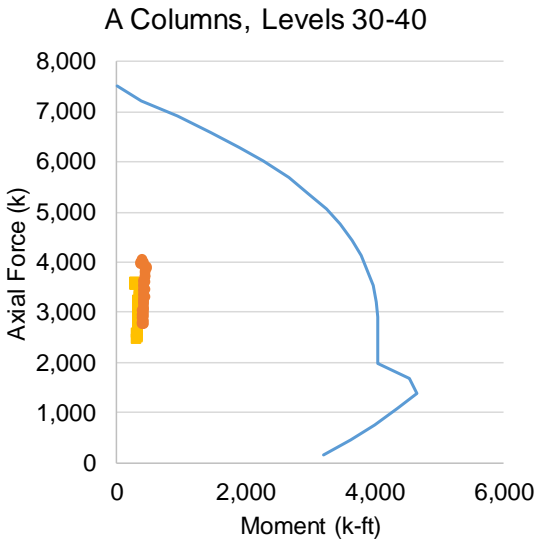
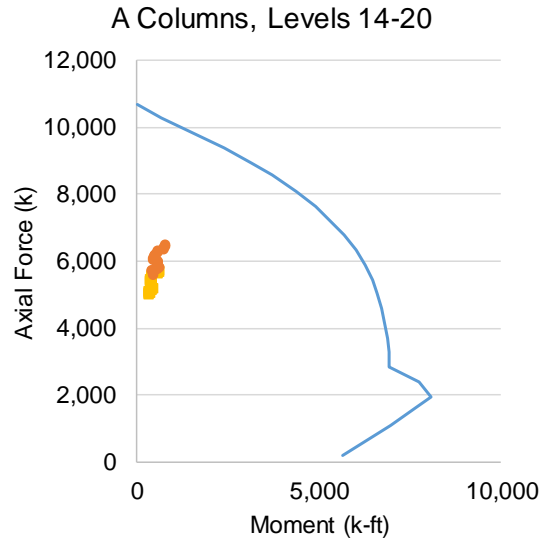
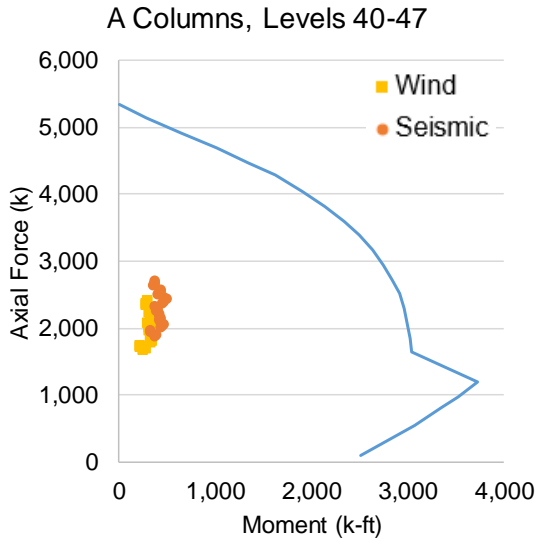
2.5.1.4 Outrigger Coupling Beams

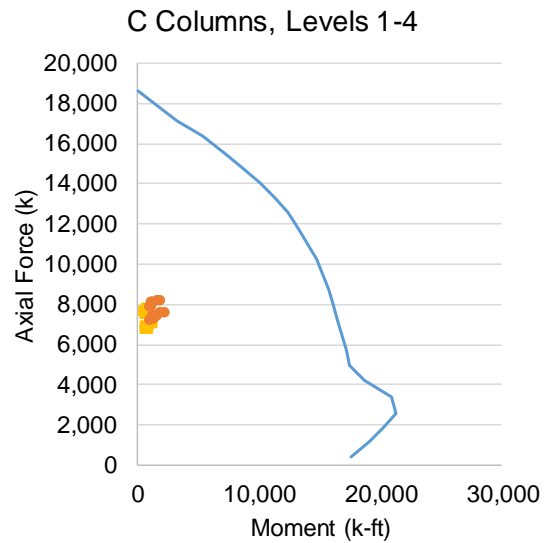
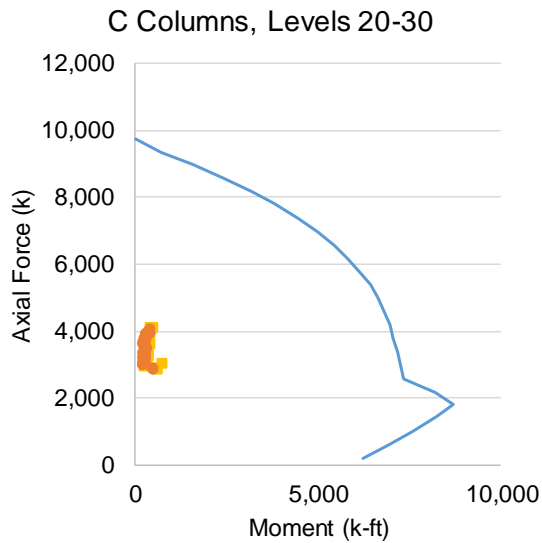
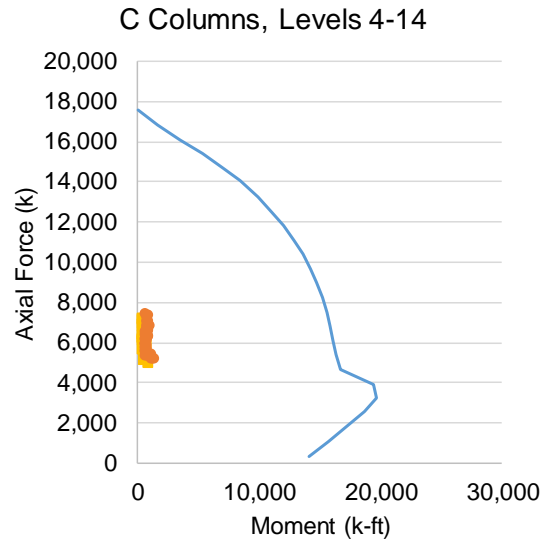
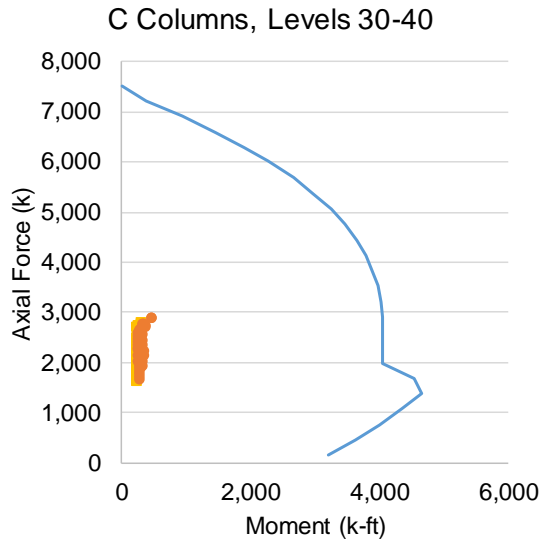
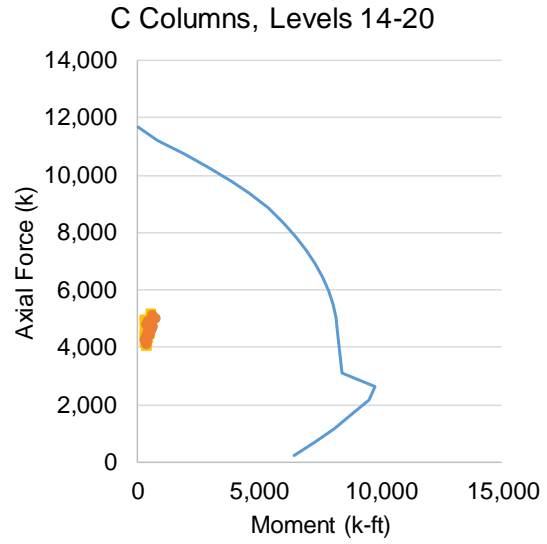
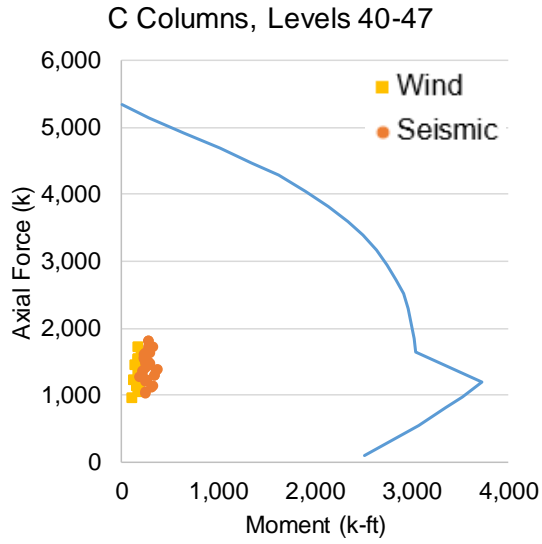
Story	Seismic				Wind			
	NW	NE	SW	SE	NW	NE	SW	SE
8	1.07	1.05	1.05	0.99	0.02	0.02	0.02	0.02
12	1.25	1.18	1.21	1.20	0.86	0.86	0.81	0.81
17	0.98	1.00	1.03	0.95	0.87	0.87	0.69	0.69
21	1.14	1.03	1.06	1.06	0.03	0.03	0.02	0.02
42	0.84	0.95	0.98	0.82	0.02	0.02	0.03	0.03
45	0.97	0.86	0.84	0.96	0.61	0.62	0.62	0.61

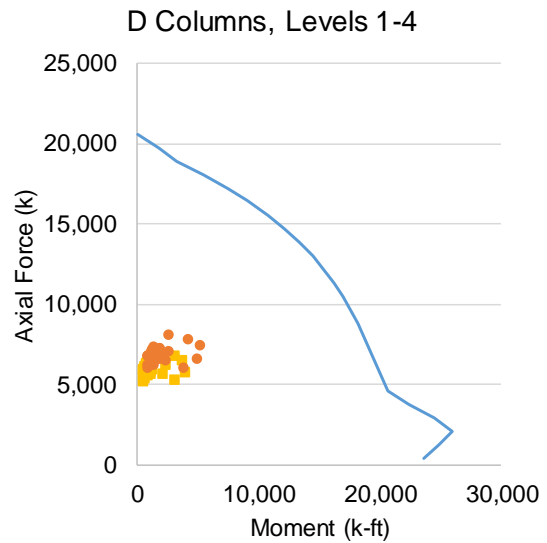
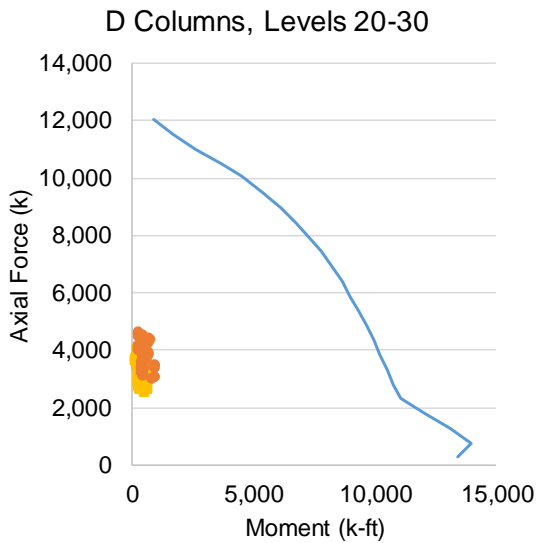
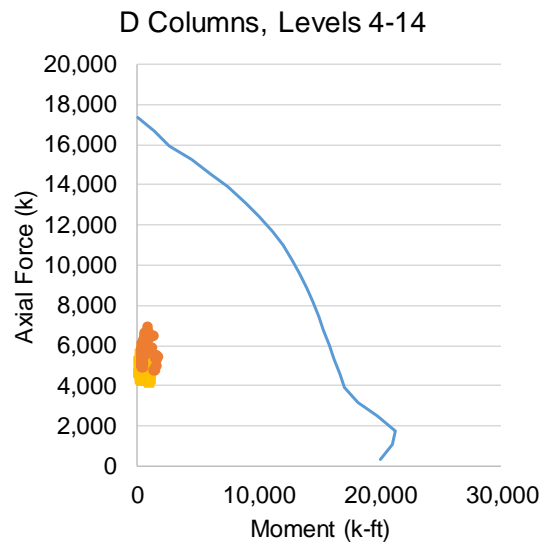
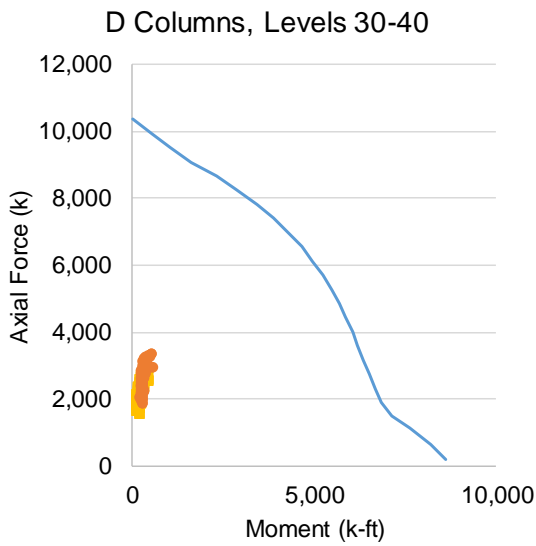
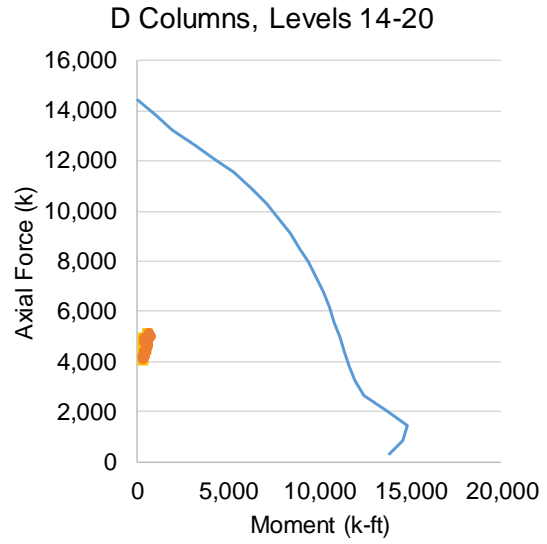
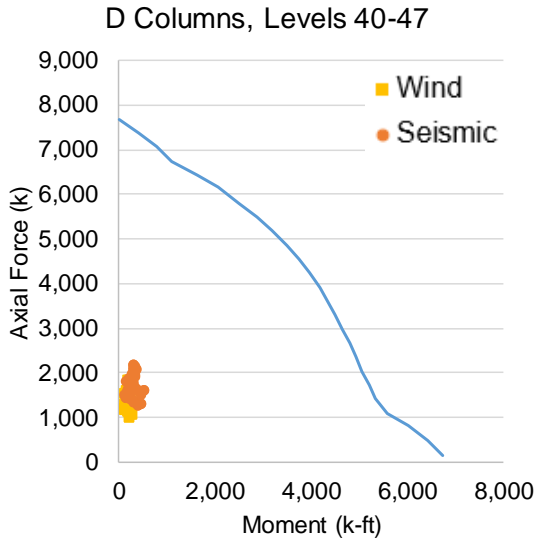
2.5.2 Moment Frames

2.5.2.1 Columns

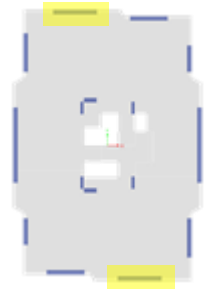
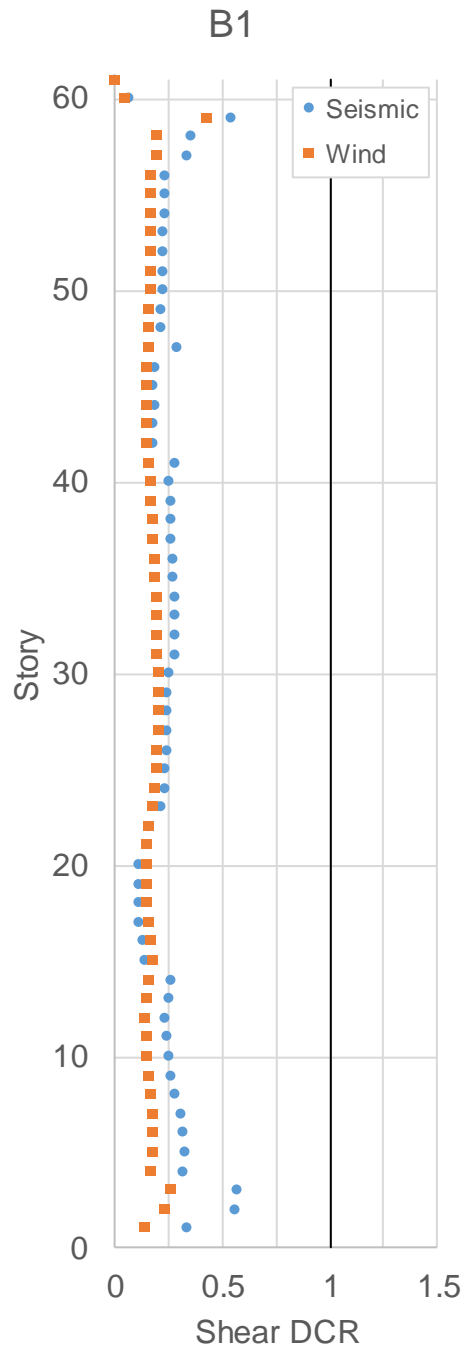
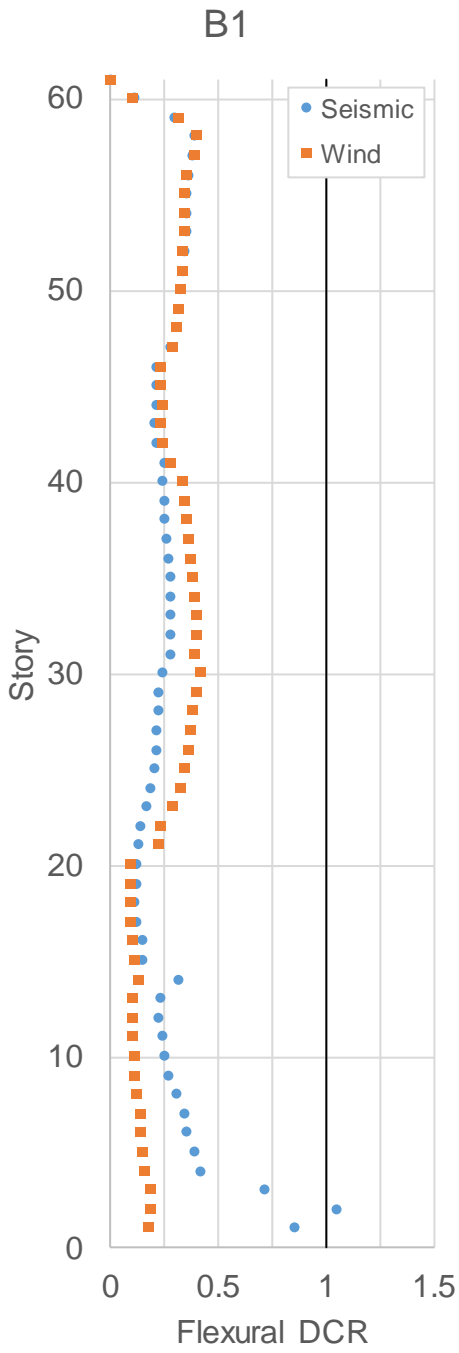


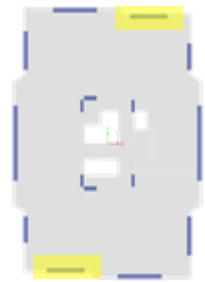
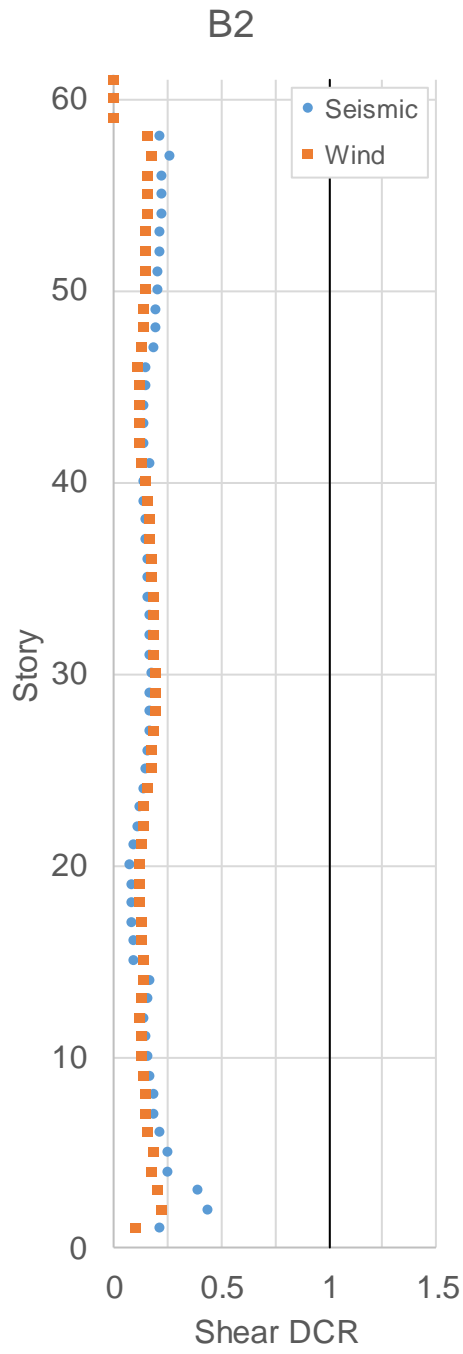
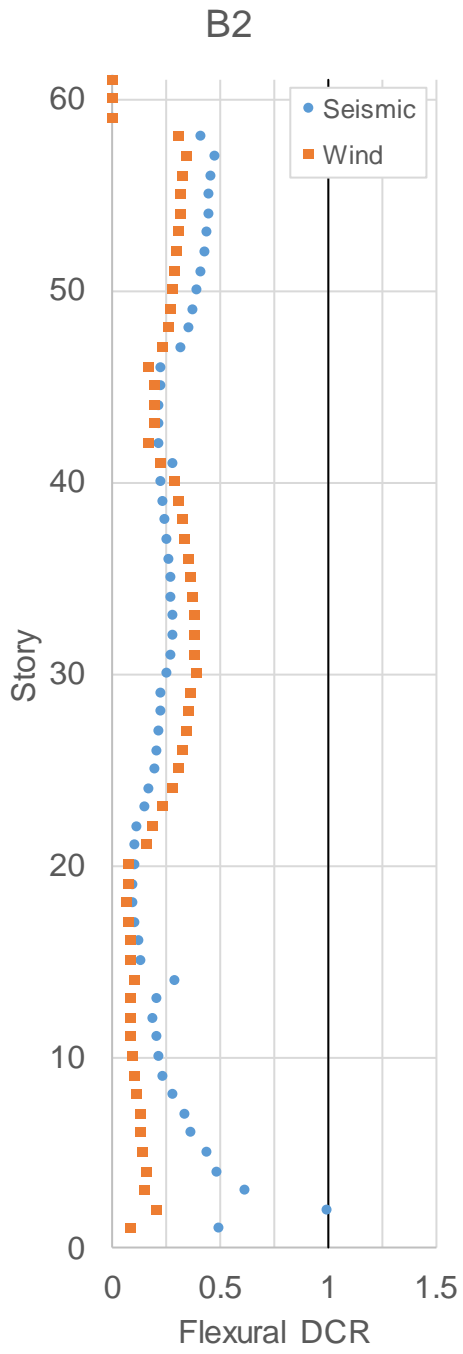


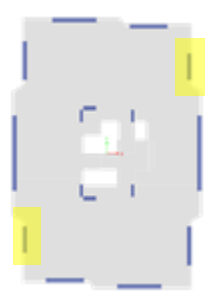
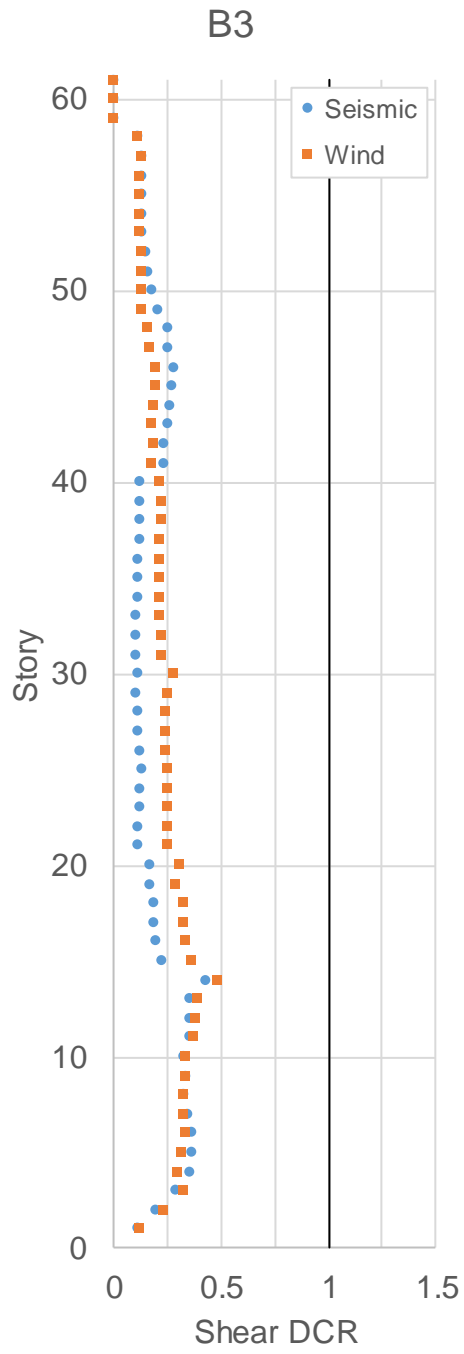
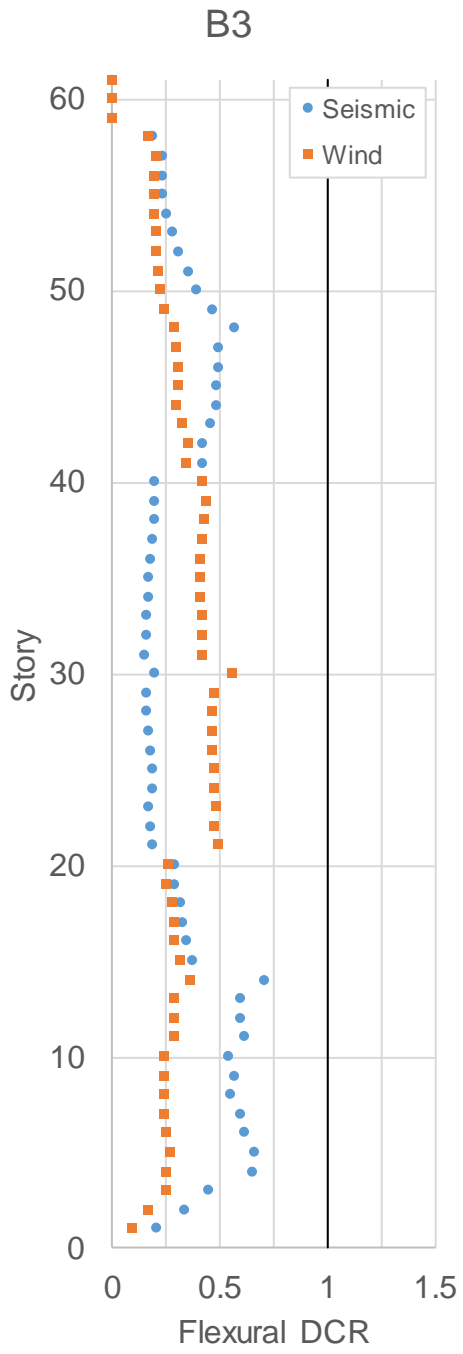


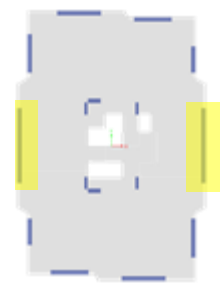
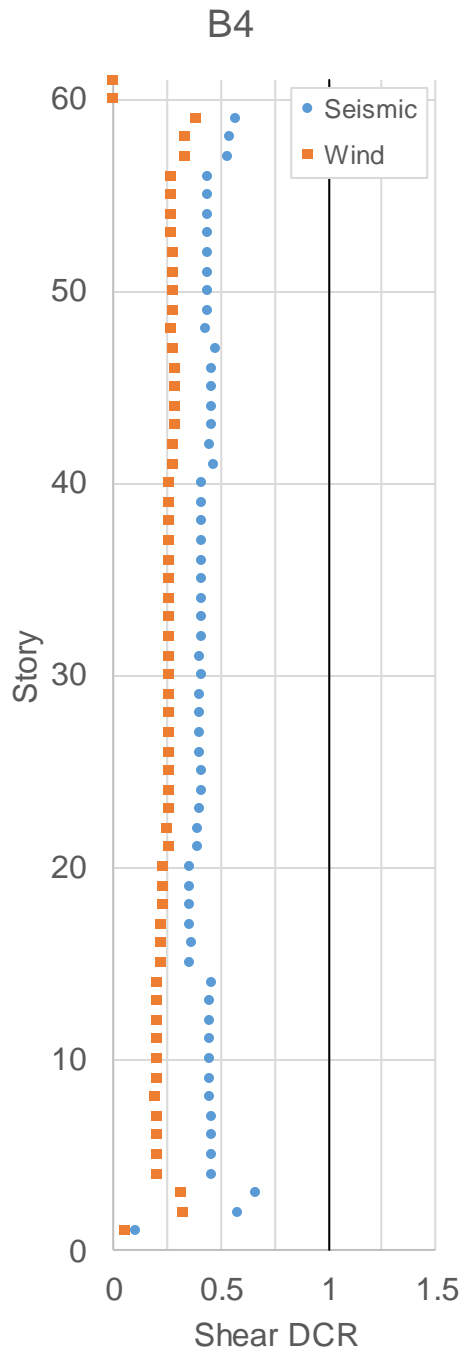
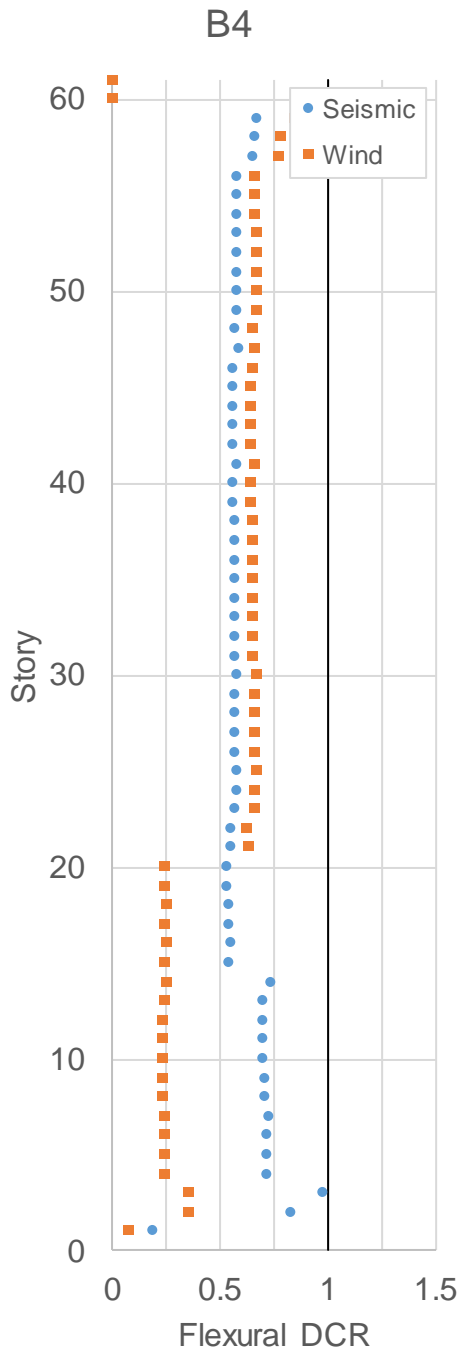


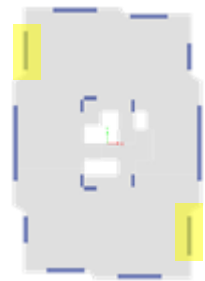
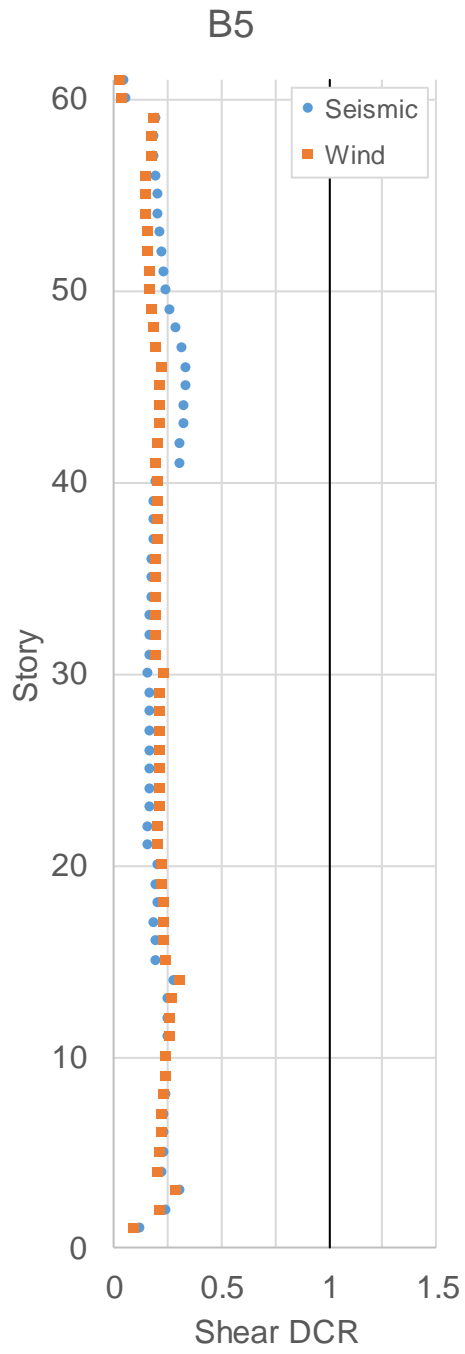
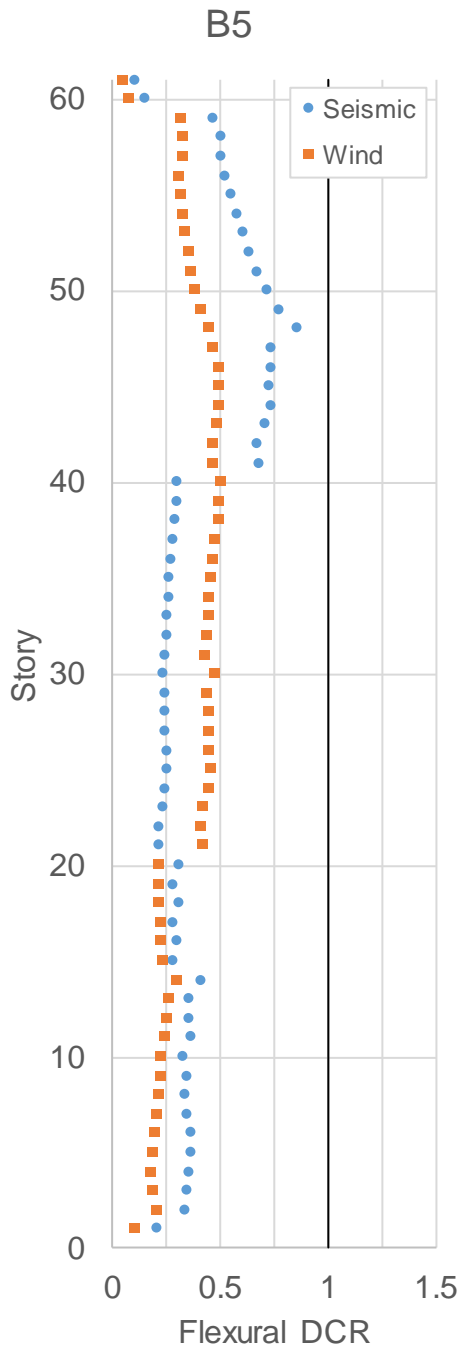
2.5.2.2 Beams











3. ANALYTICAL MODEL: XTRACT

3.1 Description and Screenshots

We used computer program XTRACT Version 3.0.7 to calculate pile cross section strength properties. We analyzed four existing pile cross sections at different depths. For each cross section, we developed a PM interaction curve and moment-curvature backbones for several axial loads.

3.1.1 Existing Pile Geometry

We determined the typical reinforcement of existing piles from review of the following documents:

1. Kie-Con Pile Drawing, Sheet No. 7 Revised (27 February 2006) shows eight prestressing strands, four #9 bars cast in the pile top, and four additional #9 bars grouted into the pile top all extending 5 ft into the tower mat foundation.
2. Webcor RFI -196 (19 April 2006) identifies that at least one pile, #608, had no exposed dowels or tendons at the pile top after installation.
3. Webcor RFI 196R1 (2 May 2006) indicates that Kie-Con proposed to chip out the top of pile and build it back to permit a total of eight #9 bars to extend into the pile cap for piles designated as tension piles.
4. Webcor RFI 212R1 (4 May 2006) identifies 66 tension piles located under the outrigger columns. The RFI also indicates a proposal to embed a total of four #9 dowels extending into the mat from typical piles and six #9 bars, plus the prestressing strands from tension piles.
5. Webcor RFI 238 (10 May 2006) confirms that pile dowels extend through the mat reinforcement.

We conservatively based our analysis of the existing piles on the reinforcing scheme of a typical as-built compression pile with only four #9 dowels extending into the mat. We conservatively neglected the increase in lateral pile capacity provided by the additional rebar and extension of prestressing tendons into the mat at the 66 tension piles identified by Webcor RFI 212R1.

We calculated the development length of the four #9 dowels following the provisions in ACI 318-14 Section 25.4.2. RFI 212R1 identifies the rebar as 60 ksi steel, and Kie-Con Pile Drawing, Sheet No 7 Revised specifies either ASTM A706 or ASTM A615 steel. We calculated existing pile properties for ASTM A615 Grade 60 material properties.

$$f_y := 68 \cdot \text{ksi} = 68 \text{ ksi}$$

$$\lambda := 1.0 \quad f'_c := 1.3 \cdot 7 \cdot \text{ksi} = 9.1 \text{ ksi}$$

$$\psi_t := 1.0$$

$$\psi_e := 1.0$$

$$\psi_s := 1.0$$

$$d_b := 1.128 \cdot \text{in} = 1.128 \text{ in} \quad n := 4$$

$$d_{\text{spiral}} := 0.374 \cdot \text{in}$$

$$\text{BarSpa} := \frac{\pi \cdot \left(10 \cdot \text{in} - d_{\text{spiral}} - \frac{d_b}{2} \right)}{n} = 7.117 \text{ in}$$

$$\text{BarCov} := 2 \cdot \text{in} + d_{\text{spiral}} + \frac{d_b}{2} = 2.938 \text{ in}$$

$$c_b := \min \left(\text{BarCov}, \frac{\text{BarSpa}}{2} \right) = 2.938 \text{ in}$$

$$A_{tr} := 2 \cdot \frac{\pi \cdot d_{\text{spiral}}^2}{4} = 0.22 \text{ in}^2$$

$$s := 2 \cdot \text{in}$$

$$K_{tr} := \frac{40 \cdot A_{tr}}{s \cdot n} = 1.099 \text{ in}$$

$$\frac{c_b + K_{tr}}{d_b} = 3.579$$

$$L_d := \frac{3}{40} \cdot \frac{f_y}{\lambda \cdot \sqrt{f'_c} \cdot \text{psi}} \cdot \frac{\psi_t \cdot \psi_e \cdot \psi_s}{\min \left(\frac{c_b + K_{tr}}{d_b}, 2.5 \right)} \cdot d_b = 24.1 \text{ in}$$

Table 25.4.2.4—Modification factors for development of deformed bars and deformed wires in tension

Modification factor	Condition	Value of factor
Lightweight λ	Lightweight concrete	0.75
	Lightweight concrete, where f_{cr} is specified	In accordance with 19.2.4.3
	Normalweight concrete	1.0
Epoxy ^[1] ψ_e	Epoxy-coated or zinc and epoxy dual-coated reinforcement with clear cover less than $3d_b$ or clear spacing less than $6d_b$	1.5
	Epoxy-coated or zinc and epoxy dual-coated reinforcement for all other conditions	1.2
	Uncoated or zinc-coated (galvanized) reinforcement	1.0
Size ψ_s	No. 7 and larger bars	1.0
	No. 6 and smaller bars and deformed wires	0.8
Casting position ^[1] ψ_t	More than 12 in. of fresh concrete placed below horizontal reinforcement	1.3
	Other	1.0

^[1]The product $\psi_e \psi_s$ need not exceed 1.7.

We calculated the development length for the eight prestressing strands following the provisions in ACI 318-14 Section 25.4.8. Kie-Con Pile Drawing, Sheet 7 Revised shows the strand area and prestress force after losses for the existing piles.

$d_b := 0.5 \text{ in}$	Nominal strand diameter
$A_{ps} := 8 \cdot 0.153 \text{ in}^2 = 1.224 \text{ in}^2$	Prestress steel area
$P_f := 188496 \text{ lbf}$	Prestress force after losses
$f_{se} := \frac{P_f}{A_{ps}} = 154 \text{ ksi}$	Effective prestress after losses
$f_{ps} := 270 \text{ ksi}$	
$l_{se} := \frac{f_{se}}{3000 \text{ psi}} \cdot d_b = 2.139 \text{ ft}$	
$l_{ps} := \left(\frac{f_{ps} - f_{se}}{1000 \text{ psi}} \right) \cdot d_b = 4.833 \text{ ft}$	
$l_d := l_{se} + l_{ps} = 6.972 \text{ ft}$	

Figure 3-1 summarizes the cutoff lengths listed in Treadwell & Rollo's Summary of Pile Driving letter dated 2 May 2006. For our analyses we used the average pile cutoff length of 3.1 ft.

Figure 3-2 shows the existing pile elevation and indicates the regions of different cross sections we analyzed. We determined the extents of these sections considering the development lengths of reinforcing bars and prestressing tendons and the average pile cutoff length of 3.1 feet. Figure 3-3 shows the configuration of reinforcement in each pile section.

The existing piles have a 14-1/4 in. square cross section with chamfered corners. Circular spiral reinforcement confines a 10 in. diameter core. We judged the unconfined corners of the cross section are likely to spall under cyclic loading. We therefore analyzed the existing piles as a 14 in. diameter effective circular cross section.

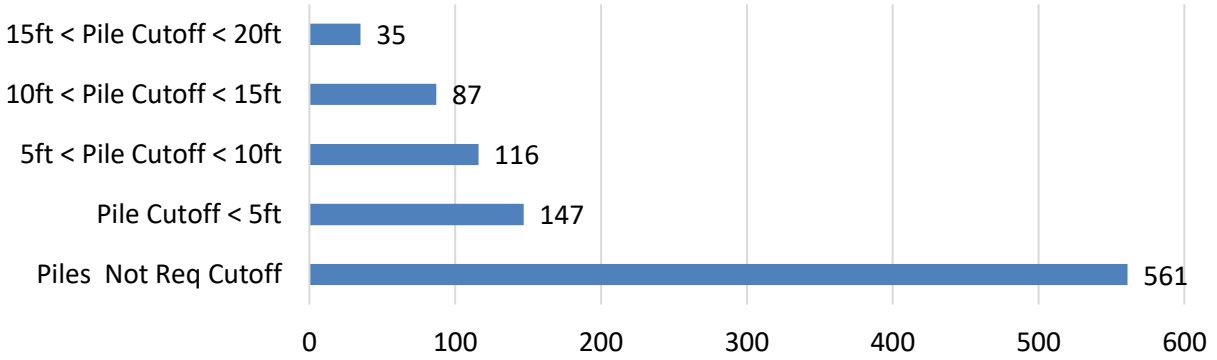


Figure 3-1 –Existing Pile Cutoffs

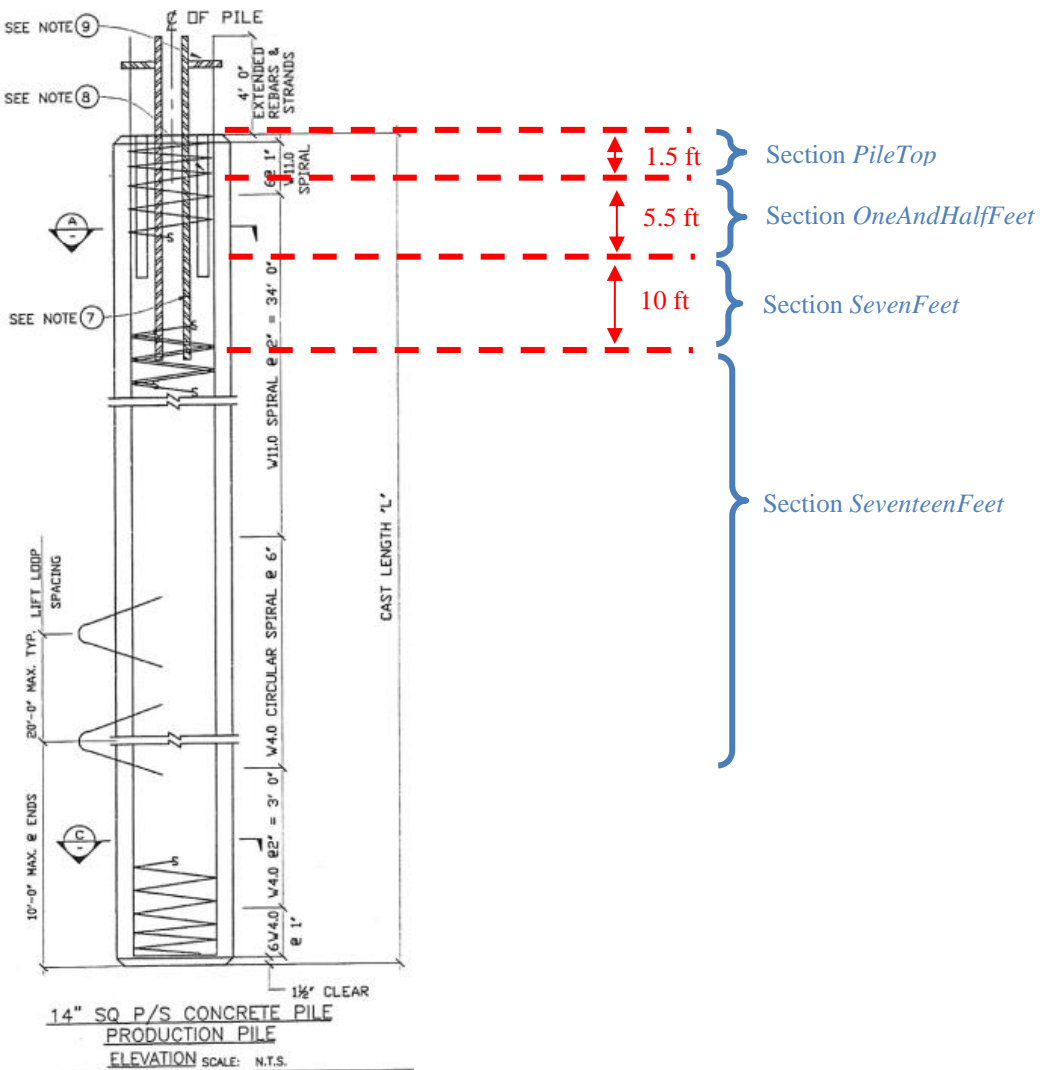
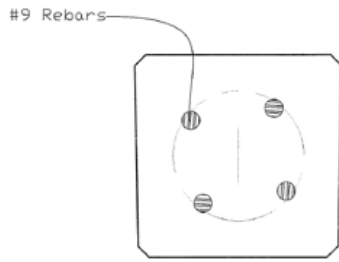
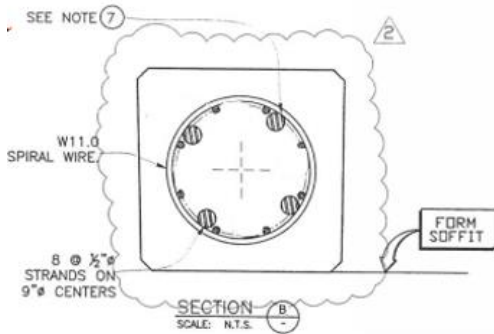


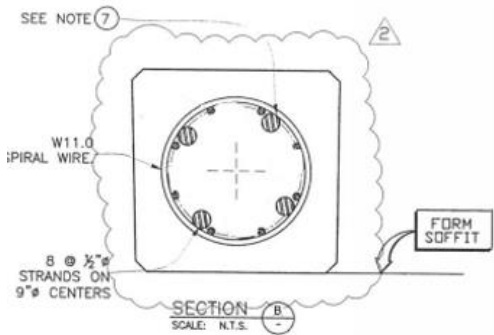
Figure 3-2 – Existing Pile Elevation



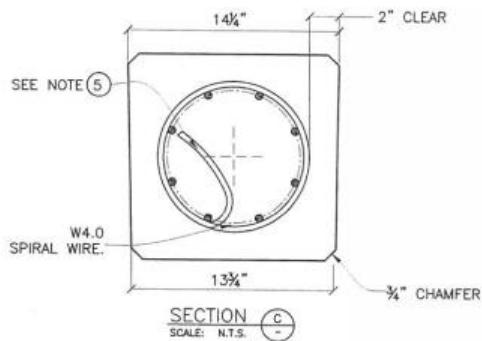
From Pile Top to 1.5 ft
 Four cast-in dowels (ASTM A615 Gr. 60)
 XTRACT Section *PileTop*
 SAP2000 Hinge Property *at top*



From 1.5 ft to 7 ft
 Four cast-in dowels (ASTM A615 Gr. 60)
 Eight strands prestressed to 108 ksi (Grade 270)
 XTRACT Section *OneAndHalfFeet*
 SAP2000 Hinge Property *at 1.5ft*



From 7 ft to 17ft 8in.
 Four cast-in dowels (ASTM A615 Gr. 60)
 Eight strands prestressed to 154 ksi (Grade 270)
 XTRACT Section *SevenFeet*
 SAP2000 Hinge Property *at 7.0 ft*



At 17ft 8in. and Below
 Eight strands prestressed to 154 ksi (Grade 270)
 XTRACT Section *SeventeenFeet*
 SAP2000 Hinge Property *at 17.67 ft*

Figure 3-3 – Existing Prestressed Precast Concrete Pile Sections

3.1.2 Existing Pile Concrete Material Properties

The existing piles were cast from concrete with a minimum specified 28-day compressive strength of 7,000 psi. We calculated existing pile capacities using an expected concrete compressive strength of $1.3 \times 7,000 \text{ psi} = 9,100 \text{ psi}$, following the recommendation of the PEER *Guidelines for Performance-Based Design of Tall Buildings* v2.03 Table 4-2. We neglected tensile concrete strength in our analyses.

We used two concrete material property definitions to model all existing pile cross sections. We assigned material property *Unconfined1* to the outer 2 in. of concrete and material property *Confined 2* to the inner 10 in. diameter core. We assigned the stress-strain relationships shown in Figure 3-4 and Figure 3-5 to material properties *Confined2* and *Unconfined1*, respectively. We calculated the material strength properties based on the material models developed by Mander et al (*Journal of Structural Engineering*, Vol 114, No. 8, August 1988) for reinforced concrete. We calculated ultimate confined concrete strain (corresponding to first hoop fracture) from the recommendations of Moehle (*Seismic Design of Reinforced Concrete Buildings*, 2015).

Concrete Material Strength Backbones	
$f'.c := 1.3 \cdot 7000 \text{ psi} = (9.1 \cdot 10^3) \text{ psi}$	Expected concrete compressive capacity
$E.c := 57000 \cdot \sqrt{\frac{f'.c}{\text{psi}}} \cdot \text{psi} = (5.437 \cdot 10^3) \text{ ksi}$	Concrete elastic modulus
Kie-Con Pile Drawing Sheet 7 indicates spiral reinforcement with ASTM A82 W11 wire spaced at 2 in. on center in the top 34 ft of the existing piles. The Kie-Con shop drawing submittal indicates welded wire reinforcement is grade 70. ASCE/SEI 41-17 Table 9-3 recommends an expected yield strength factor of 1.10 for steel materials not specifically listed in the table.	
$f_{y.s} := 1.1 \cdot 70 \text{ ksi} = 77 \text{ ksi}$	Grade 70 welded wire expected yield strength
$E.s := 29000 \text{ ksi}$	Steel elastic modulus
$cover := 2 \text{ in}$	Spiral clear cover
$D.o := 14 \text{ in}$	Pile outer dimension
$d.w := 0.374 \text{ in}$	W11 wire diameter

$A.w := 0.11 \text{ in}^2$	W11 wire area
$A.long := 4 \cdot 1 \text{ in}^2 = 4 \text{ in}^2$	Longitudinal rebar area (4 x #9 bars)
$D.s := D.o - 2 \cdot cover - d.w = 9.626 \text{ in}$	Centerline spiral diameter
$D.c := D.s - d.w = 9.252 \text{ in}$	Confined core diameter
$A.core := \frac{\pi}{4} \cdot D.c^2 = 67.23 \text{ in}^2$	Confined concrete area
$\rho.cc := \frac{A.long}{A.core} = 0.059$	Longitudinal reinforcement ratio to confined concrete area
$s := 2 \text{ in}$	Spiral reinforcement spacing
$s' := s - d.w = 1.626 \text{ in}$	Clear spacing between spiral bars

$\rho.s := \frac{\pi \cdot D.s \cdot A.w}{\frac{\pi}{4} \cdot D.c^2 \cdot s} = 0.025$	Transverse reinforcement to core concrete volumetric ratio
---	--

Mander et al [11] tested concrete specimens up to a maximum transverse reinforcement ratio of 0.025. The Mander model for confined concrete strength is therefore applicable to the existing piles.

$k.e := 1 - \frac{s'}{2 \cdot D.s} = 0.91$	Effective confinement factor (Mander Eq. 15)
--	--

Moehle [11] suggests limiting the ultimate strength of transverse reinforcement as follows.

$f.s.limit := E.s \cdot \left(0.0025 + 0.04 \cdot \sqrt[3]{\frac{k.e \cdot \rho.s}{\frac{f.c}{psi}}} \right) = 88.19 \text{ ksi}$	
--	--

$f.s := \min(fy.s, f.s.limit) = 77 \text{ ksi}$	
---	--

$f.2e := k.e \cdot \frac{\rho.s \cdot f.s}{2} = 0.867 \text{ ksi}$	Effective confining stress (Mander Eq. 19)
--	--

$f'.cc := f'.c \cdot \left(-1.254 + 2.254 \cdot \sqrt{1 + \frac{7.94 \cdot f.2e}{f'.c}} - 2 \cdot \frac{f.2e}{f'.c} \right) = 14.039 \text{ ksi}$	(Mander Eq. 29)
--	-----------------

Mander [10] suggests an unconfined concrete strain at peak stress of 0.002.

$$\varepsilon.o := 0.002$$

$$\varepsilon.cc := \varepsilon.o \cdot \left(1 + 5 \cdot \left(\frac{f'.cc}{f'.c} - 1 \right) \right) = 0.007$$

Unconfined concrete strain at peak stress

Confined concrete strain at peak stress
(Mander Eq. 5)

Moehle [11] suggests two expressions for concrete strain at first rupture of transverse reinforcement. We elect to use the more conservative of the two.

$$\varepsilon.cu := 0.004 + \frac{f.2e}{4 \cdot f'.c} = 0.028$$

Confined concrete strain at first spiral wire fracture (Moehle Eqs. 4.17 and 4.18)

$$\varepsilon.cu := 0.004 + 0.075 \cdot \frac{\rho.s \cdot f.s}{f'.c} = 0.02$$

Confined Concrete Stress-Strain Relationship

$$E.sec := \frac{f'.cc}{\varepsilon.cc} = (1.89 \cdot 10^3) \text{ ksi}$$

$$r := \frac{E.c}{E.c - E.sec} = 1.533$$

$$f.con(\varepsilon.c) := \frac{f'.cc \cdot \frac{\varepsilon.c}{\varepsilon.cc} \cdot r}{r - 1 + \left(\frac{\varepsilon.c}{\varepsilon.cc} \right)^r}$$

$$\varepsilon := 0, 0.0001 \dots \varepsilon.cu$$

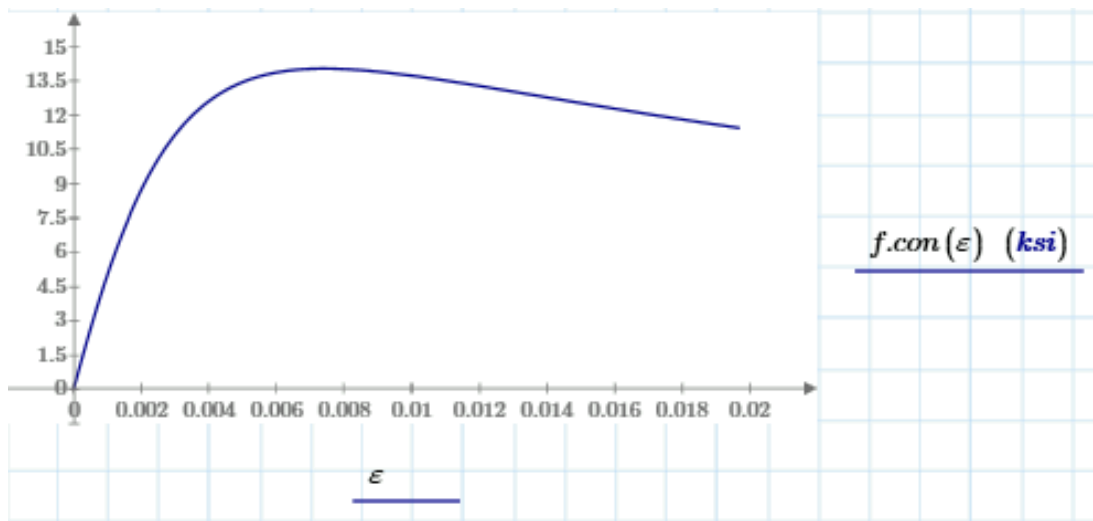


Figure 3-4 – Material Property *Confined2*

Unconfined Concrete Stress-Strain Relationship

$$\epsilon.sp := 0.005$$

Unconfined concrete spalling strain

$$E.sec := \frac{f'.c}{\epsilon.o} = (4.55 \cdot 10^3) \text{ ksi}$$

$$r := \frac{E.c}{E.c - E.sec} = 6.127$$

$$f.unc1(\epsilon.c) := \frac{f'.c \cdot \frac{\epsilon.c}{\epsilon.o} \cdot r}{r - 1 + \left(\frac{\epsilon.c}{\epsilon.o}\right)^r}$$

$$f.unc2(\epsilon.c) := \frac{2 \cdot f'.c \cdot r}{r - 1 + 2^r} \cdot \left(\frac{\epsilon.sp - \epsilon.c}{\epsilon.sp - 2 \epsilon.o}\right)$$

$$Unconfined(\epsilon.c) := \text{if}(\epsilon.c < 2 \epsilon.o, f.unc1(\epsilon.c), f.unc2(\epsilon.c)) \quad \epsilon := 0, 0.0001 \dots \epsilon.sp$$

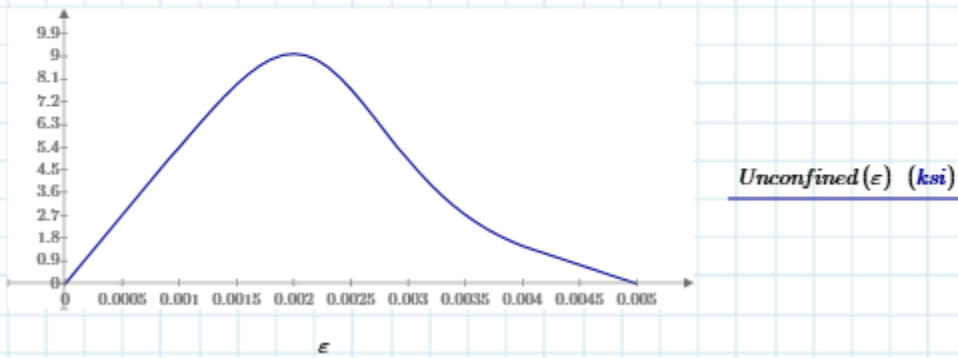


Figure 3-5 – Material Property *Unconfined1*

3.1.3 Existing Pile Steel Material Properties

We used material property *Dowels* to model ASTM A615 Grade 60 rebar with the parabolic strain hardening material model recommended in AASHTO *Guide Specifications for LRF Seismic Bridge Design*, Figure 8.4.2.1. We used the expected material properties listed in AASHTO Table 8.4.2.1.

$f_{ye} := 68 \text{ ksi}$	Expected yield stress
$f_{ue} := 95 \text{ ksi}$	Expected tensile strength
$\epsilon_{ye} := 0.0023$	Expected yield strain
$\epsilon_{sh} := 0.0125$	Onset of strain hardening
$\epsilon_{suR} := 0.06$	Reduced ultimate tensile strain
$\epsilon_{su} := 0.09$	Ultimate tensile strain
$f_{lin}(\epsilon) := \epsilon \cdot \frac{f_{ye}}{\epsilon_{ye}}$	
$q := \epsilon_{suR} - \epsilon_{sh} = 0.048$	
$m(\epsilon) := \frac{\frac{f_{ue}}{f_{ye}} \cdot (30 \cdot q + 1)^2 - 60 \cdot q - 1}{15 \cdot q^2}$	
$f_s(\epsilon) := f_{ye} \cdot \left(\frac{m(\epsilon) \cdot (\epsilon - \epsilon_{sh}) + 2}{60 \cdot (\epsilon - \epsilon_{sh}) + 2} + \frac{(60 - m(\epsilon)) \cdot (\epsilon - \epsilon_{sh})}{2 \cdot (30 \cdot q + 1)^2} \right)$	
$f_{AASHTO}(\epsilon) := \text{if}(\epsilon < \epsilon_{ye}, f_{lin}(\epsilon), \text{if}(\epsilon < \epsilon_{sh}, f_{ye}, \text{if}(\epsilon < \epsilon_{suR}, f_s(\epsilon), f_{ue})))$	

Figure 3-6 shows the material model for the steel dowels.

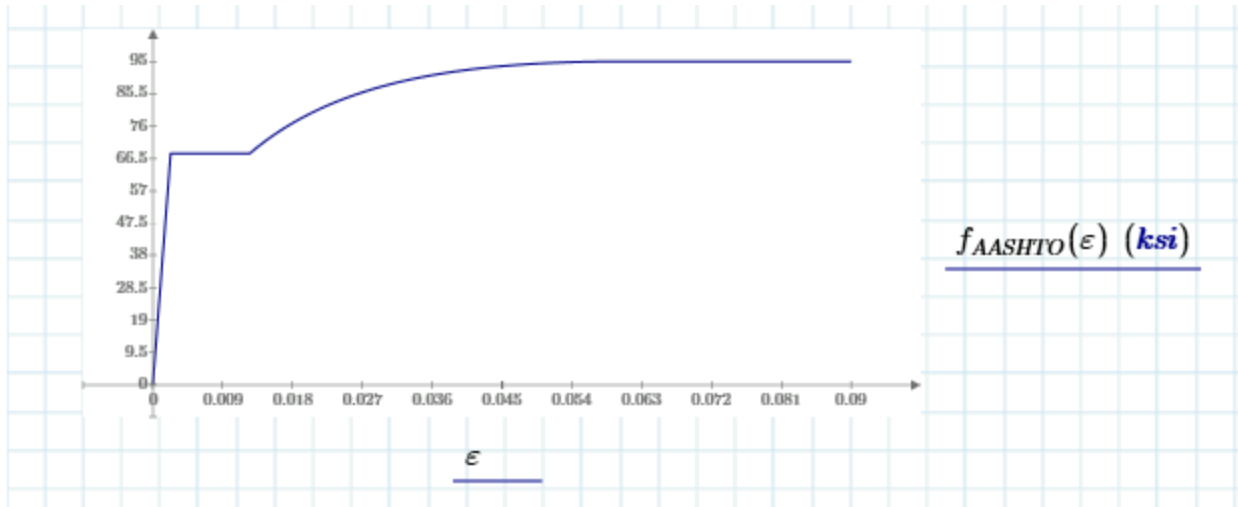


Figure 3-6 – Material Property Dowels

Kie-Con Pile Drawing Sheet No. 7 Revised specifies Grade 270 prestressing steel. We used material property *PreStress1* to model the prestressing strands. AASHTO Section 8.4.3 recommends the following material model for Grade 270 prestressing steel.

AASHTO Recommended Stress-Strain Relationship for 270 ksi Prestressing Strands

$$f_{ps,AASHTO}(\epsilon) := \text{if} \left(\epsilon < 0.0086, 28500 \text{ ksi} \cdot \epsilon, 270 \text{ ksi} - \frac{0.04 \text{ ksi}}{\epsilon - 0.007} \right)$$

Figure 3-7 shows the material model we use for Grade 270 prestressing steel.

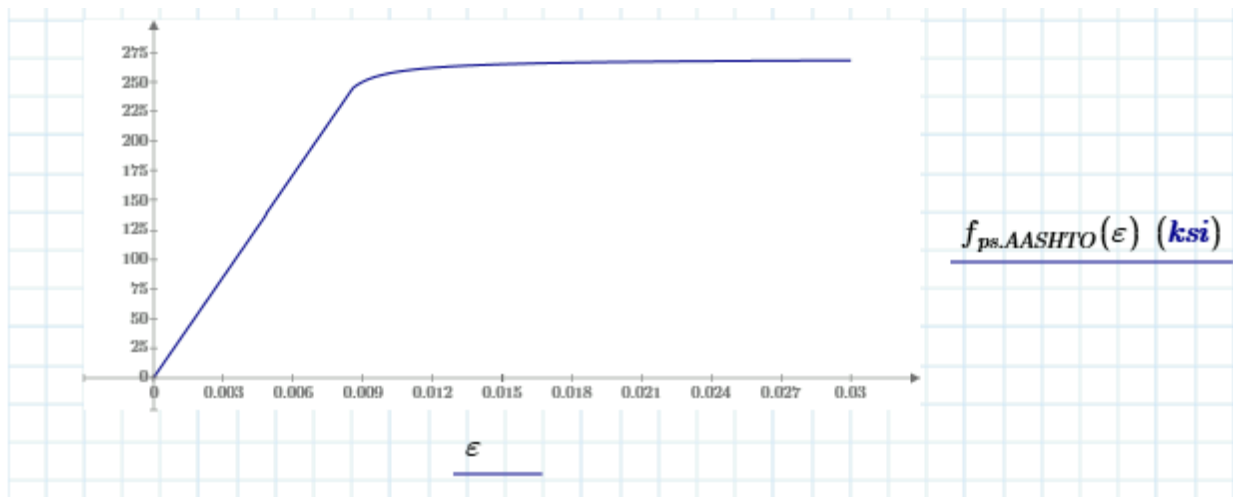


Figure 3-7 – Material Property *PreStress1*

3.1.4 Existing Pile Cross Section “PileTop”

Section *PileTop* models the existing pile just below the pilecap. The prestressing strands do not contribute to strength at the top of the pile. Therefore, the only effective steel reinforcement is four #9 bars. We modeled the cross section in XTRACT as shown in Figure 3-8.

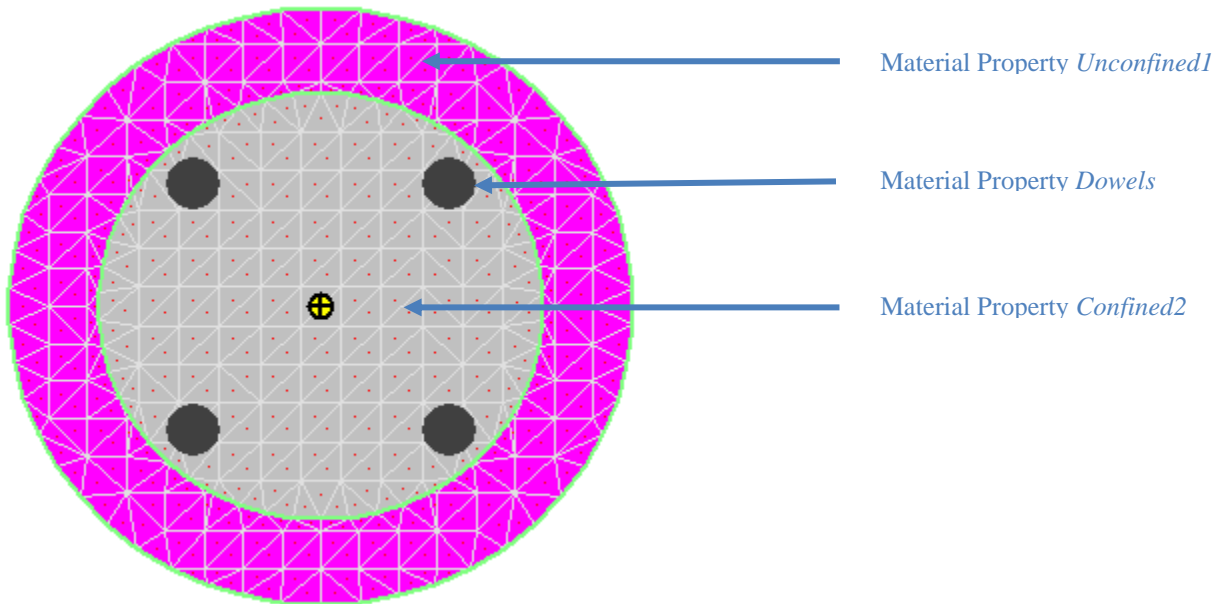


Figure 3-8 – XTRACT Model *PileTop.xpj*

3.1.5 Existing Pile Cross Section “OneAndHalfFeet”

Section *OneAndHalfFeet* models the existing pile between depths of 1.5 ft and 8 ft below the pilecap. In this region the cross section has four dowels and eight prestressing strands. We modeled the cross section in XTRACT as shown in Figure 3-9.

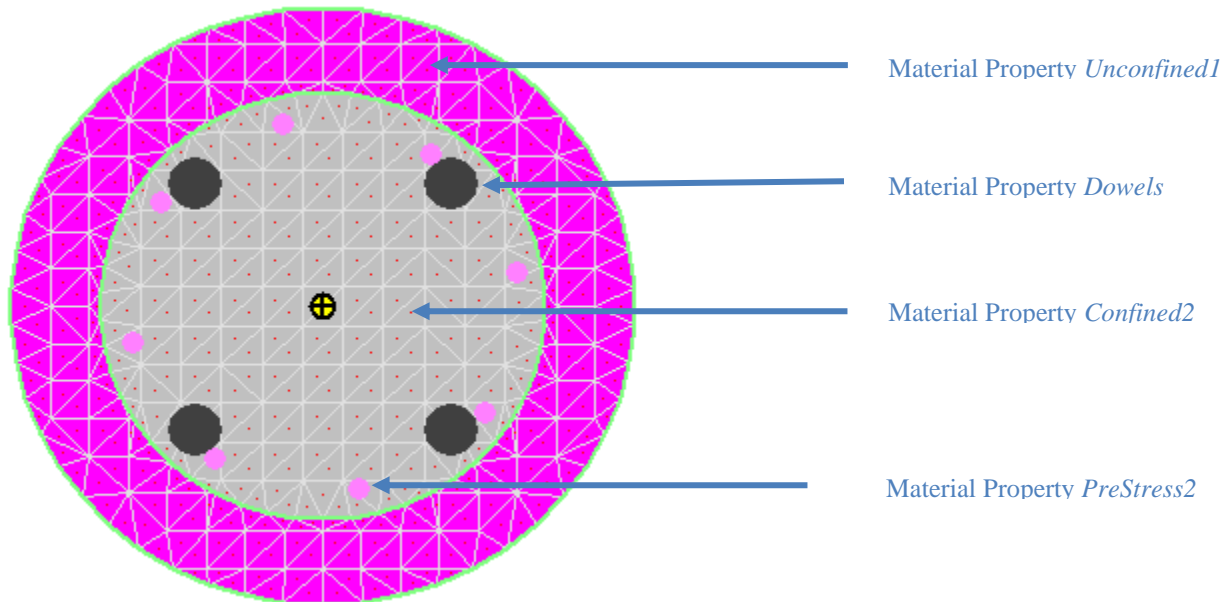


Figure 3-9 – XTRACT Model *OneAndHalfFeet.xpj*

The prestressing steel is not fully developed at distances less than about 7 ft below the pilecap (Section 3.1.1). We used material property *PreStress2* to model the prestressing strands that are not fully developed. We assigned an elastic perfectly plastic stress-strain relationship with an effective yield stress of 108 ksi, which corresponds to the maximum developed stress 1.5 ft from the pilecap, which is a lower-bound strength for the section as it occurs at the top of the segment. The ultimate material strain assigned to material property *PreStress2* does not affect the final results of our seismic analysis of the existing piles because the pushover analyses described in Section 5 show that response of the existing piles remains elastic in the region where the prestressing strands are not fully developed. Figure 3-10 shows the stress-strain relationship we assigned material property *PreStress2*.

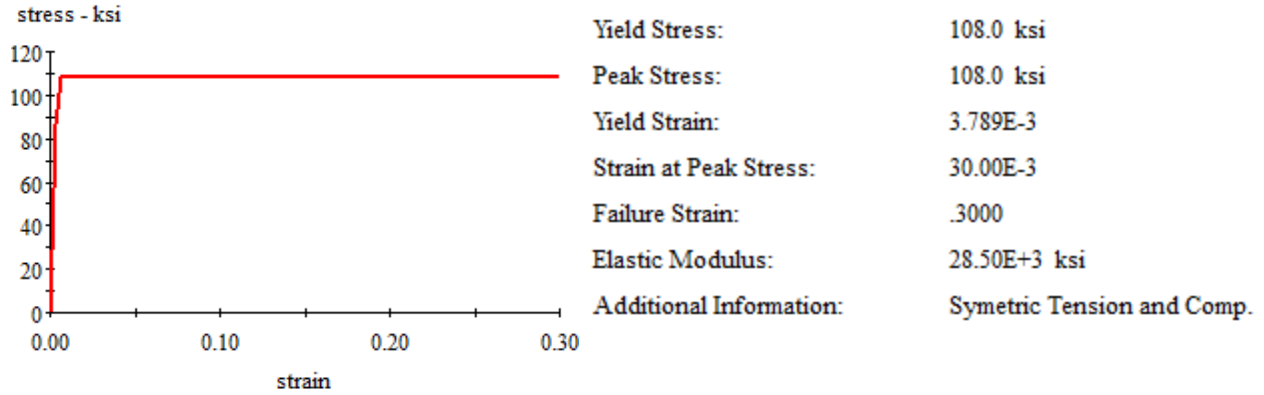


Figure 3-10 – Material Property “PreStress2”

3.1.6 Existing Pile Cross Section “SevenFeet”

Section *SevenFeet* models the existing pile between 7 ft and 17 ft below the pilecap. The prestressing strands and plain dowels are both fully developed in this region of the pile. We modeled the cross section in XTRACT as shown in Figure 3-11.

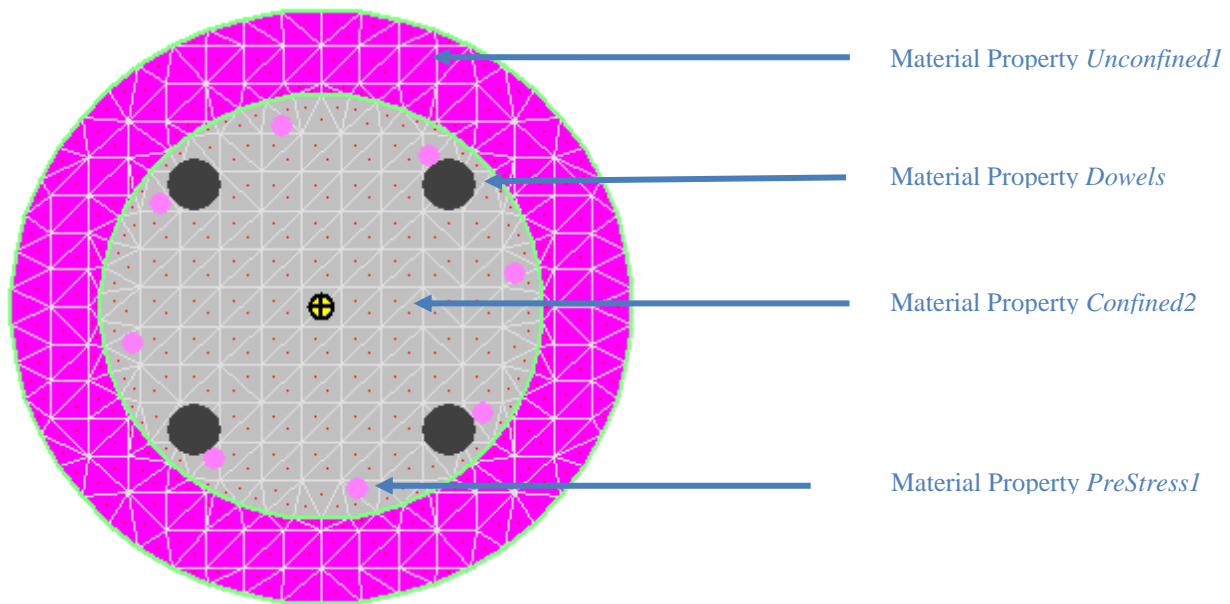


Figure 3-11 – XTRACT Model *SevenFeet.xpj*

3.1.7 Existing Pile Cross Section “SeventeenFeet”

Section *SeventeenFeet* models the existing pile beyond 17 ft below the pilecap. We only include the prestressing strands in this region of the pile. We modeled the cross section in XTRACT as shown in Figure 3-12.

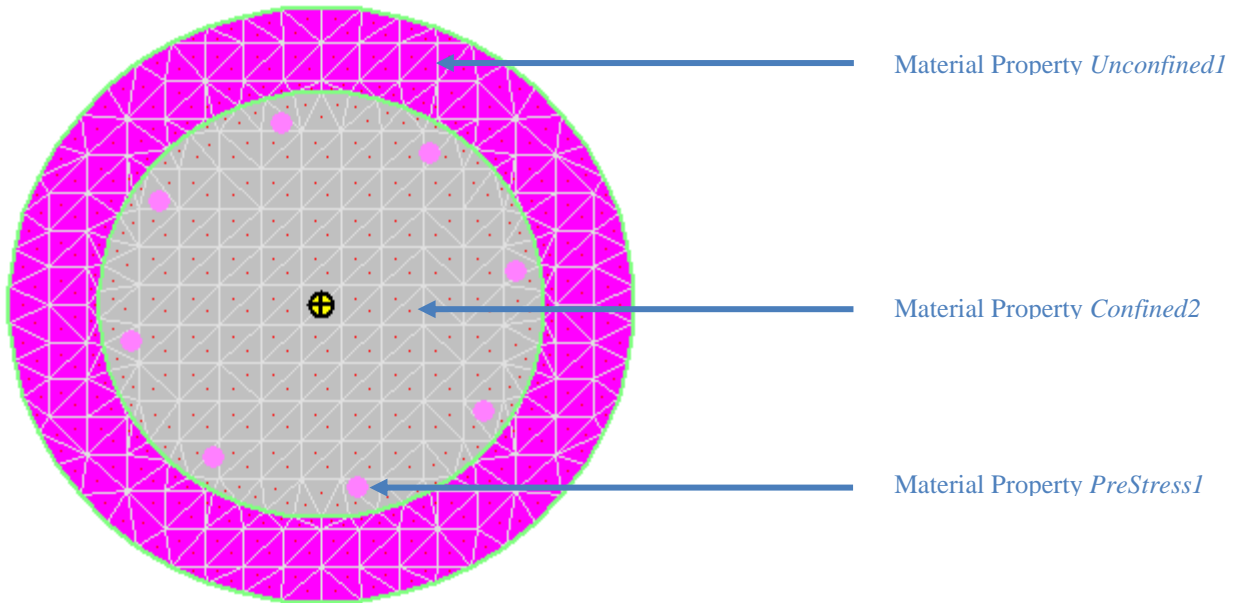


Figure 3-12 – XTRACT Model *SeventeenFeet.xpj*

3.1.8 Proposed Pile Geometry and Material Properties

The proposed rock piles have a uniform cross section from the top of the pile to bedrock. Figure XX shows the proposed pile cross section. The outer pipe casing is A252 Gr3, the center bar is A615 Gr80, and the pile casing is filled with 6,000 psi concrete. We modeled the cross section in XTRACT with expected material properties as shown in Figure 3-14.

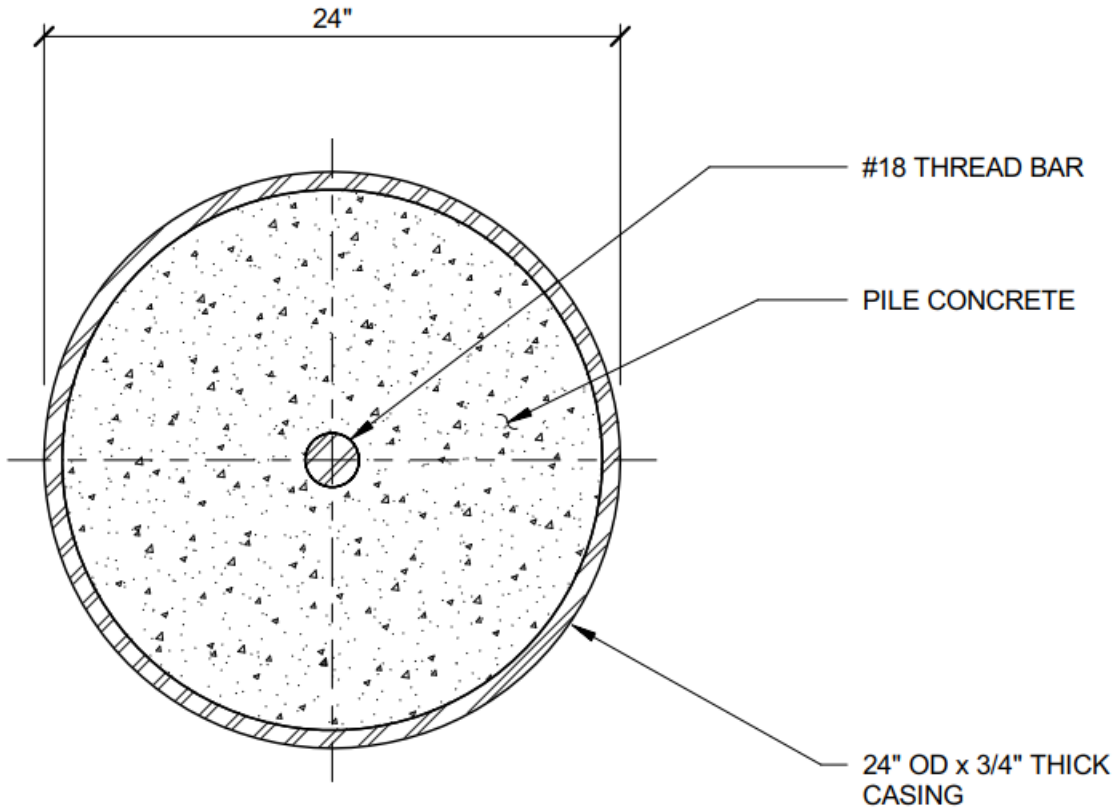
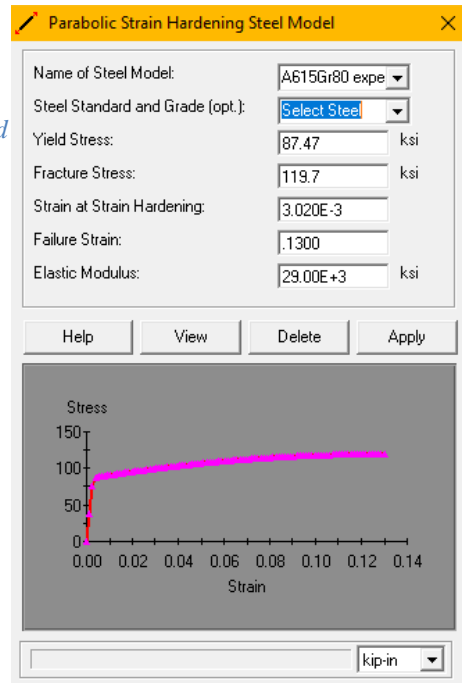
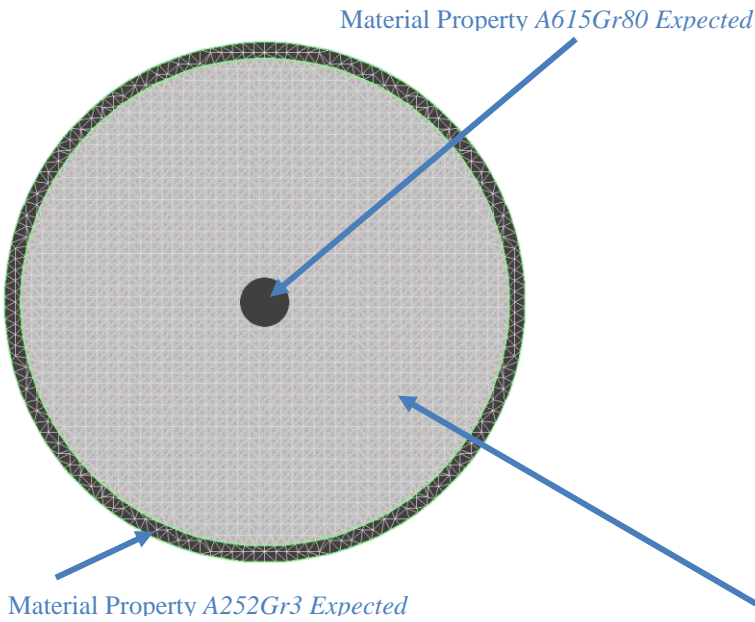


Figure 3-13 – Proposed Pile Cross Section



Material Property Confined1

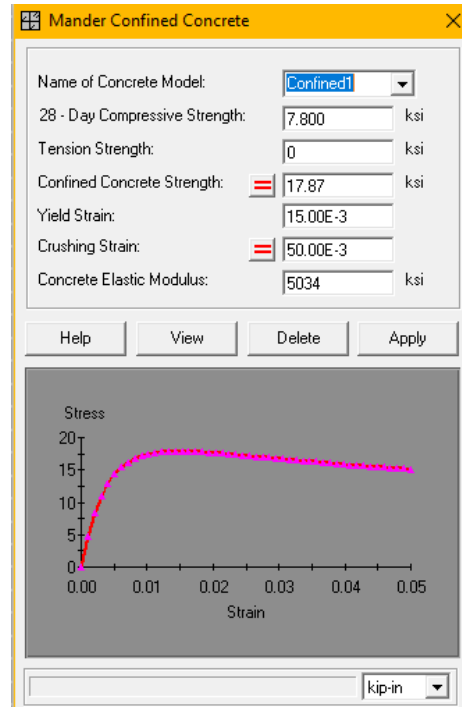
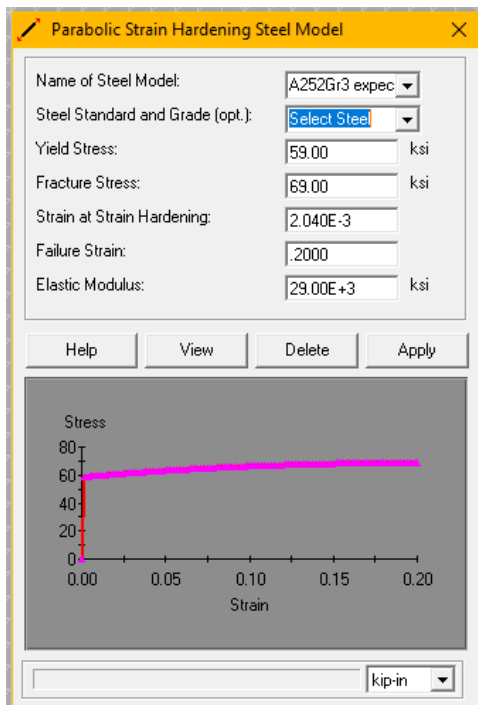


Figure 3-14 – XTRACT Model of Proposed Pile Cross Section

We obtained expected yield and ultimate strengths for A252 Gr3 steel from the paper A *Contribution to the Study of the Performance of Steel Pipe Piles Welded to Concrete Pier Cap Beams Under Seismic Loads* by M. Steunenberg (1994). We obtained ultimate strain from the ASTM specification for A252 steel.

We estimated expected material strength properties for A615 Gr80 steel from the paper *Statistical Analysis of the Mechanical Properties and Weight of Reinforcing Bars* by M. Bournonville et. al. (2004). The paper develops expected properties for A615 Gr 60 and Gr 75 reinforcing bars. We judged the ratios of expected-to-nominal strengths of Gr 75 and Gr 80 should be similar and used the ratios for Gr 75 properties to calculate expected Gr 80 properties from the nominal strengths. The paper does not present data for the ultimate strain capacity of #18 Gr 75 bars. Since the data for Gr 60 max elongation does not show a decrease in mean ultimate strain for increased bar sized, we judged the ultimate strain for #14 Gr75 bars is a reasonable approximation of ultimate strain for #18 Gr80 bars.

We calculated expected confined concrete properties for the 6,000 psi concrete as follows:

$f'.c := 1.3 \cdot 6000 \text{ psi} = 7.8 \text{ ksi}$	
$E.c := 57000 \cdot \sqrt{\frac{f'.c}{\text{psi}}} \cdot \text{psi} = (5.034 \cdot 10^3) \text{ ksi}$	
$OD.o := 24 \text{ in}$	“outer steel outer diameter”
$t.so := \frac{3}{4} \text{ in}$	“outer steel thickness”
$A.center := 4 \text{ in}^2$	“center bar area”
$f.y.s := 59 \text{ ksi}$	“steel tube yield stress”
$E.s := 29000 \text{ ksi}$	
$f.y.bar := \left(\frac{82}{75} \cdot 80\right) \text{ ksi} = 87.467 \text{ ksi}$	“center bar yield stress”

$$A_{outer} := \left(OD.o^2 - (OD.o - 2 t.so)^2 \right) \cdot \frac{\pi}{4} = 54.782 \text{ in}^2$$

$$A_{core} := OD.o^2 \cdot \frac{\pi}{4} - A_{outer} = 397.608 \text{ in}^2 \quad \text{"confined core concrete area"}$$

$$\rho.s := \frac{A_{outer}}{A_{core}} = 0.138$$

$$s := 0 \text{ in}$$

$$k.e := 1 - \frac{s}{OD.o} = 1$$

Moehle suggests limiting the ultimate strength of transverse reinforcement as follows.

$$f.s.limit := E.s \cdot \left(0.0025 + 0.04 \cdot \sqrt[3]{\frac{k.e \cdot \rho.s}{\frac{f'.c}{psi}}} \right) = 102.71 \text{ ksi}$$

$$f.s := \min(f.y.s, f.s.limit) = 59 \text{ ksi}$$

$$f.2e := k.e \cdot \frac{\rho.s \cdot f.s}{2} = 4.064 \text{ ksi} \quad \text{Effective confining stress (Mander Eq. 19)}$$

XTRACT enforces limit to confining stress of $0.3 \cdot f'.c$

$$f.2e := 0.3 \cdot f'.c = 2.34 \text{ ksi} \quad f'.c = 7.8 \text{ ksi}$$

$$f'.cc := f'.c \cdot \left(-1.254 + 2.254 \cdot \sqrt{1 + \frac{7.94 f.2e}{f'.c}} - 2 \cdot \frac{f.2e}{f'.c} \right) = 17.871 \text{ ksi} \quad \text{(Mander Eq. 29)}$$

Mander suggests an unconfined concrete strain at peak stress of 0.002.

$$\varepsilon.o := 0.002$$

Unconfined concrete strain at peak stress

$$\varepsilon.cc := \varepsilon.o \cdot \left(1 + 5 \cdot \left(\frac{f'.cc}{f'.c} - 1 \right) \right) = 0.015$$

Confined concrete strain at peak stress
(Mander Eq. 5)

Moehle suggests two expressions for concrete strain at first rupture of transverse reinforcement. We elect to use the more conservative of the two.

$$\varepsilon.cu := 0.004 + \frac{f.2e}{4 \cdot f'.c} = 0.079$$

Confined concrete strain at first spiral wire fracture (Moehle Eqs. 4.17 and 4.18)

$$\varepsilon.cu := 0.004 + 0.075 \cdot \frac{\rho.s \cdot f.s}{f'.c} = 0.082$$

Limit crushing strain to 5%

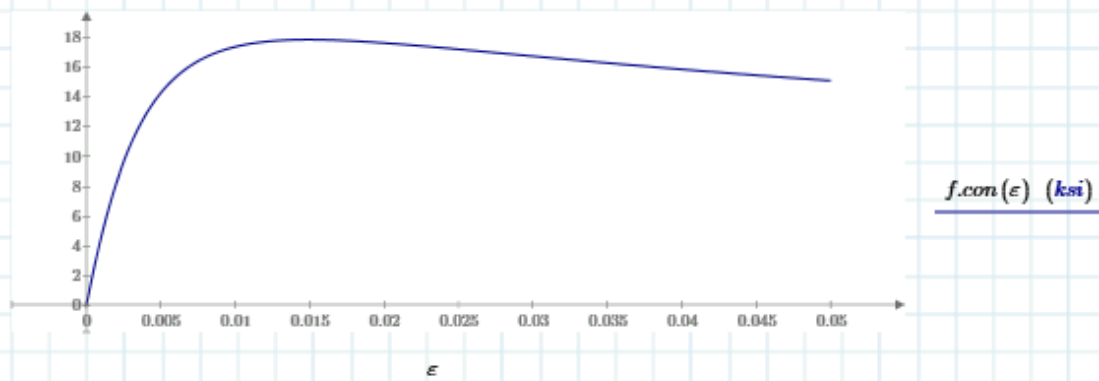
$$\varepsilon.cu := 0.05$$

Confined Concrete Stress-Strain Relationship

$$E.sec := \frac{f'.cc}{\varepsilon.cc} = (1.198 \cdot 10^3) \text{ ksi}$$

$$r := \frac{E.c}{E.c - E.sec} = 1.312$$

$$f.con(\varepsilon.c) := \frac{f'.cc \cdot \frac{\varepsilon.c}{\varepsilon.cc} \cdot r}{r - 1 + \left(\frac{\varepsilon.c}{\varepsilon.cc} \right)^r} \quad \varepsilon := 0, 0.0001 \dots \varepsilon.cu$$



3.2 Moment-Curvature Analysis

For each XTRACT cross section model discussed in Section 3.1 we generated an axial – moment (P-M) interaction diagram. Based on our analyses we expect the existing precast prestressed piles to have different compressive axial loads. We used XTRACT to generate several moment-curvature relationships for each existing pile cross section. We calculated moment-curvature for axial loads from 0 kip to 900 kip at 100 kip intervals. Figure 3-15 shows P-M interaction, and Figure 3-16 through Figure 3-19 show moment-curvature for the existing pile cross sections. Figure 3-20 shows the results of moment-curvature analysis of the proposed pile with 800 kip axial load. The effective yield moment is about 35,000 kip-in.

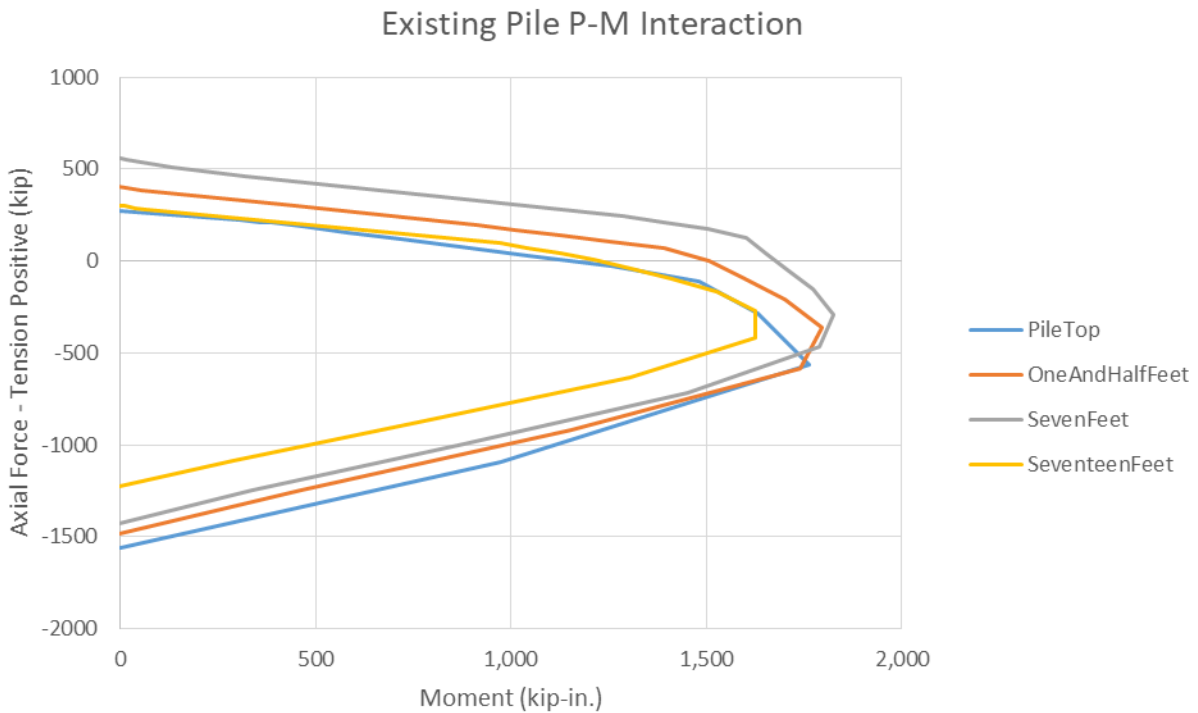


Figure 3-15 – Existing Pile P-M Interaction

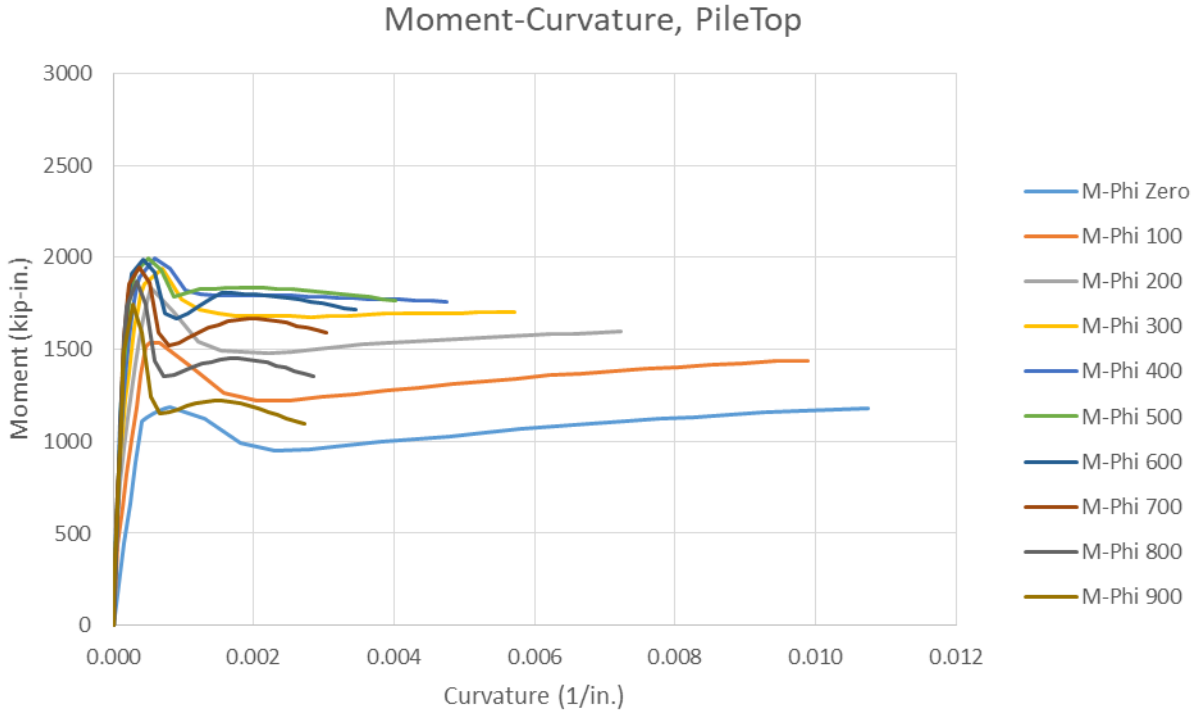


Figure 3-16 – Existing Pile Moment-Curvature at Section “PileTop”

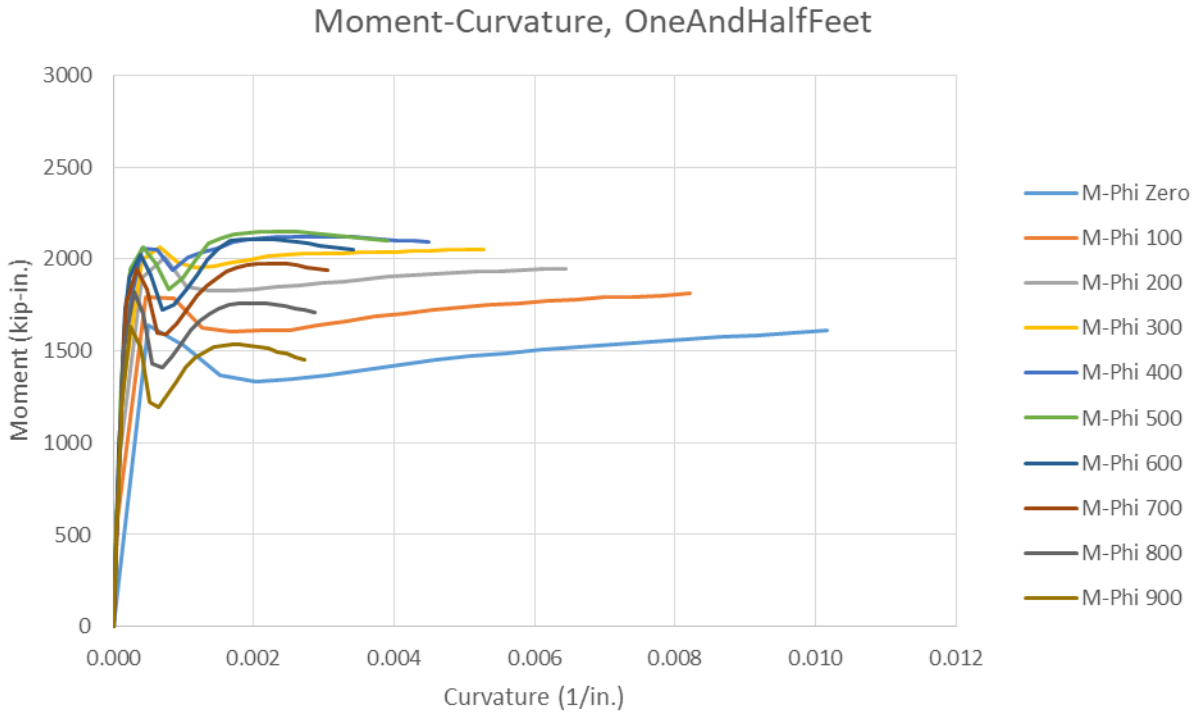


Figure 3-17 – Existing Pile Moment-Curvature at Section “OneAndHalfFeet”

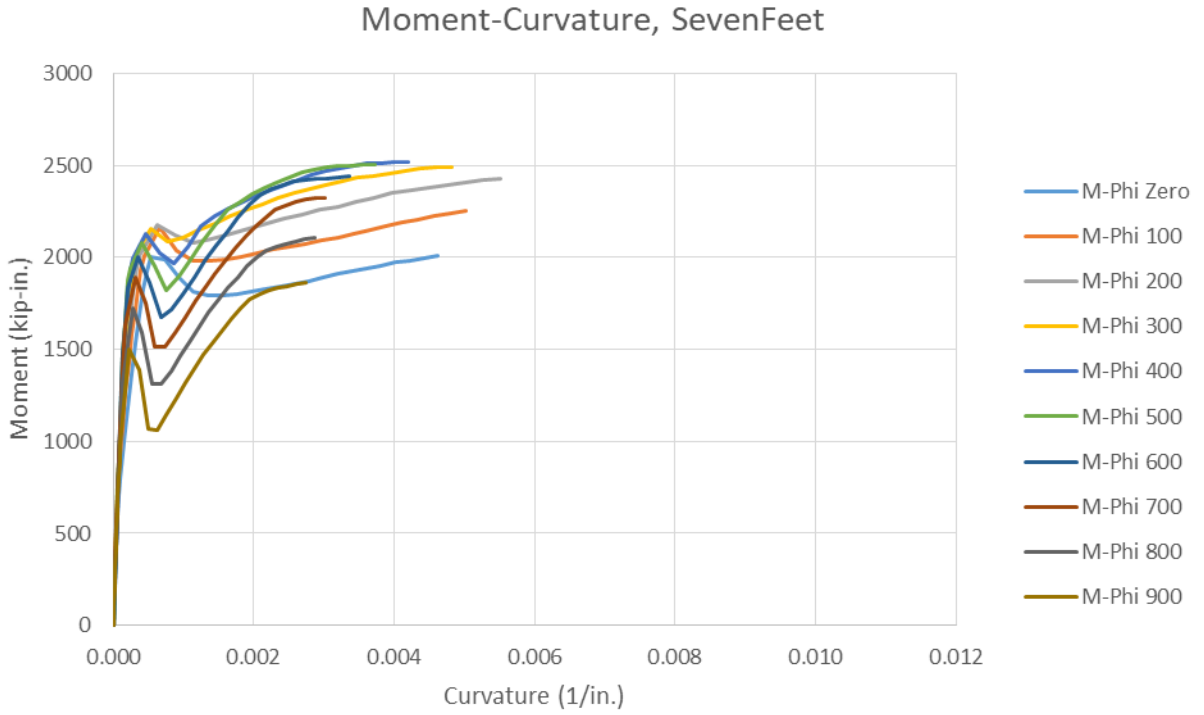


Figure 3-18 – Existing Pile Moment-Curvature at Section “SevenFeet”

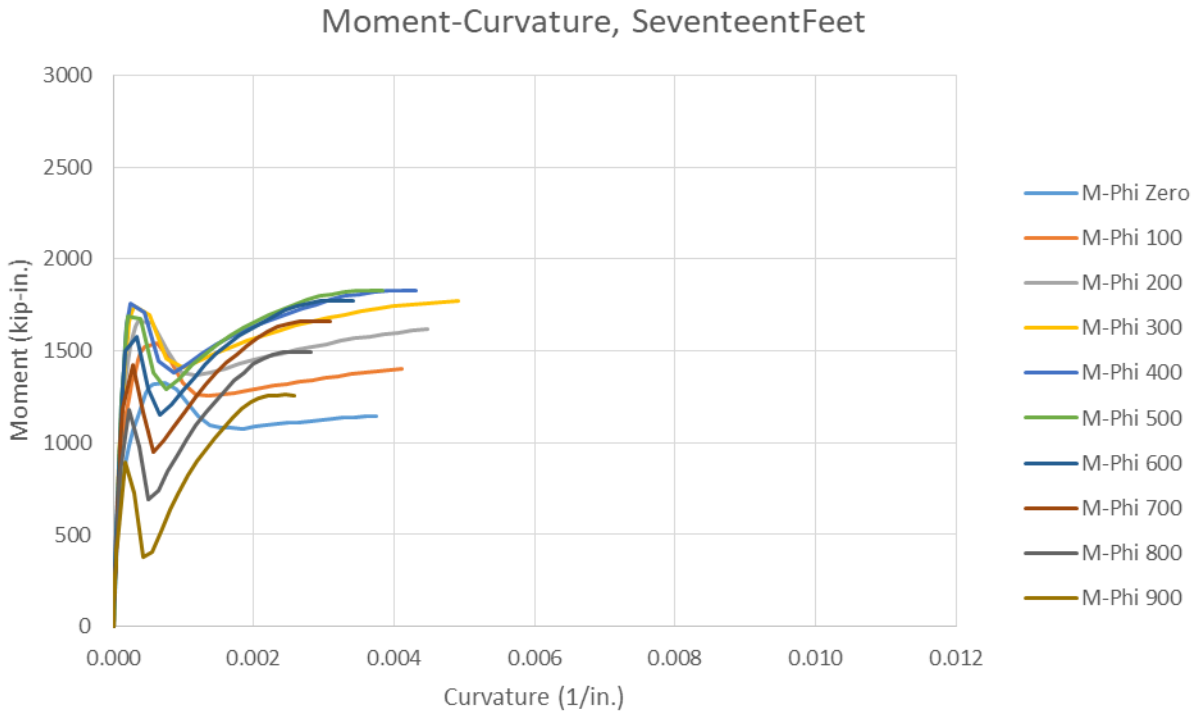


Figure 3-19 – Existing Pile Moment-Curvature at Section “SeventeenFeet”

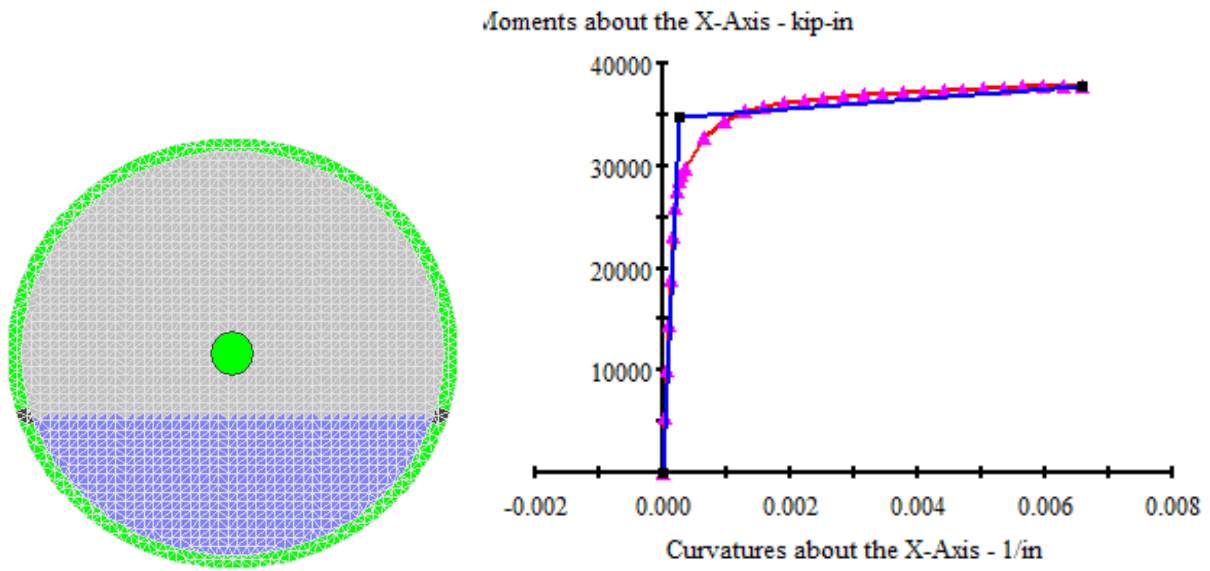


Figure 3-20 – Proposed Pile Moment-Curvature Analysis Results for Expected Properties

4. ANALYTICAL MODEL: LPILE

We used computer program LPILE, Version 2016-09.008 to calculate nonlinear force-displacement relationships (p-y curves) for lateral loading of the piles.

4.1 Group Effect Factor

To account for the effect of closely spaced piles on the piles' lateral stiffness, we used the method documented in *Analysis and Design of Shallow and Deep Foundations* by Reese et al. (2006), Section 15.5.3. This method is summarized below.

Each pile in a group is assigned plan coordinates x and y. For any two piles, we considered the direction of loading relative to the orientation of the piles. Any two piles may be oriented along the direction of loading, perpendicular to the direction of loading, or some angle in between.

For piles side-by-side, in a line oriented perpendicular to the direction of loading,

$$\beta_a = 0.64 \left(\frac{s}{b}\right)^{0.34} \leq 1.0$$

For a pile in a line oriented parallel to the load,

$$\beta_b = 0.7 \left(\frac{s}{b}\right)^{0.26} \leq 1.0 \text{ for the leading pile}$$
$$\beta_b = 0.7 \left(\frac{s}{b}\right)^{0.26} \leq 1.0 \text{ for the trailing pile}$$

Where β_a is the p-modification factor for piles side-by-side, β_b is the p-modification factor for piles aligned with the load, s is the distance between piles, and b is the pile diameter.

For piles at an arbitrary angle relative to the load,

$$\beta_s = \sqrt{\beta_a^2 \cos^2 \varphi + \beta_b^2 \sin^2 \varphi}$$

Where β_s is the p-modification factor for piles aligned at an angle to the loading direction and φ is the angle between the direction of load and a line connecting the two piles in question. For each pile in a group, the cumulative effect of the adjacency of all other piles applies. As such,

$$\beta = \frac{1}{n} \sum_{i=1}^n \prod_{j=1}^n \beta_{ij} \text{ for } i \neq j$$

Where $\beta_{i,j}$ is the p-modification factor for leading, trailing, side-by-side, or diagonal effects, as applicable between any two piles, i and j.

For each pile, we computed the modification factor between that pile and all other piles and created a cumulative product of these factors. Figure 4-1 shows the pile p-modification factors for loading in the positive X-direction (east). Figure 4-2 shows the pile p-modification factors for loading in the positive Y-direction (north). In both figures, the pile layout is indicated by an array of black dots.

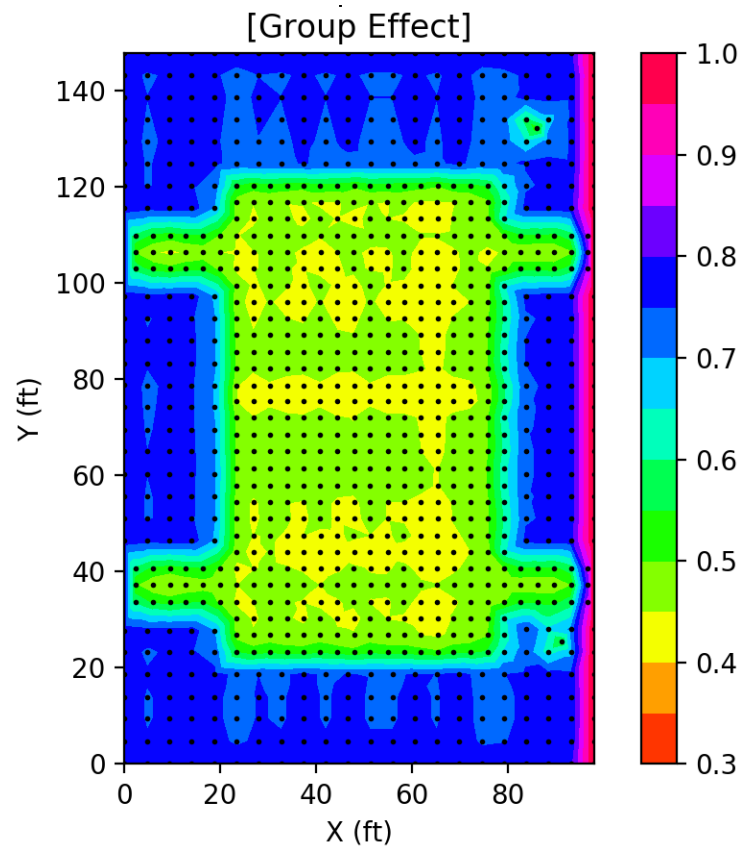


Figure 4-1 – Individual Pile Group Effect Factors for East Loading

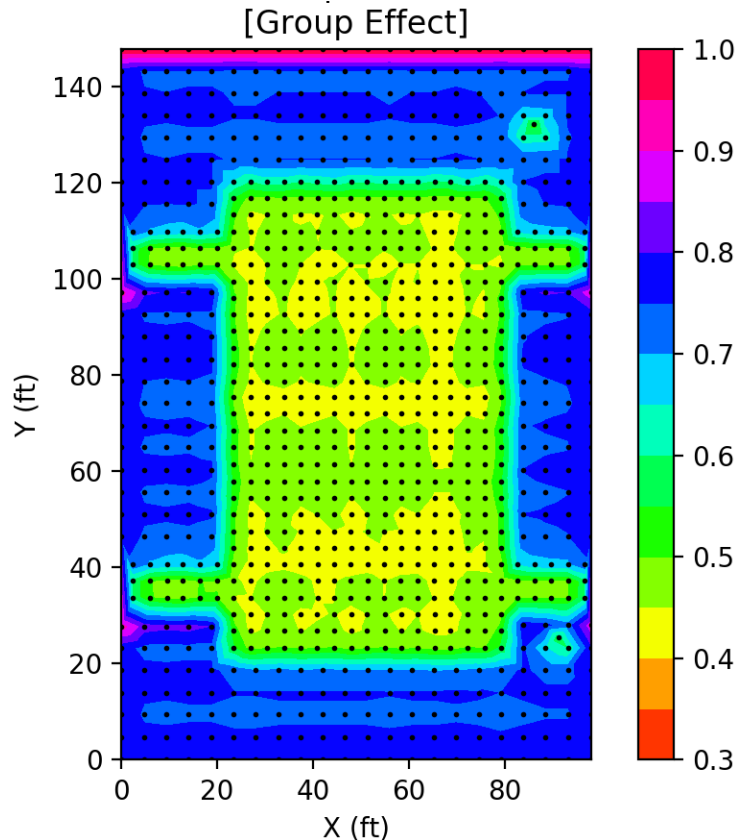


Figure 4-2 – Individual Pile Group Effect Factors for North Loading

The average pile p- modification factor is about 0.6 for both east and north loading. The pile layout is essentially symmetric about both axes, so the average p-modification factor is the same for west and south loading. We therefore developed soil p-y curves for the existing piles using a p-modification factor of 0.6 to account for lateral group effects.

4.2 Summary of Recommended Input Parameters from All Parties

We looked at soil stratigraphy and geotechnical properties recommended in two geotechnical reports for the site:

- John Egan, Slate Geotechnical Consultants, Inc. and Shannon & Wilson, Inc., *Geotechnical Evaluation for the Perimeter Pile Upgrade*, 30 November 2018.
- ENGEO, Inc., *Geotechnical Memorandum – 301 Mission Retrofit Design (Draft)*, 20 September 2018.

Recommended soil profiles from each report are indicated in Figure 4-1 and Tables 4-1 through 4-3. Depths in the tables and figure are measured from the top of the existing piles. ENGEO

Inc. recommends lower bound (LB) and upper bound (UB) soil properties, with ranges of values for clay layer undrained cohesion and strain factor. We selected the middle of the suggested ranges for our analyses and list these values in Tables 4-1 and 4-2.

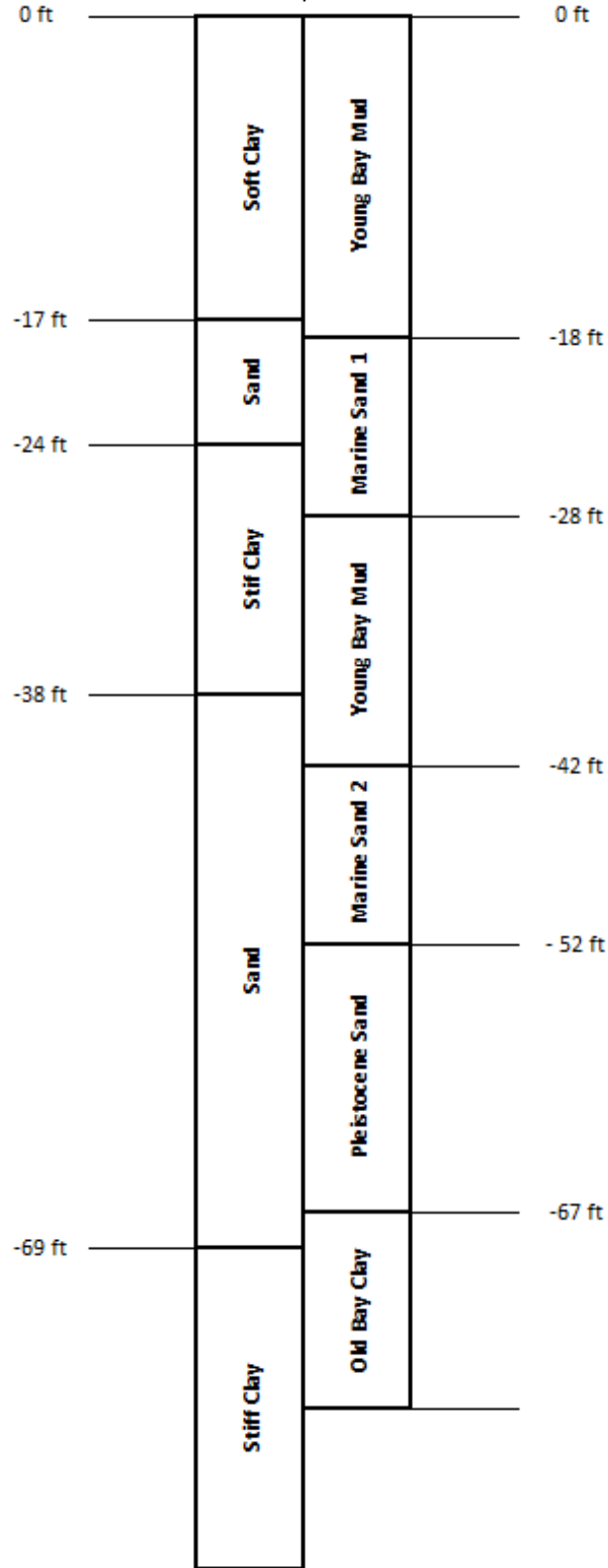


Figure 4-3 – Recommended Soil Stratigraphy

Table 4-1 – ENGEO Inc. Lower Bound Recommended Soil Properties

Layer Depth (ft)	Layer Description	LPILE Soil Type	Unit Weight γ (pcf)	Friction Angle ϕ (deg)	Undrained Cohesion c (psf)	Strain Factor E_{50} (psf)	Sand Modulus k (pci)
0 – 18	Young Bay Mud	Soft Clay	47.6	-	625	0.015	-
18 – 28	Marine Sand 1	Reese Sand	57.6	34	-	-	75
28 – 42	Young Bay Mud	Soft Clay	52.6	-	1000	0.015	-
42 – 52	Marine Sand 2	Reese Sand	67.6	35	-	-	85.6
52 – 67	Pleistocene Sand	Reese Sand	67.6	36	-	-	96.6
67 – 77	Old Bay Clay Crust	Stiff Clay without Free Water	57.6	-	2600	0.006	-

* ENGEO Inc. does not indicate recommended values for sand layer modulus ‘k’. LPILE selects the values listed above.

Table 4-2 – ENGEO Inc. Upper Bound Recommended Soil Properties

Layer Depth (ft)	Layer Description	LPILE Soil Type	Unit Weight γ (pcf)	Friction Angle ϕ (deg)	Undrained Cohesion c (psf)	Strain Factor E_{50} (psf)	Sand Modulus k (pci)
0 – 18	Young Bay Mud	Soft Clay	47.6	-	850	0.015	-
18 – 28	Marine Sand 1	Reese Sand	57.6	34	-	-	75
28 – 42	Young Bay Mud	Soft Clay	52.6	-	1250	0.015	-
42 – 52	Marine Sand 2	Reese Sand	67.6	35	-	-	85.6
52 – 67	Pleistocene Sand	Reese Sand	67.6	36	-	-	96.6
67 – 77	Old Bay Clay Crust	Stiff Clay without Free Water	57.6	-	3400	0.006	-

* ENGEO Inc. does not indicate recommended values for sand layer modulus ‘k’. LPILE selects the values listed above.

Table 4-3 – John Egan, SLATE Geotechnical Consultants Inc., and Shannon & Wilson Inc. Recommended Soil Properties

Layer Depth (ft)	LPILE Soil Type	Unit Weight γ (pcf)	Friction Angle ϕ (deg)	Undrained Cohesion c (psf)	Strain Factor E_{50} (psf)	Sand Modulus k (pci)
0 – 17	Soft Clay	131	-	880	0.02	
17 – 23.8	Sand Below the Water Table	62.6	35	-		60
23.8 – 38	Stiff Clay Without Free Water	40.6	-	1595	0.007	
38 – 69	Sand Below the Water Table	67.6	34			75
69 - 79	Stiff Clay Without Free Water	60.5	-		0.005	

4.3 Soil Spring Results

The LB soil properties from ENGEO Inc. result in the most conservative characterization of the pile lateral capacity. This is due to the fact that these properties result in both softer and weaker soil springs which directly affect pile lateral response. We calculated p-y curves for the ENGEO Inc. LB soil properties using LPILE. The p-y curve depths correspond to the locations of nonlinear springs in the individual pile pushover analysis model discussed in Section 5. We calculated soil spring force-displacement relationships by multiplying p-y curves from LPILE by the depth of soil tributary to the spring location. Table 4-4 lists soil spring locations and tributary depths. Figure 4-4 through Figure 4-7 compare soil spring force-displacement relationships for the LB properties from ENGEO Inc. and properties from John Egan, SLATE Geotechnical Consultants Inc., and Shannon & Wilson Inc.

Table 4-4 – Soil Spring Properties

Soil Spring Property	Soil Spring Depth (ft)	Tributary Length (in)
PY-B1_-12	1	12
PY-B1_-36	3	24
PY-B1_-60	5	24
PY-B1_-84	7	24
PY-B1_-108	9	24
PY-B1_-132	11	24
PY-B1_-156	13	24
PY-B1_-180	15	24
PY-B1_-204	17	24
PY-B1_-228	19	24
PY-B1_-252	21	24
PY-B1_-276	23	24
PY-B1_-300	25	24
PY-B1_-336	28	36
PY-B1_-384	32	48
PY-B1_-432	36	48
PY-B1_-480	40	48
PY-B1_-528	44	48
PY-B1_-576	48	48
PY-B1_-624	52	48
PY-B1_-672	56	48
PY-B1_-720	60	48
PY-B1_-768	64	48
PY-B1_-816	68	48

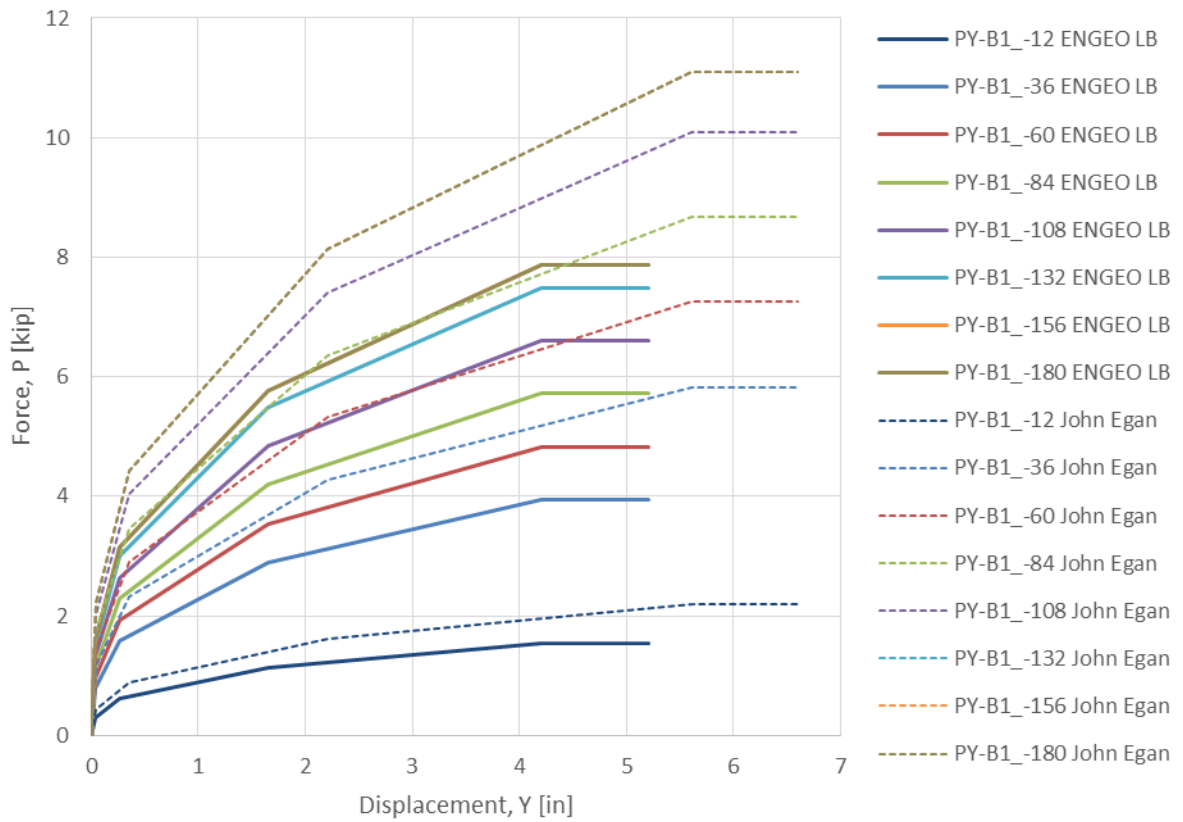


Figure 4-4 – Soil Spring Force-Displacement; Depths 1ft – 15ft

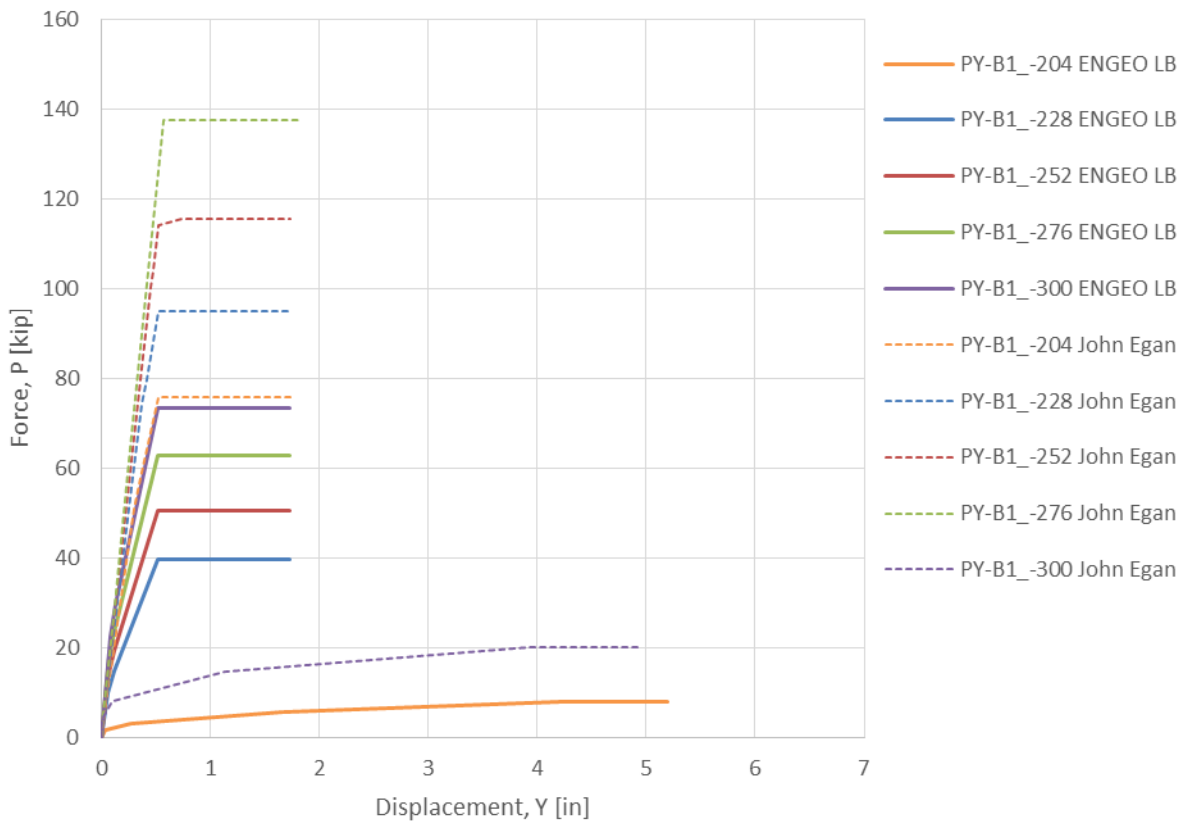


Figure 4-5 – Soil Spring Force-Displacement; Depths 17ft – 25ft

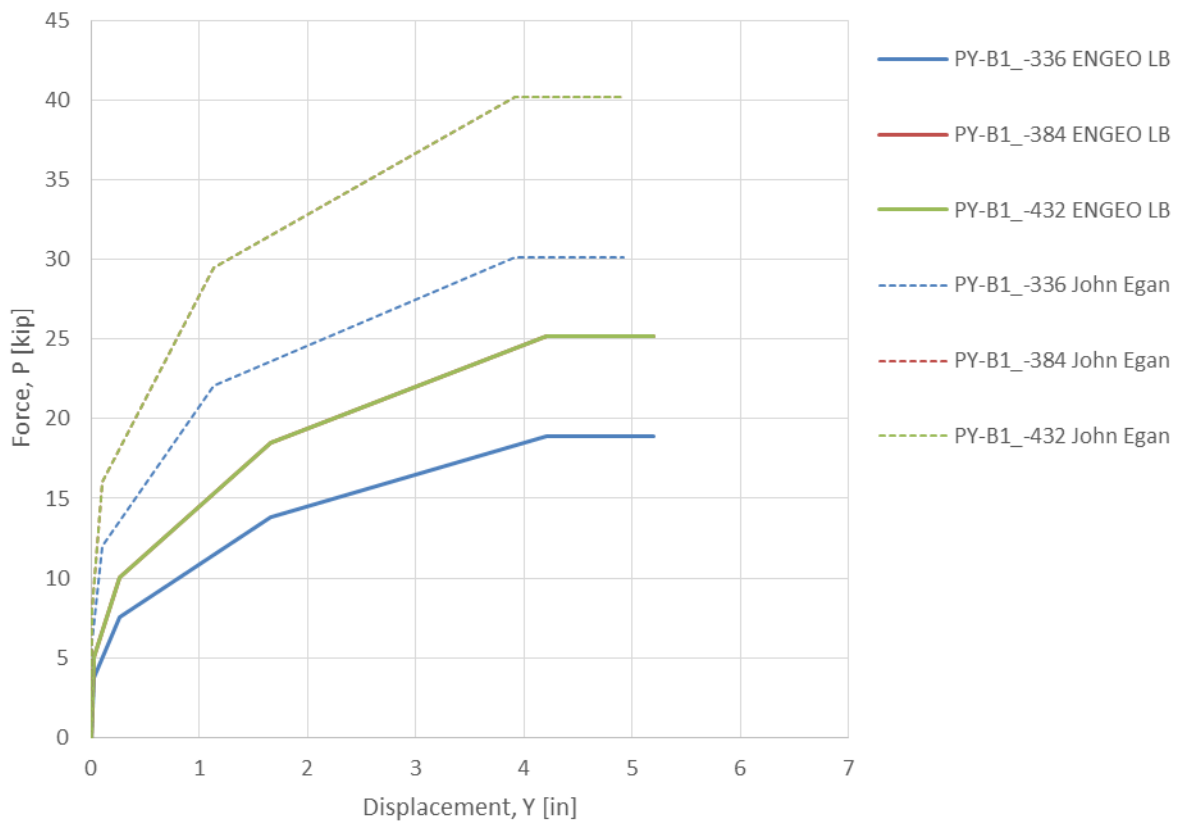


Figure 4-6 – Soil Spring Force-Displacement; Depths 28ft – 36ft

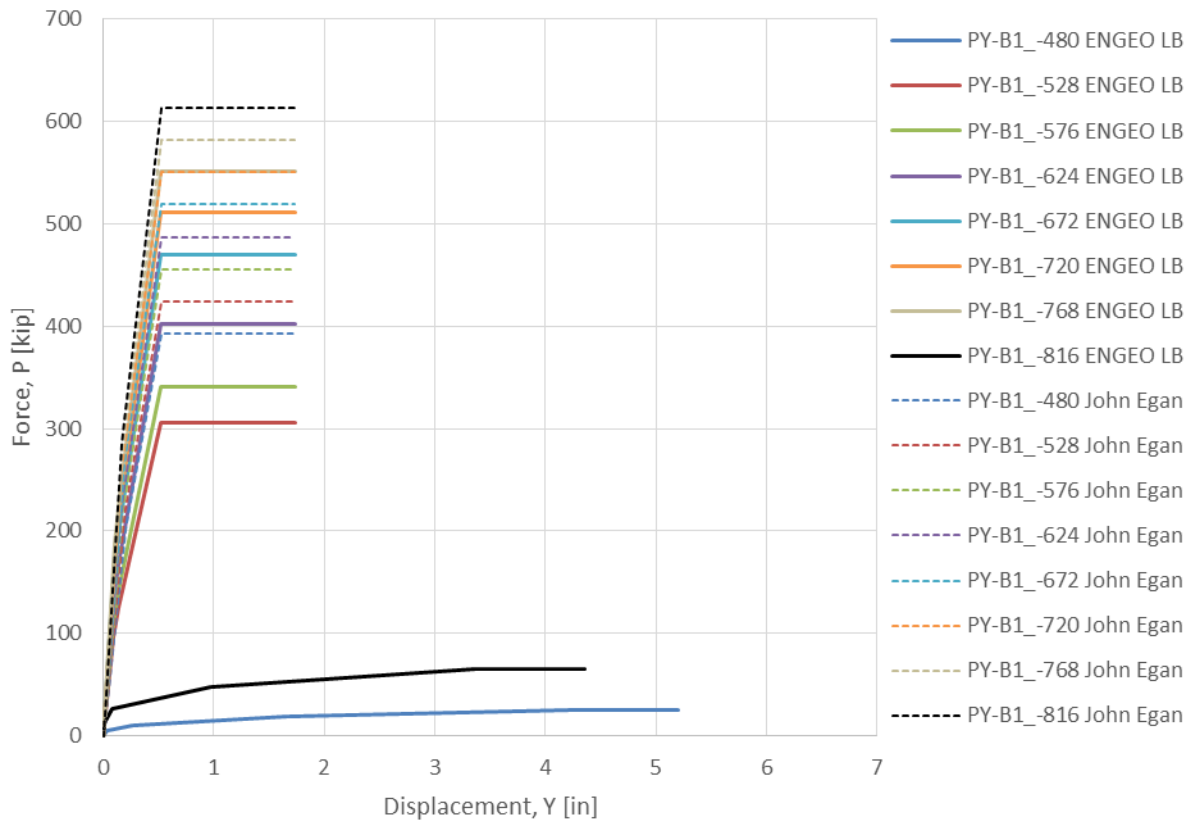


Figure 4-7 – Soil Spring Force-Displacement; Depths 40ft – 68ft

5. ANALYTICAL MODEL: SAP2000

5.1 Description and Screenshots

We used computer program SAP2000, Version 19.2.2 to conduct nonlinear pushover analyses of the existing and proposed piles. We modeled the existing piles with frame elements to a depth of 68 ft below the pile cap. The pushover analyses show that lateral forces are negligibly small below depths of about 25 ft. We modeled both types of pile with a fixed head condition; we restrained rotations at the top joint of the models. This is because the #9 dowel reinforcement in the existing piles is fully developed into the pile cap.

The model incorporates the following nonlinear elements:

- Frame element hinges with properties from XTRACT analyses described in Section 3.
- Soil springs with properties from LPILE analyses described in Section 4.

We assigned soil springs to the pile model at the locations shown in Figure 5-1. We used multi-linear elastic link elements to model the soil springs with the force-displacement relationships shown in Figure 4-4 through Figure 4-7.

We assigned frame element hinges at the locations shown in Figure 5-2. The lowest hinge in the model is at a depth of 25 ft. We confirmed that maximum pile bending moments below 25 ft remain in the elastic range of pile behavior. The frame element hinges are deformation-controlled interacting P-M3 hinges. We defined the hinge properties with P-M interaction contours developed in XTRACT and shown in Figure 3-15. We assigned bilinear, elastic-perfectly plastic approximations of the moment-curvature relationships developed for each cross section in XTRACT. Table 5-1 summarizes hinge property definitions in the SAP2000 model.

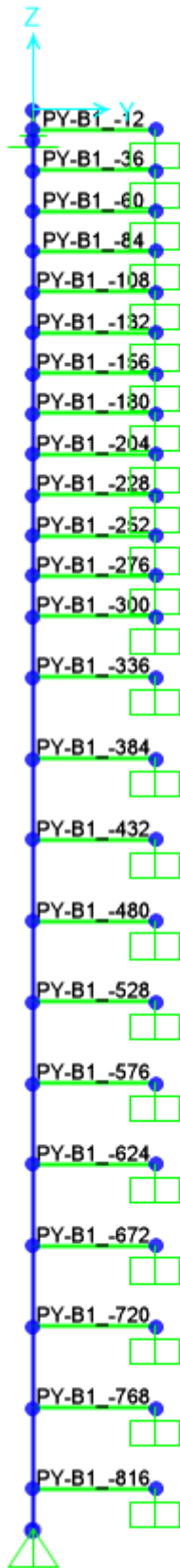


Figure 5-1 – SAP2000 Model Soil Spring Locations

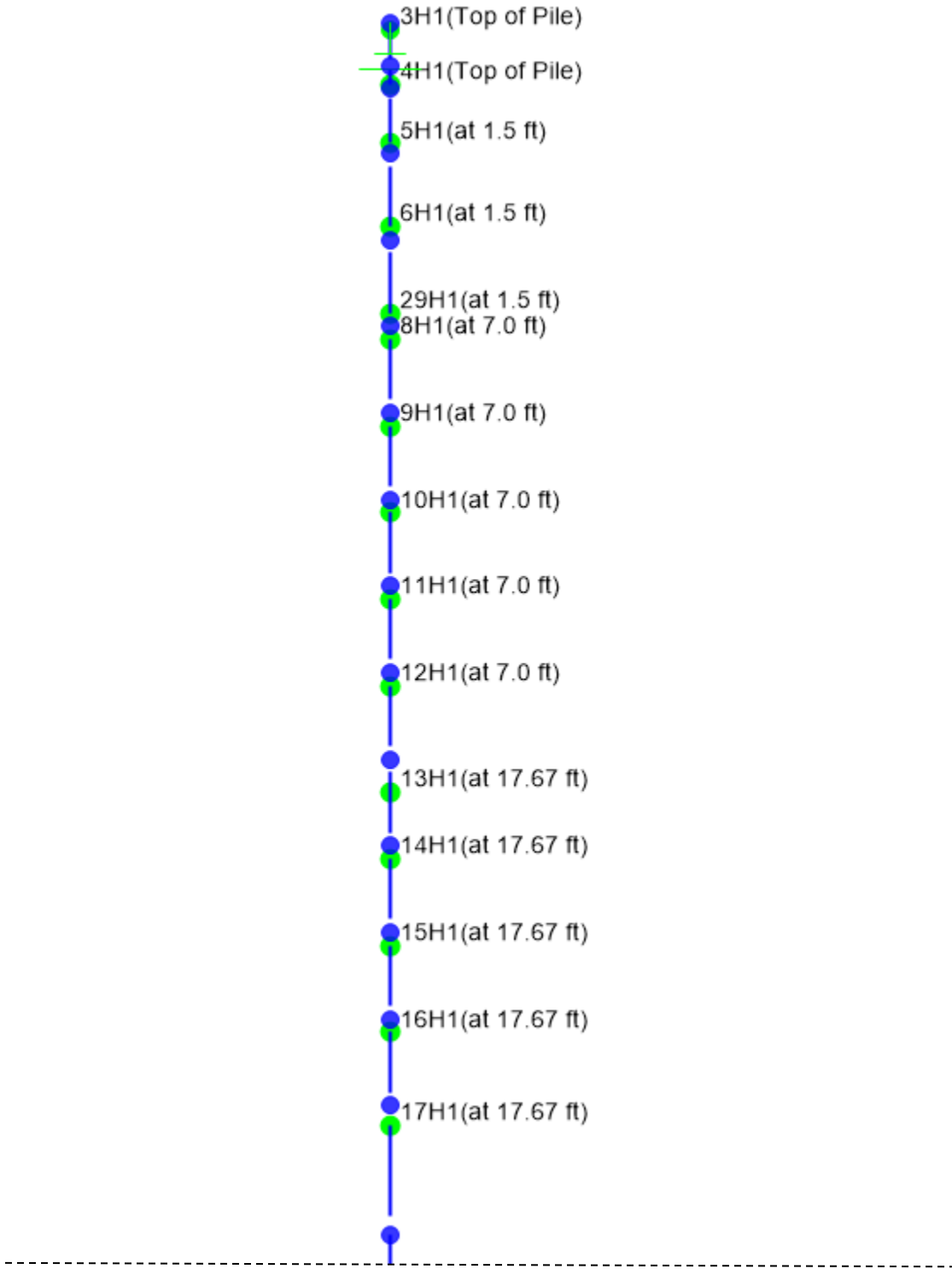


Figure 5-2 – SAP2000 Model Hinge Locations

Table 5-1 – Nonlinear Hinge Properties

SAP2000 Hinge Property	XTRACT Model
Top of Pile	PileTop.xpj
at 1.5 ft	OneAndHalfFeet.xpj
at 7.0 ft	SevenFeet.xpj
At 17.67 ft	SeventeenFeet.xpj

We defined hinge property *at 1.5 ft* based on a conservative combination of the strength properties of XTRACT models *PileTop* and *OneAndHalfFeet*. The partially developed prestressing steel between 1.5 ft and 7 ft below the pilecap would not traditionally be accounted for when assessing the cross section moment capacity. Neglecting the partially developed prestressing steel is conservative when applied axial loads are small. However, at high compression loads, the partial prestress can reduce the section's flexural capacity due to earlier crushing of the confined concrete core. Figure 5-3 compares P-M behavior of the cross section with and without the partially developed prestressing steel. From the P-M plots, we concluded that neglecting the prestressing steel is conservative for axial compression with magnitude less than 500 kip. For axial compression with magnitude greater than 500 kips, accounting for the partially developed prestressing strands is conservative.

Figure 5-4 through Figure 5-11 compare our bilinear approximations to the output from XTRACT.

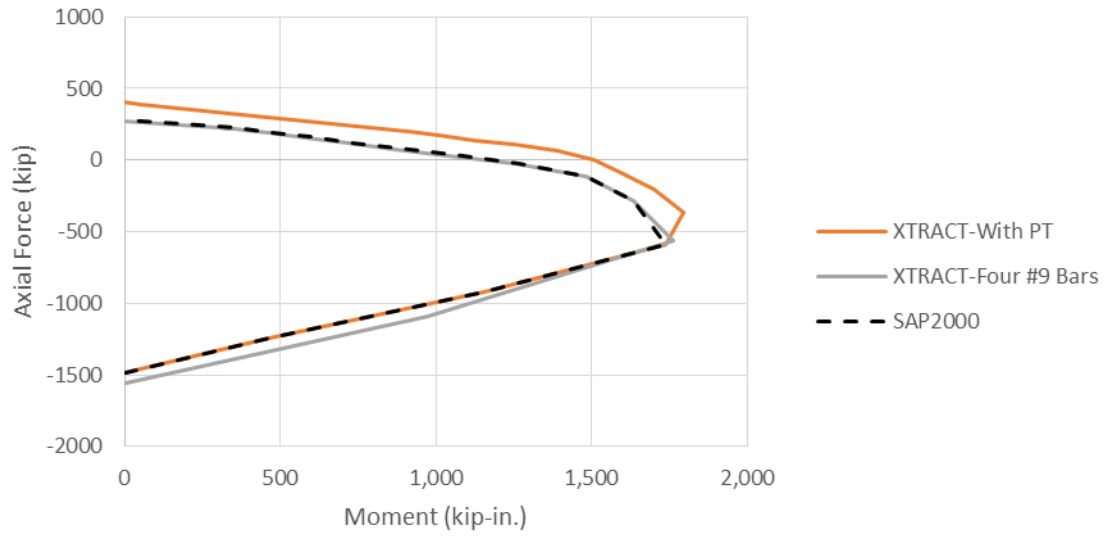


Figure 5-3 – SAP2000 P-M Interaction for Hinge Property at 1.5 ft

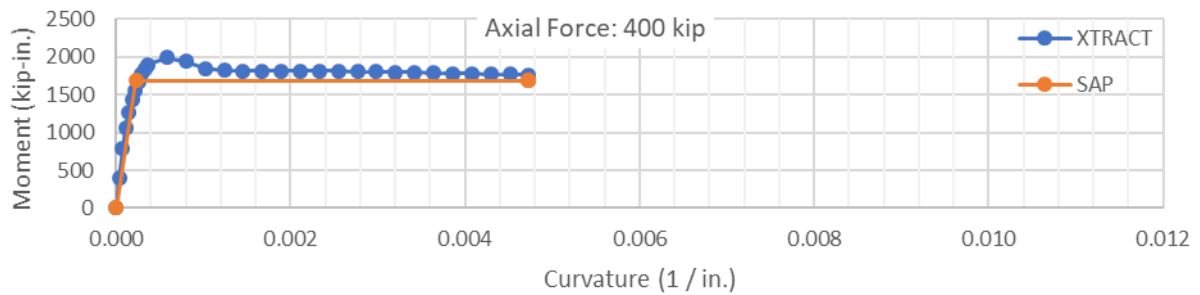
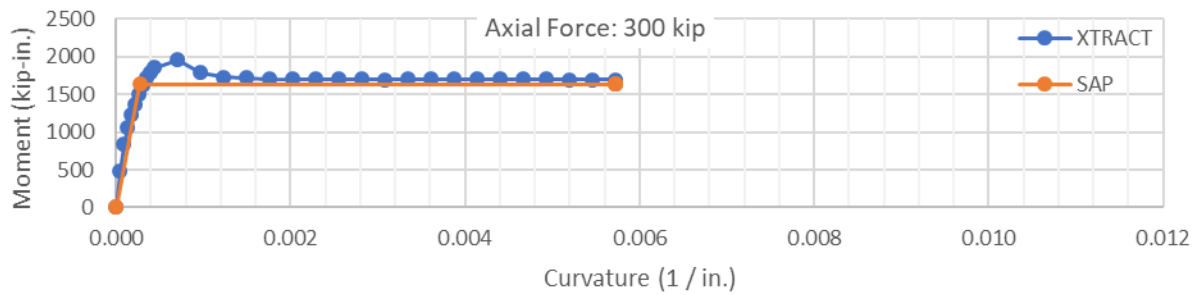
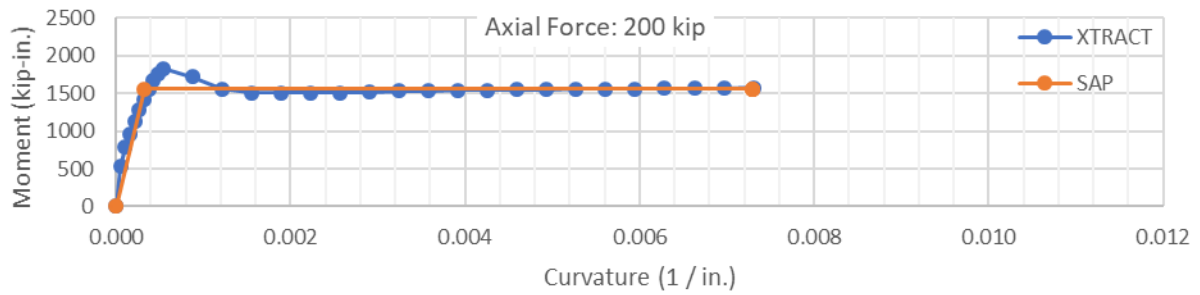
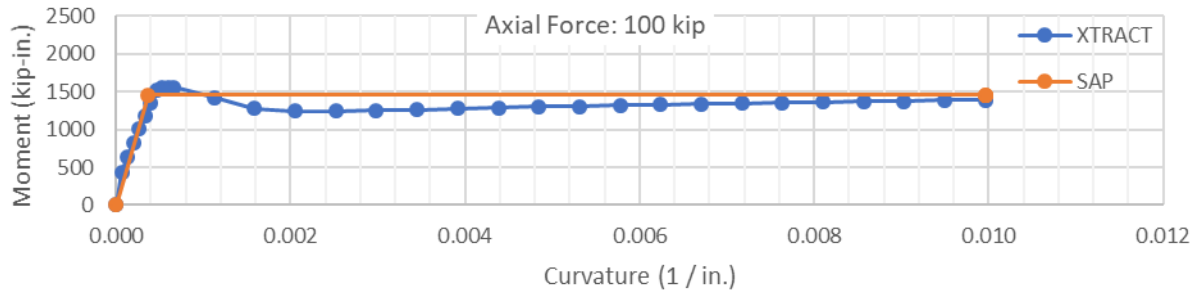
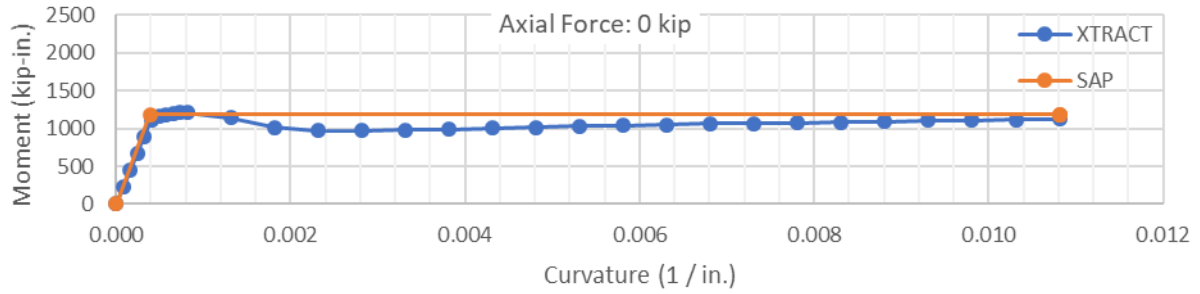


Figure 5-4 – Hinge Property *Top of Pile* Moment-Curvature for 0-400 kip Axial Force

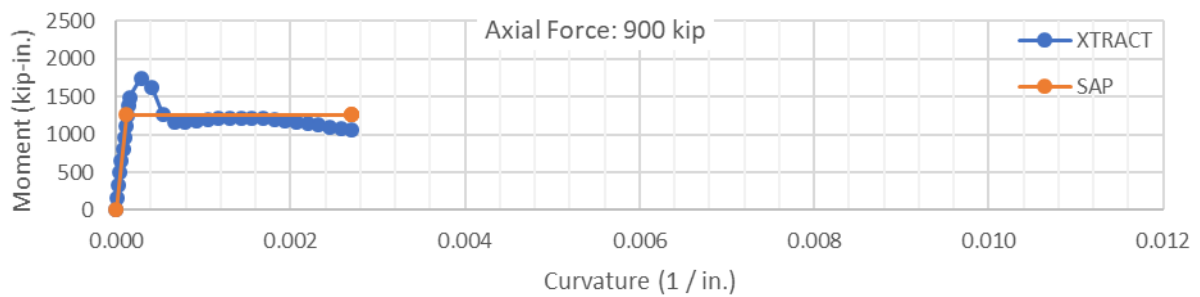
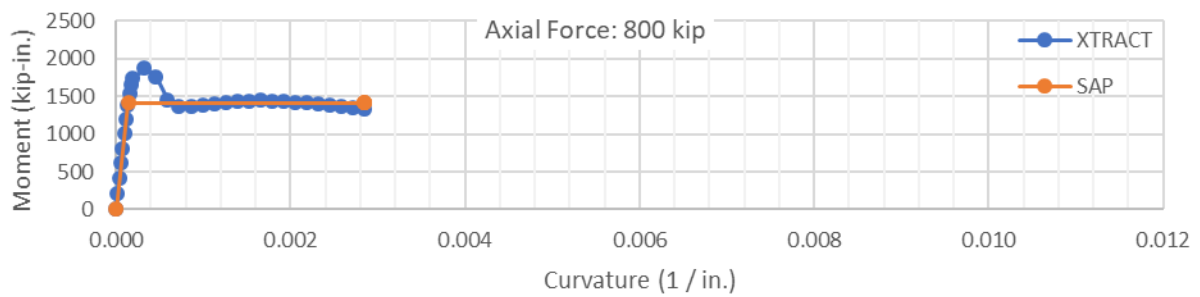
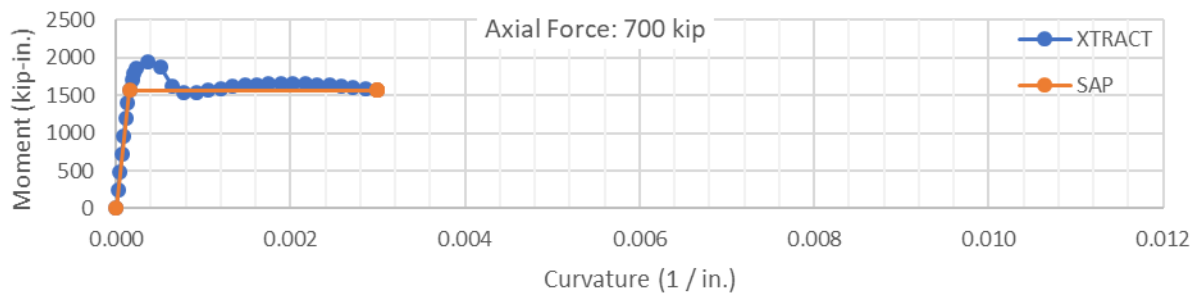
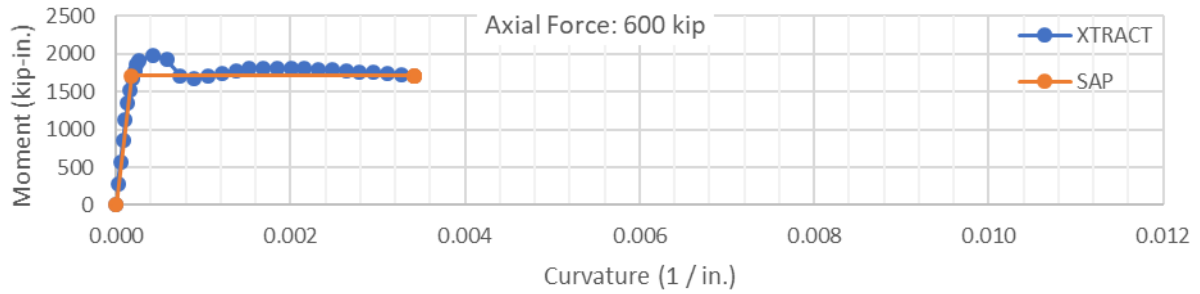
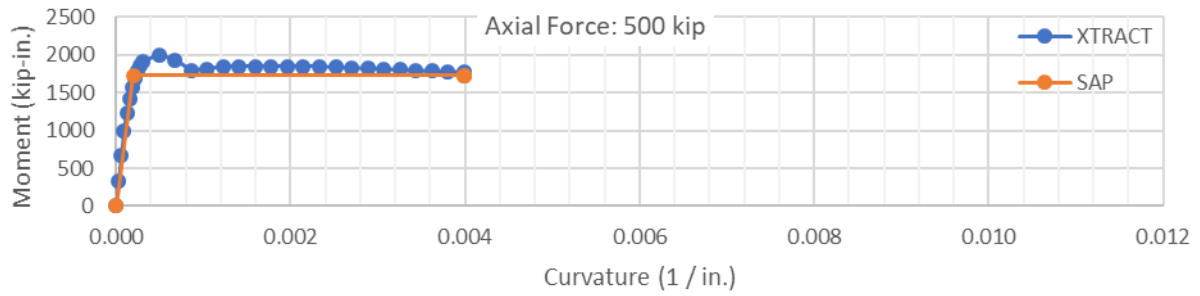


Figure 5-5 – Hinge Property *Top of Pile* Moment-Curvature for 500-900 kip Axial Force

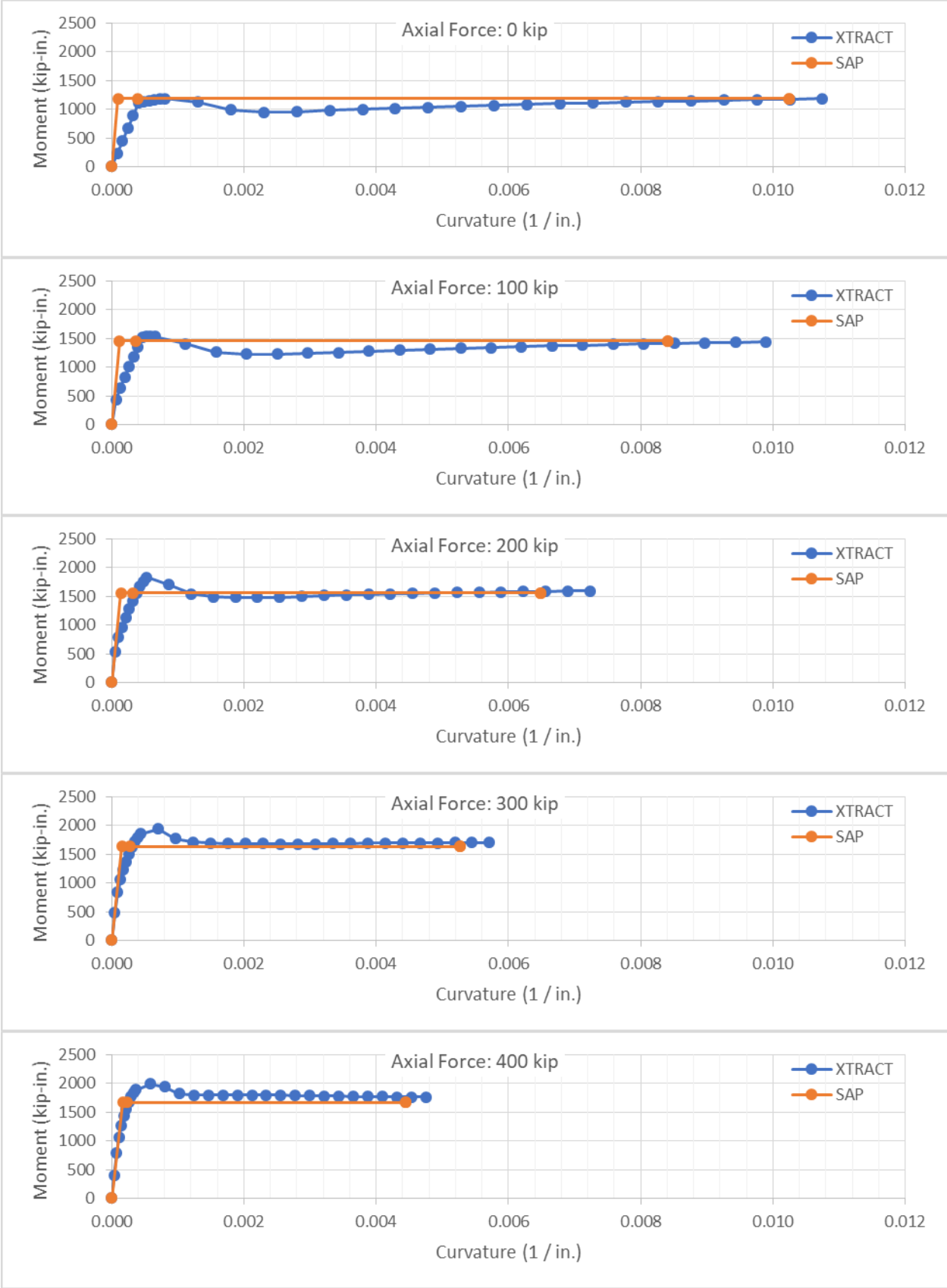


Figure 5-6 – Hinge Property at 1.5 ft Moment-Curvature for 0-400 kip Axial Force

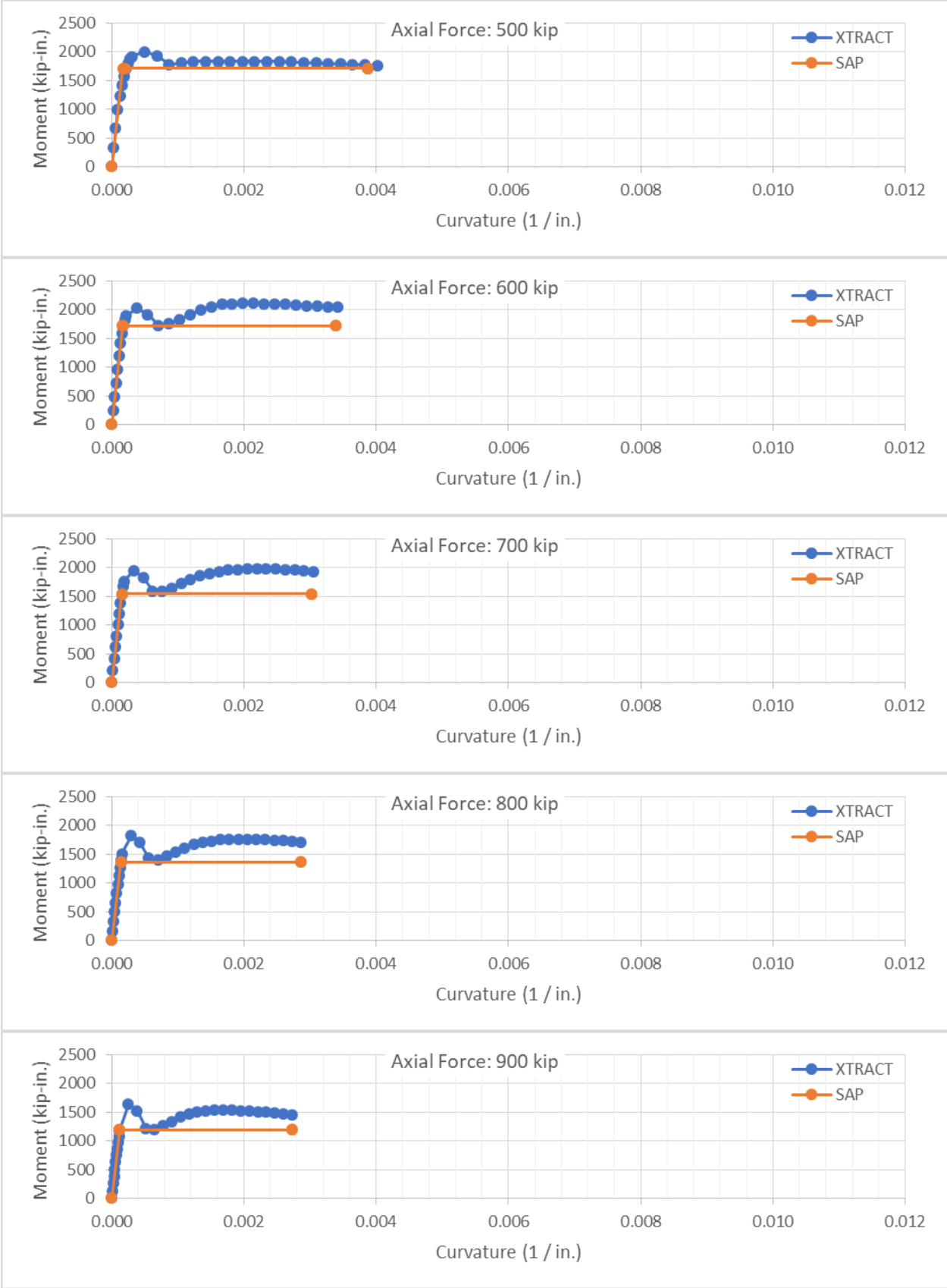


Figure 5-7 – Hinge Property at 1.5 ft Moment-Curvature for 500-900 kip Axial Force

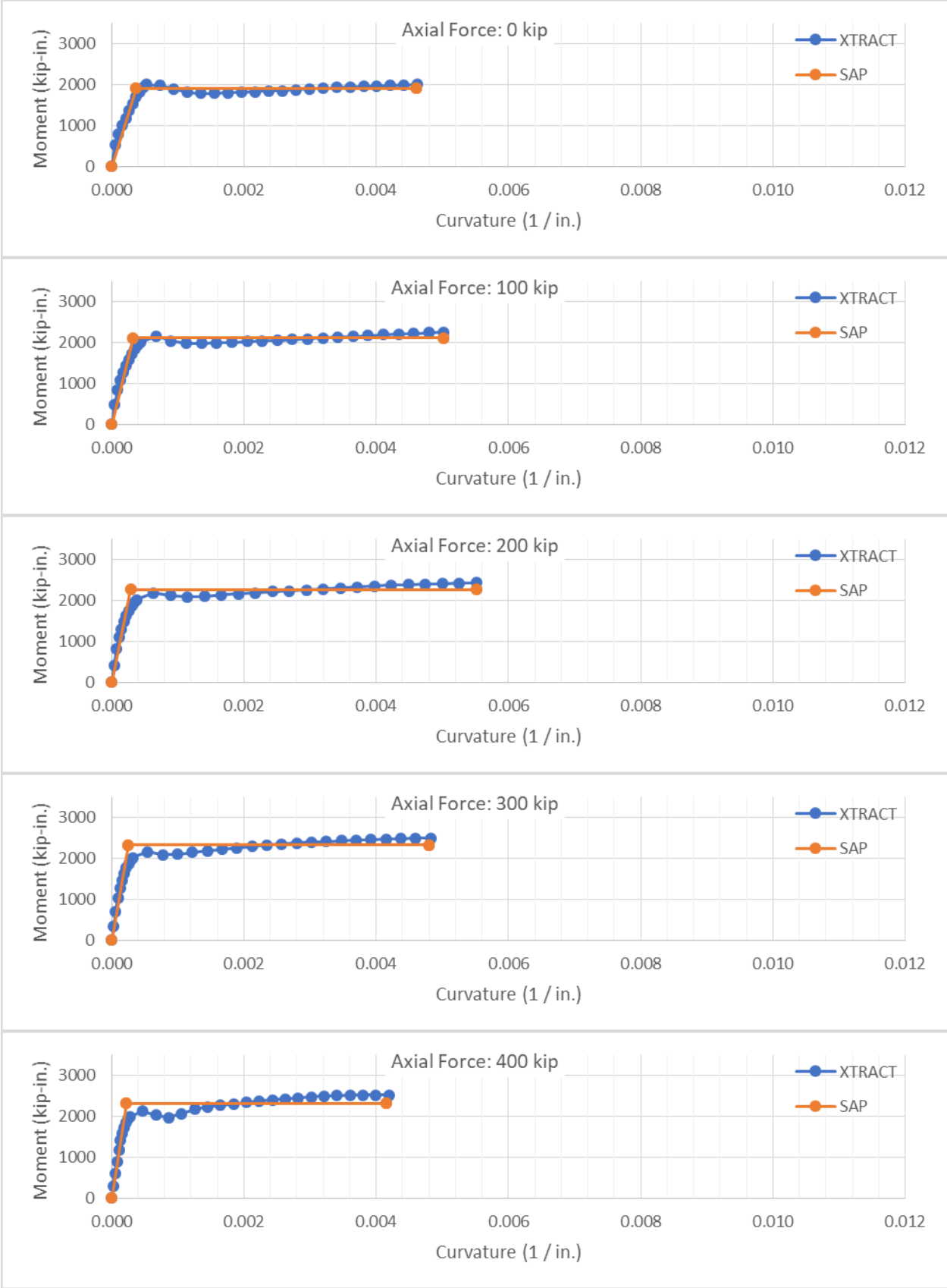


Figure 5-8 – Hinge Property at 7 ft Moment-Curvature for 0-400 kip Axial Force

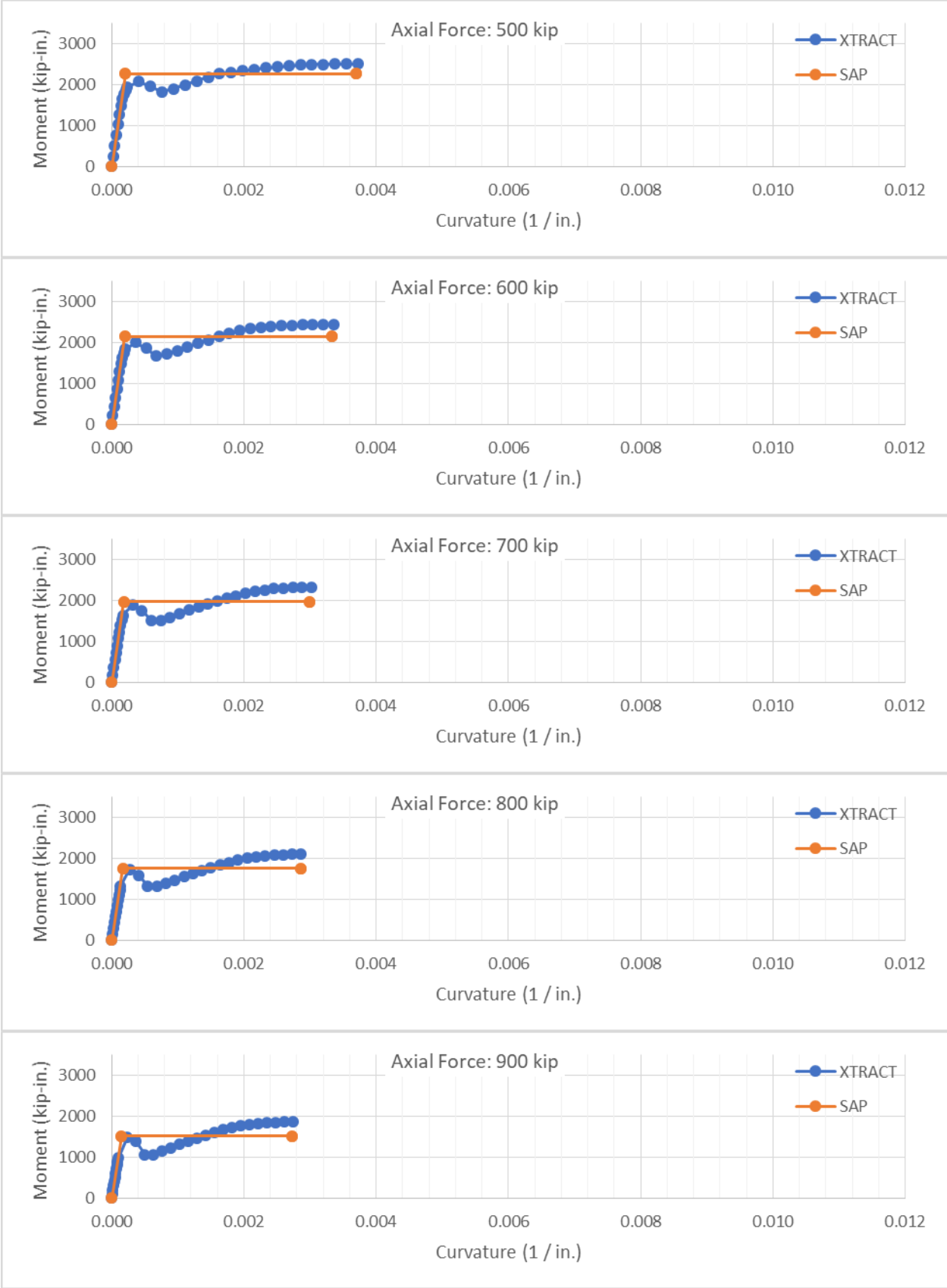


Figure 5-9 – Hinge Property at 7 ft Moment-Curvature for 500-900 kip Axial Force

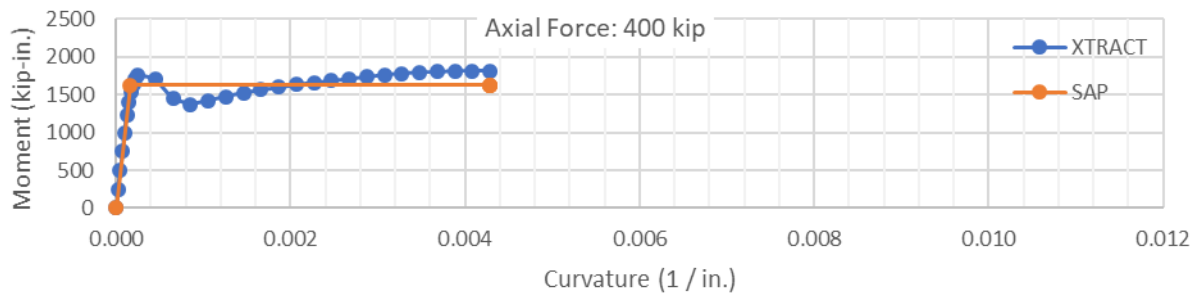
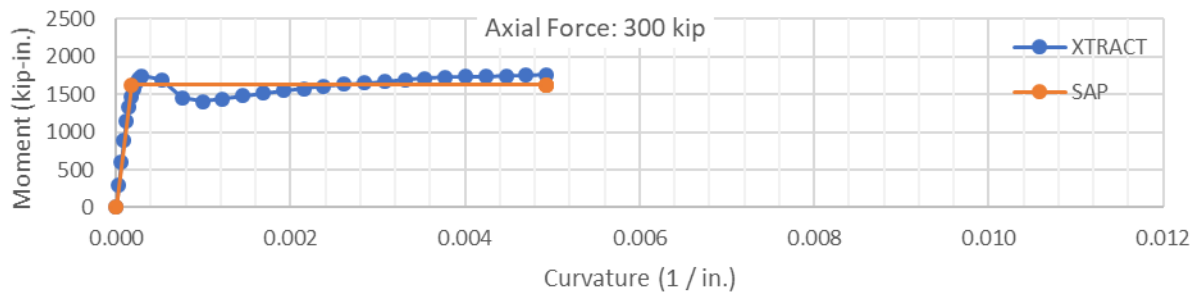
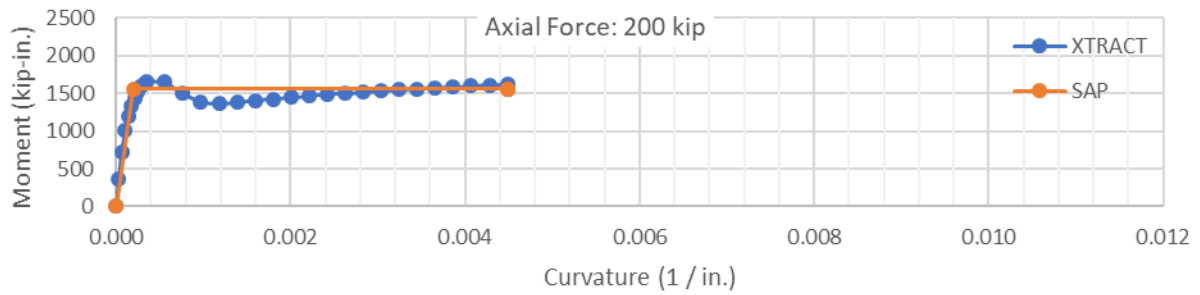
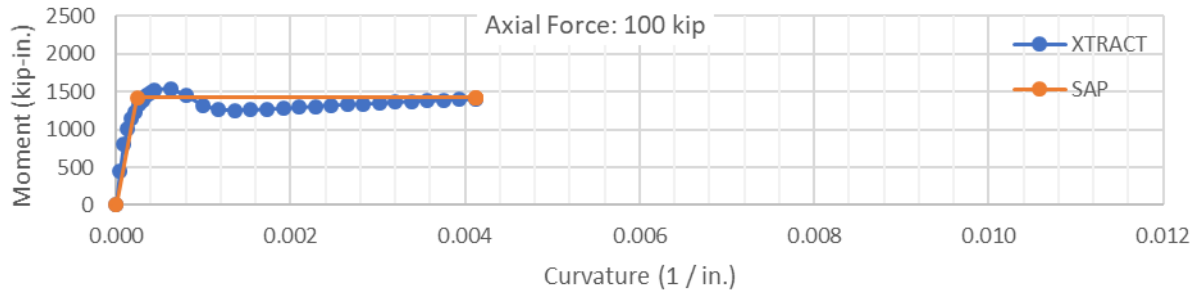
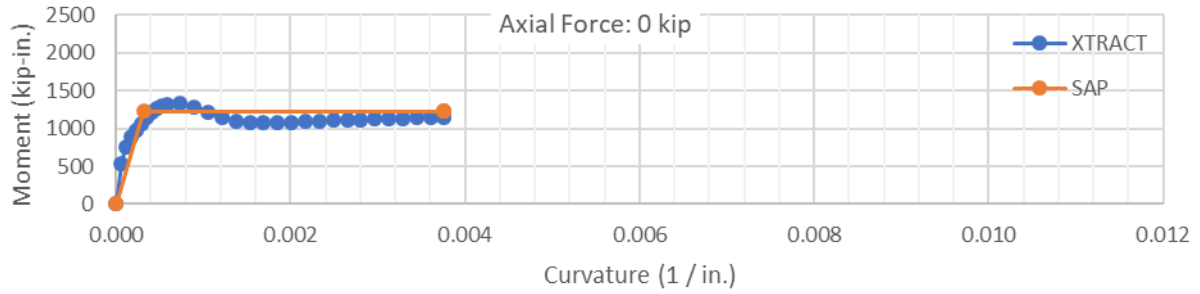


Figure 5-10 – Hinge Property at 17.67 ft Moment-Curvature for 0-400 kip Axial Force

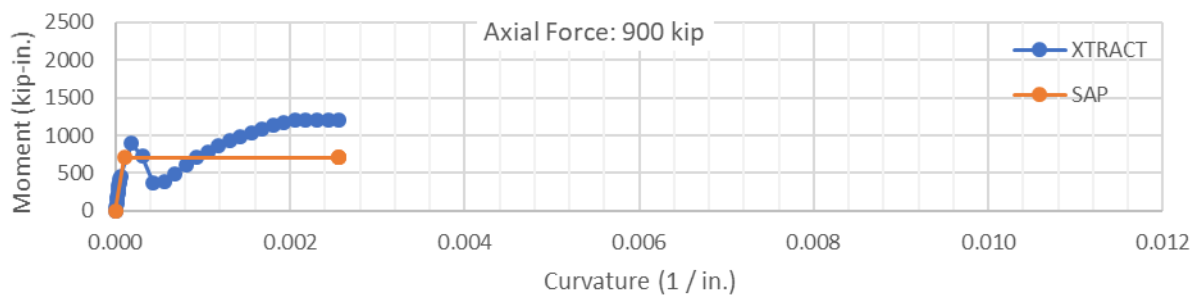
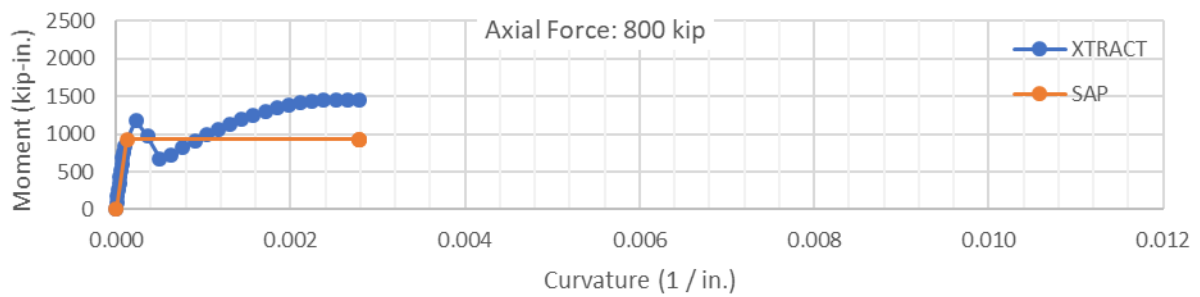
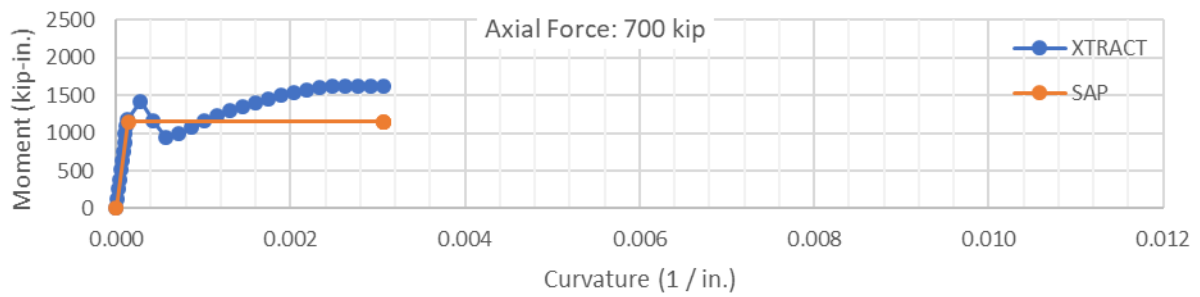
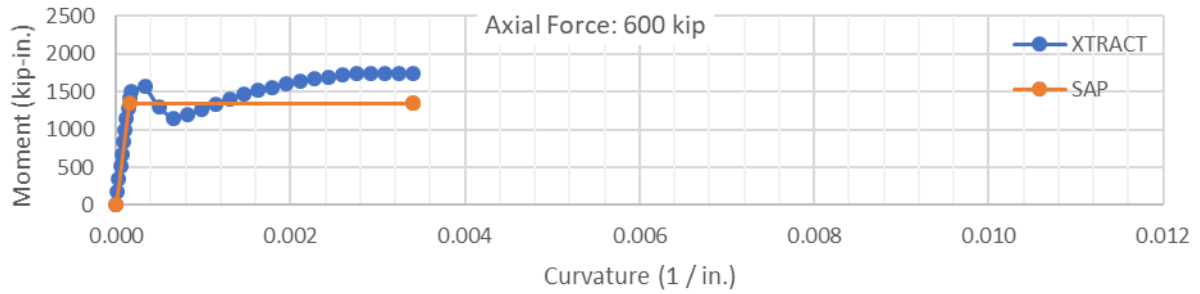
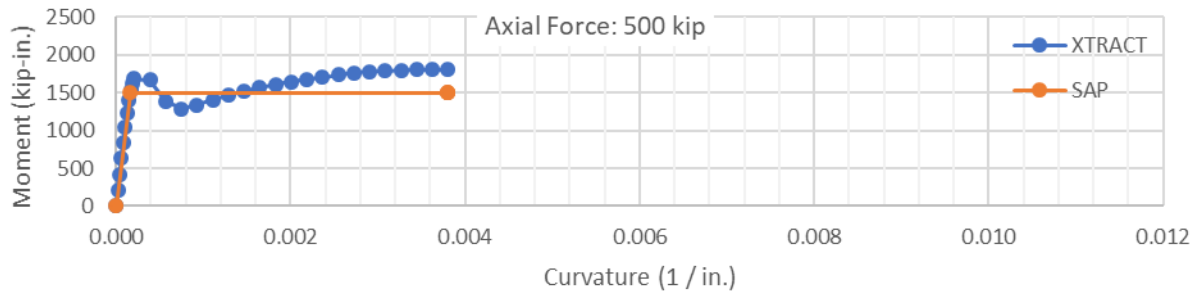


Figure 5-11 – Hinge Property at 17.67 ft Moment-Curvature for 500-900 kip Axial Force

Table 5-2 – SAP2000 Model Frame Element Section Properties

Section Property	Elastic Modulus (ksi)	Area (in²)	Moment of Inertia (in⁴)
14 in Square Pile	5437	196	3205

We analyzed the existing piles for 30 pushover analysis cases. These pushover load cases start from combinations of the following initial loads:

- Ten compressive axial loads from 0 kip to 900 kip
- Three initial pile head rotations: -1.09%, 0%, and +1.09%

All initial condition and pushover load cases considered both material (soil link and frame hinge) nonlinearities and P- Δ geometric nonlinearities. Each pushover analysis applies a Y-direction acceleration load to a unit mass lumped at the pile head, causing pile head displacements in the negative Y-direction. The pushover load case increments the magnitude of lateral acceleration load in subsequent steps, iterating until a target pile head displacement is achieved.

5.2 Individual Pile Pushover Results

For each load increment (analysis step) of the pushover load cases we record the pile head displacement and pile shear force at the pile head. We plot the individual pile force-displacement results in Figure 5-12.

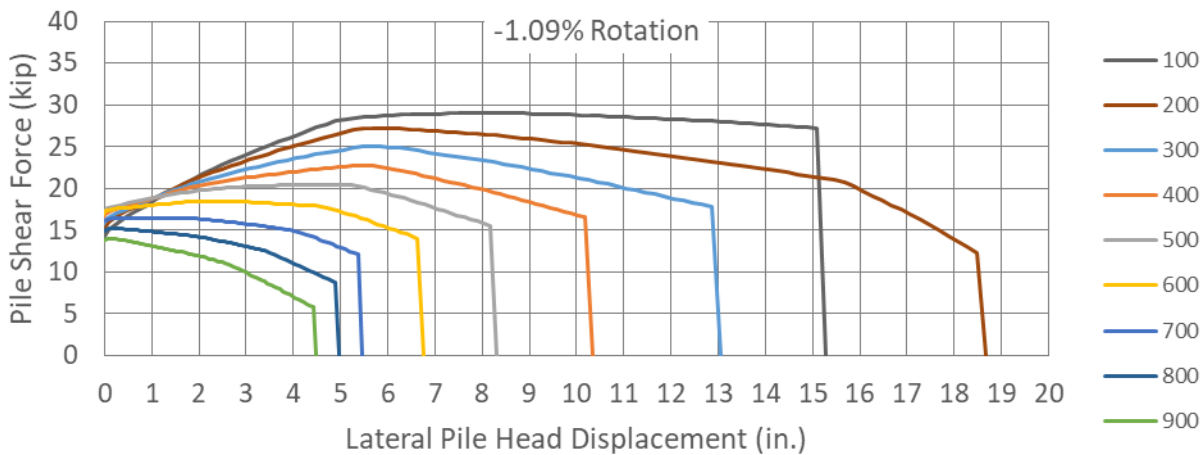
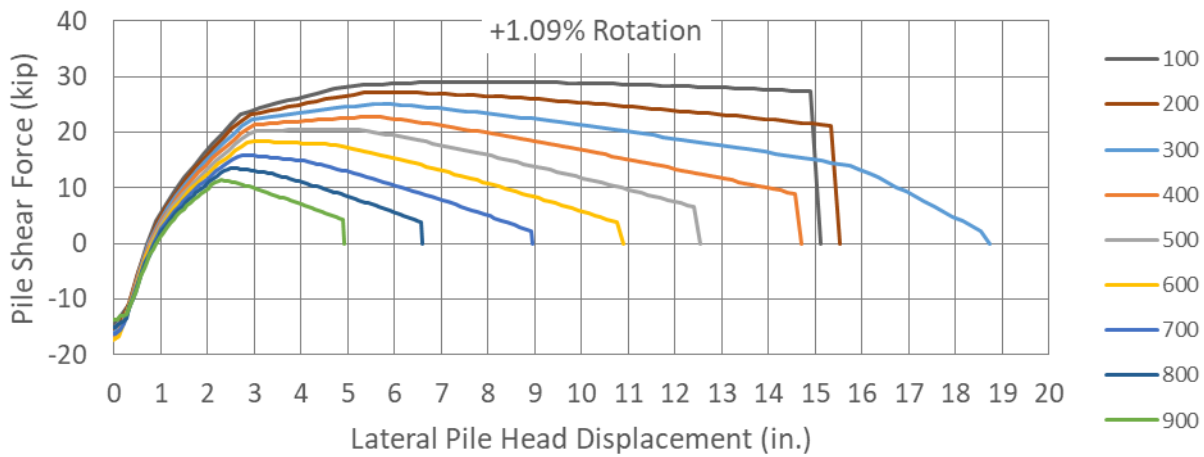
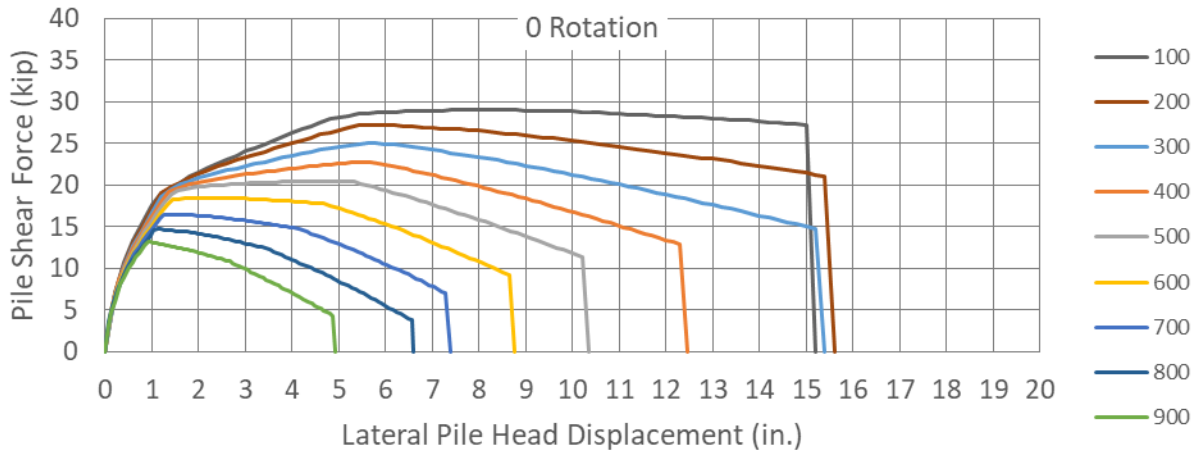


Figure 5-12 – Existing Pile Pushover Curves

When initial pile head rotations are applied, pushover results show non-zero pile shear forces at zero displacement. These initial shear forces hold the fixed pile head in place at locations where dishing and settlement of the mat have caused pile head rotation. Figure 5-13 illustrates the direction of static shear force occurring due to positive or negative pile head rotation.

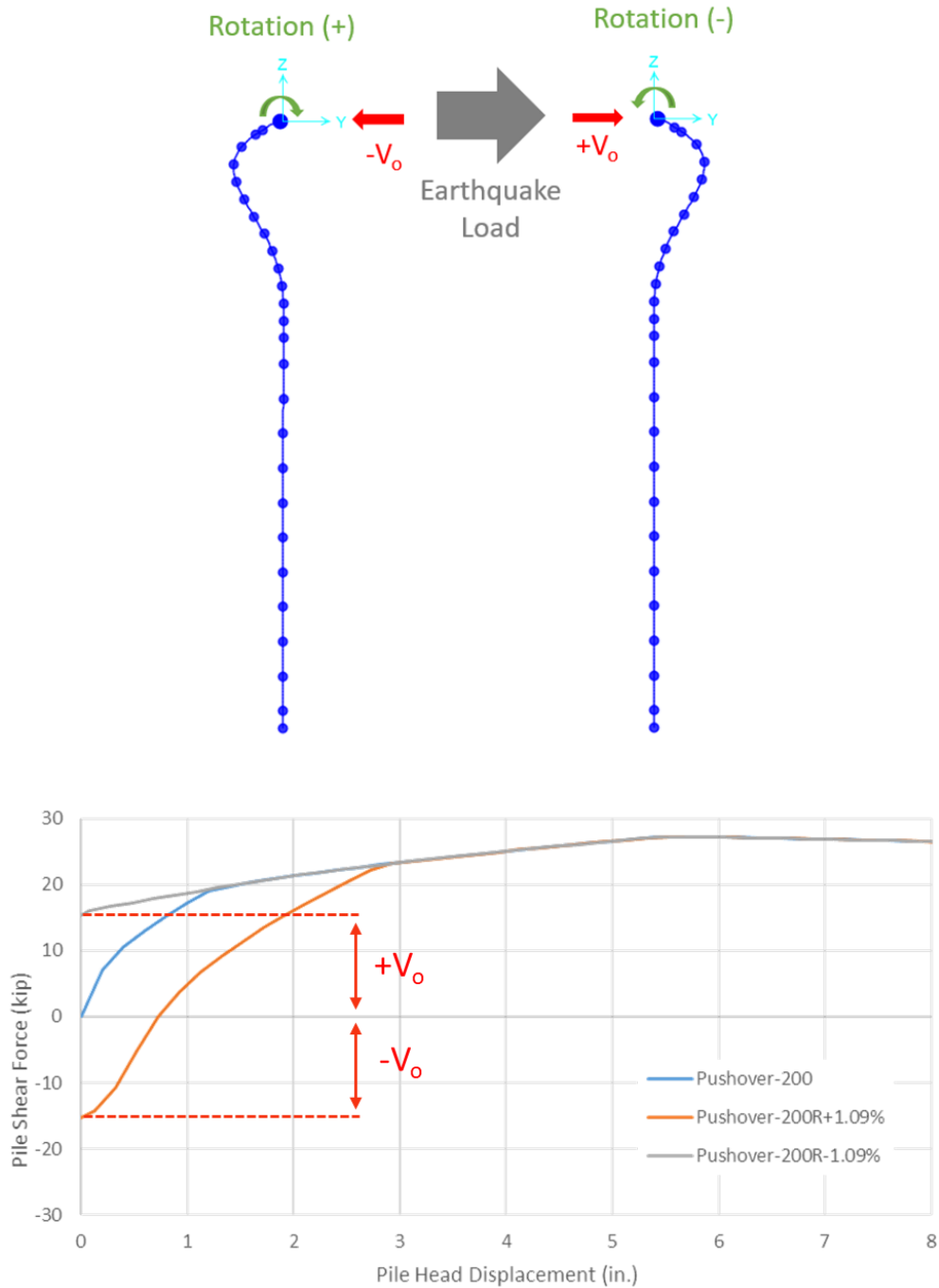


Figure 5-13 – At-Rest Pile Head Rotation and Shear

Ultimate lateral displacement capacities are indicated in Figure 5-12 as the sudden drop to zero shear force. We found that the ultimate displacement capacity of the existing piles is governed by one of two failure modes, dependent on the axial loading and initial pile head rotation:

- Exceeding the ultimate pile section curvature.
- Geometric (P- Δ) instability due to formation of three plastic hinges.

Figure 5-14 illustrates the yielding sequence of a pile with zero pile head rotation loaded to 700 kips compression. This progression of pile yield is typical for piles governed by ultimate section curvature.

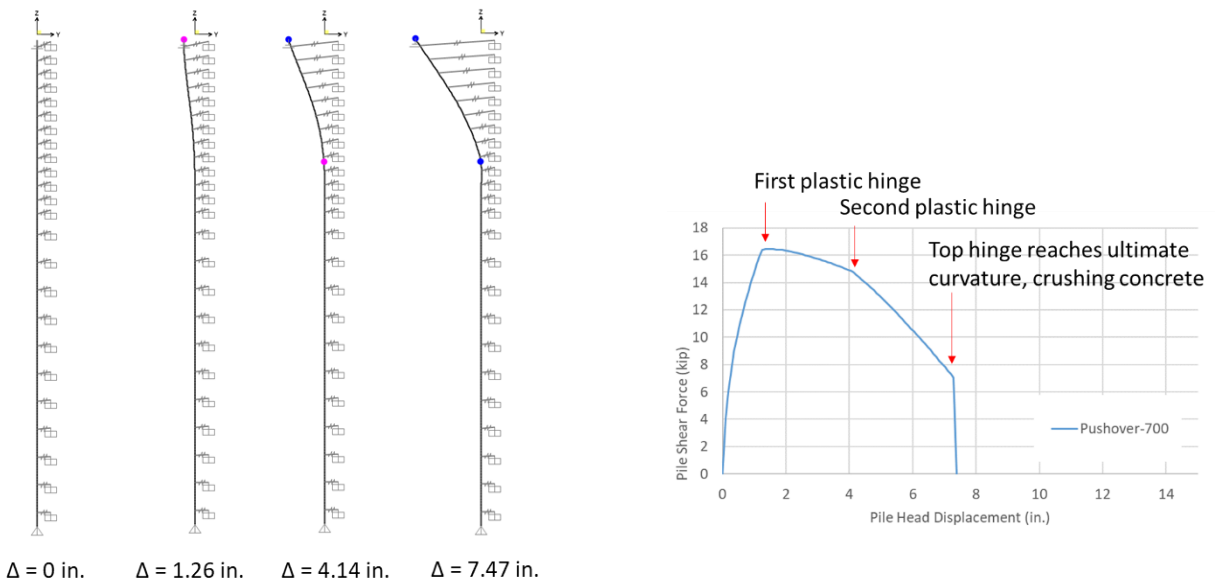


Figure 5-14 – Pile Yield Progression, 700 kip and Zero Pile Head Rotation

Figure 5-15 illustrates the yielding sequence of a pile with zero initial pile head rotation loaded to 800 kips. This progression of pile yield is typical for piles governed by P- Δ instability.

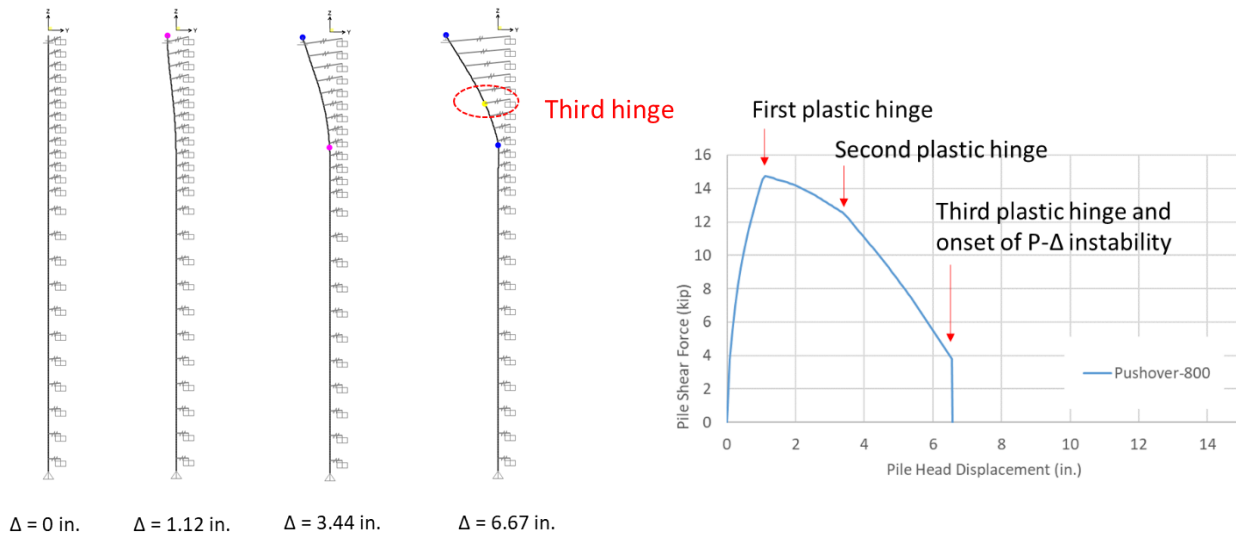


Figure 5-15 – Pile Yield Progression, 800 kip and Zero Pile Head Rotation

5.3 Combination of Pushover Results to Obtain Composite Foundation Backbones

We combined the individual pile pushover results into composite lateral foundation backbones following the steps below.

1. For each existing pile, we linearly interpolated between pushover curves shown in Figure 5-12 to the pile's axial force. We did this separately for initial pile head rotations of 0%, +1.09%, and -1.09%.
2. For each existing pile, we linearly interpolated between the three pushover curves developed in Step 1 to the pile's initial head rotation. We did this separately for the initial pile head rotation relative to earthquake loading in the four principal directions of the tower (+X, -X, +Y, and -Y).
3. For each principal direction, we summed the individual pile pushover curves developed in Step 2. This resulted in the four cumulative lateral foundation backbones shown in Figure 5-16. These backbones quantify the contribution of the existing piles to the lateral strength of the foundation (strength prior to installing retrofit piles).

In Steps 1 and 2 above, we interpolated to the pile axial loads recommended in the 30 November 2018 geotechnical report by John Egan, SLATE Geotechnical Consultants Inc., and Shannon & Wilson, Inc. The maximum pile force is 829 kip, the minimum pile force is 119 kip, and the average force for the 942 piles is 247 kip. Figure 5-17 shows the distribution of pile forces in plan. Table 5-3 lists the number of existing piles within different ranges of axial load. The majority of existing piles carry between 100 and 300 kip.

We calculated pile head rotations from the displaced shape of the PERFORM-3D mat grillage due to gravity loads and settlement. The PERFORM 3D gravity load analyses are discussed in Volume II. We extracted nodal rotations from the model and interpolated to the pile locations corresponding to the axial loads. Figure 5-18 shows contours in plan of pile head rotations. Rotation directions follow the right-hand rule, such that negative rotations YY indicate a downward slope in the negative X-direction, and positive rotations XX indicate a downward slope in the negative Y-direction.

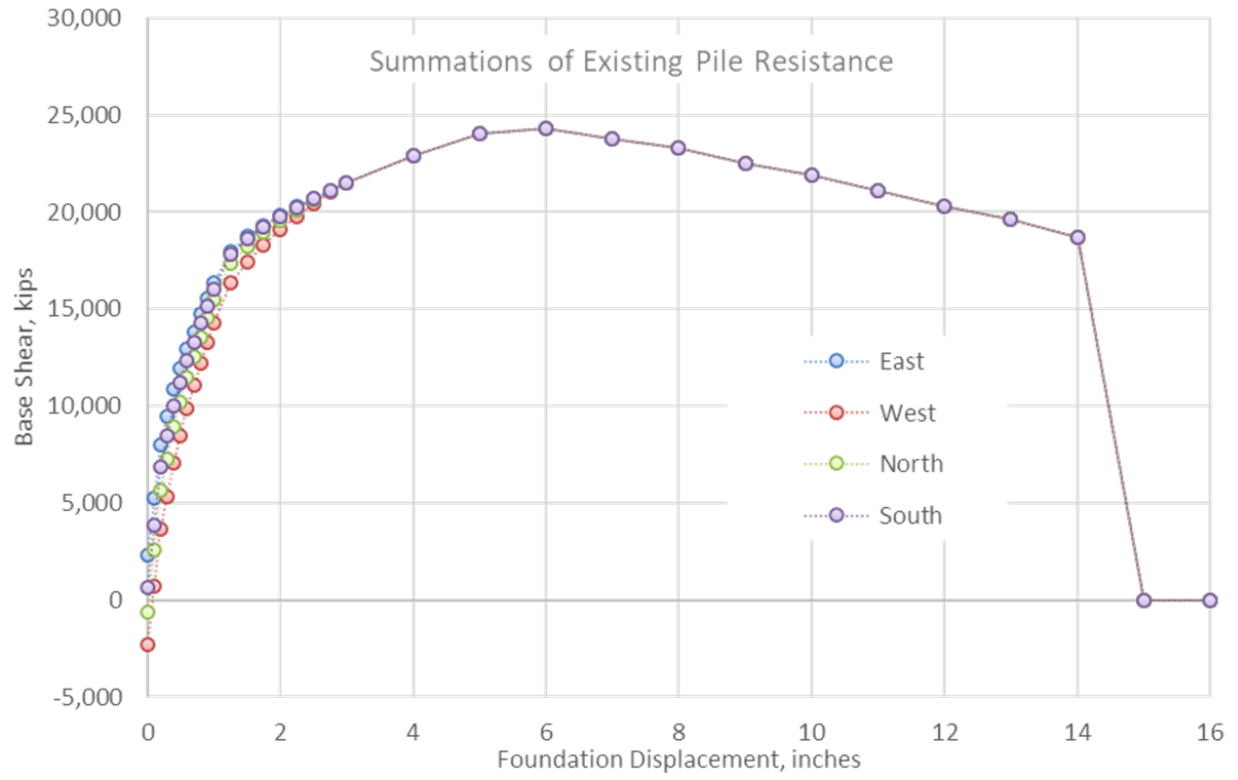


Figure 5-16 – Existing Pile Cumulative Lateral Backbones

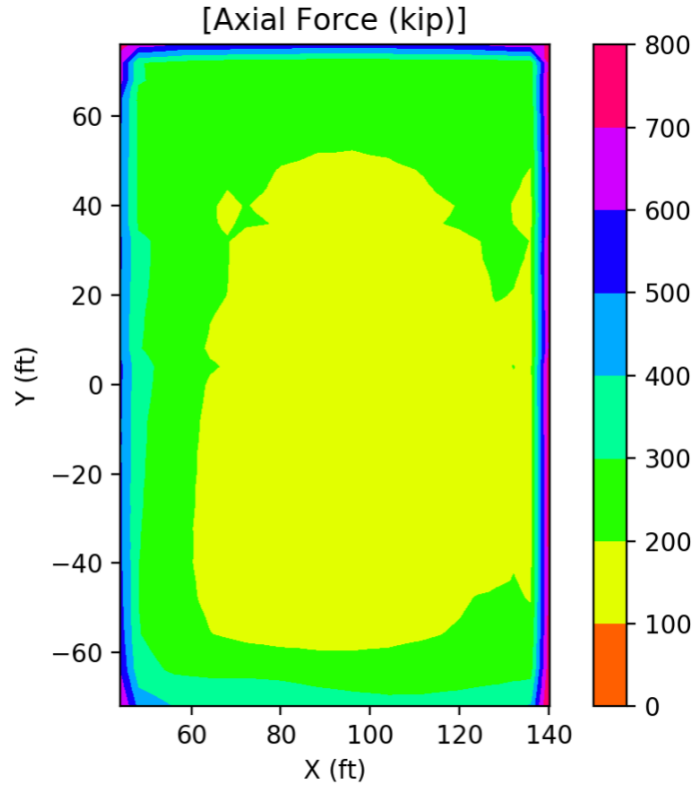


Figure 5-17 – Existing Pile Axial Load Distribution

Table 5-3 – Existing Pile Axial Loads

Pile Count	Axial Load
0	0 kip - 100 kip
453	100 kip - 200 kip
333	200 kip - 300 kip
61	300 kip - 400 kip
13	400 kip - 500 kip
41	500 kip - 600 kip
12	600 kip - 700 kip
36	700 kip - 800 kip
1	800 kip - 900 kip

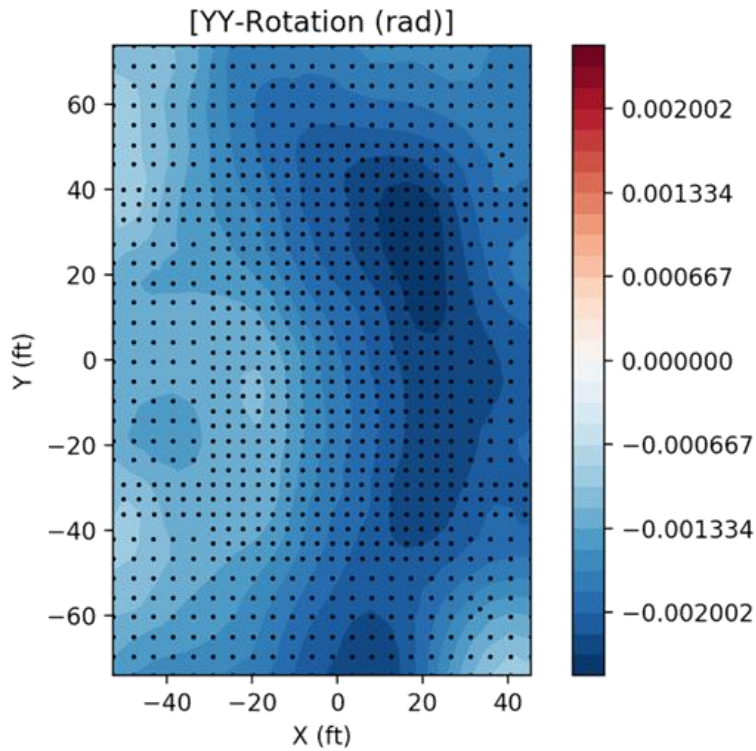
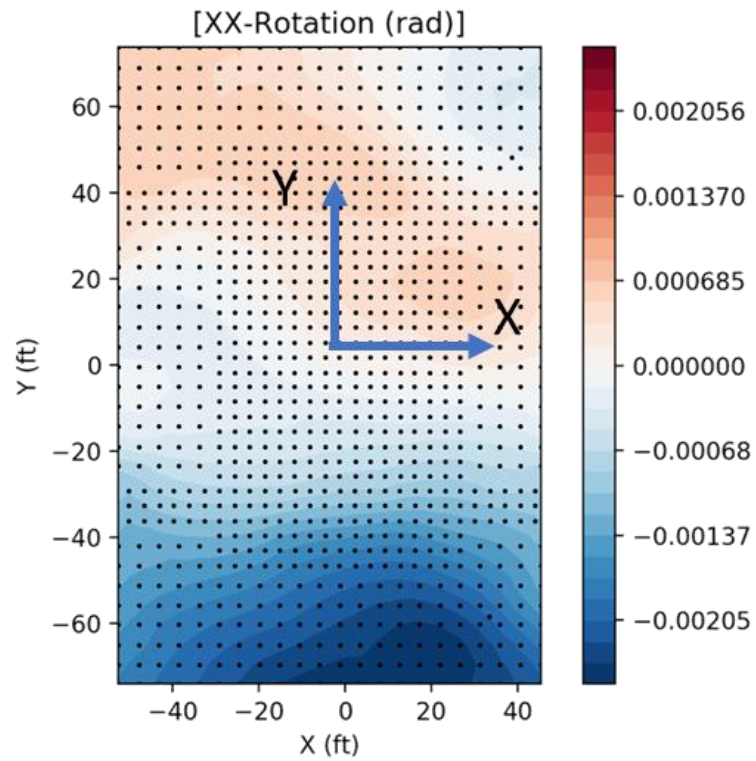


Figure 5-18 – Pile Head Rotations

5.4 Existing Pile Backbone Modifications

5.4.1 Correction for Pile Head Rotations

Settlement of the tower has induced rotations at the pile heads. The pile head rotations induce static shear forces in the foundation, as described in Section 5.2. The static shear in the piles at zero displacement is captured in the cumulative backbones shown in Figure 5-16. The cumulative static shear force in the piles is apparent as an offset of the shear force in each direction at zero displacement. We applied these cumulative static shear forces to the tower foundation in our nonlinear time history analyses described in Section 6.

We applied the following static foundation shear forces:

- 649 kip in the (-)Y –direction (i.e., to the south)
- 2,287 kip in the (+)X –direction (i.e., to the east)

5.4.2 Correction for Tower Overturning Moment

We calculated cumulative existing pile lateral force-displacement relationships (Section 5.3) based on pile axial loads due to gravity. During an earthquake, overturning of the tower is resisted by moment fixity of the foundation. The 10 ft thick foundation mat is approximately rigid relative to the soil and piles. We conducted nonlinear time history analysis of a sub-group of existing piles to investigate the effect of overturning on the cumulative foundation lateral capacity. Results of the study show a minor decrease in lateral capacity when overturning is considered (about 3% reduction in ultimate strength).

5.4.2.1 Analysis Model Description

We used SAP2000 Version 19.2.2 to model a group of nine existing piles. We used two models to study the effect of axial loads due to overturning on the total pile shear capacity. One model applies both lateral shear force and overturning moment due to earthquake loading, while the second model applies only shear.

5.4.2.2 Pile Group Model with Overturning

Figure 5-19 shows the pile group model that includes overturning in the analysis. The pile group model consists of:

- Nine identical piles, equally spaced with fixed pile-head boundary conditions and no static rotation. Each pile includes nonlinear P-M interacting hinges and nonlinear p-y soil springs identical to the ones used in the individual pile model described in Section 5.
- A cantilever SDOF oscillator with length, mass, and stiffness calibrated to the tower period and producing the desired seismic pile loading described below.
- A rigid frame to transfer shear and axial forces from the base of the cantilever to the piles. Moments are released at the connection to the pile heads to avoid loading the piles in flexure due to rotation of the superstructure. The pile heads are instead restrained against rotation in the model.

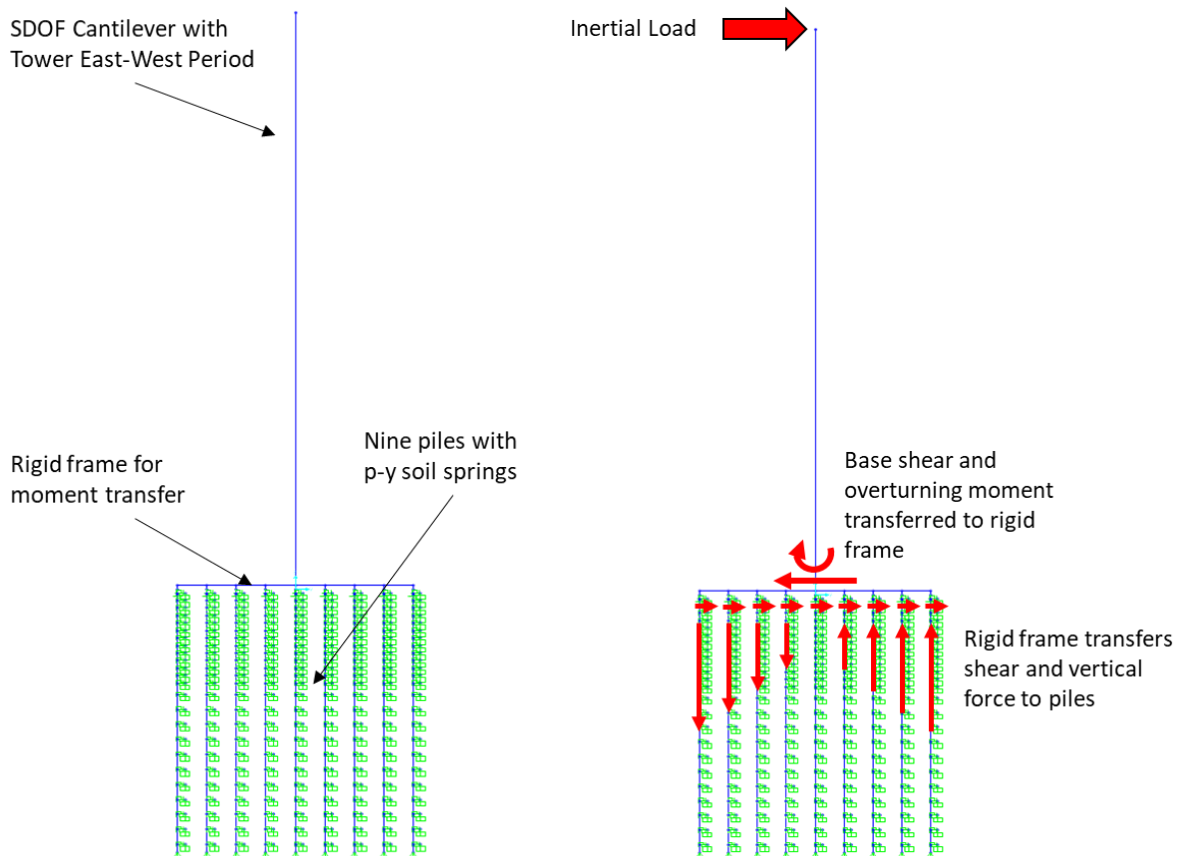


Figure 5-19 – Pile Sub-Group Model Including Overturning

The pile group was subjected to gravity load and was then analyzed for two of the time history records used in the MCE nonlinear response history analysis of the tower structure. The pile group loading resulted in:

- 250 kip initial static compression at each of the nine piles.
- Approximately 230 kip maximum seismic shear force on the pile group.
- Approximately (+/-)300 kip maximum axial force at the outermost piles due to seismic overturning.

We selected 250 kips static compression because this is the average pile loading due to gravity loads. We targeted 230 kips seismic shear force because we estimate this is the ultimate lateral capacity for a group of nine piles under an axial load of 250 kips. We targeted 300 kips as a conservative maximum axial load on the piles in the tower due to MCE-level overturning effects.

We introduced overturning to the pile group model by offsetting the cantilever mass 153.5 ft above the tops of the nine piles. We selected this height based on a preliminary time history analysis of the tower: 153.5 ft is the ratio of maximum base moment to maximum base shear of the tower. We equally spaced the piles at about 7 ft - 10 in. on center to achieve (+/-)300 kip axial force at the outermost piles simultaneous with the maximum applied seismic shear of 230 kip.

The tower X-direction (east-west) response would produce greater overturning demands on the piles because the X-direction foundation dimension is smaller than the Y-direction dimension. We therefore apply the X-direction components of the following two ground motions:

- We selected RSN#184 because in preliminary analyses it results in the greatest tower foundation lateral displacement.
- We selected RSN#178 for comparison.

Section 6 describes these ground motion records and the relative orientations of the tower principal axes to fault-parallel and fault-normal directions.

We calibrated the pile group model period to match the approximate X-direction fundamental period of the tower, accounting for period lengthening due to nonlinear response of the

superstructure. We obtained the elastic X-direction tower fundamental period from Eigen value modal analysis of the PERFORM 3D model described in Section 6.

$$\begin{aligned} T_{xe} &= \text{Elastic fundamental X-direction period} \\ &= 4.76 \text{ s} \end{aligned}$$

$$\begin{aligned} T_{xi} &= \text{Approximate inelastic X-direction period} \\ &= 1.2 * T_{xe} \\ &= 1.2 * 4.76 \\ &= 5.71 \text{ s} \end{aligned}$$

We achieved the above period of 5.71 s by adjusting the mass and stiffness of the cantilever element in conjunction with one another. We first selected the cantilever mass such that applying our selected acceleration time histories will produce the maximum desired shear force of 230 kips on the pile group. We calculated the mass from the smaller of the 2% damped spectral accelerations at 5.71 s:

$$\begin{aligned} Sa_{178X}(5.71s) &= \text{RSN\#178 X-direction 2\% damped spectral acceleration at 5.71 s} \\ &= 0.198 \text{ g} \end{aligned}$$

$$\begin{aligned} Sa_{184X}(5.71s) &= \text{RSN\#184 X-direction 2\% damped spectral acceleration at 5.71 s} \\ &= 0.209 \text{ g} \end{aligned}$$

$$\begin{aligned} m &= \text{Cantilever mass assignment} \\ &= 230 \text{ kip} / Sa_{178X}(5.71s) \\ &= 230 / 0.198 \\ &= 1,162 \text{ kip} \\ &= 3.01 \text{ kip-s}^2 / \text{in.} \end{aligned}$$

We conducted nonlinear time history analyses using the direct-integration method, which allows us to capture all the modeled nonlinearities of the pile group, including P-Delta effects. We applied initial gravity load of 250 kip at each pile with a nonlinear static load case, and continue the time history analyses from the initial loading. The ground motions are digitized at 0.005 s intervals. We computed response over at least 10 sub-steps for each input timestep to increase numerical stability and promote convergence. To avoid generating excessive data, we saved analysis output at a time interval of 0.1 s, which is adequate considering the period of the structure subject to this study.

We applied mass- and stiffness-proportional Rayleigh damping in the time history analyses. We selected Rayleigh damping parameters such that effective damping is less than 2% for periods between 0.025 s – 12 s (0.08 Hz – 40 Hz). The resulting effective damping at the system fundamental period of 5.71 s is about 1%, and the resulting effective damping at 0.01 s (100 Hz) is about 5%. We assigned this relatively low damping as a precaution; SAP2000 uses initial element stiffness values to calculate damping matrices, which can result in unrealistic damping forces in yielded nonlinear elements when using stiffness-proportional damping. Our analysis results do not suggest that these types of unrealistic damping forces occur. Hysteresis loops adhere closely to the pile group lateral resistance backbones predicted by static pushover analysis, as shown in Figure 5-21. Had we assigned excessive damping to the system, we would see total shear forces at inelastic displacements increase above those predicted by the static backbone. The results do not show these large damping forces, and we therefore conclude the assigned damping is appropriate and possibly conservative.

5.4.2.3 Pile Group Model without Overturning

We developed the pile group model without earthquake overturning moment by modifying the model described in Section 5.4.2.2. We adjusted the height of the cantilever SDOF oscillator, placing the mass at 1 in. above the pile heads to essentially remove overturning from the system lateral response. We adjusted the stiffness properties of the cantilever to match the fundamental system period of the model that includes overturning. We did not otherwise modify the pile group model. Figure 5-20 shows the pile group model that does not include overturning in the analysis.

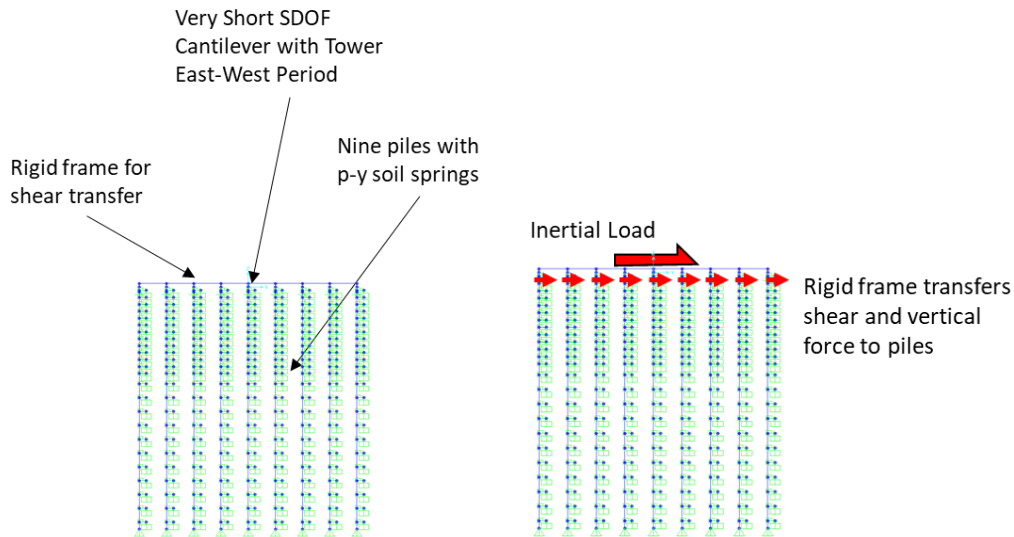


Figure 5-20 – Pile Sub-Group Model without Overturning

5.4.2.4 Analysis and Results

We conducted nonlinear time history analysis with the pile group models described above. We analyzed the models for the same two earthquake ground motion acceleration records and compared the results.

Figure 5-21 shows hysteresis results for the pile group analyses. The plots show time history results with blue dots, plotting lateral displacement at the pile heads versus the total shear force resisted by the pile group. The plots also show the predicted pile group force-displacement backbones as orange lines. We developed these static backbones by summing interpolated results of individual pile pushover analyses discussed in Section 5.2.

The hysteretic behavior of the pile group is similar whether overturning moment is included or not. The results show that maximum displacements are slightly greater when overturning is included. Figure 5-22 more clearly shows the increase in peak displacements. We compared the pile group shear force resistance at equal displacements. For both ground motions, we found that the shear force displacements of 2 in., 3 in., and 4 in. is consistently lower by about 3% when we include overturning in the analysis.

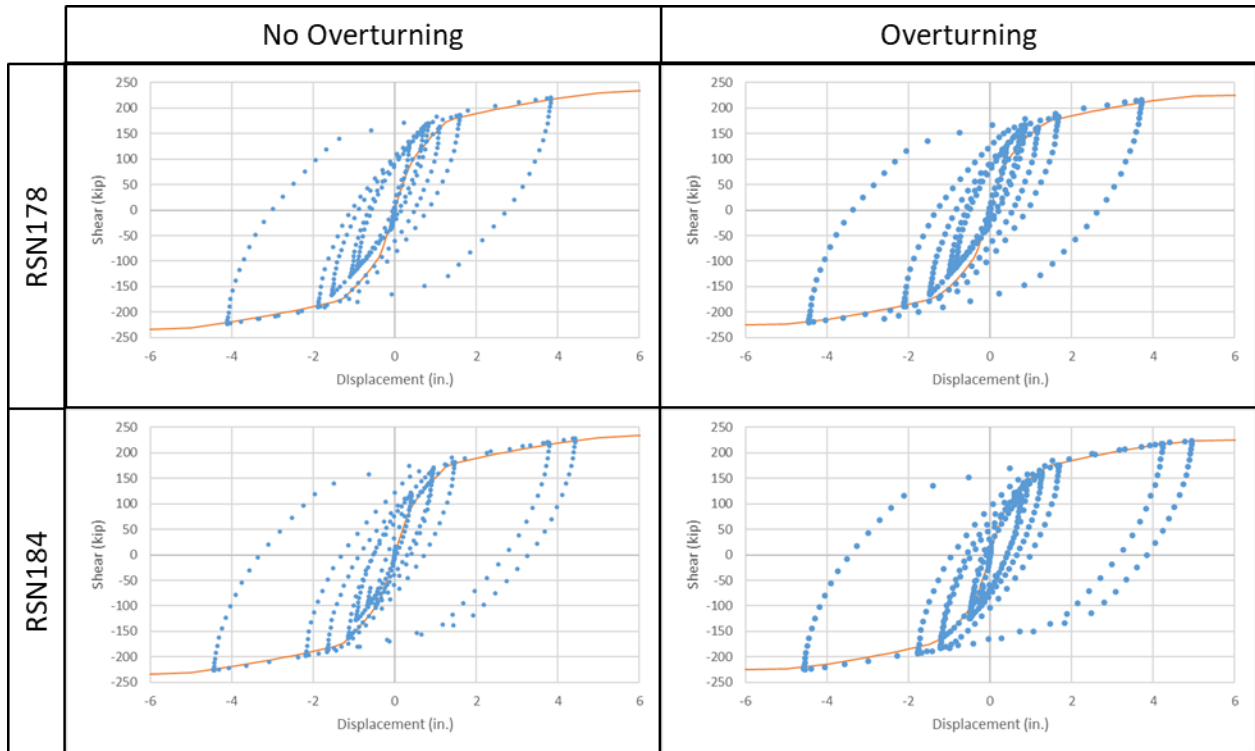


Figure 5-21 – Pile Group Overturning Study Hysteresis Results

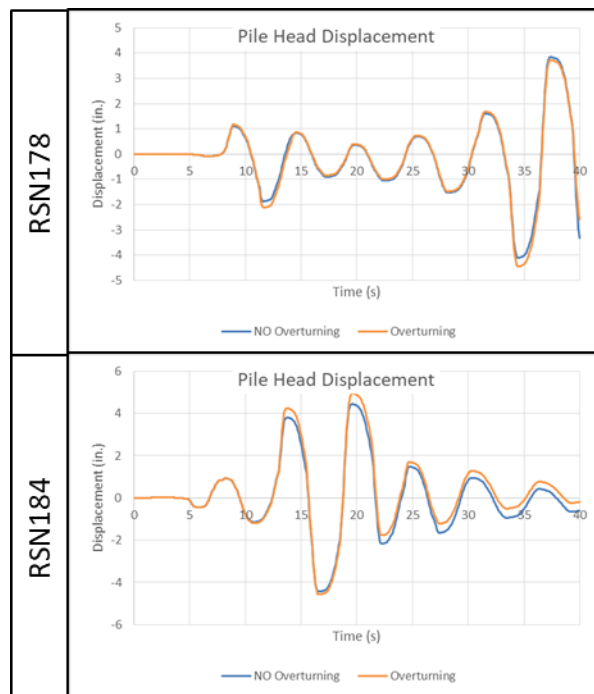


Figure 5-22 – Pile Group Overturning Study Displacement Results

6. ANALYTICAL MODEL: PERFORM 3D

We used PERFORM-3D version 6.0.1 to conduct nonlinear time history analysis of the tower. We used different models to evaluate the superstructure and substructure. We conservatively analyzed the superstructure for a pinned-base condition. The tower is a tall, long period structure experiencing large lateral displacements in an earthquake. Refined modeling at the base of the structure for analysis of the existing piles is insignificant to the superstructure response. The model we used for analysis of the superstructure includes jacking loads from the retrofit piles, capturing the change in demand on the foundation mat. We used the model described in Volume II, Section 1 to calculate superstructure seismic demands.

To analyze the tower substructure, we modified the PERFORM-3D model of the tower to account for interaction of the foundation with the surrounding soil and adjacent podium structure foundation. We used this model to evaluate the capability of the existing foundation to resist seismic base shear forces. The modified model we used for analysis of the substructure conservatively neglects the contribution of the retrofit piles to foundation capacity. Additions to the model for substructure analysis are discussed in Section 6.1.

6.1 Substructure Analysis Model Modifications

We modified the model described in Volume II, Section 1 to include soil-structure interaction effects consistent with the ‘rigid bathtub’ modeling approach recommended by PEER TBI Figure 4-6 (c). Figure 6-1 – Conceptual Soil-Structure Interaction Modeling shows conceptually how we modeled various soil-structure interaction effects. We added the following to the PERFORM-3D model of the tower:

- A lumped-mass stick model approximating east-west direction seismic response of the podium basement and above-ground mid-rise structure.
- Gap elements modeling the separation between the tower and podium embedded foundations.
- Inelastic elements modeling cumulative lateral resistance from the existing piles and embedded tower foundation in all four principal plan directions.
- Inelastic elements modeling east-west direction lateral resistance at the podium embedded foundation.

- An isolator element modeling soil friction resistance on the embedded podium foundation.

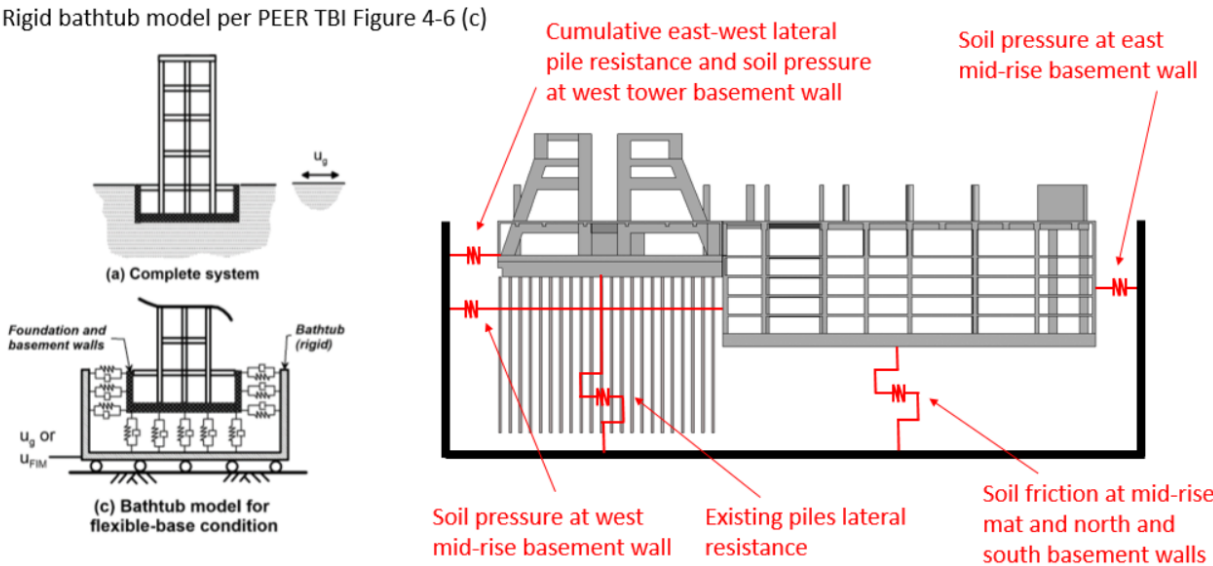


Figure 6-1 – Conceptual Soil-Structure Interaction Modeling

6.1.1 Podium Structure Model

We modeled the podium structure with a lumped mass stick model. We used the DeSimone structural drawings, dated 4 April 2008 as the basis for our model. Figure 6-2 shows an overview of the podium model, and Figure 6-3 shows the model incorporation into the PERFORM-3D model of the tower. We modeled the expected mass of the podium, including superimposed dead loads and 25% of live loads. We assumed a self-weight of 145 pcf for normalweight concrete and estimated superimposed dead and live loads based on our understanding of the occupancy and finishes in the building. We used a curtain wall weight of 15psf vertical at the perimeter of the podium and tower. Table 6-1 and Table 6-2 summarize our assumptions used for each occupancy and floor level.

We included the self-weight of the mat foundation and superimposed dead and 25% live loads at level B5. The majority of the mat is 6ft thick, but a portion at the east side is 8ft thick. The self-weight of the 8ft thick portion of the mat is 9,309 kip, and the self-weight of the 6ft thick portion of the mat is 19,632 kip. We estimated the superimposed dead and unreduced live load acting on the mat at 214 kip and 1,224 kip, respectively.

Table 6-3 lists the total expected weight (Dead + Superimposed Dead + 25% Live) at each floor of the podium structure and the floor heights relative to the ground level (L1).

Table 6-1 – Live Loads Used in Podium Structure Mass Estimate

Occupancy	Live Load, psf
Residential	40
Mechanical	75
Lobby	100
Parking	40

Table 6-2 – Summary of Loads at Each Podium Floor

Level	Height	Slab	DL, psf	Floor Finish	CMEP	Partitions	Concrete Pads	Curtain Wall, lb/ft	SDL, psf	Occupancy	0.25LL
14	11.00	12-in. NWC	145	30	15	0	12	165	57	Mechanical	18.75
13	12.83	12-inch NWC	145	7	5	10	0	193	22	Residential	10
12	10.75	12-in. NWC	145	7	5	10	0	161	22	Residential	10
11	10.75	9-in. PT NWC	109	7	5	10	0	161	22	Residential	10
10	10.75	9-in. PT NWC	109	7	5	10	0	161	22	Residential	10
9	10.75	9-in. PT NWC	109	7	5	10	0	161	22	Residential	10
8	10.75	9-in. PT NWC	109	7	5	10	0	161	22	Residential	10
7	10.75	9-in. PT NWC	109	7	5	10	0	161	22	Residential	10
6	10.75	9-in. PT NWC	109	7	5	10	0	161	22	Residential	10
5	10.75	9-in. PT NWC	109	7	5	10	0	161	22	Residential	10
4	10.75	9-in. PT NWC	109	7	5	10	0	161	22	Residential	10
3	15.42	12-in. NWC	145	20	5	10	0	231	35	Lobby	25
2	17.33	12-in. NWC	145	20	5	10	0	260	35	Lobby	25
1	15.00	12-in. NWC	145	20	5	10	0	225	35	Lobby	25
B1	9.00	12-in. NWC	145	2	5	0	0	135	7	Parking	10
B2	9.00	12-in. NWC	145	2	5	0	0	135	7	Parking	10
B3	9.00	12-in. NWC	145	2	5	0	0	135	7	Parking	10
B4	9.00	12-in. NWC	145	2	5	0	0	135	7	Parking	10
B5				2	5	0	0	0	7	Parking	10

Table 6-3 – Podium Structure Weights

	Level	Weight (kip)	Height (ft)
13-Story Mid-Rise	14	2201	142.58
	12	2669	131.58
	11	2214	118.75
	10	2237	108
	9	2247	97.25
	8	2237	86.5
	7	2237	75.75
	6	2237	65
	5	2237	54.25
	4	2366	43.5
	3	4191	32.75
	2	8563	17.33
Basement (Parking Garage)	1	10256	0
	B1	7078	-15.75
	B2	7609	-25
	B3	7525	-34
	B4	7616	-43
	B5	29461	-52
Mid-Rise Sum		35637	
Basement Sum		69545	
Structure Total		105182	

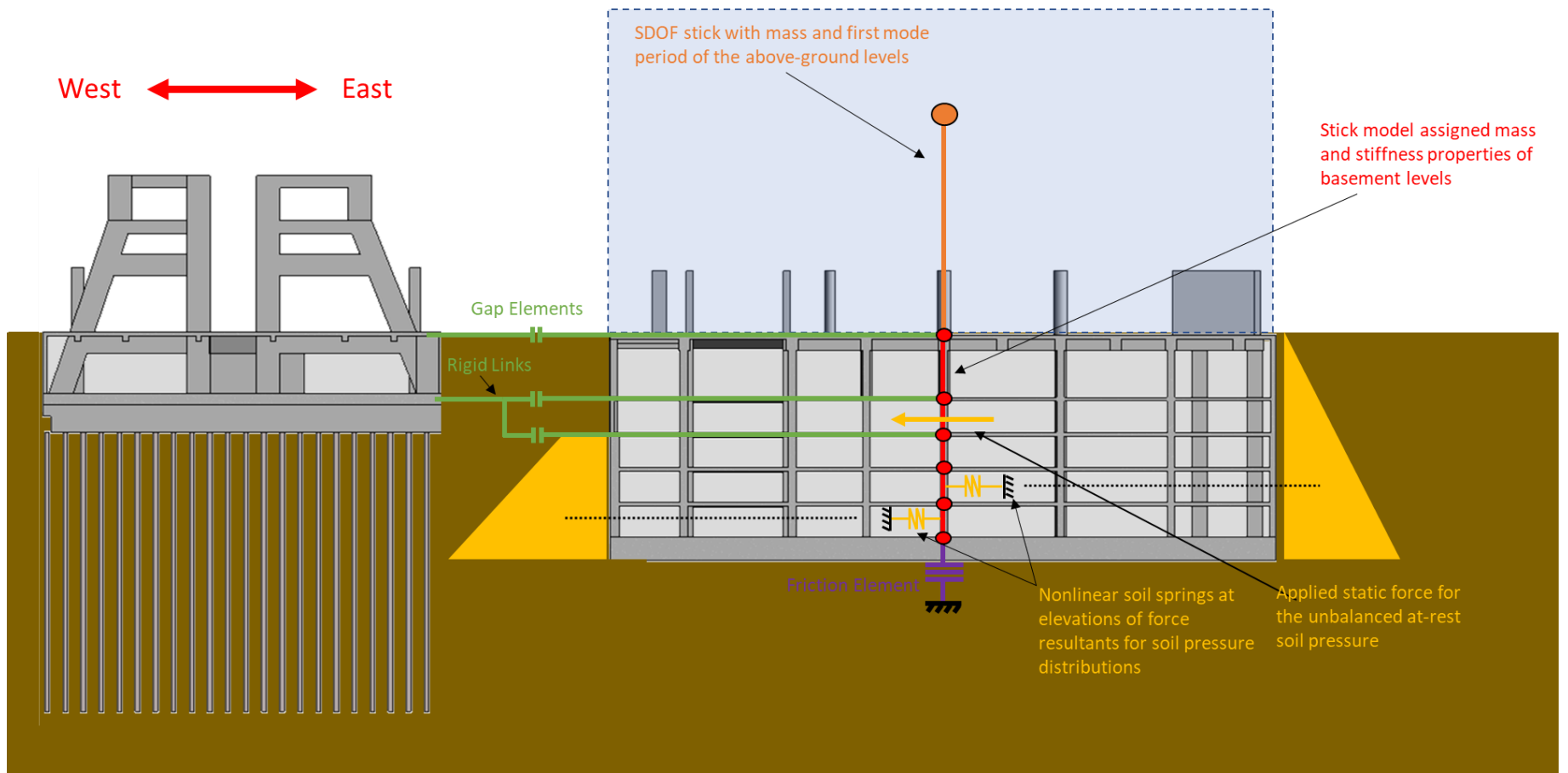


Figure 6-2 – Podium Basement and Mid-Rise Model Schematic

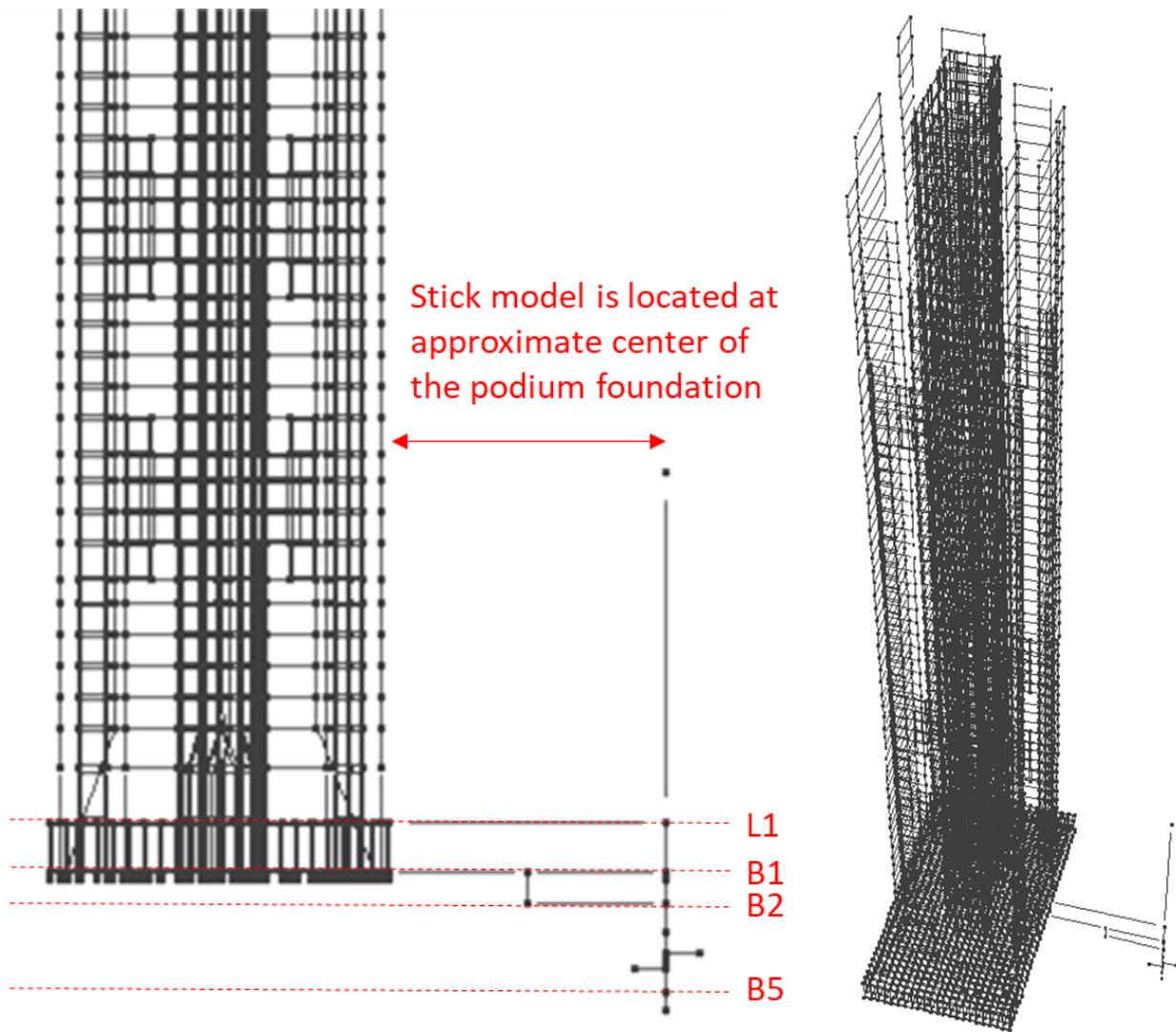


Figure 6-3 – Podium Basement and Mid-Rise Model in PERFORM 3-D

As shown in Figure 6-2, we modeled the above-ground 13-story mid-rise using a single-degree-of-freedom cantilever. The model conservatively assumes 100% of the above-ground mass participating in the first mode of the mid-rise. We estimated the east-west direction first mode period of the mid-rise using ASCE/SEI 7-10 Equation 12.8-7 for concrete shear wall structures.

$$T_a = \frac{0.0019}{\sqrt{C_w}} h_n \quad (\text{ASCE/SEI 7-10 Equation 12.8-9})$$

$$C_w = \frac{100}{A_B} \sum_{i=1}^x \frac{A_i}{\left[1 + 0.83 \left(\frac{h_i}{D_i} \right)^2 \right]} \quad (\text{ASCE/SEI 7-10 Equation 12.8-10})$$

A_B	=	Area of base of structure
	=	10,114 ft ² (typical midrise floor area)
h_n	=	Structure height
	=	142.58 ft
A_i	=	Web area of shear wall i
D_i	=	Length of shear wall i
h_i	=	Height of shear wall i
x	=	Number of shear walls in the building effective in resisting lateral forces in the direction under consideration

Figure 6-4 highlights the six east-west direction mid-rise reinforced concrete shear walls. All six walls extend the full height of the structure. Table 6-4 lists the shear wall dimensions needed for ASCE/SEI 7-10 Equation 12.8-10.

Table 6-4 – Mid-Rise East-West Direction Shear Walls

Shear Wall	Length (D) ft	Height (h) ft	Area (A) ft ²	A / (1+0.83(h/D) ²)
E.4	17.250	142.58	34.5	0.598
C.8	17.250	142.58	34.5	0.598
C.4	13.250	142.58	33.125	0.341
D.5	13.250	142.58	26.5	0.273
E.1	13.250	142.58	26.5	0.273
F.1	6.250	142.58	12.5	0.029
SUM:				2.112

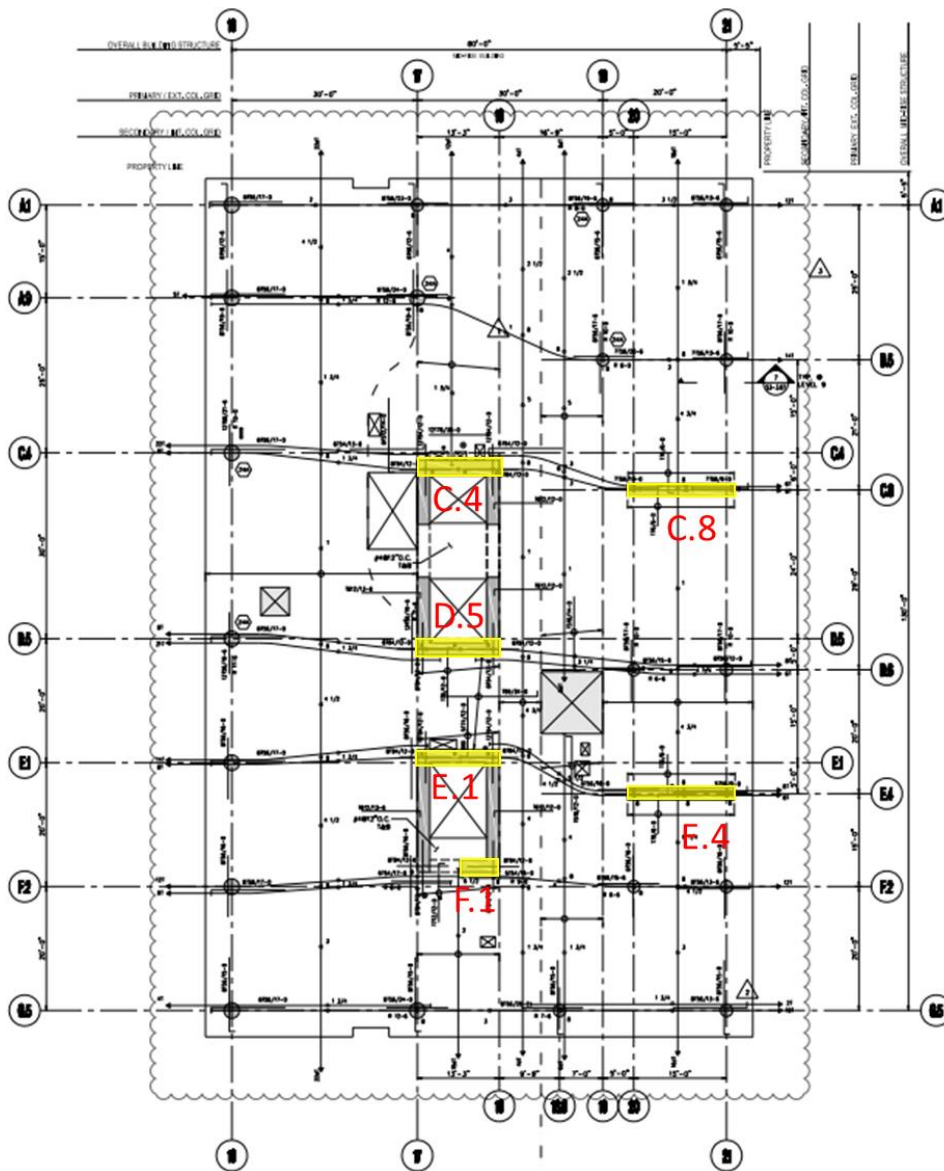


Figure 6-4 – Mid-Rise East-West Direction Shear Walls

$$\begin{aligned}
\sum_{i=1}^x \frac{A_i}{\left[1 + 0.83 \left(\frac{h_i}{D_i}\right)^2\right]} &= 2.112 && \text{(Table 6-4)} \\
C_v &= (100 / 10,114) * 2.112 \\
&= 0.02088 \\
T &= [0.0019 / (0.02088)^{0.5}] * 142.58 \\
&= 1.87 \text{ s}
\end{aligned}$$

To account for period lengthening due to inelastic response of the mid-rise to the MCE, we applied a factor of 1.2 to the elastic east-west direction period calculated above.

$$1.2 * T = 2.25 \text{ s}$$

We used ASCE/SEI 7-10 Equation 12.8-12 to estimate the ratio of overturning moment to base shear consistent with the equivalent lateral force procedure.

$$C_{vx} = \frac{w_x h_x^k}{\sum_{i=1}^n w_i h_i^k} \quad \text{(ASCE 7-10 Equation 12.8-12)}$$

Where C_{vx} is the vertical distribution factor for level x , equal to the percentage of total base shear acting at level x . The exponent k , is dependent on the structure period. For $T \leq 0.5$ s, k is 1. For $T \geq 2.5$, k is 2. For the effective east-west period of 2.25 s, we linearly interpolate between the above values to $k = 1.87$. We calculated the vertical distribution factors using the mid-rise weights (w_x , w_i) and heights (h_x , h_i) of each above-ground level listed in Table 6-3. The sum of the products of the distribution factors and story heights is equal to the effective height of the mid-rise mass.

$$H_{\text{eff}} = \sum_{i=1}^n C_{vi} * h_i = 108 \text{ ft}$$

We lumped all of the above-ground mid-rise mass at the top of the modeled cantilever, at the effective height of 108 ft. We assigned the cantilever an equivalent flexural stiffness to calibrate its period to the expected east-west direction mid-rise period of 2.25 s. We modeled the cantilever as relatively rigid in the north-south direction. North-south direction response of the podium structure is de-coupled from the tower response.

$$\begin{aligned}
W &= 35,637 \text{ kip} \\
M &= W / g \\
&= 35,637 / 32.2 \\
&= 1,107 \text{ kip-s}^2/\text{ft} \\
T_e &= 2.25 \text{ s} \\
K_{\text{eff}} &= M / (T / 2\pi)^2 \\
&= 8632 \text{ kip / ft}
\end{aligned}$$

We calculated the following section properties to model the mid-rise cantilever in PERFORM-3D:

$$\begin{aligned}
E &= \text{Arbitrary elastic modulus} \\
&= 10,000 \text{ ksf} \\
A &= \text{Select axial stiffness 100 times the flexural stiffness} \\
&= 100 * K_{\text{eff}} * H_{\text{eff}} / E \\
&= 100 * 8632 * 108 / 10,000 \\
&= 9332 \text{ ft}^2 \\
A_v &= \text{Use zero shear area so that PERFORM-3D neglects shear deformation} \\
&= 0 \text{ ft}^2 \\
I_{22} &= \text{East-west flexural stiffness is determined by bending about the element 2-2 axis} \\
&= K_{\text{eff}} * H_{\text{eff}}^3 / (3 * E) \\
&= 8632 * 108^3 / (3 * 10,000) \\
&= 3.636 * 10^4 \text{ ft}^4 \\
I_{33} &= \text{Select north-south direction stiffness 100 times the east-west stiffness} \\
&= 3.636 * 10^7 \text{ ft}^4 \\
I_{11} &= \text{Use 100 times the moment of inertia for the torsional moment of inertia.} \\
&= 3.636 * 10^7 \text{ ft}^4
\end{aligned}$$

Figure 6-5 shows the PERFORM-3D section property definition.

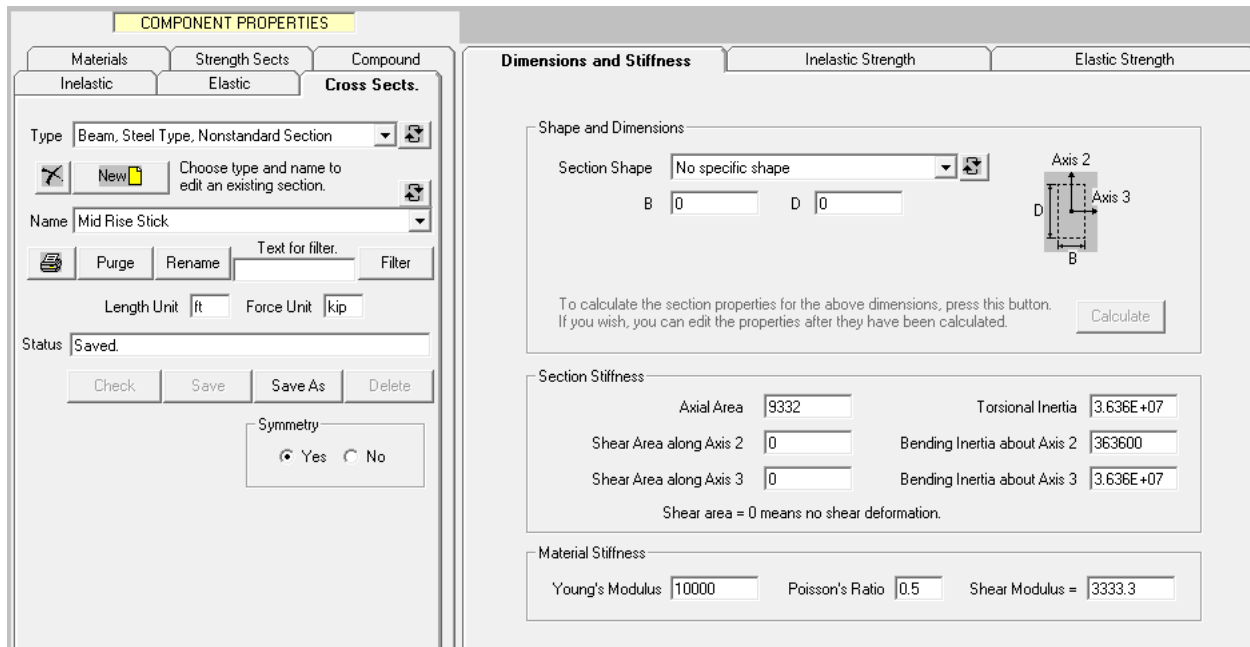


Figure 6-5 – Podium Above Ground Structure Stick Model Component Property Definition

As shown in Figure 6-2, we modeled the podium basement with a multiple-degree-of-freedom lumped-mass stick. We modeled the basement masses, including the mass of the mat at level B5, at the elevations listed in Table 6-3.

We estimated the east-west direction basement story stiffness properties based on the outer north and south shear walls. We did not model the stiffness of the core shear walls because they are much smaller than the outer basement walls. The outer north and south shear walls are both 167ft-7in. long. Above Level B2, the walls are 14in. thick. Below Level B2, the walls are 18 in. thick.

We modeled the basement stiffness with elastic beam elements assigned effective section properties based on the wall dimensions and material properties. We applied cracked section property modifiers from PEER TBI Table 4-3 for basement walls. We oriented the elements with the local element 3-axis in the east-west direction. Total effective shear areas and east-west direction moments of inertia are calculated for the walls between Levels L1 and B2 as follows:

$$\begin{aligned} \alpha_{crv} &= \text{Cracked section modifier for in-plane shear stiffness of basement walls} \\ &= 0.20 \end{aligned}$$

$$\begin{aligned} \alpha_{crf} &= \text{Cracked section modifier for in-plane flexural stiffness of basement walls} \\ &= 0.80 \end{aligned}$$

$$\begin{aligned}
A &= \text{Total shear wall area, Levels B1 and B2} \\
&= 2 * 14 \text{ in.} * 167\text{ft-7in.} \\
&= 391 \text{ ft}^2 \\
\\
A_{v3} &= \text{Effective total east-west shear area} \\
&= \frac{5}{6} * A * \alpha_{crv} \\
&= 65.17 \text{ ft}^2 \\
\\
A_{v2} &= \text{Select north-south direction stiffness 100 times the east-west stiffness} \\
&= 100 * A_{v3} \\
&= 6517 \text{ ft}^2 \\
\\
I_{22} &= \text{Effective total moment of inertia about north-south axis} \\
&= 2 * 14 \text{ in.} * (167\text{ft-7in.})^3 / 12 * \alpha_{crf} \\
&= 7.321 * 10^5 \text{ ft}^4 \\
\\
I_{11}, I_{33} &= \text{Select torsional moment of inertia and moment of inertia about east-west axis 100} \\
&\quad \text{times the moment of inertia about the north-south axis} \\
&= 7.321 * 10^7 \text{ ft}^4
\end{aligned}$$

We assigned the material properties calculated below to the podium basement elements.

$$\begin{aligned}
f_c' &= \text{Expected concrete compressive strength} \\
&= 1.3 * 5,000 \text{ psi} \\
&= 6,500 \text{ psi} \\
\\
E &= \text{Concrete elastic modulus} \\
&= 57,000 * [f_c']^{0.5} \\
&= 4,595 \text{ ksi} \\
\\
\nu &= \text{Concrete Poisson's ratio} \\
&= 0.17
\end{aligned}$$

Figure 6-6 shows the PERFORM-3D component property definitions for the podium basement walls.

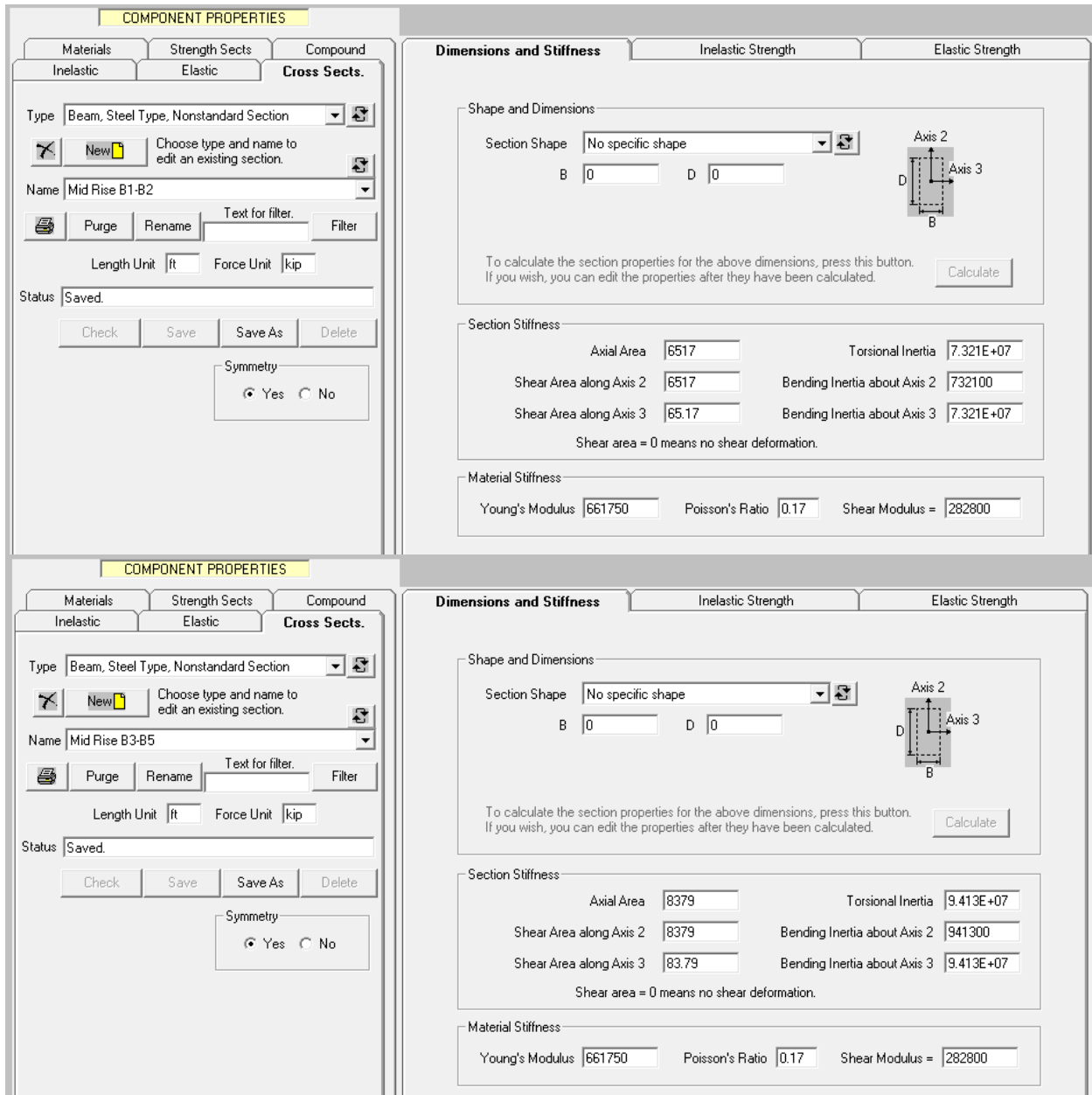


Figure 6-6 – Podium Basement Wall PERFORM-3D Component Property Definitions

We modeled the interface between the tower and podium basements with nonlinear elastic gap-hook elements. DeSimone structural drawings dated 4 April 2008 show a 1 in. gap between the east side of the tower basement and the west side of the podium basement. The gap can close in an earthquake when the tower and podium move towards one another. Upon gap closure, the following below grade structural components can transfer force between the two structures:

- Tower and podium diaphragms at Level L1.
- Tower and podium north and south basement shear walls between Levels L1 and B1.
- Tower mat and podium diaphragms at Levels B1 and B2.
- Tower mat and north and south podium shear walls between Levels B1 and B2.

The gap between all above listed components is consistently 1 in. We used three gap-hook elements to model force transfer between the tower and podium at Levels L1, B1, and B2. We assigned the same properties to all three elements.

The only degree of freedom for the gap-hook element is axial deformation. It has zero stiffness in both tension and compression when it is not closed. To allow independent response of the tower and podium away from each other, we assigned a large tension “hook” distance of 40 in. We assigned a compression “gap” distance of 1 in. We assigned a relatively rigid axial stiffness that is 20 times the elastic stiffness of the podium foundation lateral soil springs, which are described in Section 6.1.2. Figure 6-7 shows the PERFORM-3D component property definitions for the foundation gap elements.

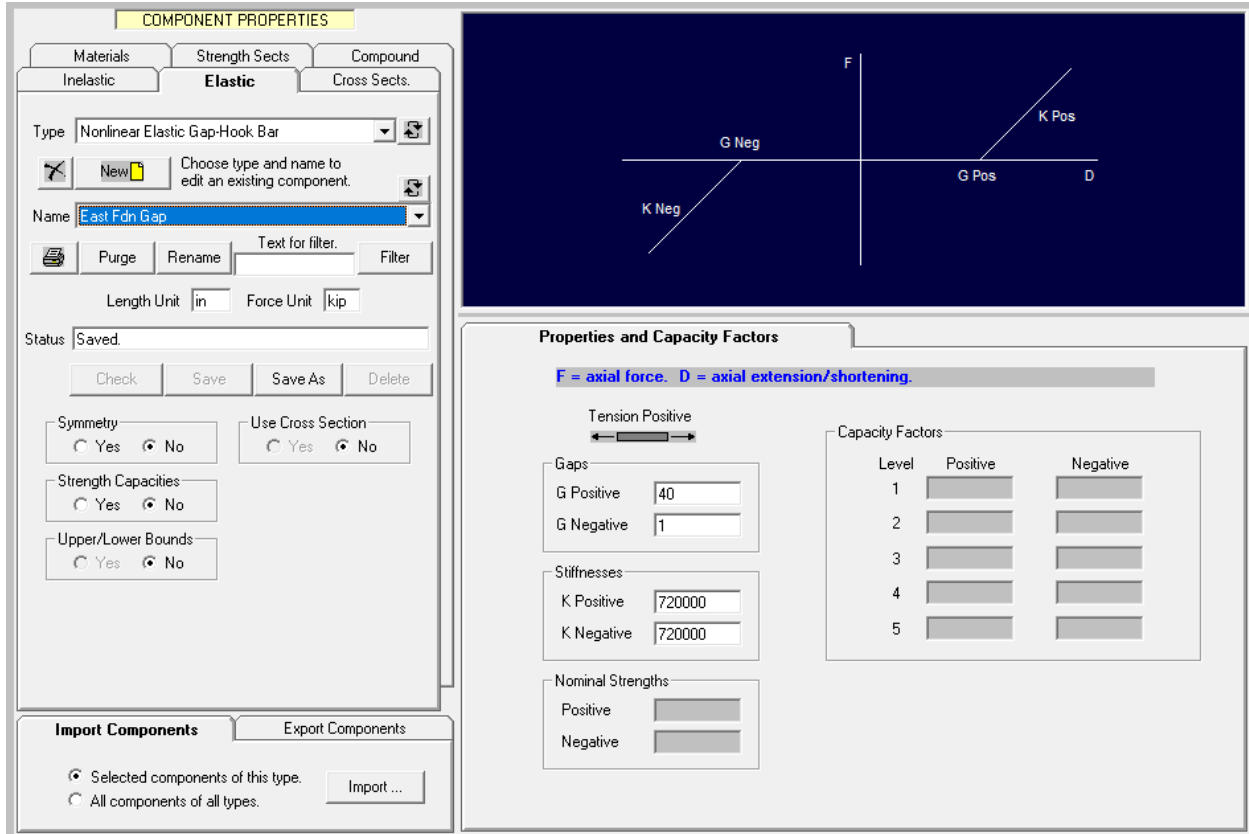


Figure 6-7 – PERFORM-3D Component Definition for Foundation Gap Elements

We used two rigid elastic bars to transfer force from the tower mat to the two foundation gap elements at Levels B1 and B2. As shown in Figure 6-2 and Figure 6-3, a horizontally oriented rigid link connects the east side of the tower mat to a vertically oriented rigid link. We released moment continuity at the eastern end of the horizontal link where it connects to the tower mat. We modeled moment continuity between the two rigid links. The vertically oriented link is connected to the gap elements at Levels B1 and B2. To avoid instabilities, we assigned vertical and lateral H2 nodal support conditions at both top and bottom of the vertical rigid link.

We modeled the rigid links as a nonstandard elastic section. We assigned relatively rigid axial and flexural stiffness properties as calculated below.

$$\begin{aligned}
 K_{\text{soil}} &= \text{Mid-rise foundation soil spring initial stiffness} \\
 &= 36,000 \text{ kip / in.} \quad (\text{Section 6.1.2})
 \end{aligned}$$

$$\begin{aligned}
 K_{\text{rigid}} &= 20 * K_{\text{soil}} \\
 &= 720,000 \text{ kip / in.}
 \end{aligned}$$

- E = Arbitrary elastic modulus
= 29,000 ksi.
- L = Distance between east side of tower mat and modeled location of podium
= 1,029 in.
- A = $K_{\text{rigid}} * L / E$
= 25,548 in²
- H = Story height between B1 and B2
= 111 in.
- I = $K_{\text{rigid}} * H^3 / (12 * E * I)$
= 2,830,000 in⁴

Figure 6-8 shows the PERFORM-3D component property definitions for the rigid link elements.

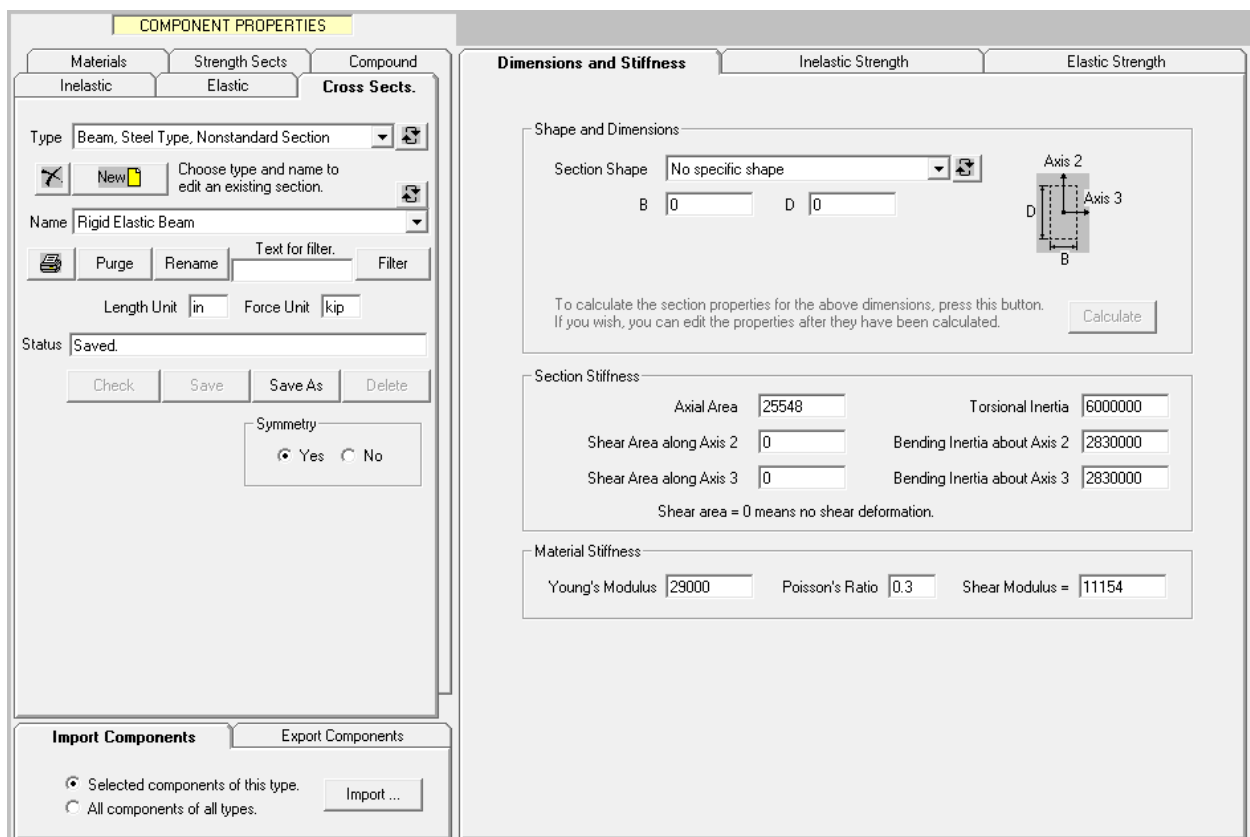


Figure 6-8 – PERFORM-3D Component Definition for Rigid Links

6.1.2 Basement Wall Lateral Resistance

Soil pressure acting normal to the embedded foundations affects the lateral response characteristics of the tower and podium structures. To account for the effects of soil-structure interaction, we used the lateral earth pressure characterizations from the 30 November 2018 geotechnical report by John Egan, SLATE Geotechnical Consultants Inc., and Shannon & Wilson Inc. These force-displacement relationships account for the following interactions between the embedded foundations and surrounding soil mass:

- Passive pressure normal to the mat face and basement walls acting opposite to the direction of foundation displacement. It is engaged as the foundation displaces into the soil mass.
- Active pressure normal to the mat face and basement walls acting in the same direction as foundation displacement. It is engaged as the foundation displaces away from the soil mass.

Figure 6-9 shows the locations and directions of soil pressure affecting lateral displacement of the embedded tower foundation. Soil pressure acts directly at the north and west sides of the tower basement. We neglected soil pressure south of the tower basement because the Transbay Terminal foundation is directly adjacent to the south. A 1 in. gap separates the east side of the tower basement from the podium structure basement. When the tower foundation displaces to the east, the gap can close and transfer force through the podium basement and into the soil mass to the east. We accounted for the 1 in. gap as discussed in Section 6.1.1 by including nonlinear gap elements in the analysis model, as well as modeling the podium foundation mass, stiffness, and the dynamic properties of the above-ground podium structure. We accounted for soil pressure at both east and west podium basement walls. We did not model soil pressure at the north podium basement wall because north-south response of the podium does not affect the tower. We accounted for friction forces in our model of the podium foundation.

Figure 6-10 shows cumulative force displacement relationships for active and passive pressure at each basement wall. Forces acting at the podium basement walls are significantly higher than at the tower foundation because the podium foundation is much deeper. Positive displacements in the figure engage passive pressure, and negative displacements engage active pressure. Soil pressure is non-zero at zero displacement. This magnitude of pressure is the at-rest soil pressure occurring at static (non-earthquake) conditions. At-rest soil pressure at the north and west sides

of the tower are not counteracted by pressures at the south and east sides, resulting in an unbalanced soil load condition. Realistically, these unbalanced pressures decrease according to the active pressure force-displacement curves as the foundation moves away from the soil mass. However, the decrease is relatively small so we conservatively modeled the unbalanced tower foundation soil pressure as static loads acting on the tower foundation towards south and east. Cumulative forces due to unbalanced at-rest soil pressures are:

- 1,906 kip south
- 3,008 kip east

Figure 6-11 through Figure 6-14 show elevations of the soil-structure interaction forces we considered in the PERFORM-3D model.

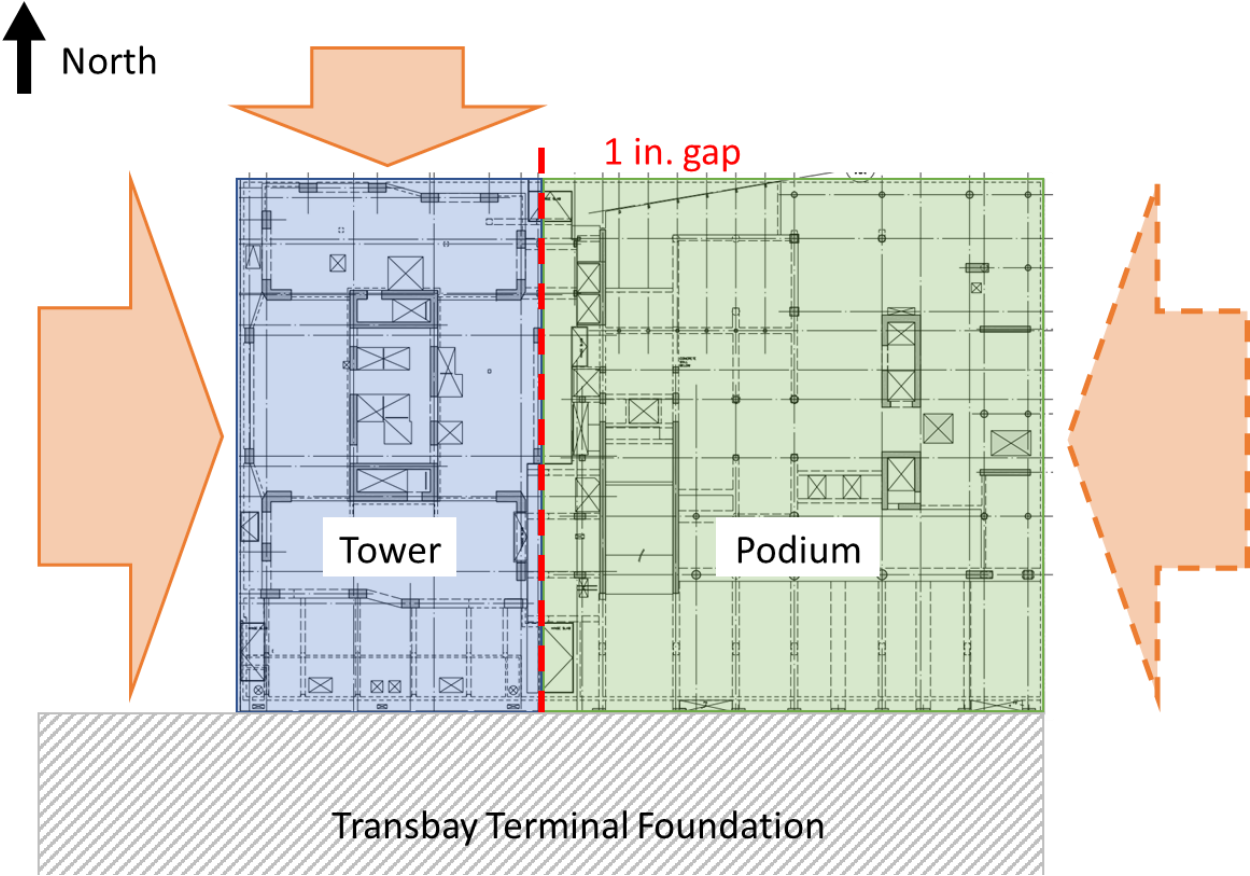


Figure 6-9 – Embedded Foundation Lateral Earth Pressures

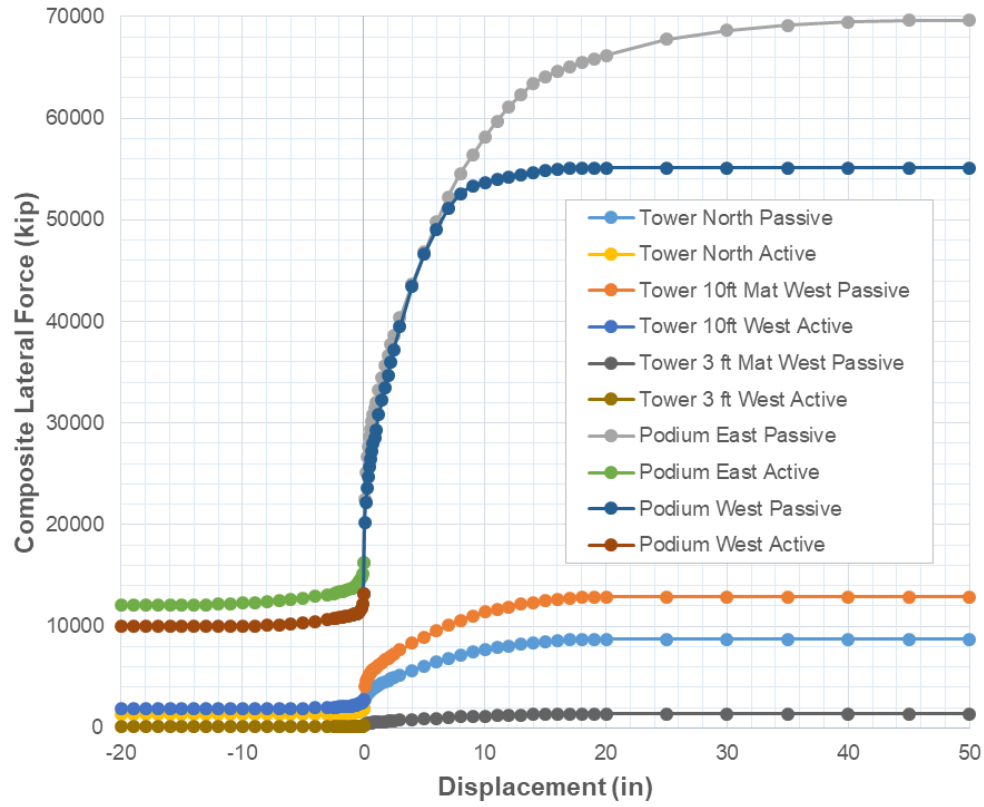


Figure 6-10 – Embedded Foundation Lateral Force-Displacement Relationships

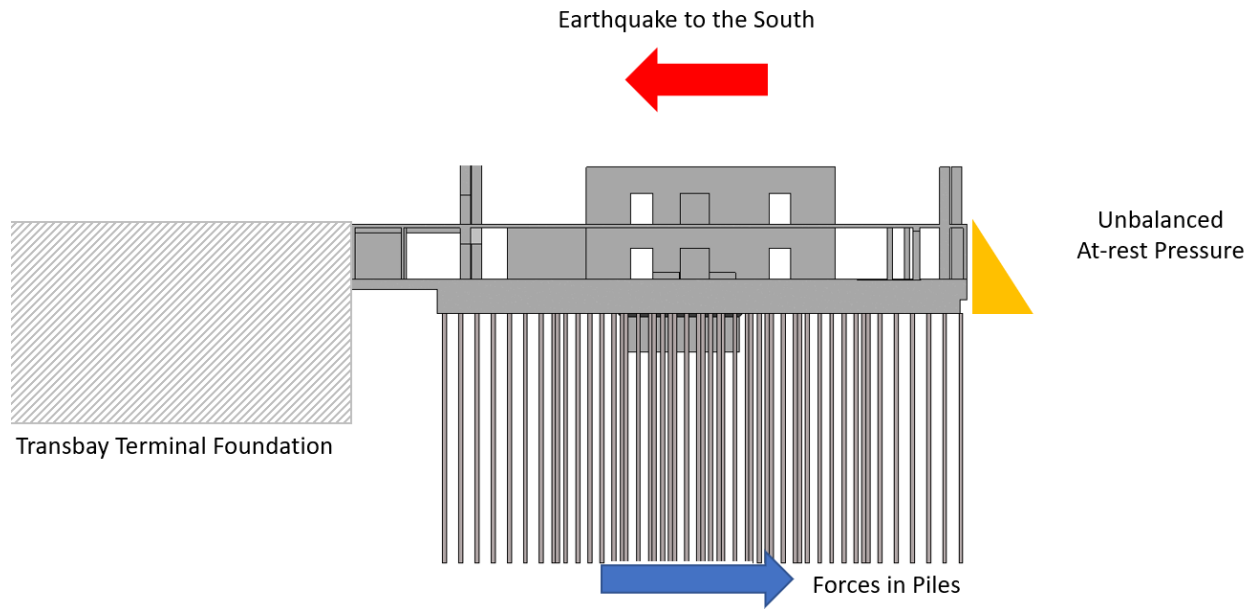


Figure 6-11 – Soil Contributions to South Lateral Resistance

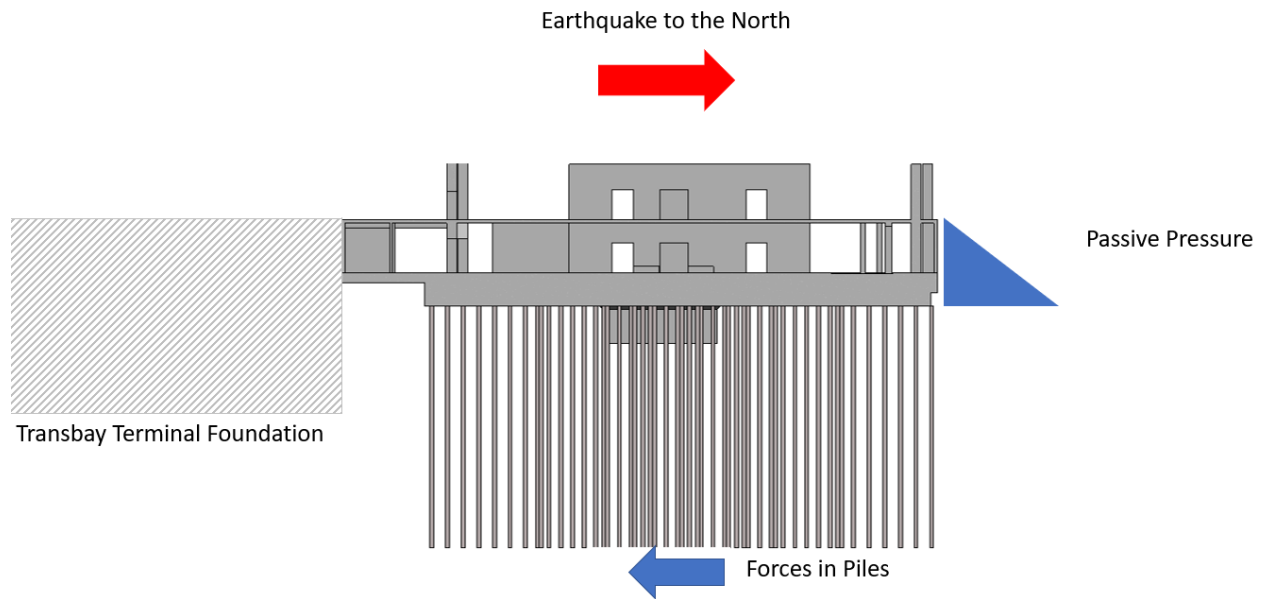


Figure 6-12 – Soil Contributions to North Lateral Resistance

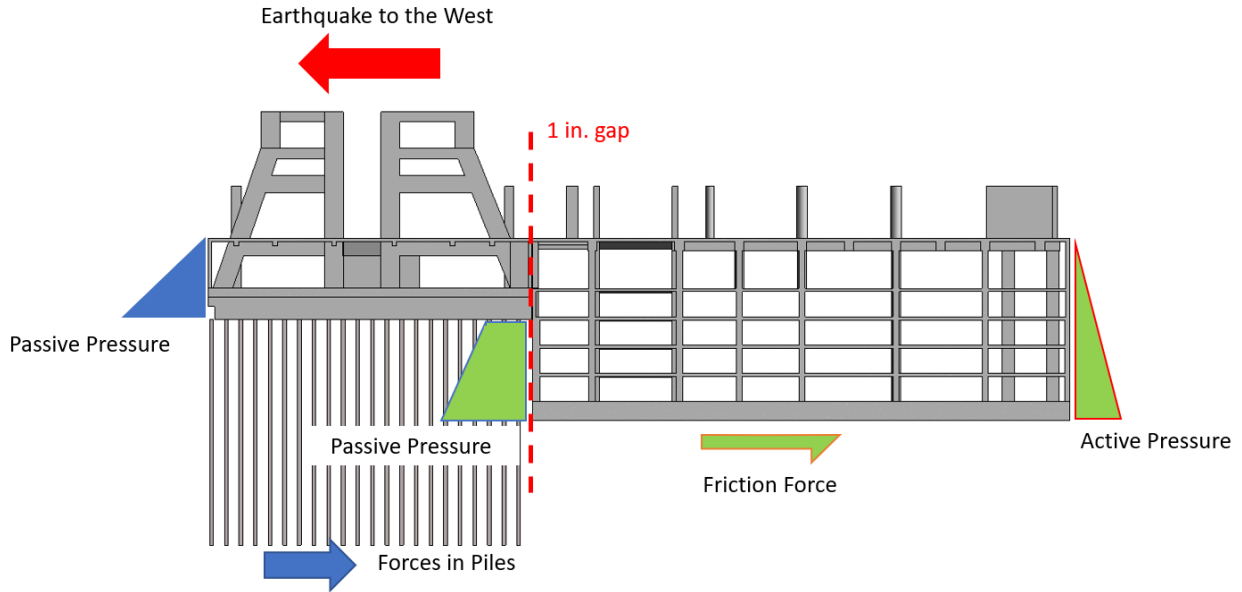


Figure 6-13 – Soil Contributions to West Lateral Resistance

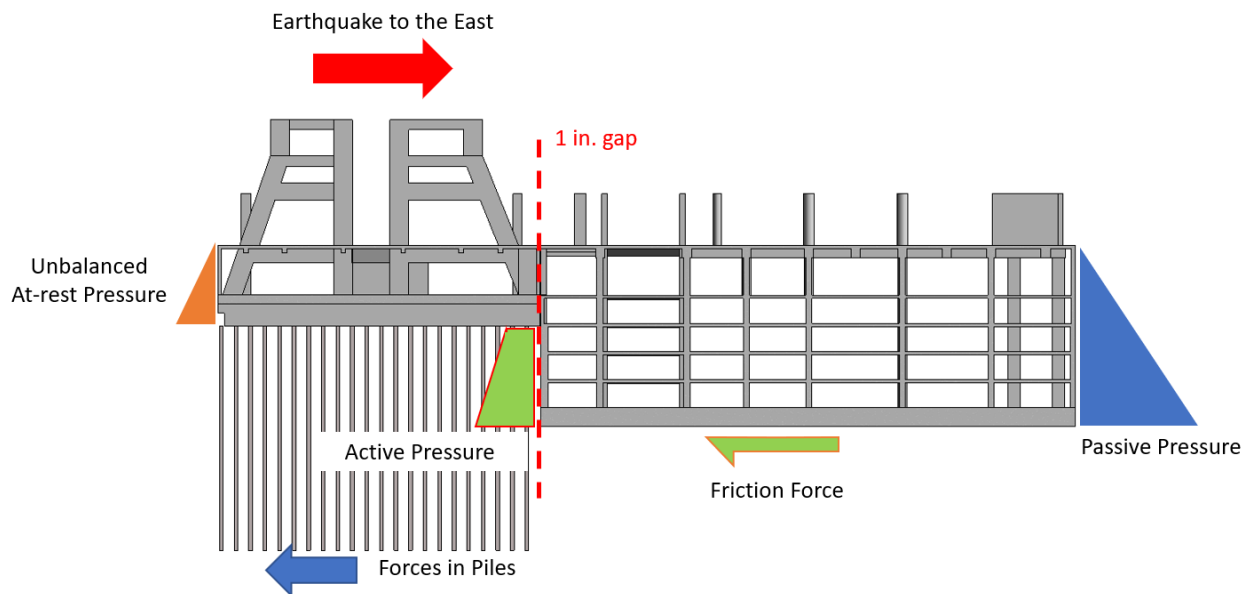


Figure 6-14 – Soil Contributions to East Lateral Resistance

A greater height of soil loads the east podium basement wall relative to the west wall. Therefore, similarly to the tower foundation, the podium foundation is subjected to unbalanced at-rest soil pressure. At-rest forces due to soil pressure are 16,251 kip and 13,243 kip at the east and west podium basement walls, respectively. The 30 November 2018 geotechnical report by John Egan et.al. indicates east and west soil pressures act at centroid heights of 20 ft and 15 ft above the

bottom of the podium mat, respectively. We modeled the unbalanced at-rest pressure on the podium basement by applying a static force acting at an effective height causing equal overturning moment.

$$\begin{aligned} F_{\text{rest,E}} &= \text{Podium basement force due to east at-rest soil pressure} \\ &= 16,251 \text{ kip} \end{aligned}$$

$$\begin{aligned} F_{\text{rest,W}} &= \text{Podium basement force due to west at-rest soil pressure} \\ &= 13,243 \text{ kip} \end{aligned}$$

$$\begin{aligned} F_{\text{rest,Net}} &= \text{Podium net basement force due to unbalanced at-rest soil pressure} \\ &= F_{\text{rest,E}} - F_{\text{rest,W}} \\ &= 3,008 \text{ kip} \end{aligned}$$

$$\begin{aligned} h_E &= \text{Centroid height of east soil pressure} \\ &= 20 \text{ ft} \end{aligned}$$

$$\begin{aligned} h_W &= \text{Centroid height of west soil pressure} \\ &= 15 \text{ ft} \end{aligned}$$

$$\begin{aligned} h_{\text{Net}} &= (F_{\text{rest,E}} * h_E - F_{\text{rest,W}} * h_W) / (F_{\text{rest,Net}}) \\ &= 42 \text{ ft} \end{aligned}$$

We modeled active and passive soil pressure at the east and west podium basement walls using two inelastic bar elements, located at the centroid heights of the east and west soil pressure distributions. Since we account for at-rest soil pressure by applying an equivalent static force to the model, we remove at-rest pressures from the soil pressure force-displacement curves as illustrated in Figure 6-15. Figure 6-16 and Figure 6-17 show the component definitions in PERFORM-3D for the east and west podium basement soil pressure, respectively.

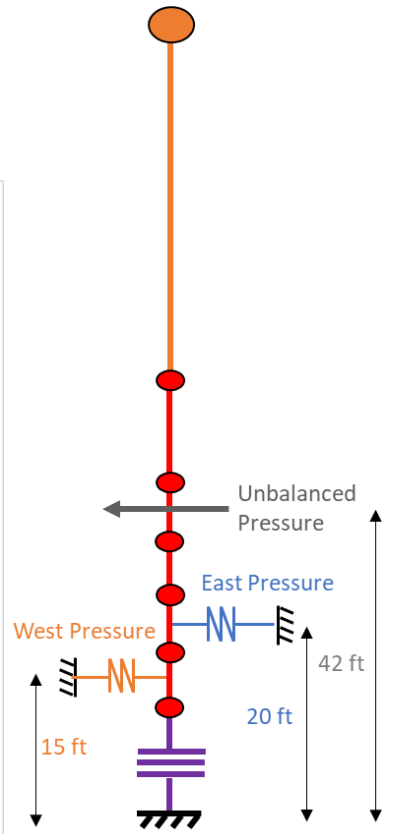
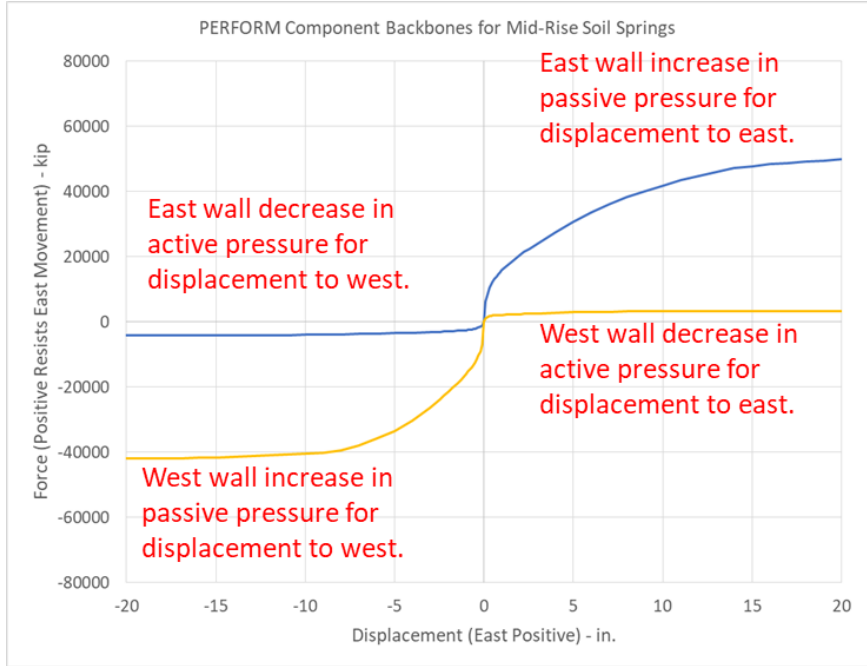
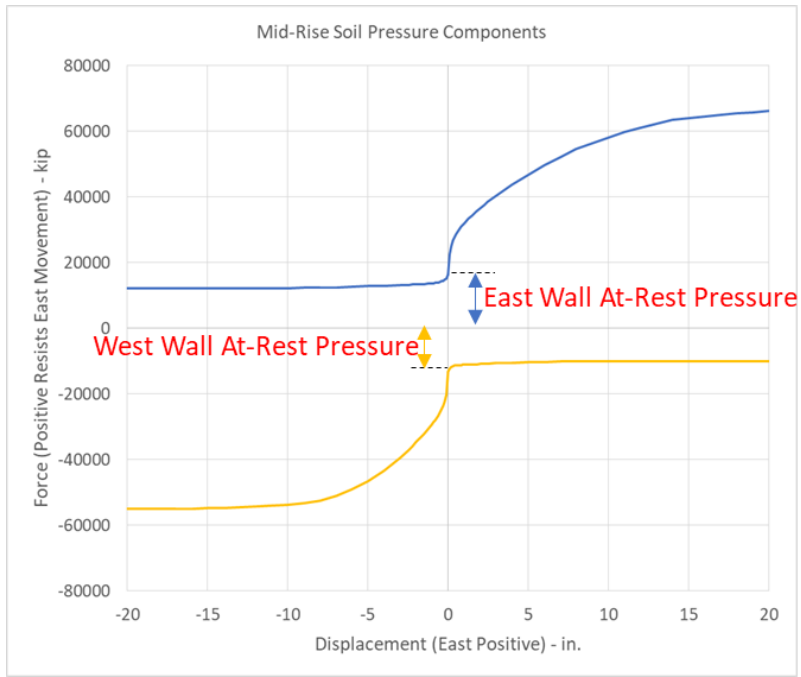


Figure 6-15 – Podium Basement Wall Pressure Modeled Force-Displacement

COMPONENT PROPERTIES

Materials | Strength Sects | Compound

Inelastic | Elastic | Cross Sects.

Type: Inelastic Bar

Name: East Mid Rise Soil Pressure

Length Unit: in | Force Unit: kip

Status: Saved

Graph | Save | Save As | Delete

Shape of Relationship: E-P-P Trilinear

Use Cross Section: Yes No

Symmetry: Yes No

Deformation Capacities: Yes No

Strength Loss: Yes No

Cyclic Degradation: None YULRX YX+3

Upper/Lower Bounds: Yes No

Import Components | Export Components

Selected components of this type. All components of all types.

Basic F-D Relationship

F = axial force. D = axial strain.

Tension Positive

Initial Stiffness, K_0 (= EA):

Youngs modulus, E:

Section area, A:

Positive Actions: FY FU

Negative Actions: FY FU

Positive Deformations: DU DX

Negative Deformations: DU DX

KH/KD: Pos = Neg =

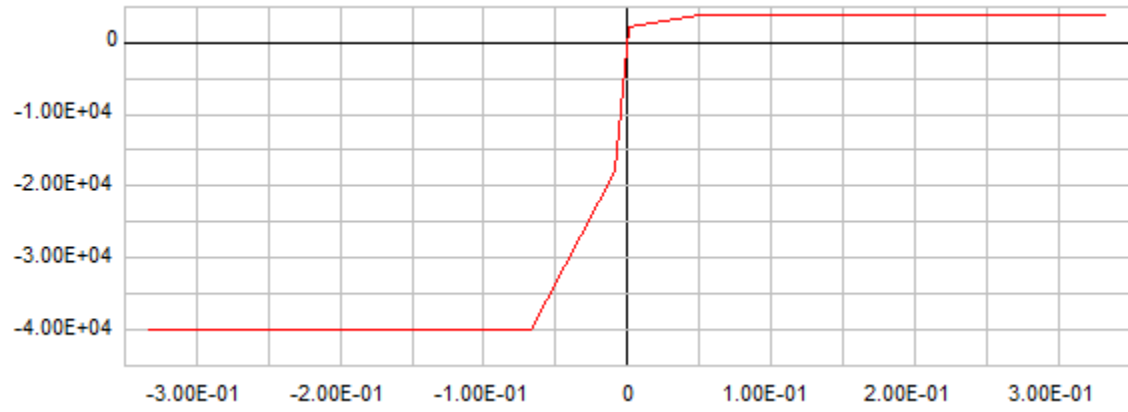


Figure 6-16 – PERFORM-3D Component Definition for Soil Pressure at the East Podium Basement Wall

COMPONENT PROPERTIES

Materials | Strength Sects | Compound

Inelastic | Elastic | Cross Sects.

Type: Inelastic Bar

Name: West Mid Rise Soil Pressure

Length Unit: in | Force Unit: kip

Status: Saved

Graph | Save | Save As | Delete

Shape of Relationship: E-P-P | Trilinear

Use Cross Section: Yes | No

Symmetry: Yes | No

Deformation Capacities: Yes | No

Strength Loss: Yes | No

Cyclic Degradation: None | YULRX | YX+3

Upper/Lower Bounds: Yes | No

Import Components | Export Components

Selected components of this type. | All components of all types. | Import ...

Basic F-D Relationship | Cyclic Degradation | Upper/Lower Bounds | Strength Loss | Deformation Capacities

F = axial force. D = axial strain.

Tension Positive

Initial Stiffness, K_0 (= EA):

Young's modulus, E: 10000

Section area, A: 216

Positive Actions: FY: 1800, FU: 3200

Negative Actions: FY: 18000, FU: 40000

Positive Deformations: DU: 0.05, DX: 0.333

Negative Deformations: DU: 0.0583, DX: 0.333

KH/ K_0 : Pos = 0.013, Neg = 0.204

Paste | Copy | Clear

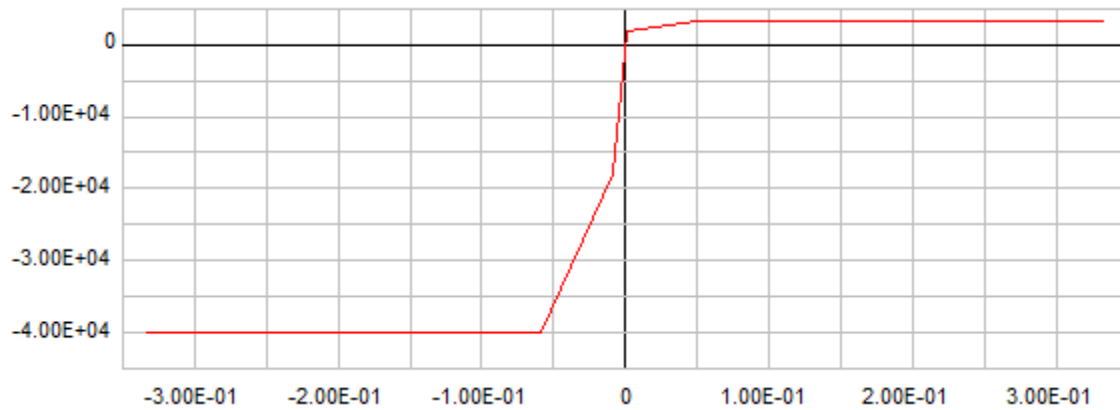


Figure 6-17 – PERFORM-3D Component Definition for Soil Pressure at the West Podium Basement Wall

We accounted for two sources of friction resistance between the podium foundation and surrounding soil. The 30 November 2018 geotechnical report by John Egan et.al. recommends (1) a friction coefficient of 0.5 at the bottom of the mat, applicable to the buoyant weight of the podium structure, and (2) friction resistance at the north and south podium basement walls reaching peak resistance of 27 kip per foot of wall at displacements greater than 0.10 in.

We calculated the friction resistance at the bottom of the mat based on a conservative historic water table elevation at 10 ft below ground surface. As indicated in the 30 November 2018 geotechnical report, the current ground water table is much lower than this due to recent dewatering activities at adjacent sites. We calculated an equivalent friction coefficient for the PERFORM-3D friction isolator element, as shown below.

$$\begin{aligned} L_{EW} &= \text{Podium basement east-west dimension} \\ &= 171.5 \text{ ft} \end{aligned}$$

$$\begin{aligned} L_{NS} &= \text{Podium basement north-south dimension} \\ &= 178.33 \text{ ft} \end{aligned}$$

Figure 6-18 indicates the regions where the podium mat is 6 ft thick and 8 ft thick. The areas do not include the mat directly below the basement walls.

$$\begin{aligned} A_6 &= \text{Area of 6 ft thick mat within inner wall perimeter} \\ &= 21,512 \text{ ft}^2 \end{aligned}$$

$$\begin{aligned} A_8 &= \text{Area of 8ft thick mat within inner wall perimeter} \\ &= 7,874 \text{ ft}^2 \end{aligned}$$

$$\begin{aligned} L_8 &= \text{Length of east wall above the 8 ft thick mat} \\ &= 106.33 \text{ ft} \end{aligned}$$

$$\begin{aligned} t &= \text{Basement wall thickness} \\ &= 1.5 \text{ ft} \end{aligned}$$

$$\begin{aligned} D_{mat} &= \text{Depth to top of mat} \\ &= 52 \text{ ft} \end{aligned}$$

$$\begin{aligned} D_{water} &= \text{Depth to water table} \\ &= 10 \text{ ft} \end{aligned}$$

$$\begin{aligned} V_{above} &= \text{Displaced volume of water above the mat} \\ &= L_{EW} * L_{NS} * (D_{mat} - D_{water}) \\ &= 1,285,000 \text{ ft}^3 \end{aligned}$$

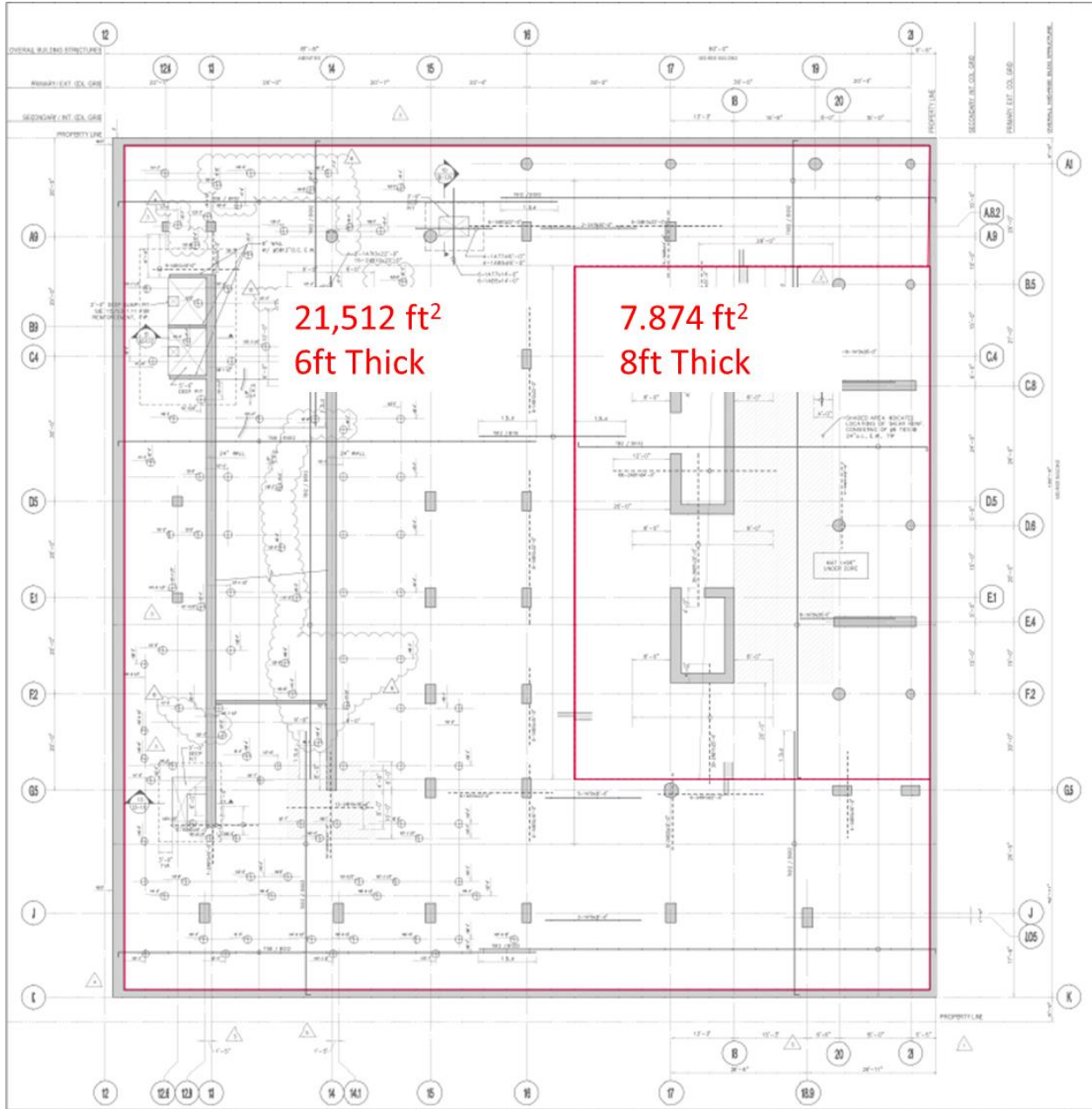


Figure 6-18 – Podium Basement Mat Thickness Regions

$$\begin{aligned}
 V_{\text{mat}} &= \text{Mat volume} \\
 &= 6\text{ft} * (A_6 + A_8 + t * 2 * (L_{\text{EW}} + L_{\text{NS}})) + 2\text{ft} * (A_8 + t * L_8) \\
 &= 198,700 \text{ ft}^3
 \end{aligned}$$

$$\begin{aligned}
 \gamma_{\text{water}} &= \text{Unit weight of water} \\
 &= 62.4 \text{ pcf}
 \end{aligned}$$

$$B = \text{Buoyant uplift force}$$

$$\begin{aligned}
&= \gamma_{\text{water}} * (V_{\text{above}} + V_{\text{mat}}) \\
&= 92,600 \text{ kip} \\
W &= \text{Expected weight of the podium structure (1.0 Dead + 0.25 Live)} \\
&= 105,200 \text{ kip} \\
\mu &= \text{Friction coefficient} \\
&= 0.5 \\
F_{\text{mat}} &= \text{Total resistance due to friction at the bottom of the mat} \\
&= \mu * (W - B) \\
&= 6,300 \text{ kip} \\
f_{\text{wall}} &= \text{Resistance per foot of wall due to friction at north and south basement walls} \\
&= 27.42 \text{ kip / ft} \\
F_{\text{wall}} &= \text{Total resistance due to friction at north and south basement walls} \\
&= 2 * L_{\text{EW}} * f_{\text{wall}} \\
&= 9,405 \text{ kip} \\
F_{\text{fr}} &= \text{Total friction resistance at podium embedded foundation} \\
&= F_{\text{mat}} + F_{\text{wall}} \\
&= 15,705 \text{ kip}
\end{aligned}$$

Gravity loading in the PERFORM-3D model does not account for hydrostatic uplift. Therefore, we assigned an equivalent friction coefficient to correct for the modeled axial load on the friction isolator element.

$$\begin{aligned}
\mu_{\text{eff}} &= \text{Effective podium foundation friction coefficient} \\
&= F_{\text{fr}} / W \\
&= 0.15
\end{aligned}$$

The 30 November 2018 geotechnical report indicates the side wall friction force engages at a displacement of 0.1 in. We modeled the friction element in PERFORM-3D with an initial elastic stiffness at displacements less than 0.1 in., as calculated below. Figure 6-19 shows the PERFORM-3D component property definition.

$$\begin{aligned}
\Delta 0 &= \text{Displacement to engage friction resistance} \\
&= 0.1 \text{ in.} \\
K 0 &= \text{Initial friction pendulum component stiffness} \\
&= F_{\text{fr}} / \Delta 0 \\
&= 157,000 \text{ kip / in.}
\end{aligned}$$

COMPONENT PROPERTIES

Materials | Strength Sects | Compound

Inelastic | Elastic | Cross Sects.

Type: Seismic Isolator, Friction Pendulum

Name: Mid Rise Soil Friction

Length Unit: in | Force Unit: kip

Status: Saved

Graph | Save | Save As | Delete

Friction Type: Constant Coeff. Variable Coeff.

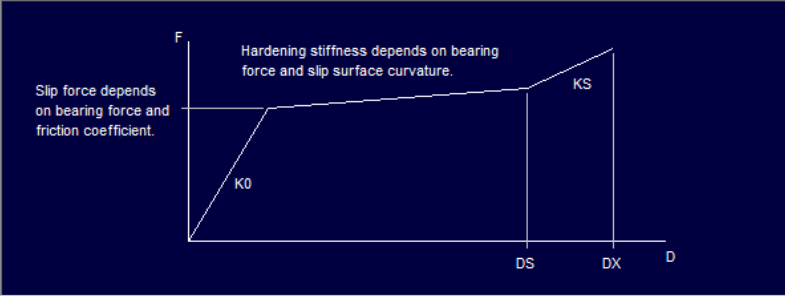
Axis 1-2 Symmetry: Yes No

Deformation Capacities: Yes No

Strength Capacities: Yes No

Import Components | Export Components

Selected components of this type. All components of all types. Import ...



Shear Behavior | Bearing Behavior | Capacities

F = shear and bearing forces. D = shear and bearing deformations.

Axis 3
Axis 2 | Axis 1

Boundary is circular. For no stiffening at boundary, leave DS and KS blank.

Stiffnesses and Deformations:

	Along Axis 1	Along Axis 2
K0	158859	
DX	40	
DS	0	
KS	0	

Friction Properties:

Slip Rate	Coefficient
All rates	0.151
Coefficient for push-over analysis: 0.151	

Shear Stiffness for Gravity Load: 0.01

Slip Surface Radi (0 = Flat Surface):
Along Axis 1: 0 | Along Axis 2:

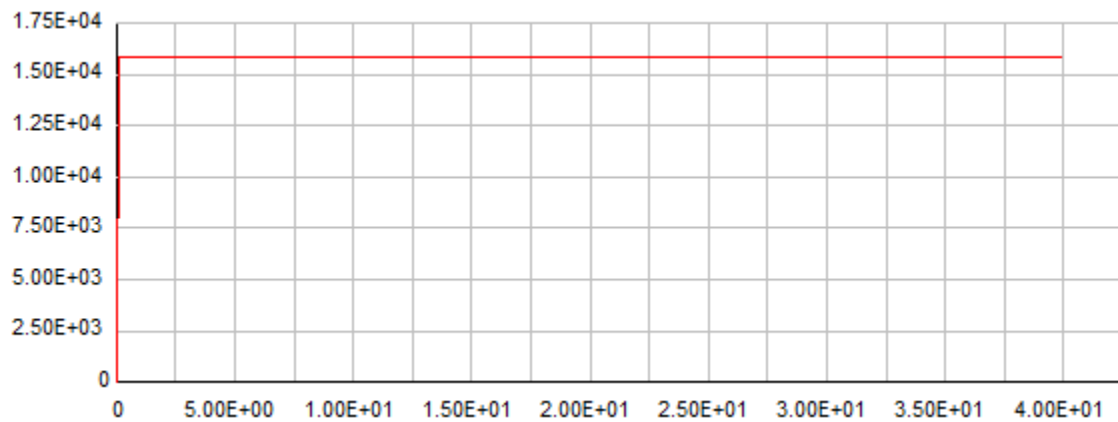


Figure 6-19 – PERFORM-3D Component Definition for Podium Foundation Friction

6.1.3 Cumulative Lateral Foundation Backbones

We used the following nonlinear elements to model the various sources of lateral resistance at the tower and podium foundations:

- One inelastic bar element accounting for the cumulative resistance of piles in the east and west directions, plus passive soil pressure resistance at the west tower basement wall (Figure 6-24).
- One inelastic bar element accounting for the cumulative resistance of piles in the north and south directions, plus passive soil pressure resistance at the north tower basement wall (Figure 6-25).
- One inelastic bar element accounting for active and passive soil pressure at the east podium basement wall (Figure 6-16).
- One inelastic bar element accounting for active and passive soil pressure at the west podium basement wall (Figure 6-17).
- One friction isolator element accounting for friction on the embedded podium foundation (Figure 6-19).

We added the lateral resistance from the existing piles to that of the basement walls to compute the cumulative foundation resistance to base shear in each of the four principal coordinate directions. Figure 5-16 shows the cumulative resistance of the existing piles in each direction. Figure 6-10 shows passive pressure resistance at each basement wall. Figure 6-20 through Figure 6-23 show the combined lateral resistance in each direction accounting for both piles and passive soil pressure. In each direction, the cumulative lateral resistance of the foundation to seismic loading was calculated as the sum of resistance from the piles and the embedded mat and basement walls. We accounted for the effects of overturning on the lateral resistance of the piles (Section 5.4.2) by reducing the pile resistance by 3%.

We fit idealized trilinear curves with strength loss to the backbones, using trilinear relationships that we implemented in our PERFORM 3D nonlinear time history analyses. The elastic stiffness of the east-west backbone is the same in both directions, and the elastic stiffness of the north-south backbone is the same in both directions. Figure 6-24 shows the PERFORM-3D component definition for the east-west direction backbones. Tension on the component corresponds to the foundation's resistance to movement west. Figure 6-25 shows the

PERFORM-3D component definition for the north-south direction backbones. Tension on the component corresponds to the foundation's resistance to movement south.

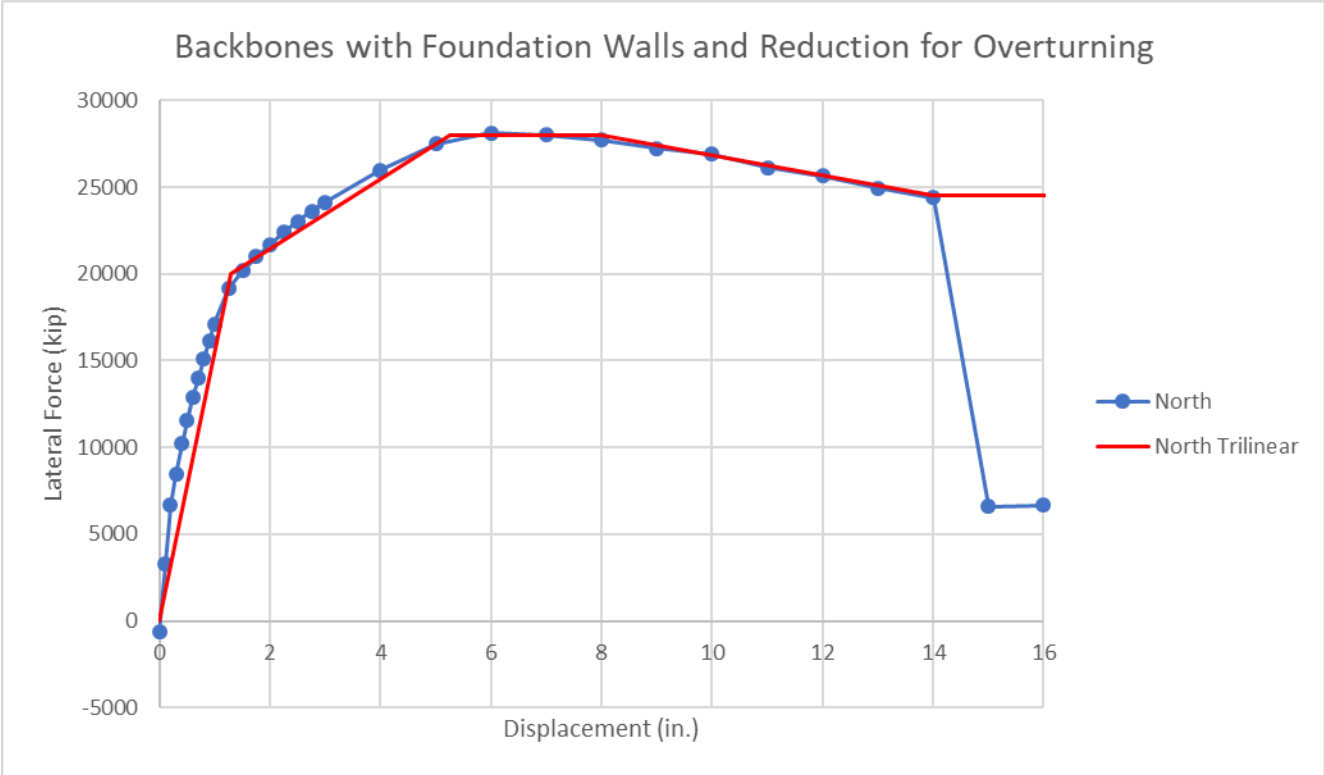


Figure 6-20 – Existing Condition North Foundation Lateral Backbone

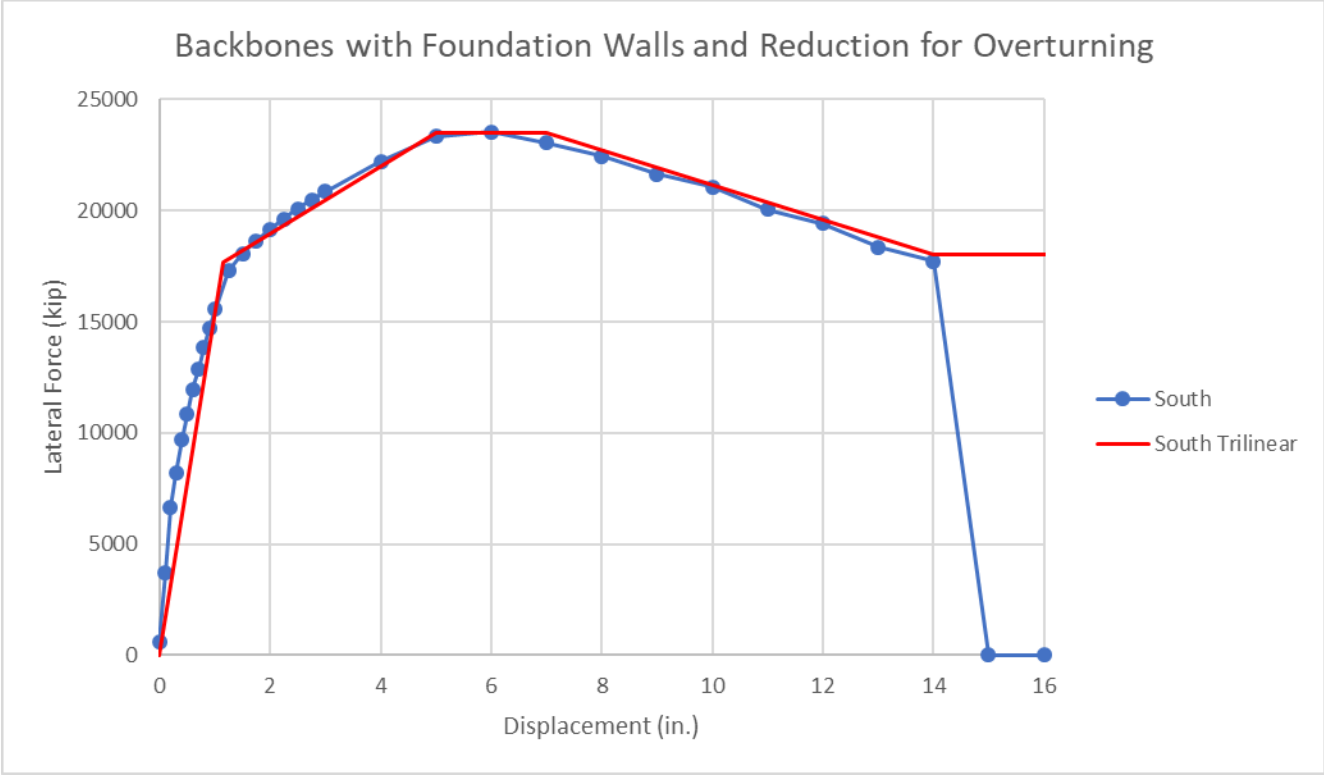


Figure 6-21 – Existing Condition South Foundation Lateral Backbone

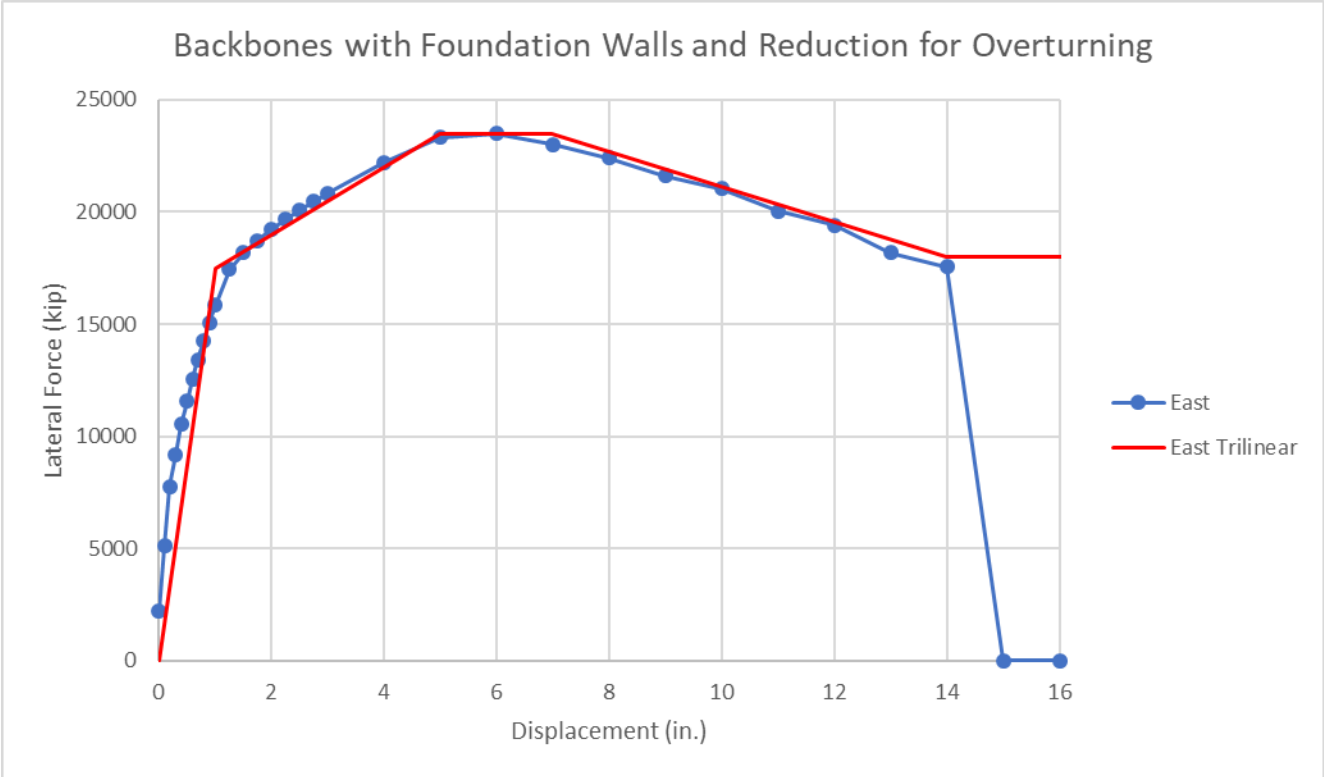


Figure 6-22 – Existing Condition East Foundation Lateral Backbone

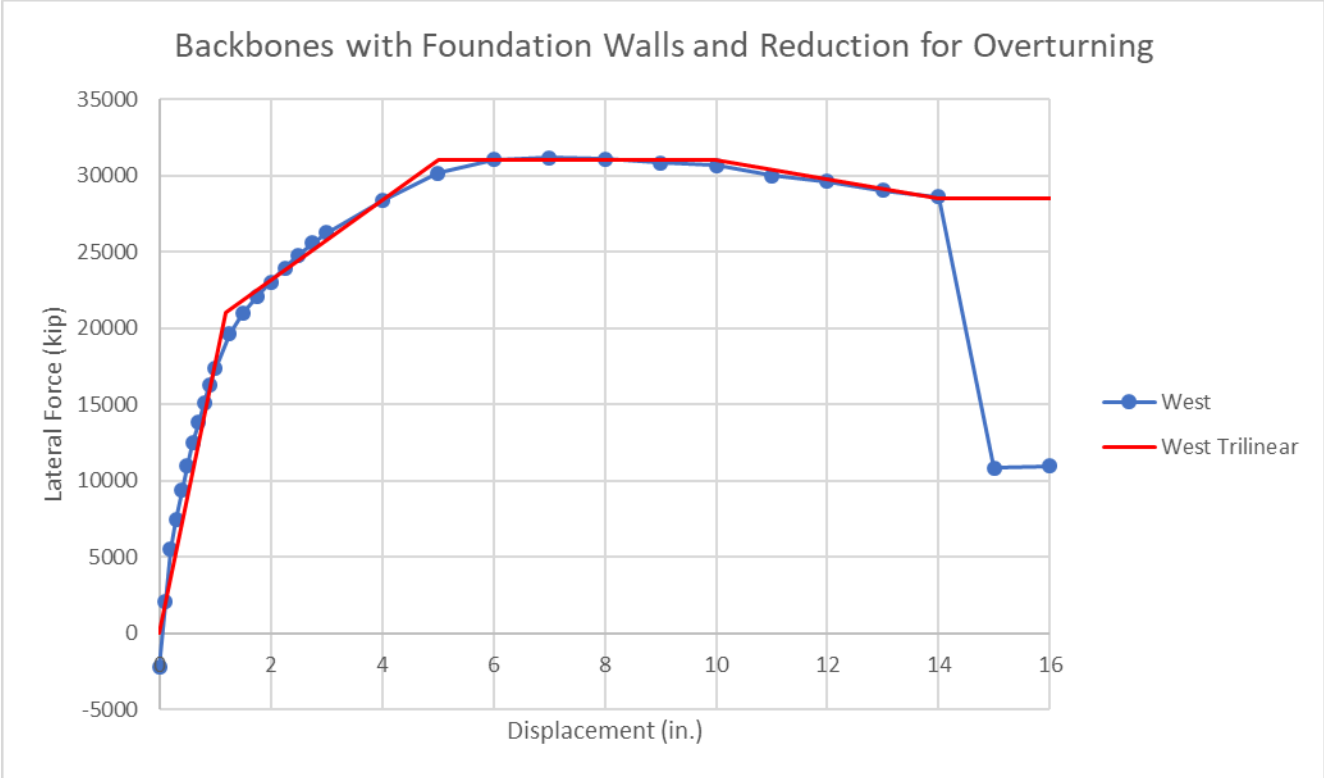


Figure 6-23 – Existing Condition West Foundation Lateral Backbone

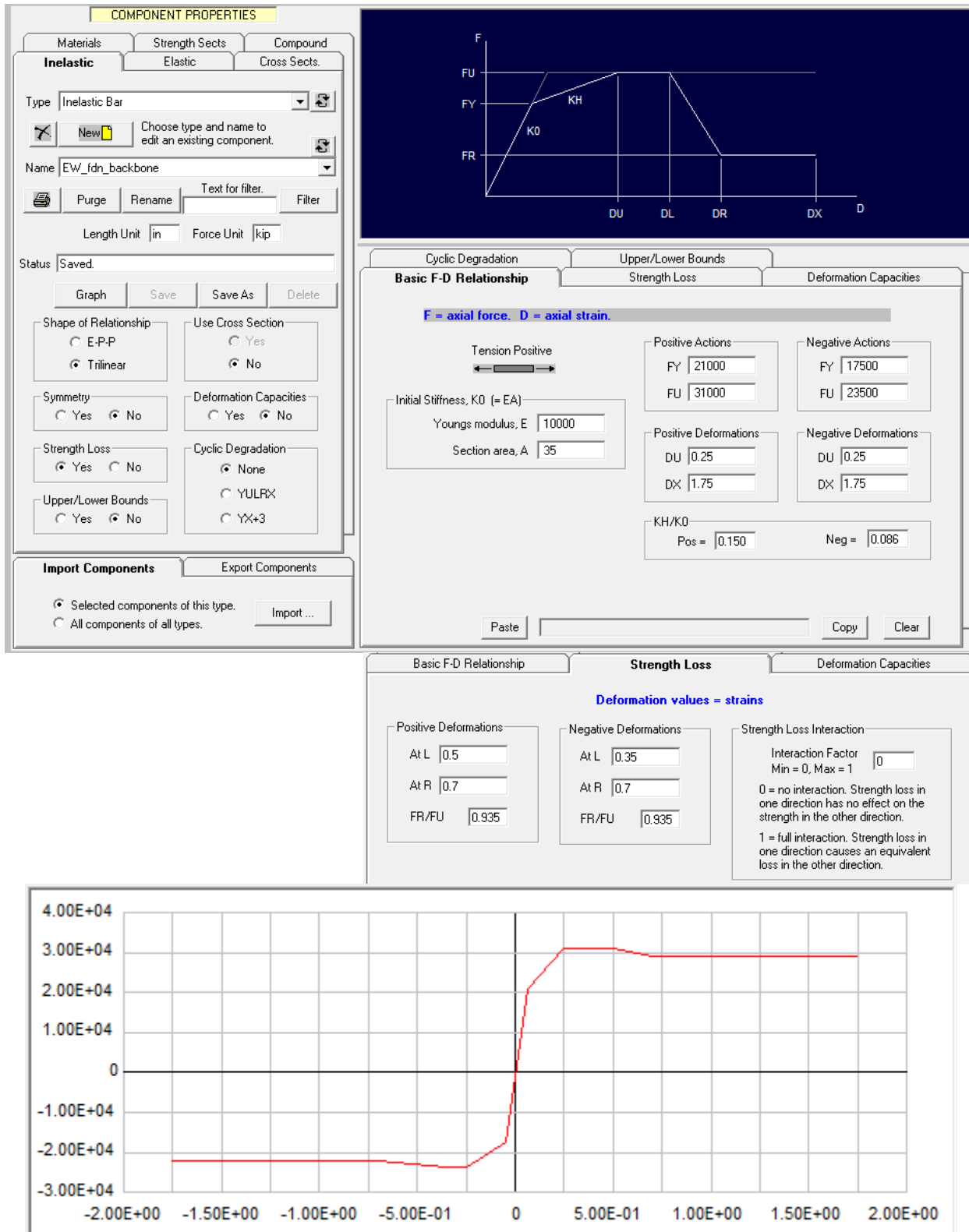


Figure 6-24 – PERFORM-3D Component Definition for Combined East-West Resistance of Existing Piles and Passive Soil Pressure

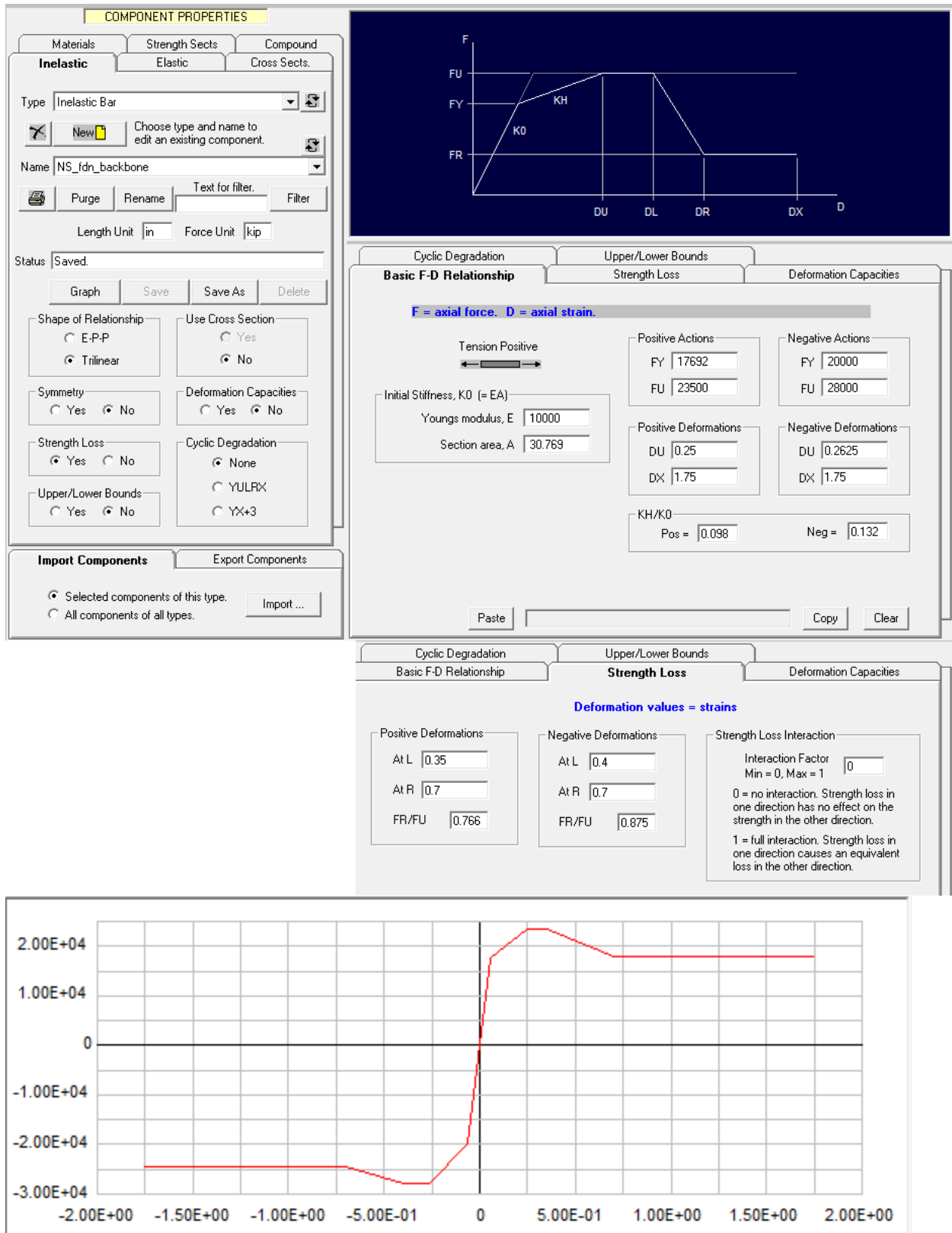


Figure 6-25 – PERFORM-3D Component Definition for Combined North-South Resistance of Existing Piles and Passive Soil Pressure

As an example, calculation of the PERFORM-3D component properties for the north tower foundation backbone is shown below. The trilinear approximation of the foundation backbone is in Table 6-5.

Table 6-5 – Tower North Foundation Backbone Trilinear Fit

Displacement North. (in.)	Force (kip)
0	0
1.3	20,000
5.25	28,000
8	28,000
14	24,500

L = Inelastic bar element length
 = 20 in.

FY = Component yield strength
 = 20,000 kip

ΔY = Component deformation at yield
 = 1.3 in.

K0 = Elastic stiffness
 = $FY / \Delta Y$
 = 15,385 kip / in.

E = Arbitrary elastic modulus
 = 10,000 ksi

A = Component cross section area
 = $K0 * L / E$
 = 30.77 in²

FU = Component ultimate strength
 = 28,000 kip

ΔU = Component deformation at ultimate strength
 = 5.25 in.

DU = Component strain at ultimate strength
 = $\Delta U / L$
 = 0.2625

ΔL = Component deformation at onset of strength loss
 = 8 in.

DL	=	Component strain at onset of strength loss
	=	$\Delta L / L$
	=	0.40
ΔR	=	Component deformation at end of strength loss
	=	14 in.
DR	=	Component strain at end of strength loss
	=	$\Delta R / L$
	=	0.70
FR	=	Component resistance at end of strength loss
	=	24,500 kip
FR / FU	=	0.875

6.2 Analysis Load Cases

We applied expected gravity loads simultaneous with lateral MCE seismic loading. Gravity dead and live loads on the tower are described in Volume I, Section 3. Gravity loads on the podium structure are described in Volume III, Section 6.1.1. The seismic hazard is described in Volume III, Section 1.

We conducted nonlinear time history analysis for 11 ground motion records spectrally matched to the MCE seismic hazard. We used the ground motion records selected by ENGEO Inc. in their September 2018 geotechnical memorandum. John Egan, Slate Geotechnical Consultants, Inc., and Shannon & Wilson, Inc. spectrally matched the ground motion records, as documented in their 30 November 2018 report. The spectrally matched records were provided to SGH as pairs of horizontal acceleration time histories oriented in the fault-normal and fault-parallel directions. Figure 6-26 illustrates the 301 Mission site relative to fault orientation. In each PERFORM-3D dynamic earthquake load case, we specified that the applied ground motions occur at a rotation of 10 degrees clockwise from the tower principle axes. Table 6-6 lists record sequence numbers from the PEER NGA West 2 database for the 11 ground motions applied in the dynamic earthquake load cases.

Table 6-6 – PERFORM-3D Nonlinear Time History Analyses

Ground Motion	PERFORM-3D Dynamic Earthquake Load Case
1	RSN#178 Imperial Valley-06
2	RSN#184 Imperial Valley-06
3	RSN#316 Westmorland
4	RSN#802 Loma Prieta
5	RSN#832 Landers
6	RSN#1163 Kocaeli
7	RSN#1261 Chi-Chi
8	RSN#1511 Chi-Chi
9	RSN#5827 El Mayor-Cucupah_Mexico
10	RSN#6890 Darfield NZ
11	RSN#6959 Darfield NZ

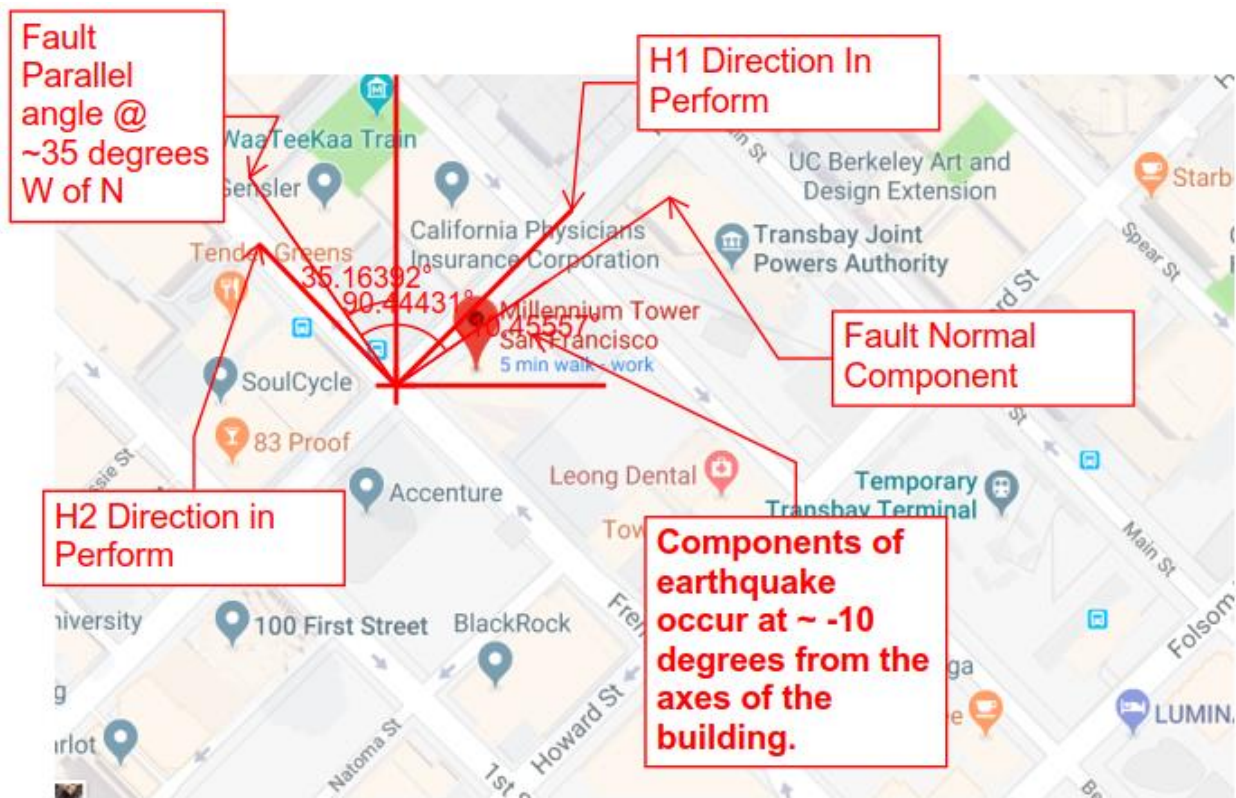


Figure 6-26 – 301 Mission Site Relative to Fault Orientation

6.2.1 Superstructure Analysis Series

We ran eleven analyses, one for each ground motion record. Each of the analyses consists of three loads applied in series:

1. Static nonlinear analysis: expected gravity load (1.0 Dead + 0.25 Live)
2. Static nonlinear analysis: retrofit pile jacking
3. Nonlinear dynamic earthquake analysis: one of the eleven ground motions

Retrofit pile jacking loads are discussed in Volume II. For these analyses we used a model with a pinned base.

6.2.2 Substructure Analysis Series

We ran eleven analyses, one for each ground motion record. Each of the analyses consists of three loads applied in series:

1. Nonlinear static analysis: expected gravity load (1.0 Dead + 0.25 Live)
2. Nonlinear static nonlinear analysis: base shear preload
3. Nonlinear dynamic earthquake analysis: one of the eleven ground motions

The effect of settlement on the substructure capacity is captured in our model of the foundation backbone, as described in Sections 4 and 5. Base shear preload refers to static lateral forces acting at the tower and podium foundation from two sources: (1) unbalanced at-rest soil pressure, and (2) existing pile shear forces induced by settlement of the tower. These static lateral forces are described in Sections 5.4.1 and 6.1.2.

6.3 Superstructure Analysis Results

6.3.1 Shear Walls

6.3.1.1 Axial Strains

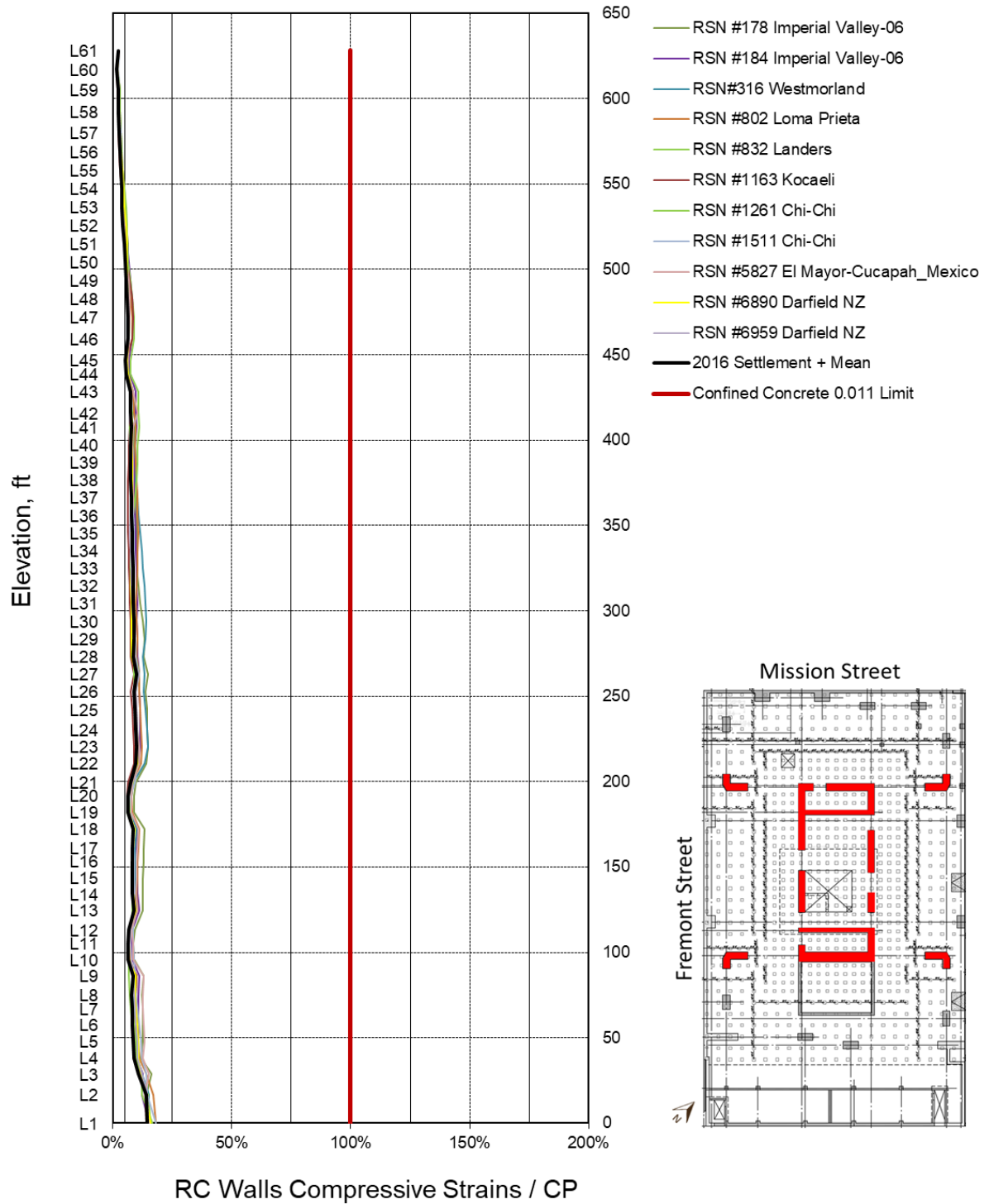


Figure 6-27 – Shear Wall Concrete Compressive Strains

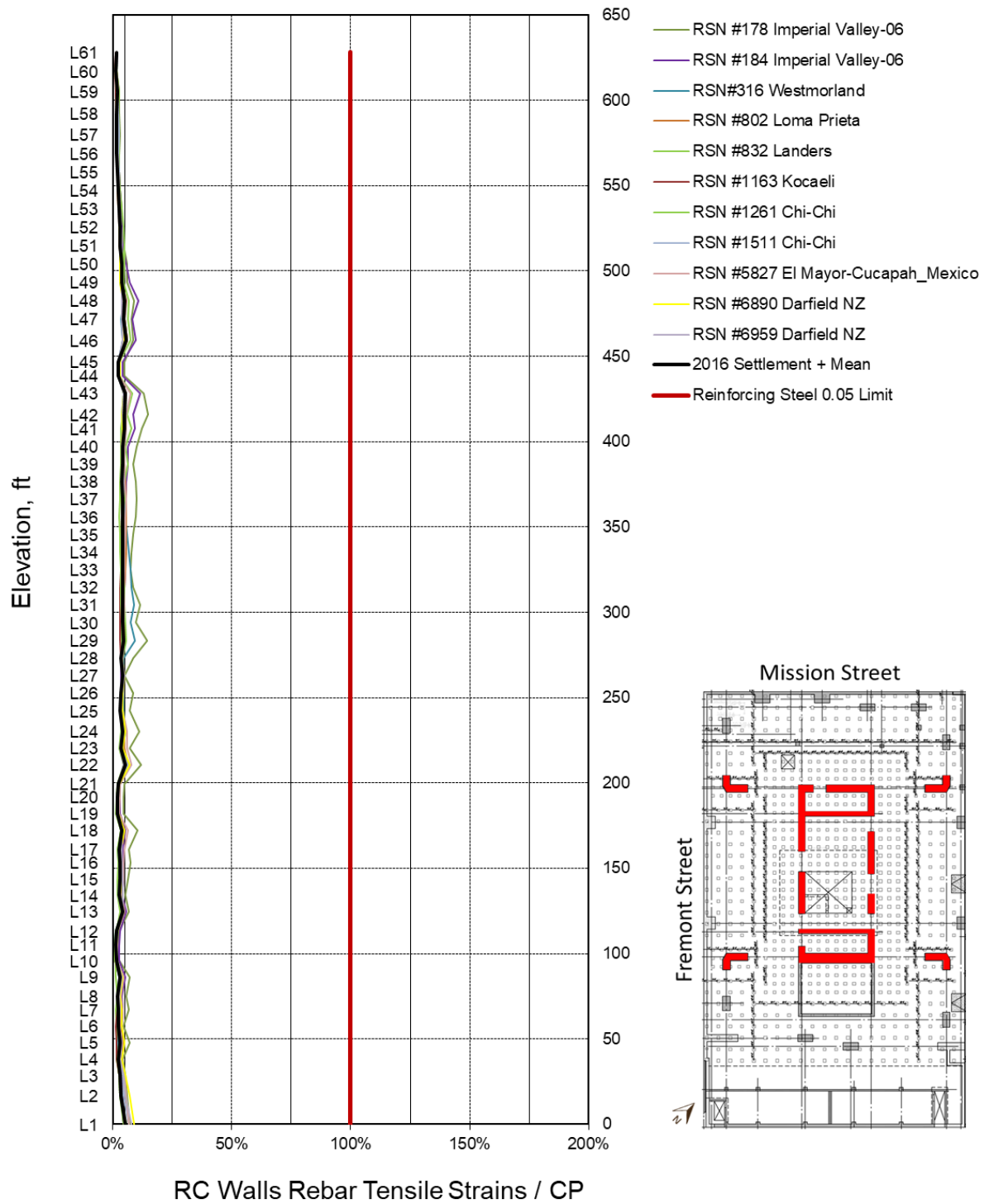


Figure 6-28 – Shear Wall Steel Tensile Strains

6.3.1.2 Steel Coupling Beam Rotations

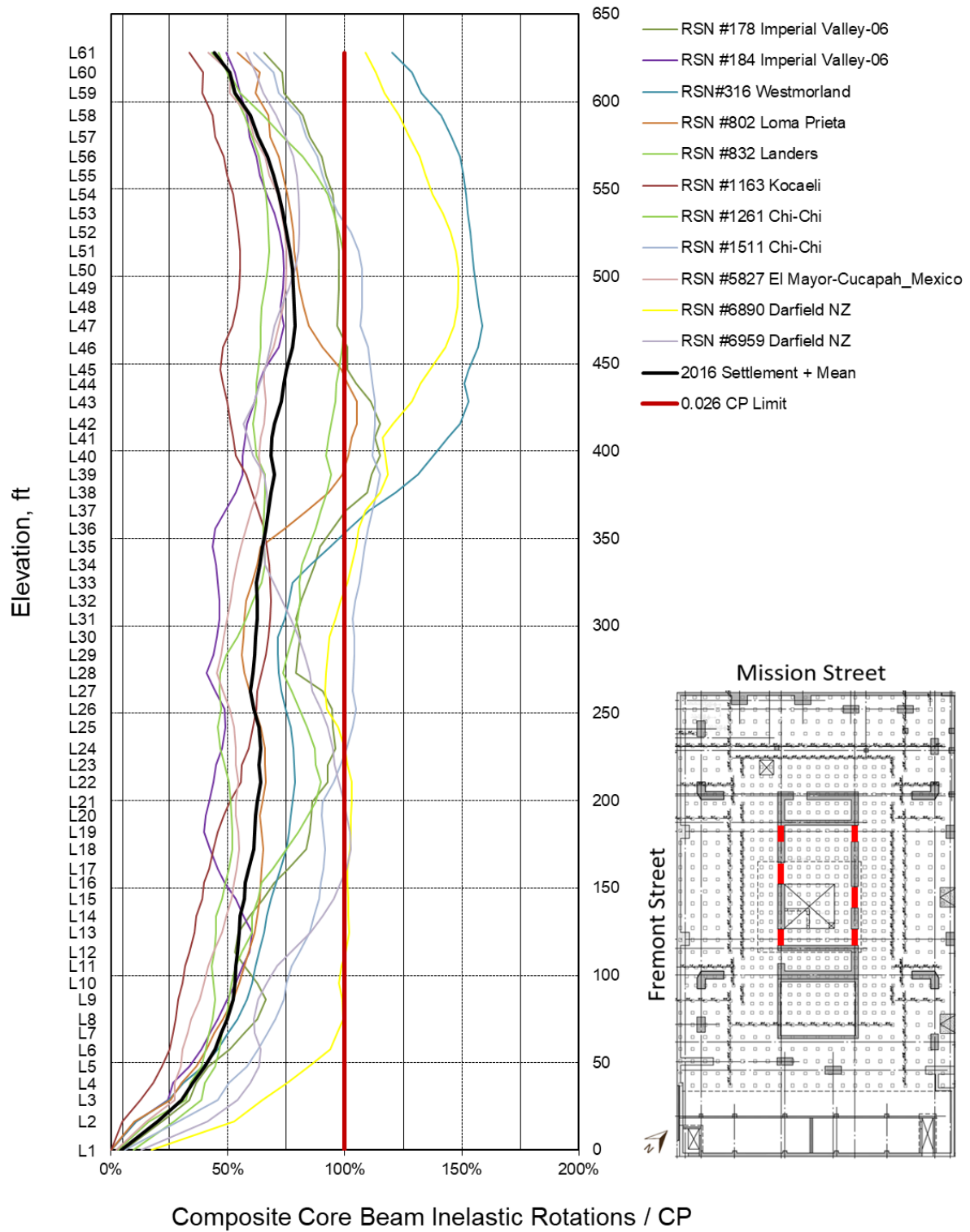
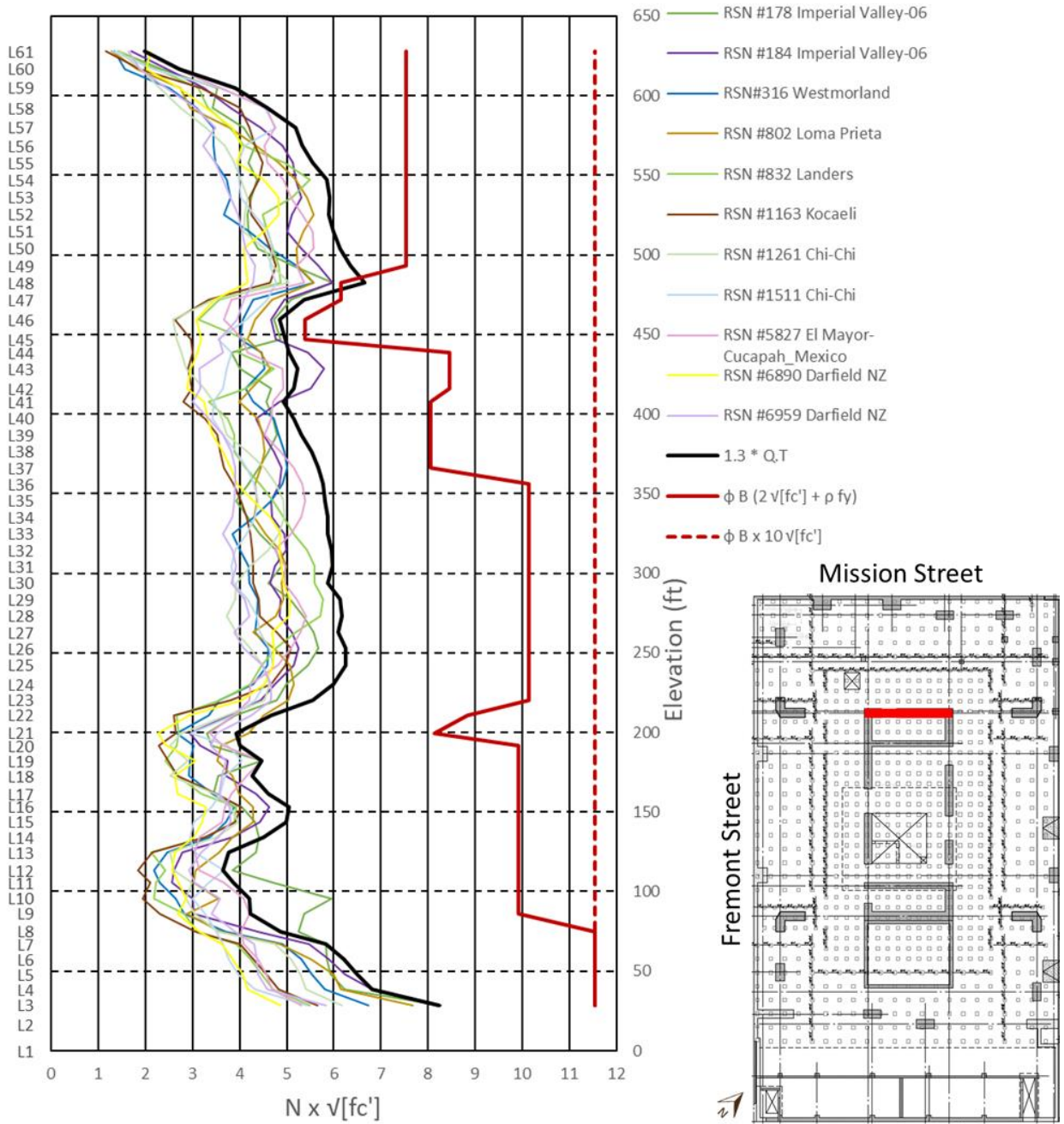


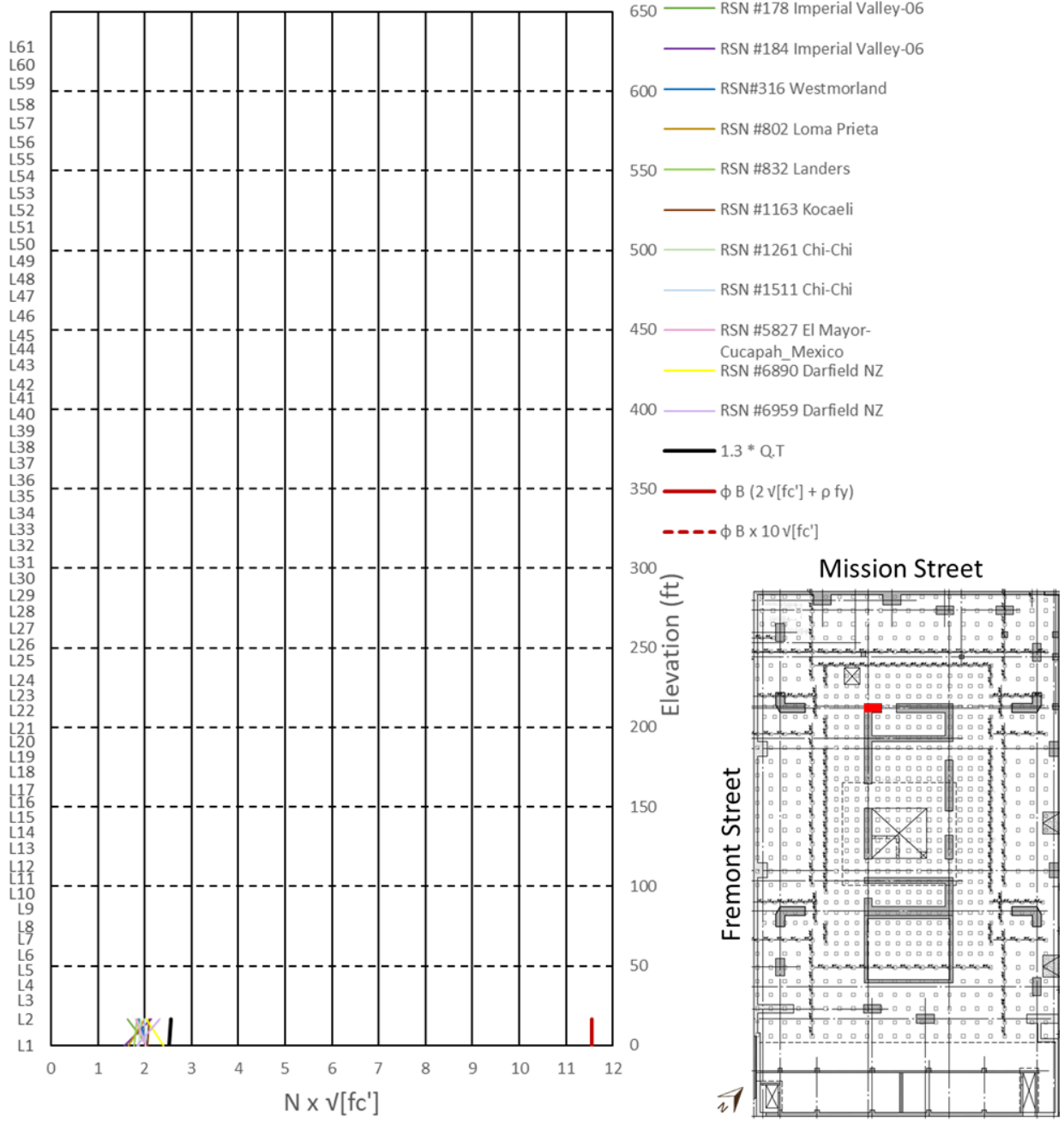
Figure 6-29 – Steel Coupling Beam Inelastic Rotations

6.3.1.3 Shear Wall Forces

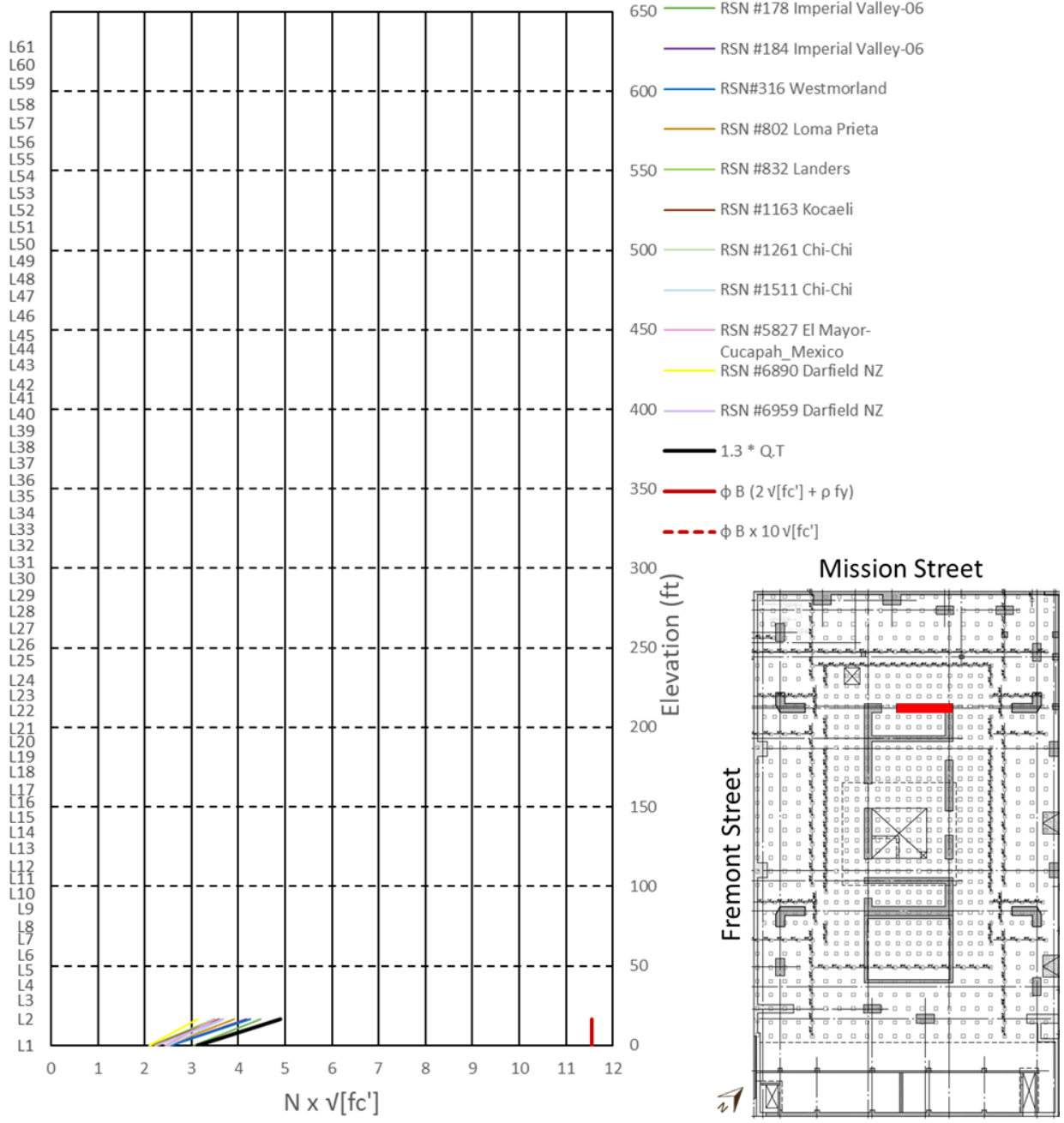
Pier C-49 Force-Controlled Shear



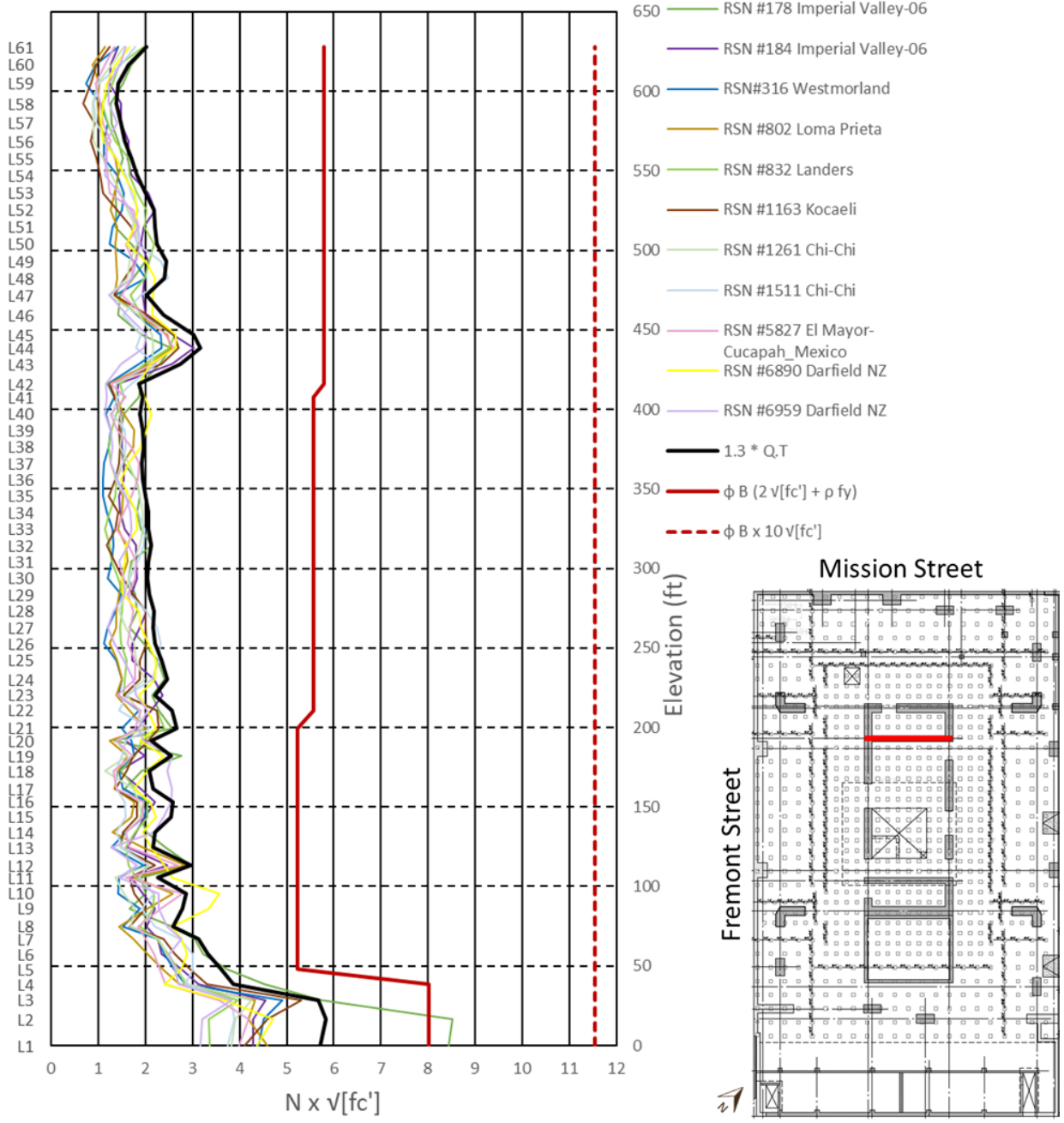
Pier C-4 Force-Controlled Shear



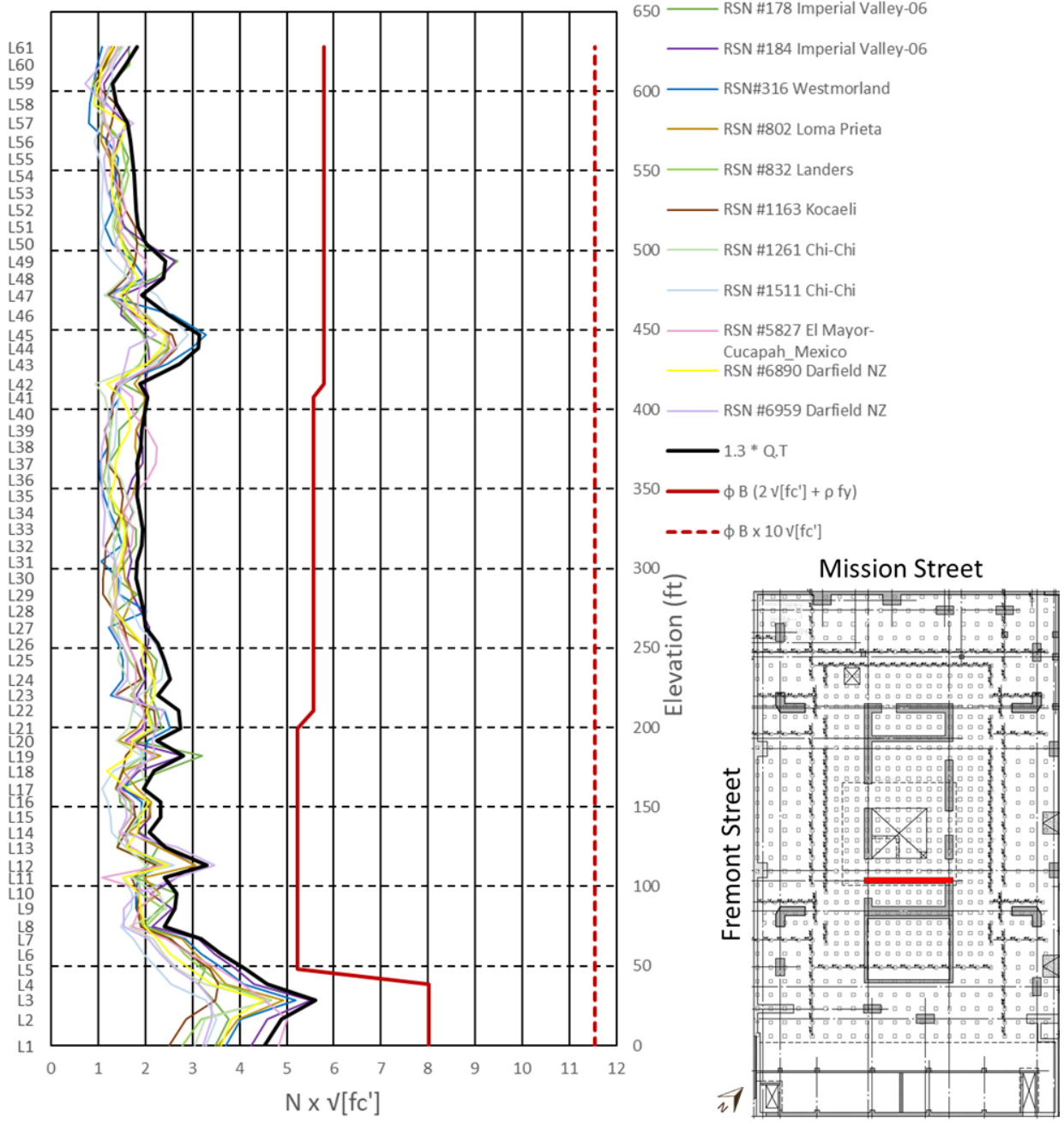
Pier C-9 Force-Controlled Shear



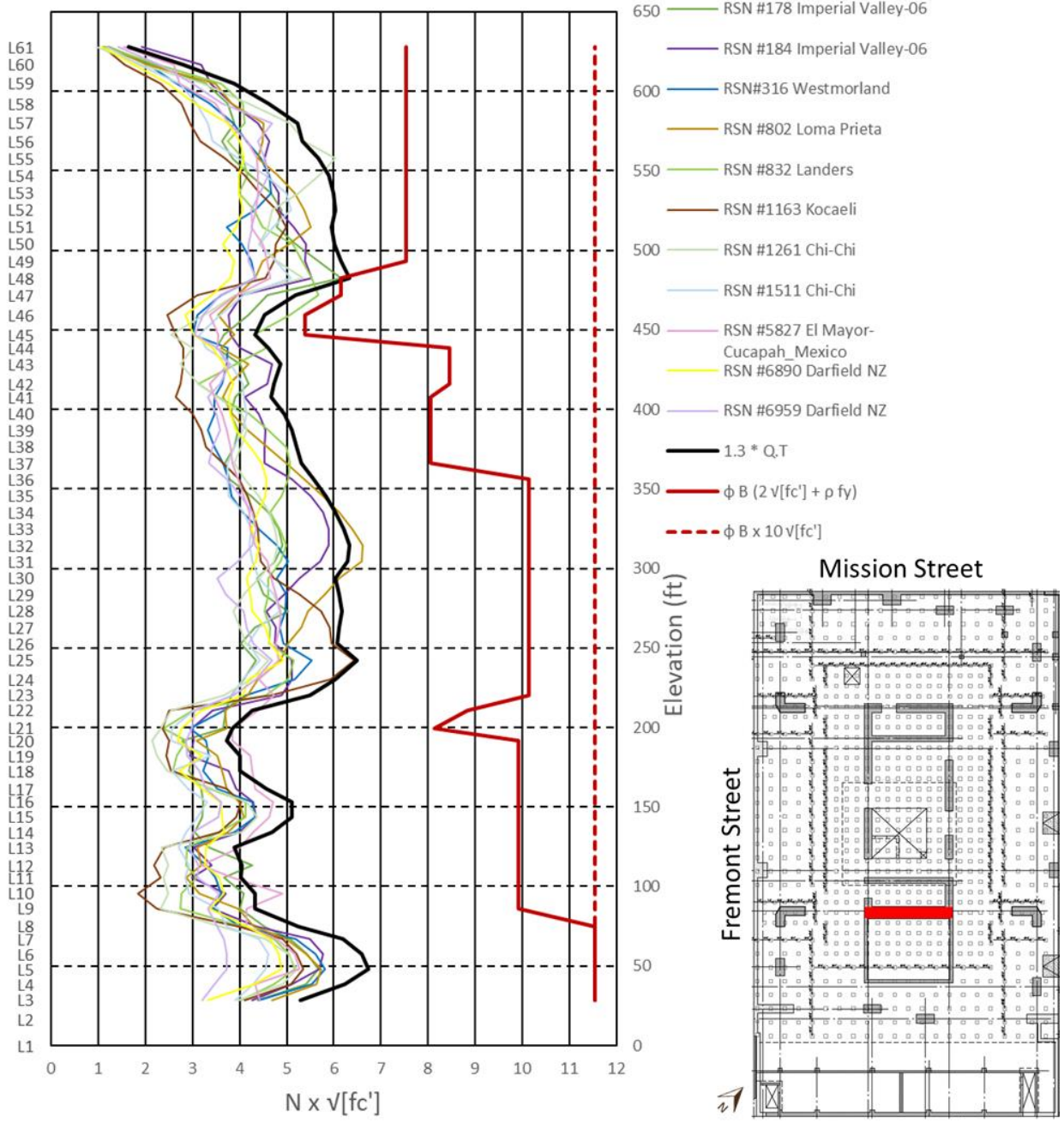
Pier C.7-49 Force-Controlled Shear



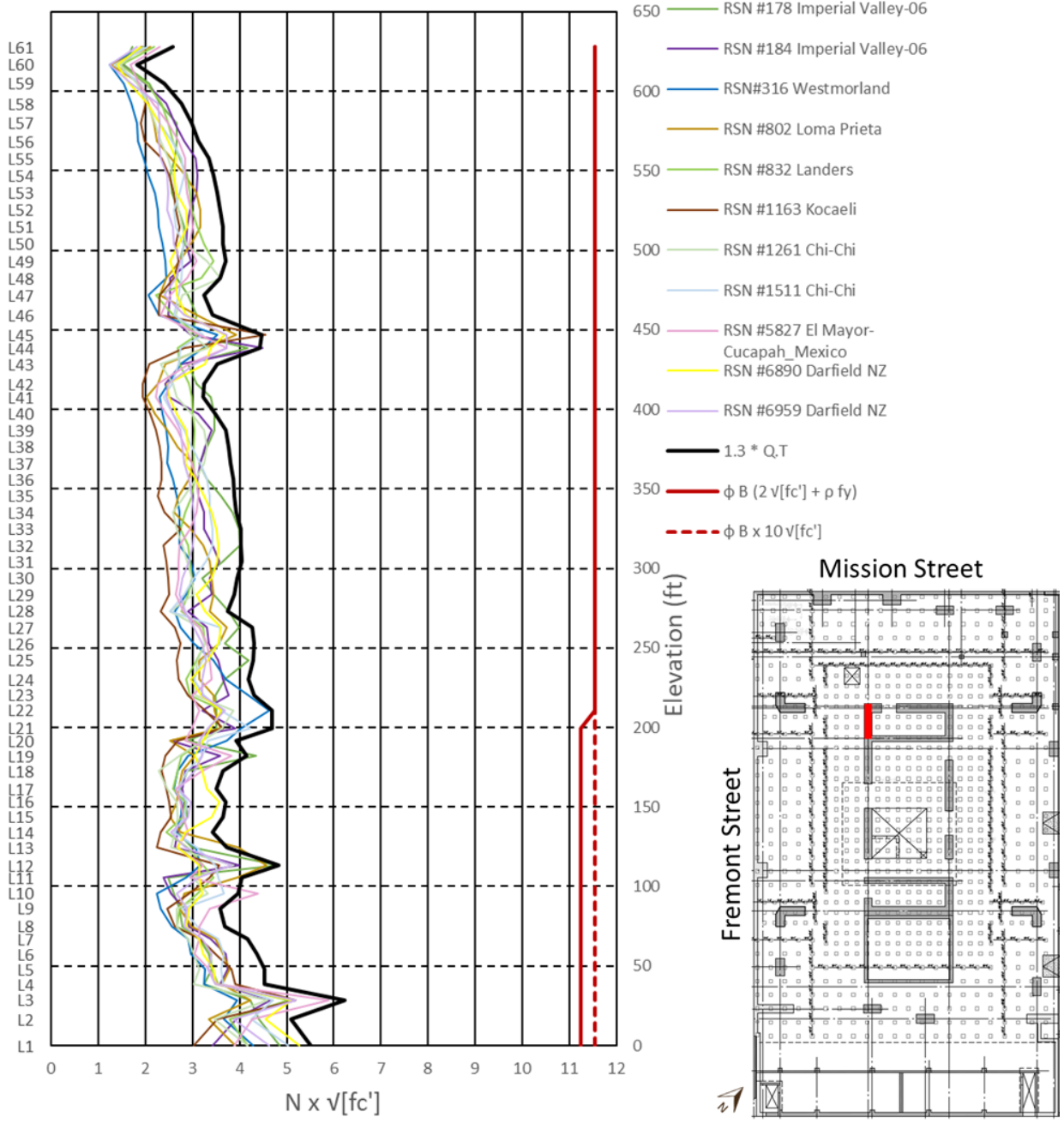
Pier E.3-49 Force-Controlled Shear



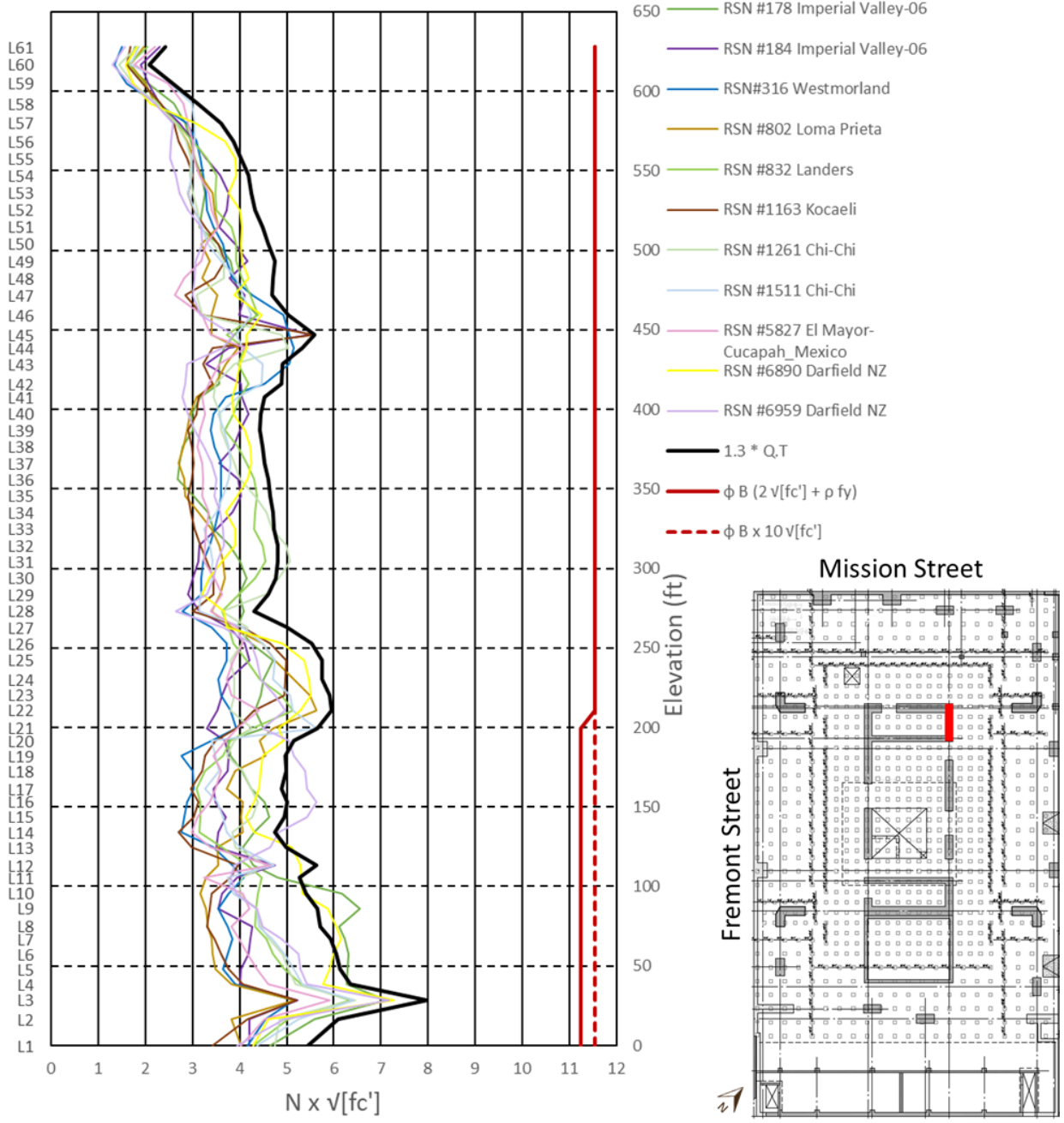
Pier F-49 Force-Controlled Shear



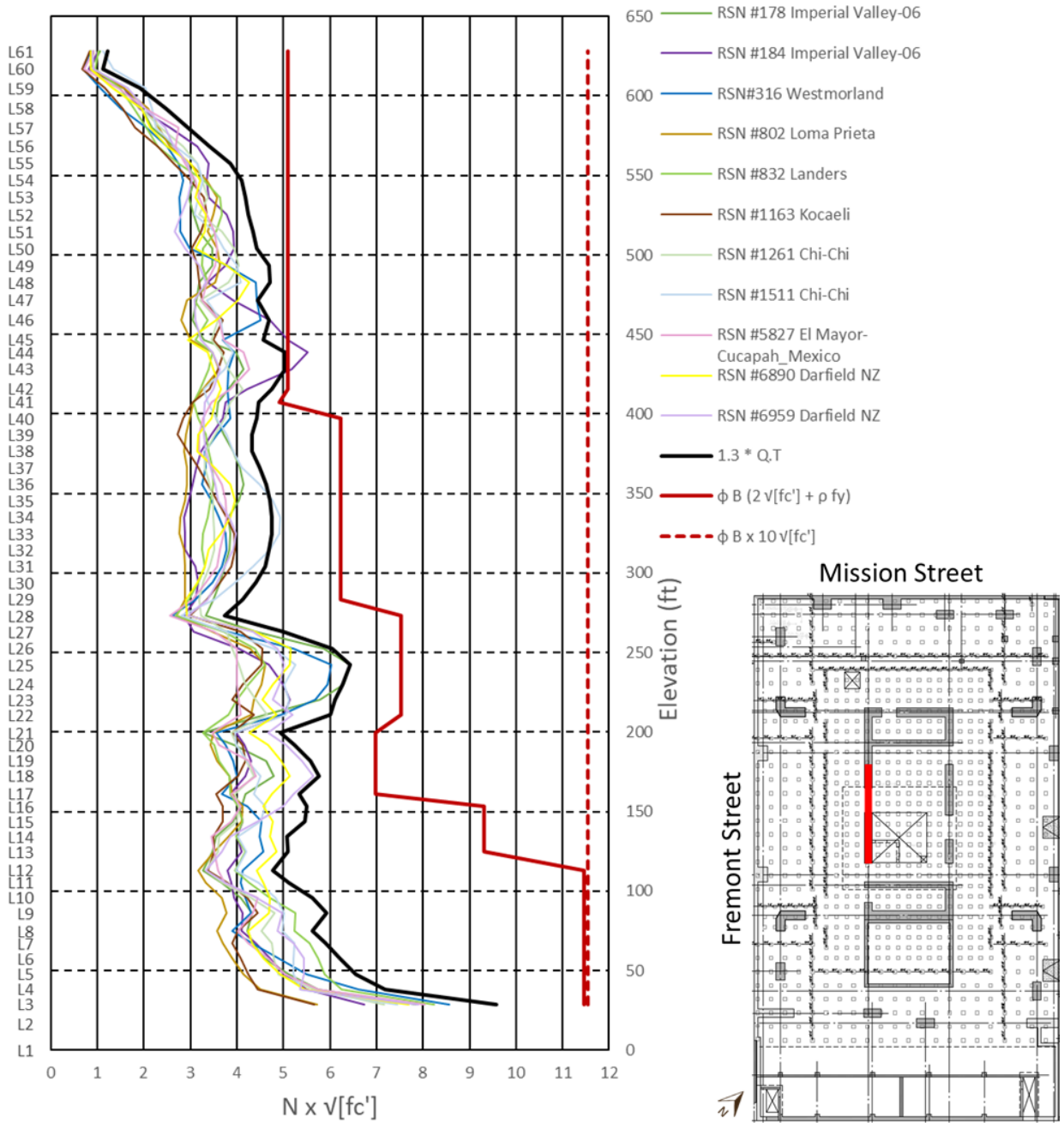
Pier 4-C Force-Controlled Shear



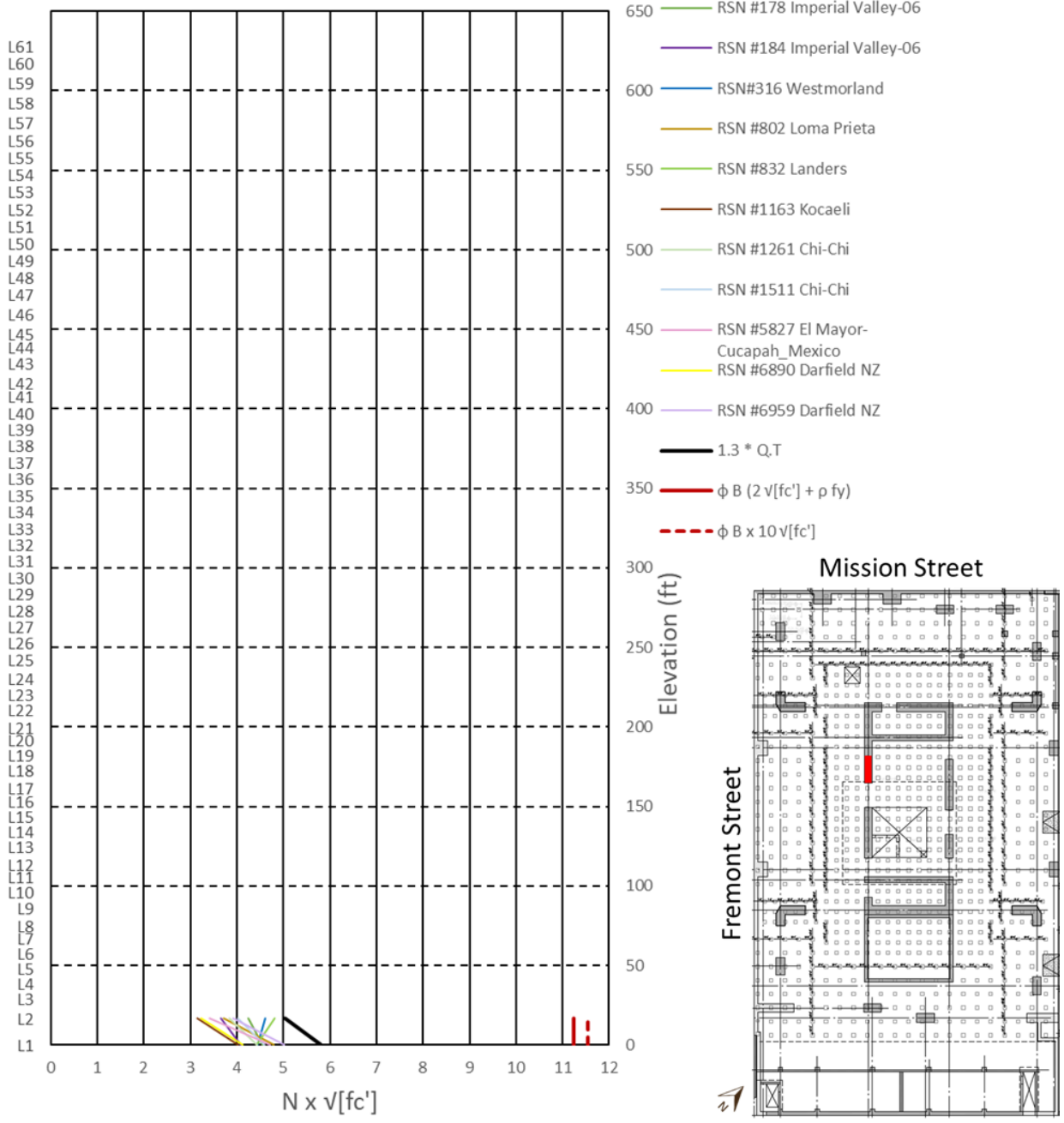
Pier 9-C Force-Controlled Shear



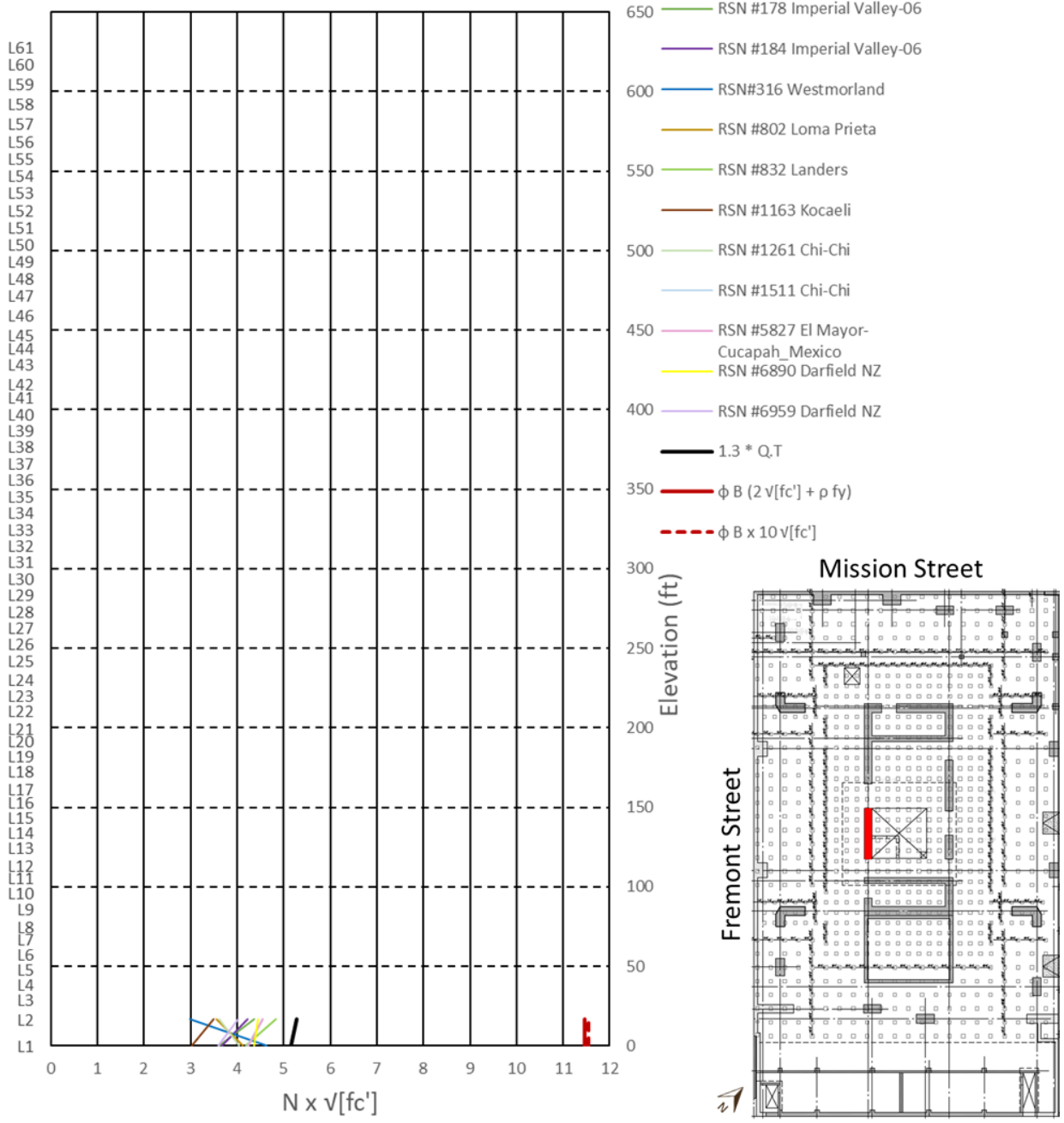
Pier 4-DE Force-Controlled Shear



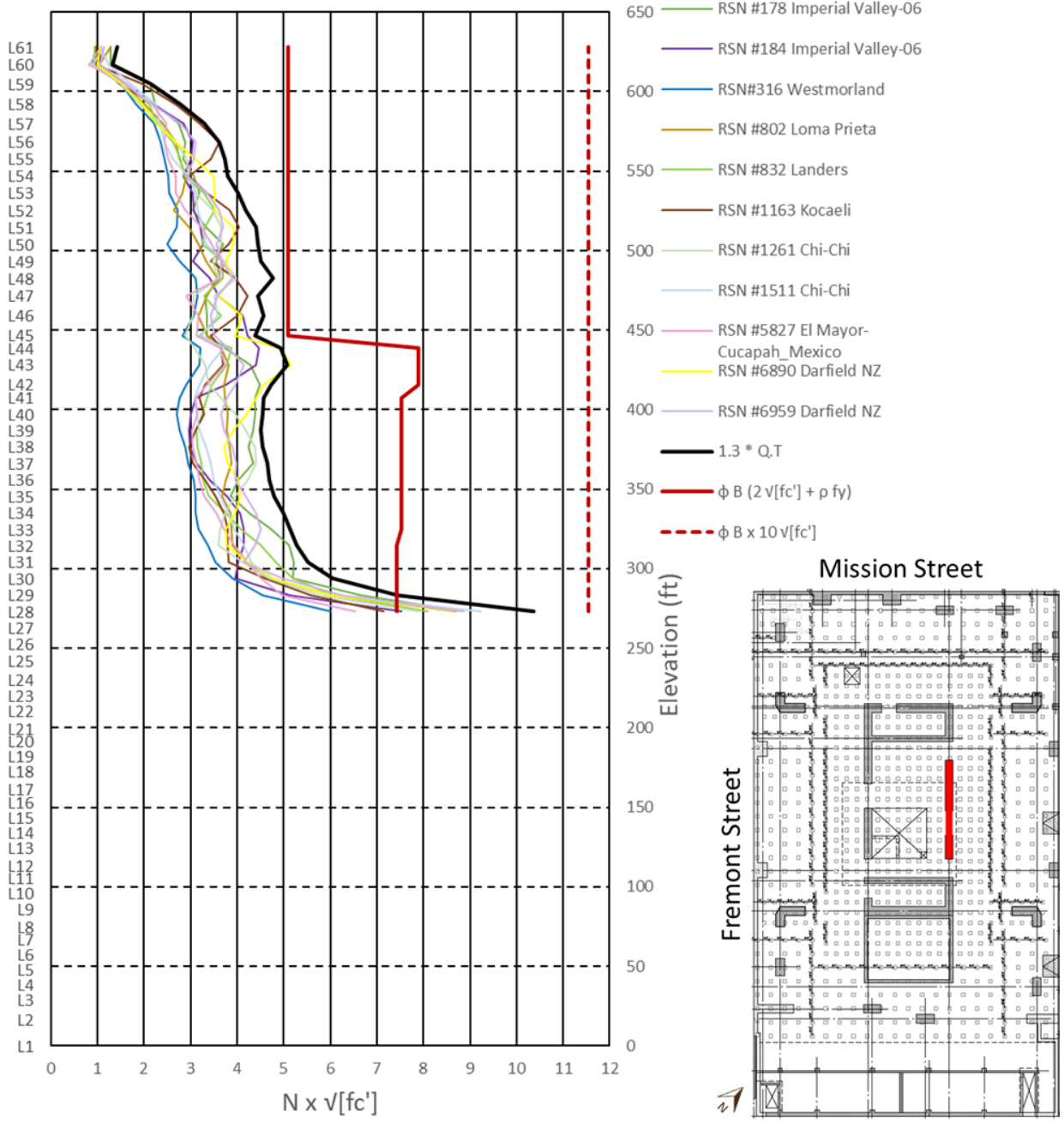
Pier 4-D Force-Controlled Shear



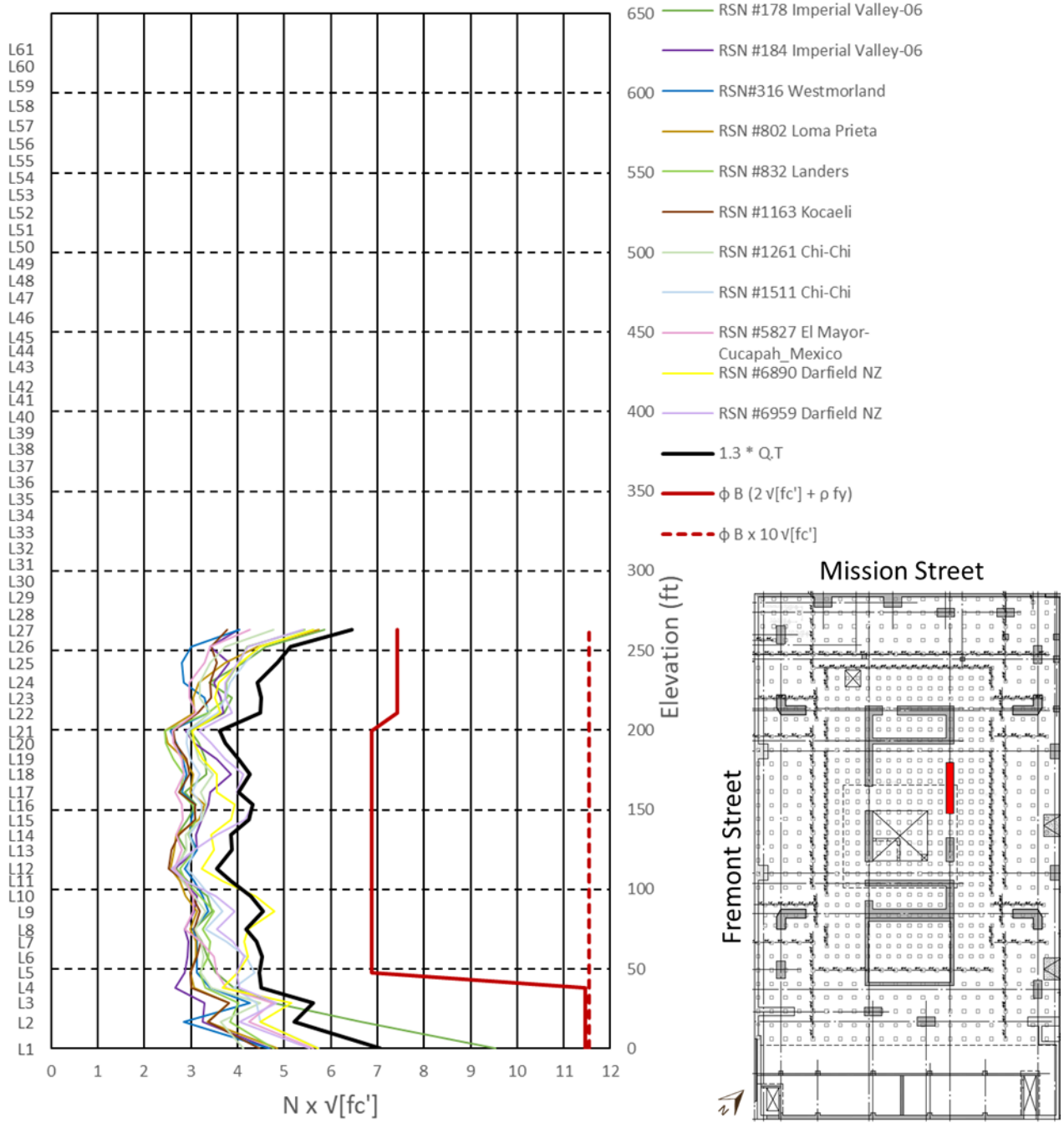
Pier 4-E Force-Controlled Shear



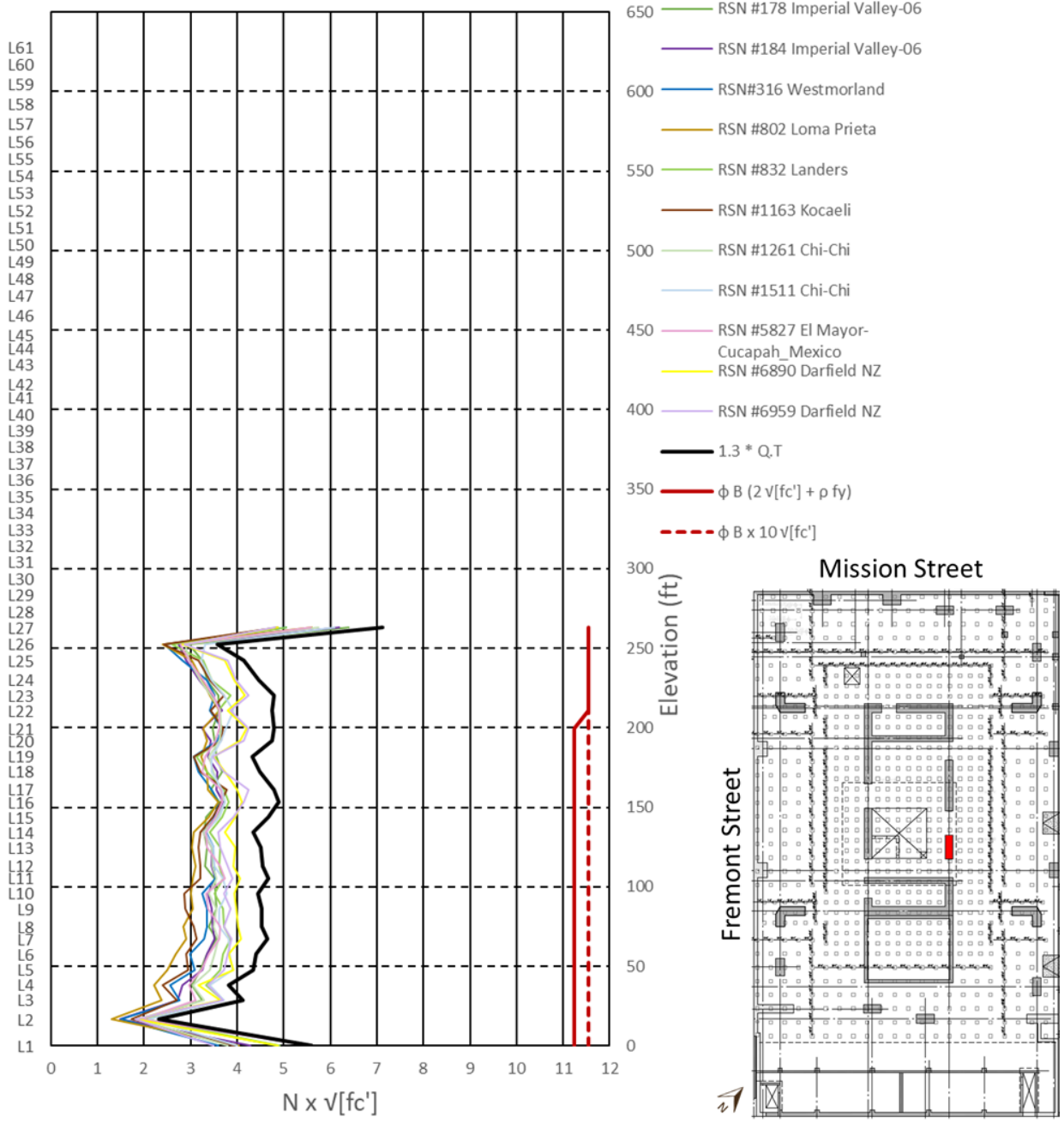
Pier 9-DE Force-Controlled Shear



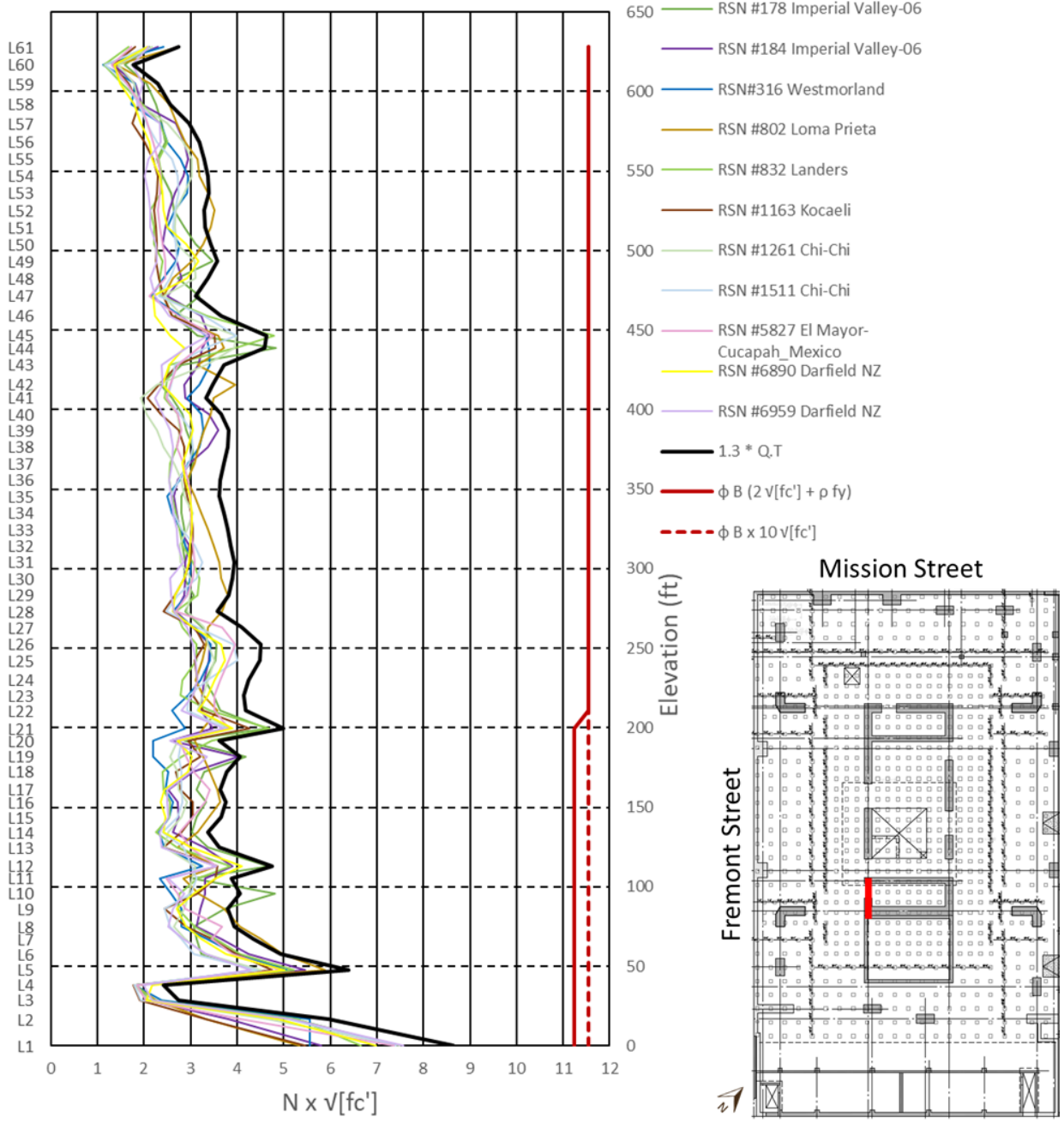
Pier 9-D Force-Controlled Shear



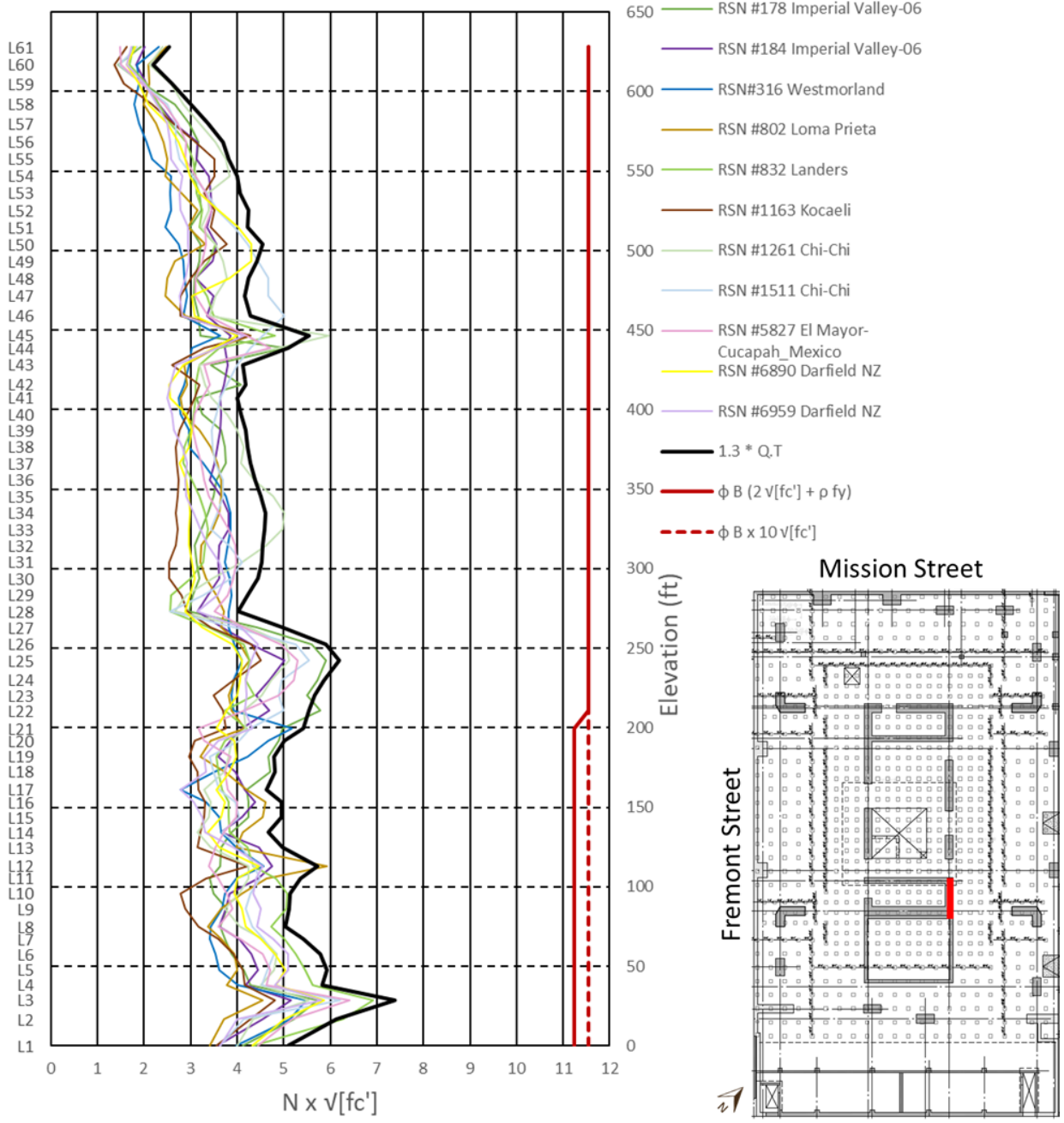
Pier 9-E Force-Controlled Shear



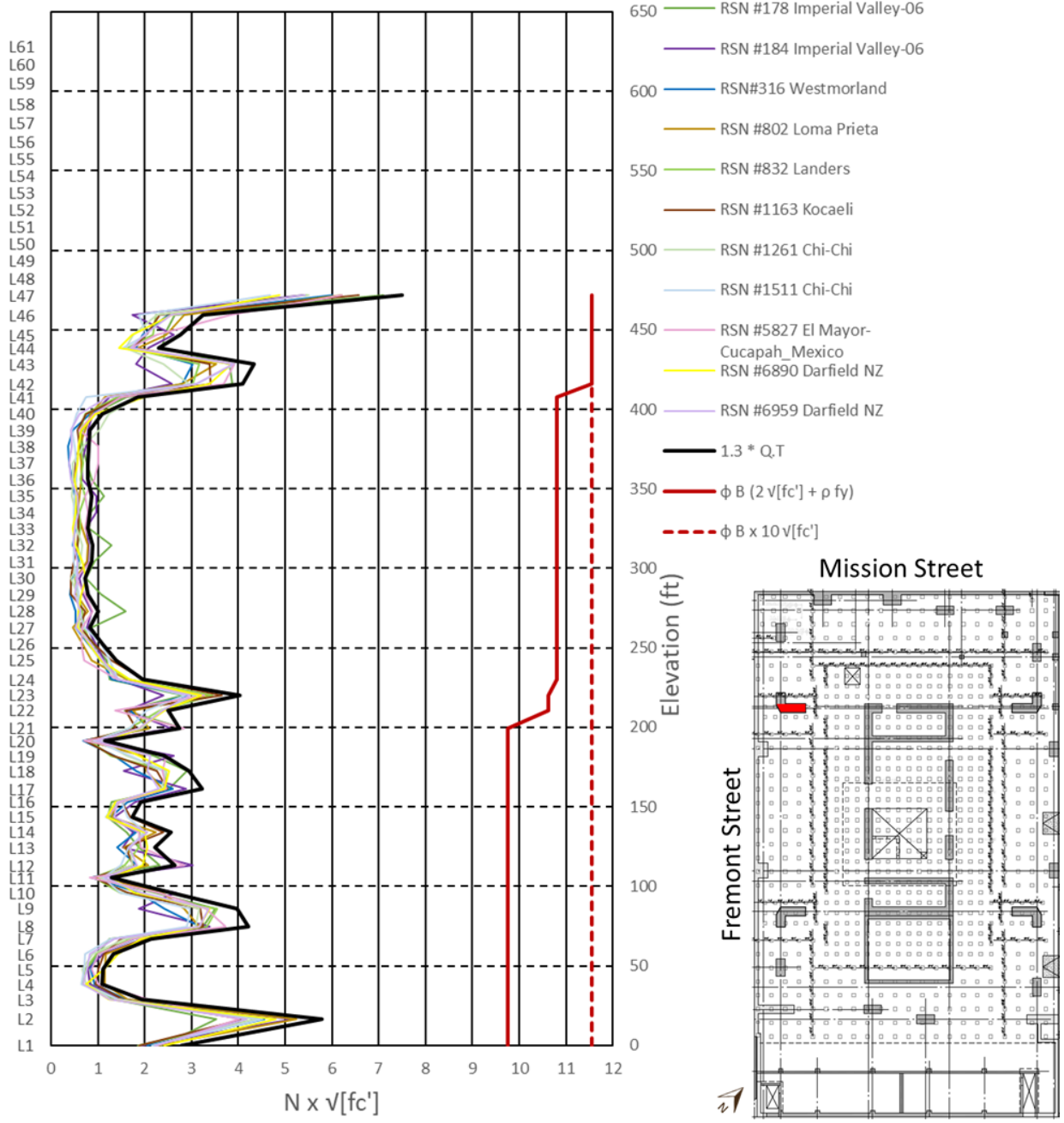
Pier 4-F Force-Controlled Shear



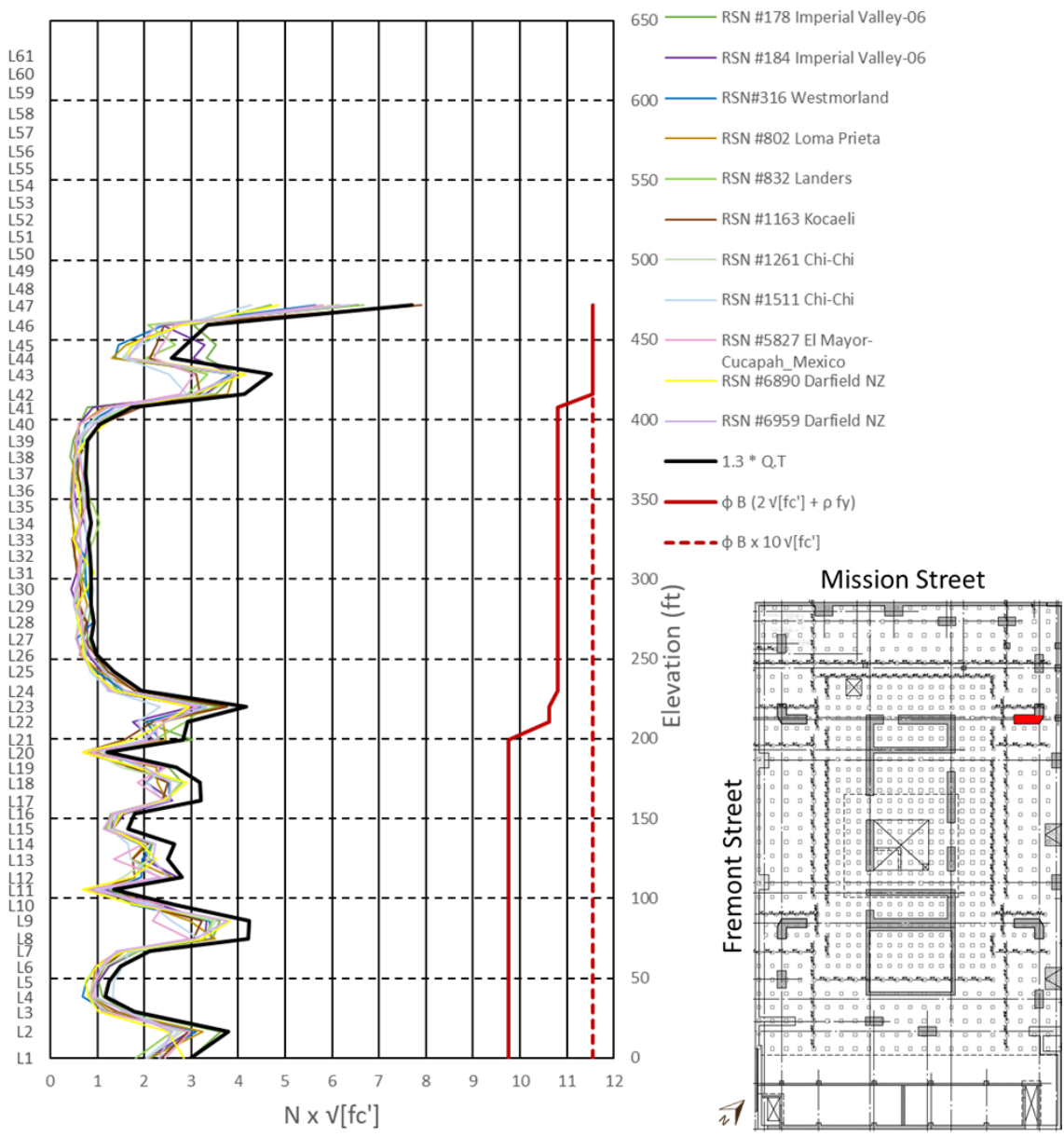
Pier 9-F Force-Controlled Shear



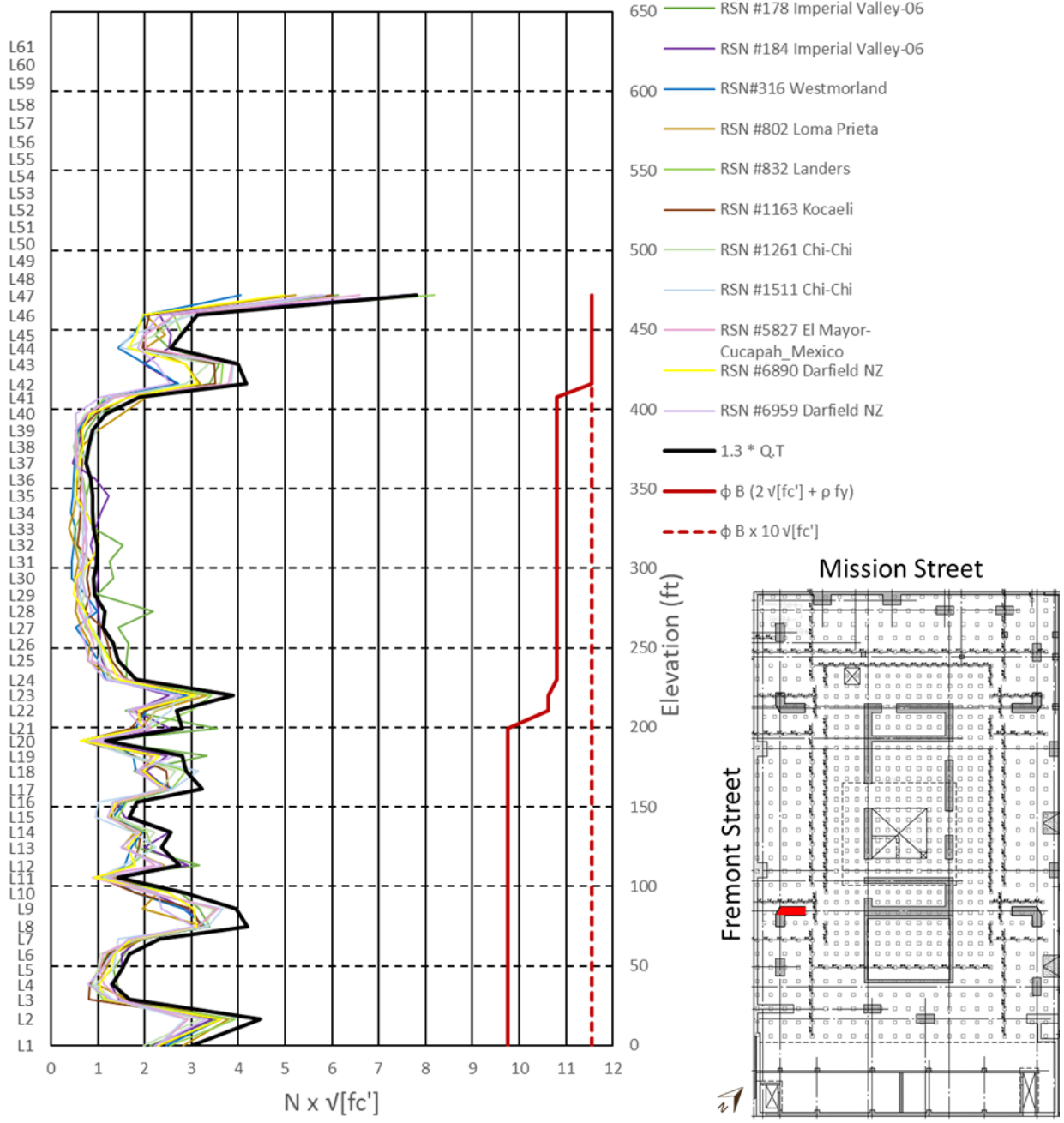
Pier C-2 Force-Controlled Shear



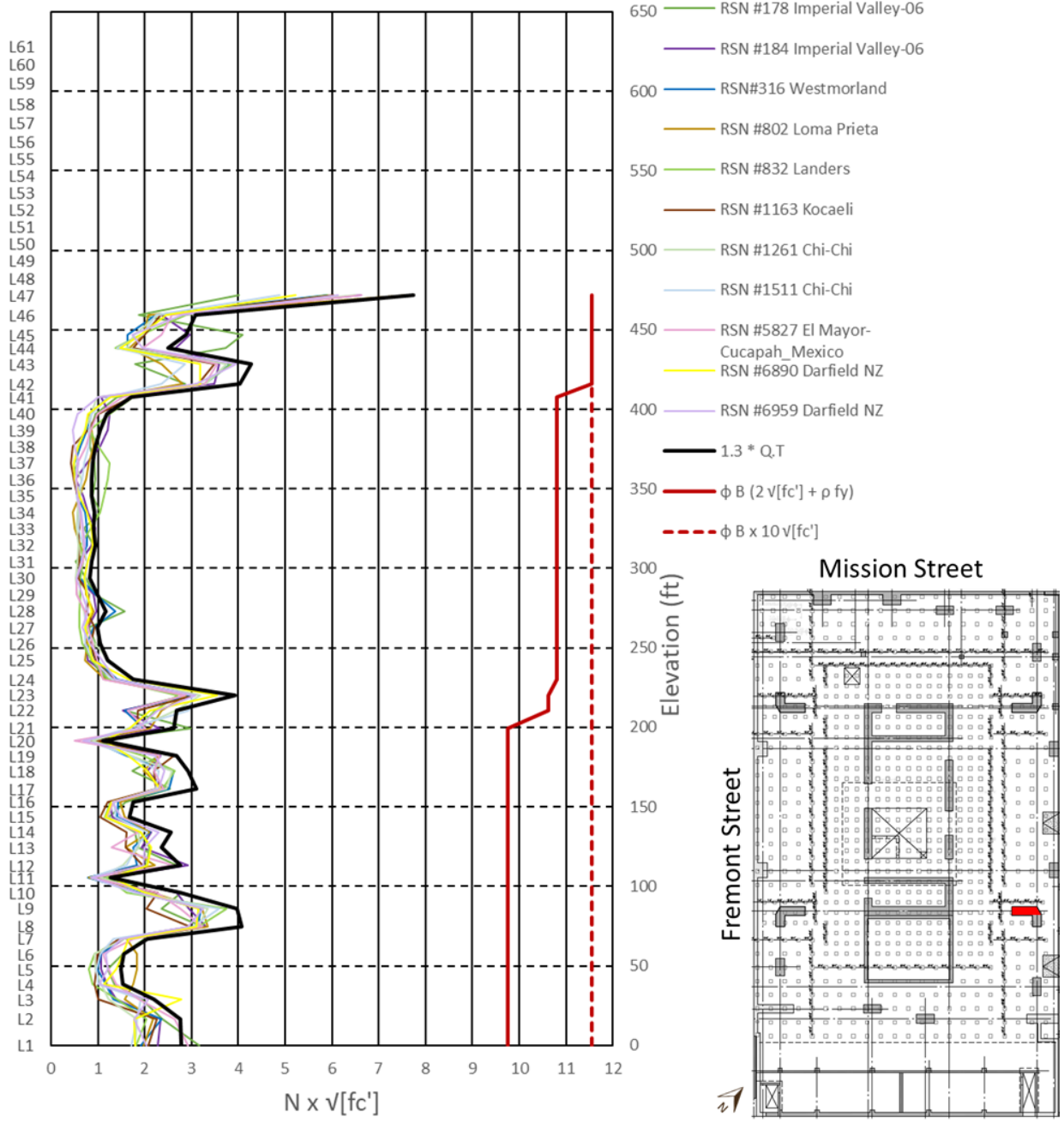
Pier C-11 Force-Controlled Shear



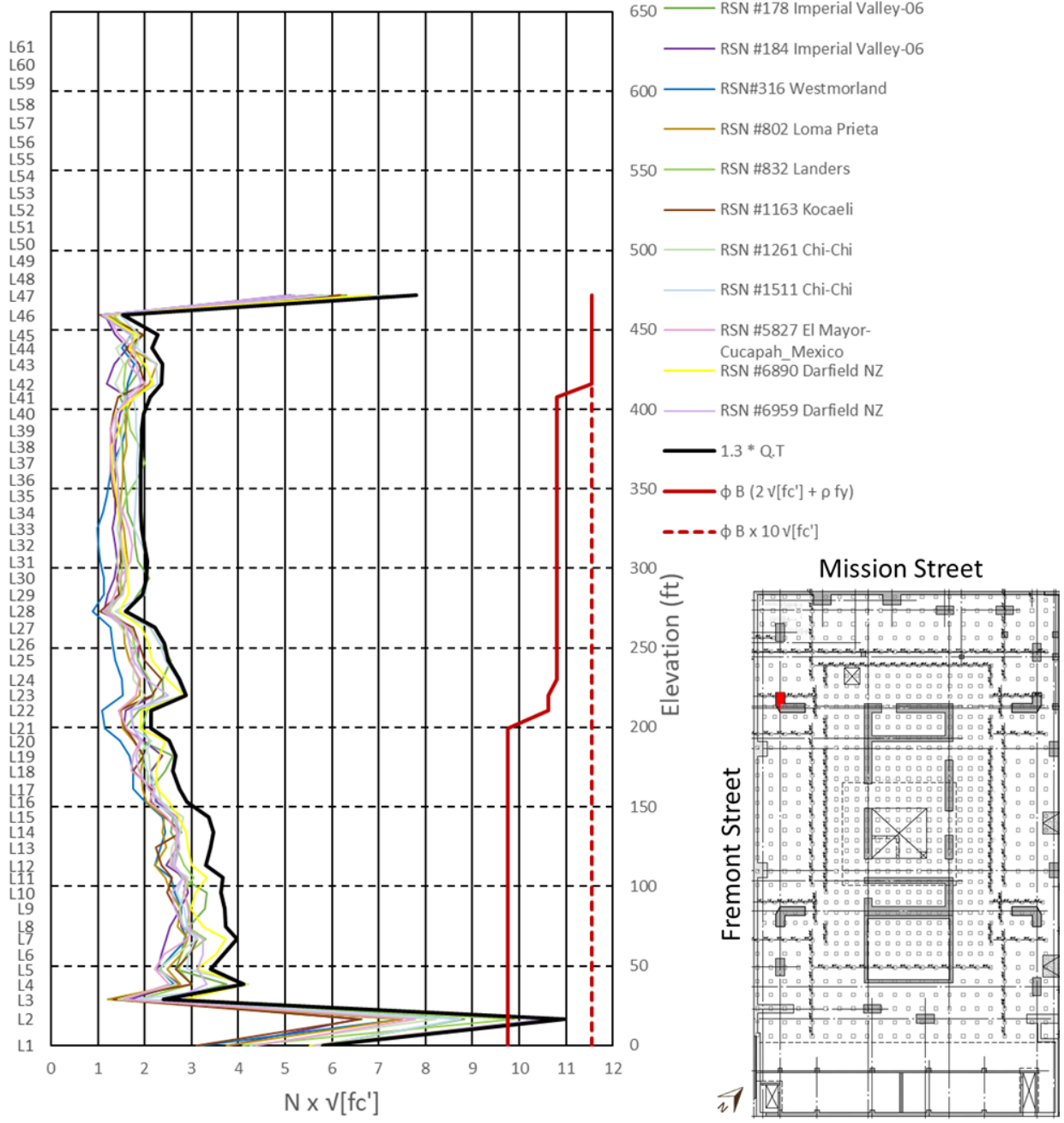
Pier F-2 Force-Controlled Shear



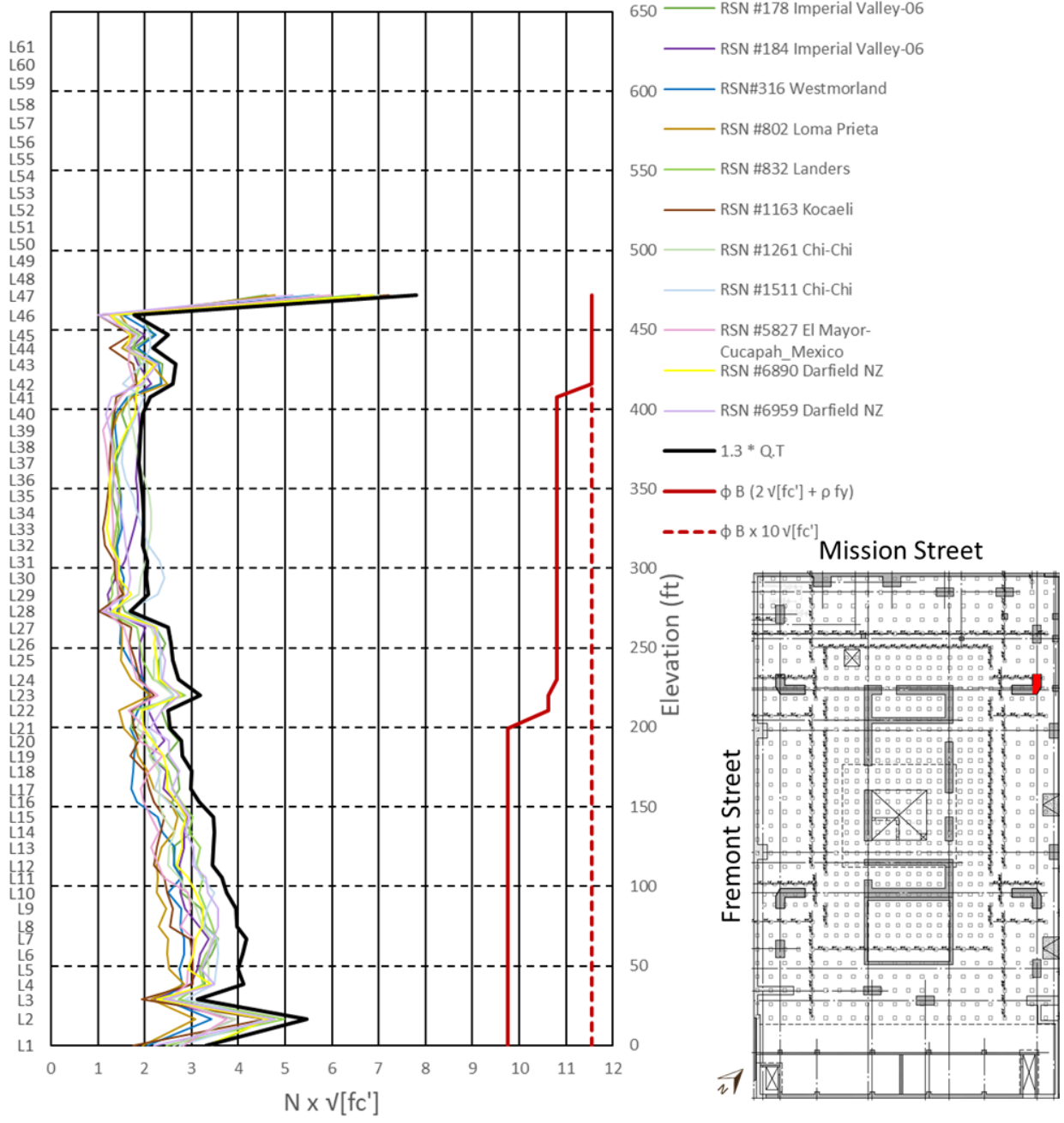
Pier F-11 Force-Controlled Shear



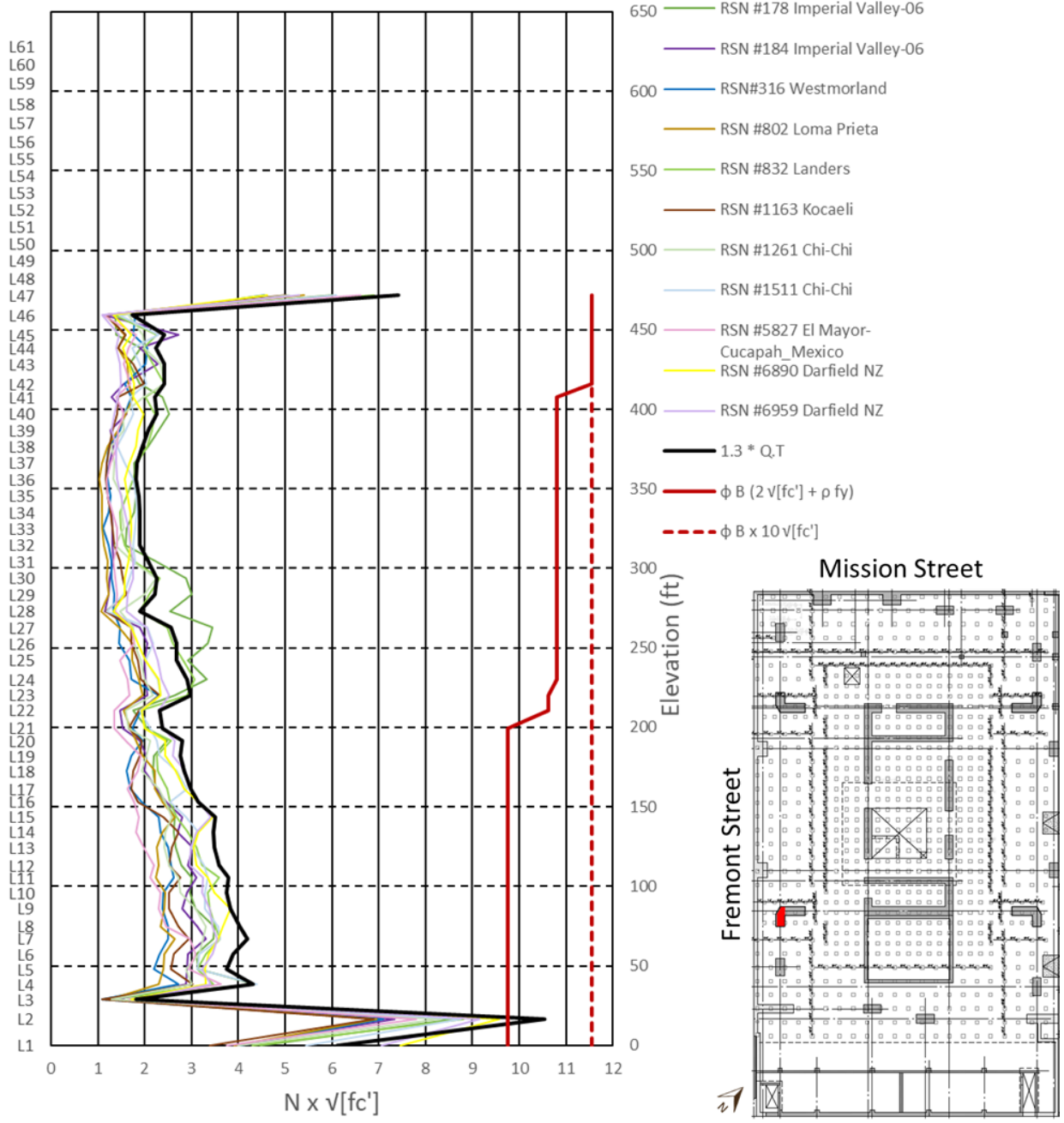
Pier 2-C Force-Controlled Shear



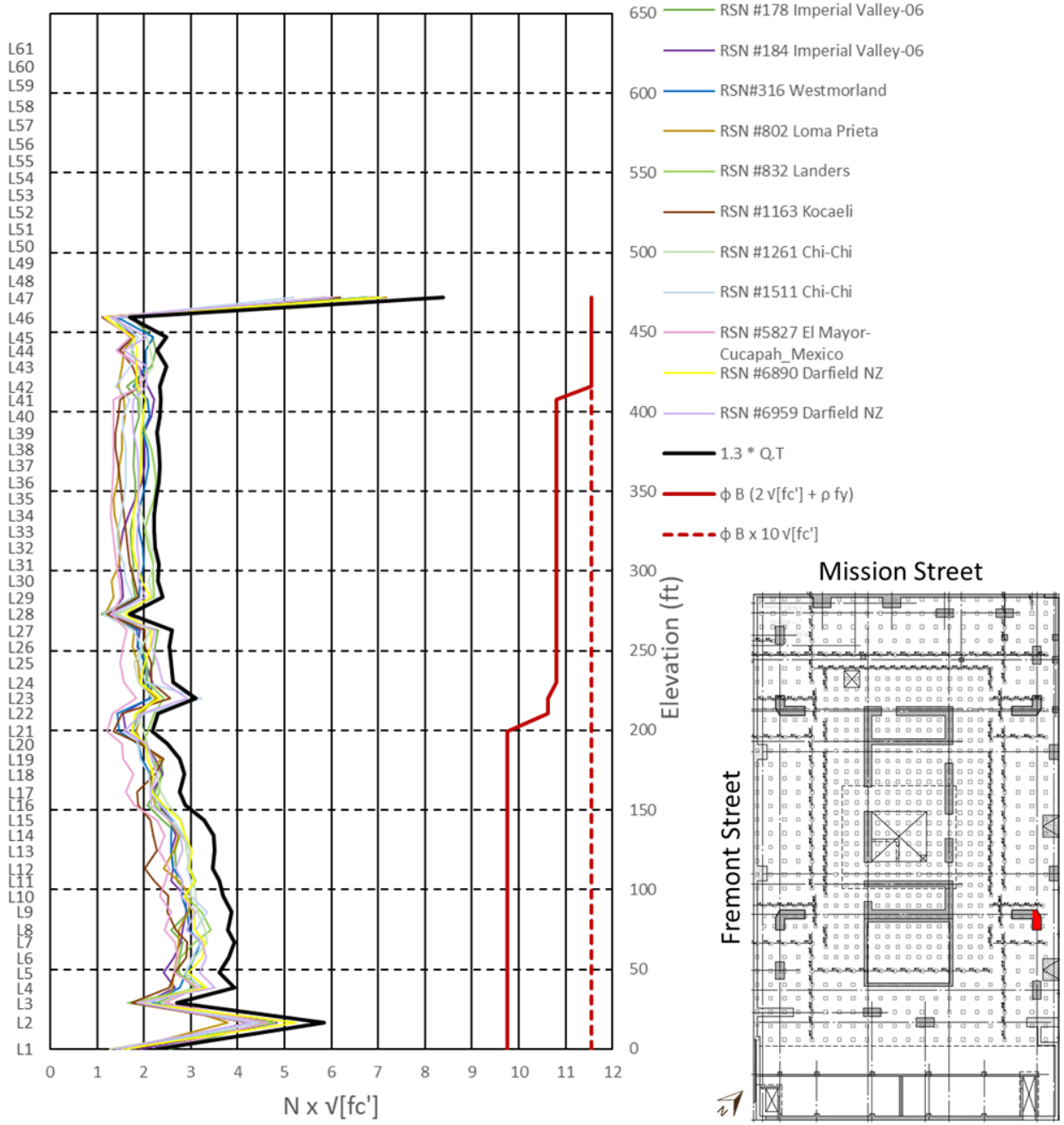
Pier 11-C Force-Controlled Shear



Pier 2-F Force-Controlled Shear



Pier 11-F Force-Controlled Shear



6.3.2 Perimeter Moment Frames

6.3.2.1 Column Plastic Rotations

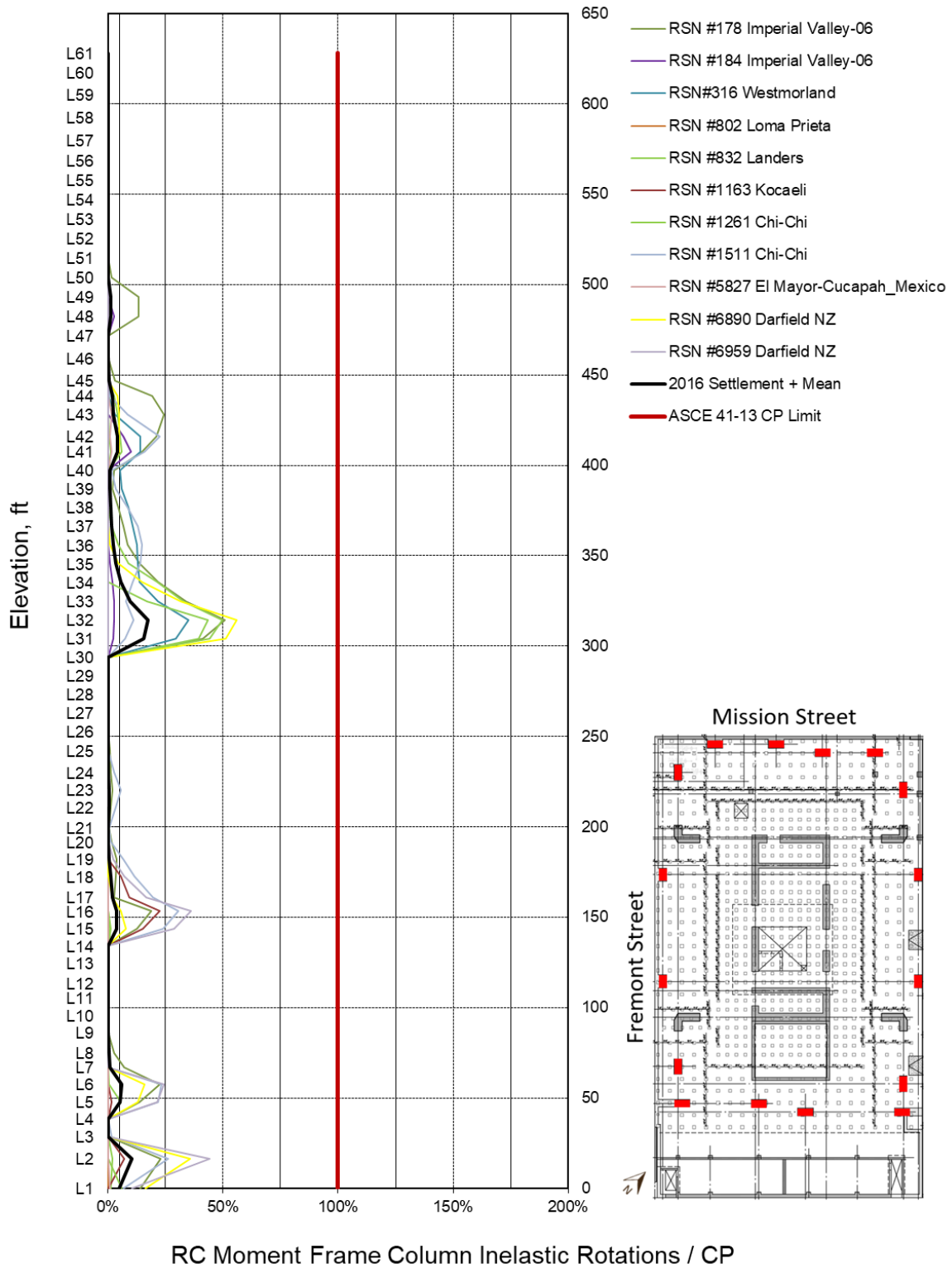
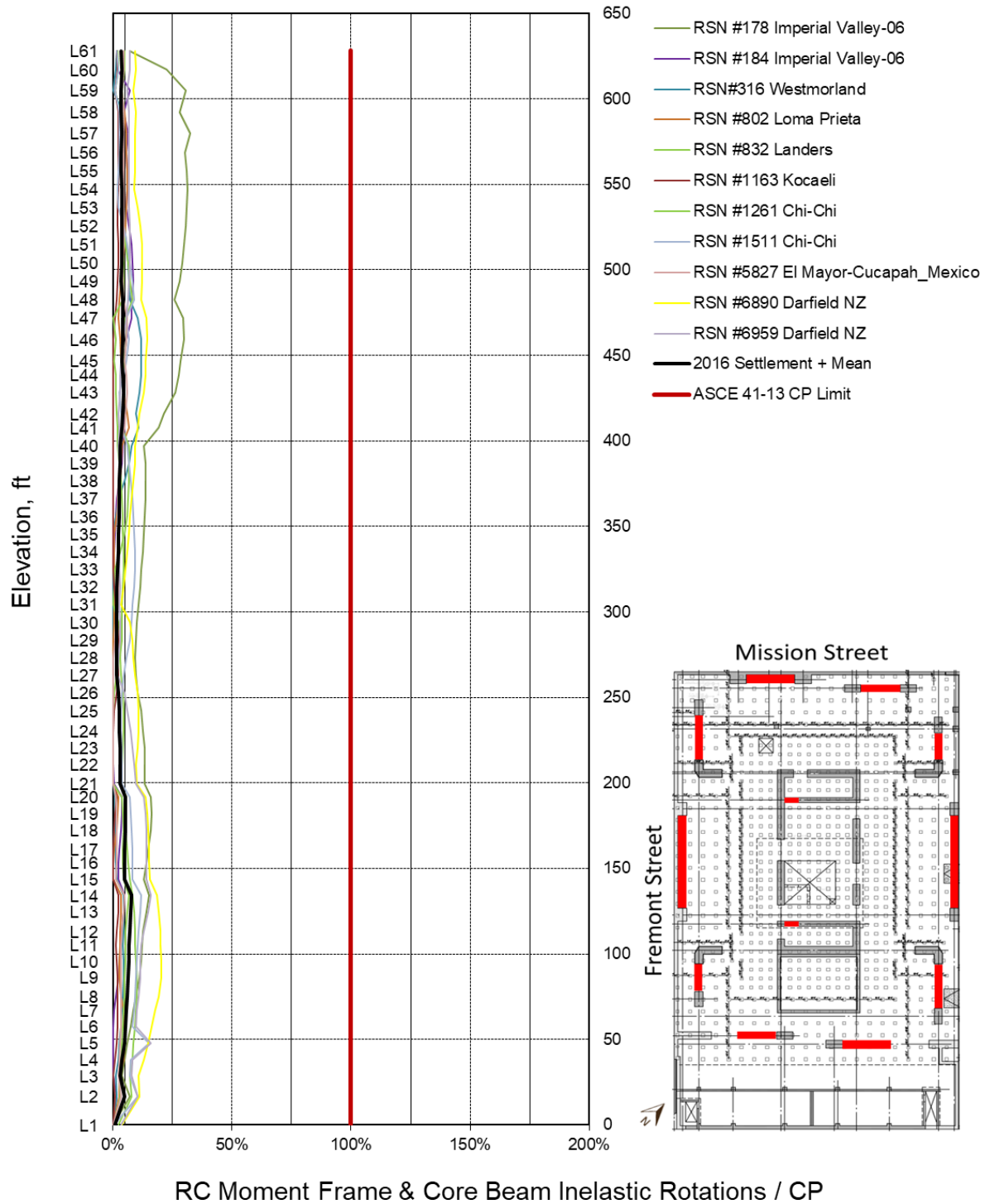


Figure 6-30 – Moment Frame Column Inelastic Rotations

6.3.2.2 Beam Plastic Rotations



RC Moment Frame & Core Beam Inelastic Rotations / CP

Figure 6-31 – Moment Frame Beam Inelastic Rotations

6.3.3 Outrigger Beam Rotations

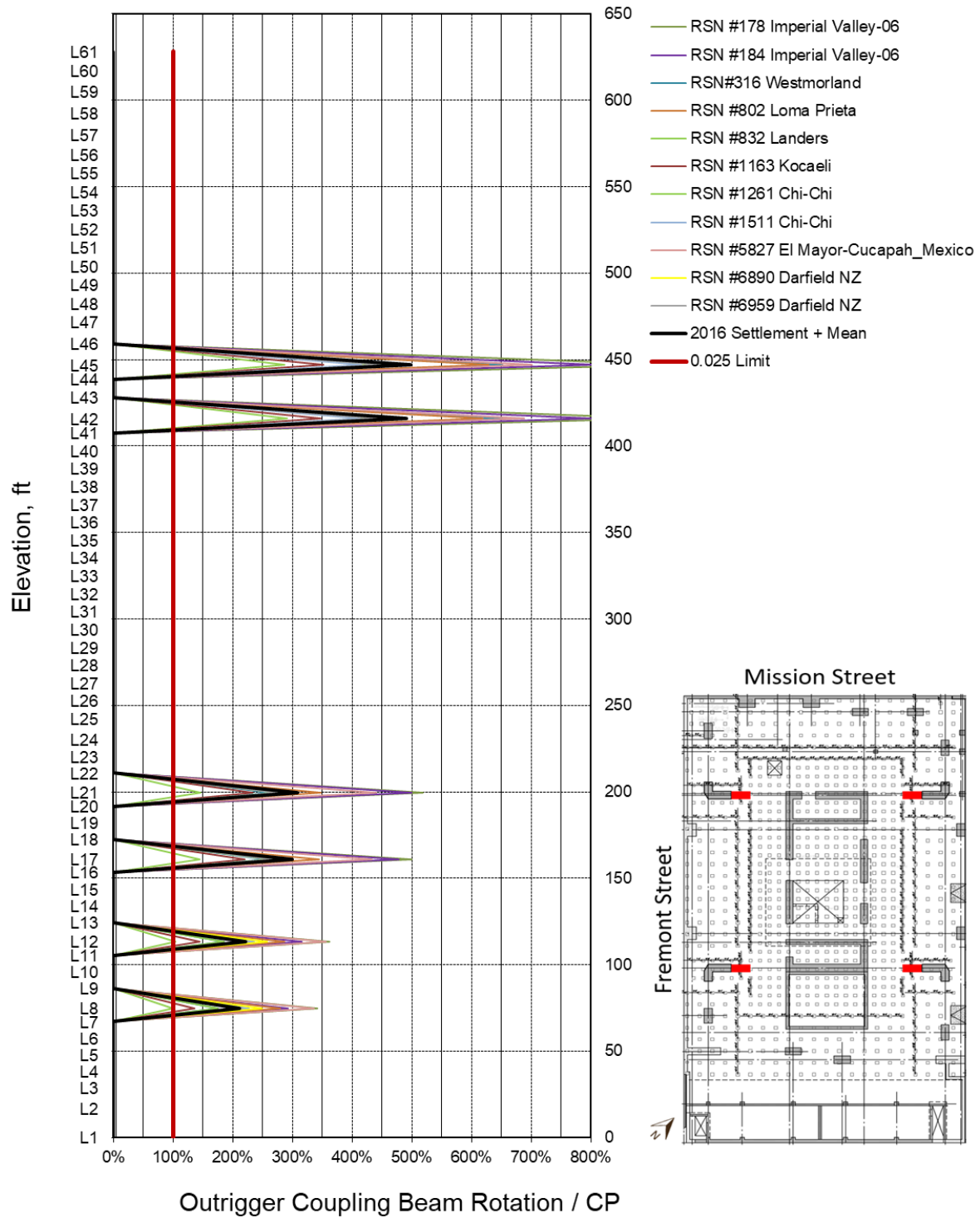


Figure 6-32 – Outrigger Coupling Beam Rotations

6.4 Substructure Analysis Results

6.4.1 Grillage Inelastic Beam Rotations

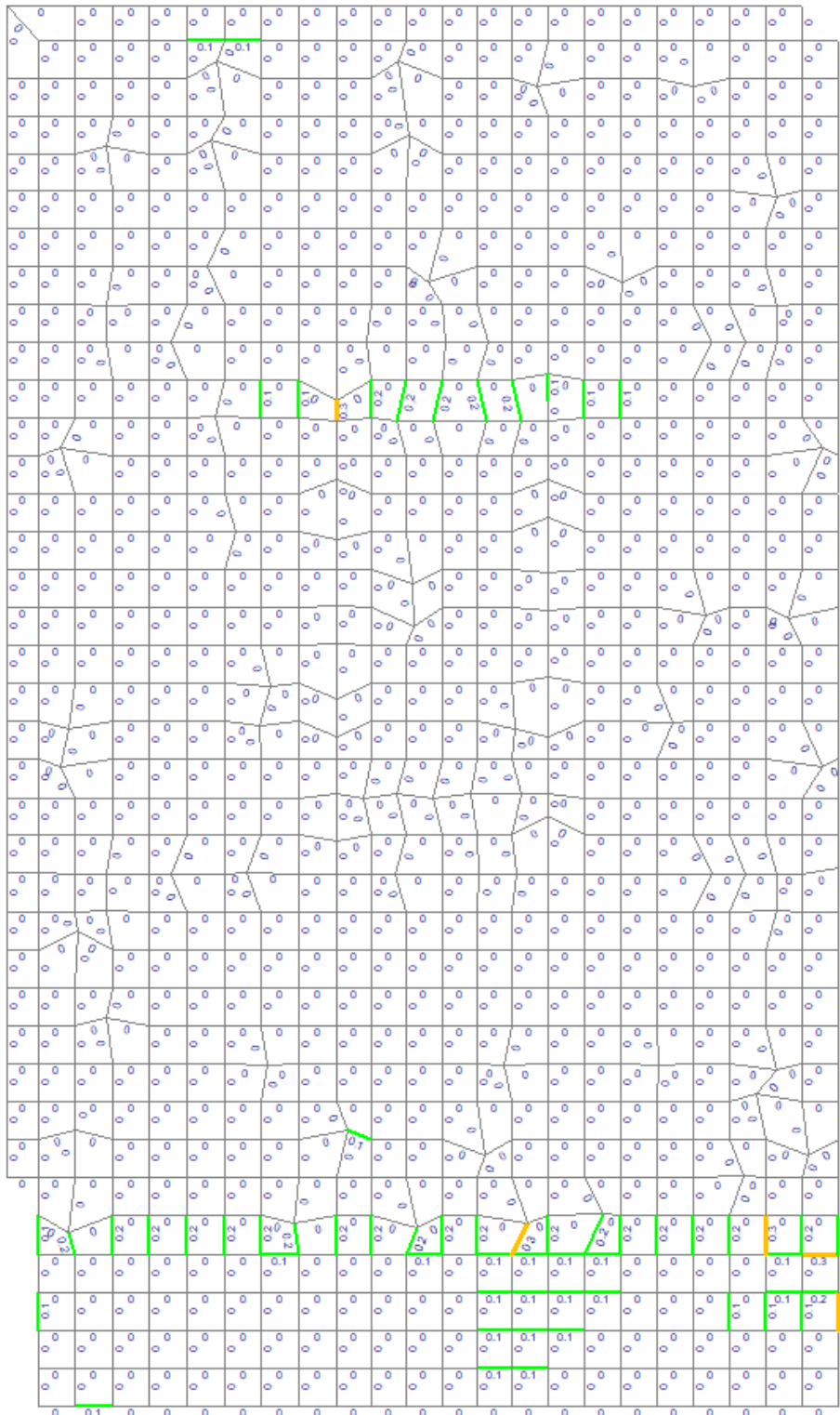


Figure 6-33 – Mat Flexural DCRs due to the MCE (Average of 11 Ground Motions)

6.4.2 Foundation Lateral Displacements

Peak displacements of the tower foundation due to the 11 ground motions are listed in Table 6-7. Figure 6-34 and Figure 6-35 show these peak displacements relative to the cumulative foundation backbones. The largest peak displacement is 5.8 in. This displacement does not exceed the displacement capacity of any existing piles.

Table 6-7 – Maximum Tower Foundation Displacements due to the MCE

Ground Motion Record	East	West	North	South
RSN#178 Imperial Valley-06	4.0	0.5	1.3	3.1
RSN#184 Imperial Valley-06	3.9	3.0	0.8	1.9
RSN#316 Westmorland	1.3	3.1	1.9	1.6
RSN#802 Loma Prieta	1.7	0.8	0.8	2.2
RSN#832 Landers	1.8	0.6	0.3	5.3
RSN#1163 Kocaeli	1.9	1.2	0.9	1.7
RSN#1261 Chi-Chi	1.5	0.7	0.8	3.8
RSN#1511 Chi-Chi	1.5	0.1	1.0	4.9
RSN#5827 El Mayor-Cucapah_Mexico	2.1	0.6	0.8	3.5
RSN#6890 Darfield NZ	1.6	1.1	0.4	5.8
RSN#6959 Darfield NZ	1.1	0.9	1.1	3.0
Average of 11 Ground Motions	2.0	1.1	0.9	3.3

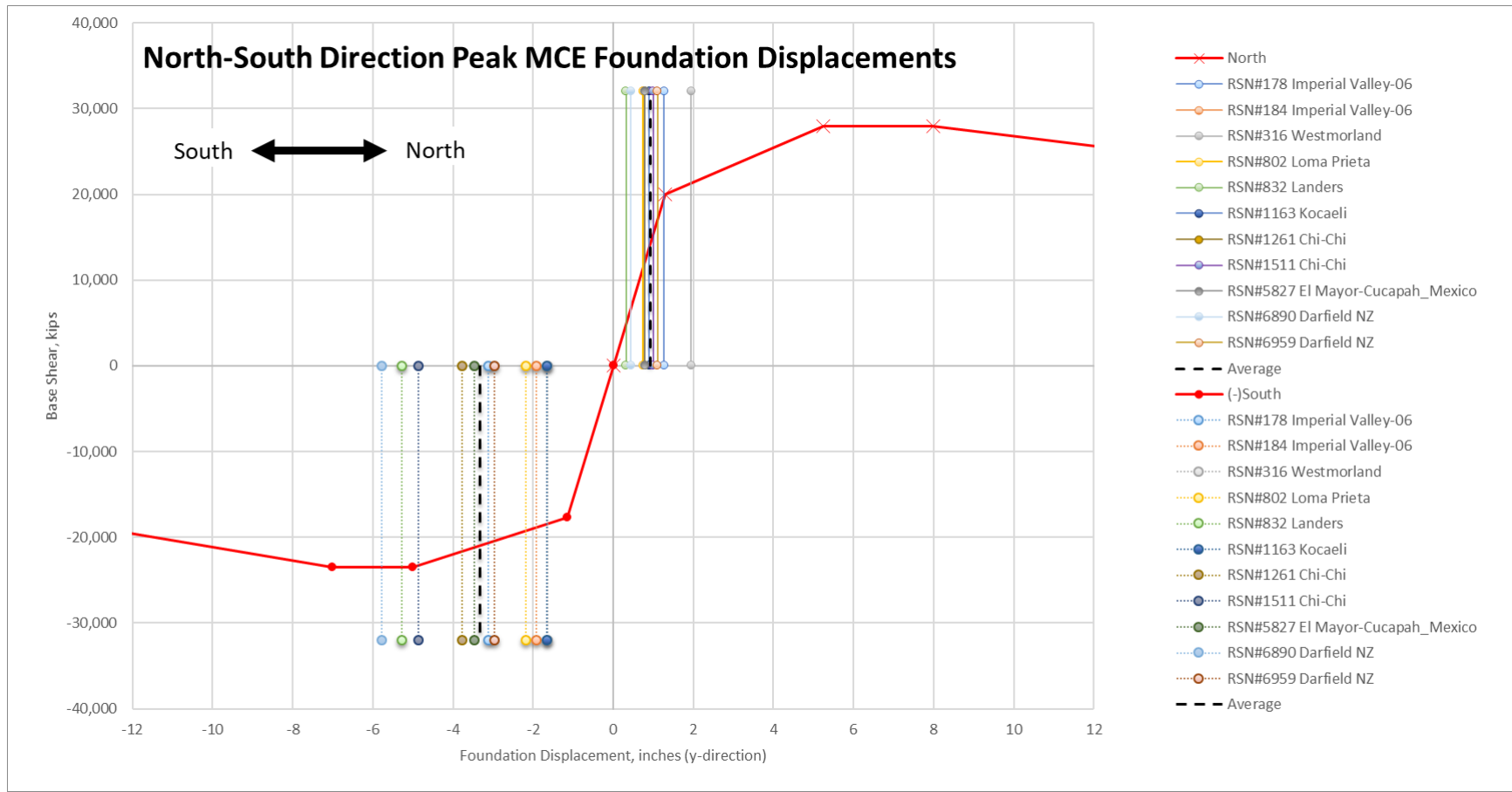


Figure 6-34 – North-South Peak Tower Foundation Displacements due to the MCE

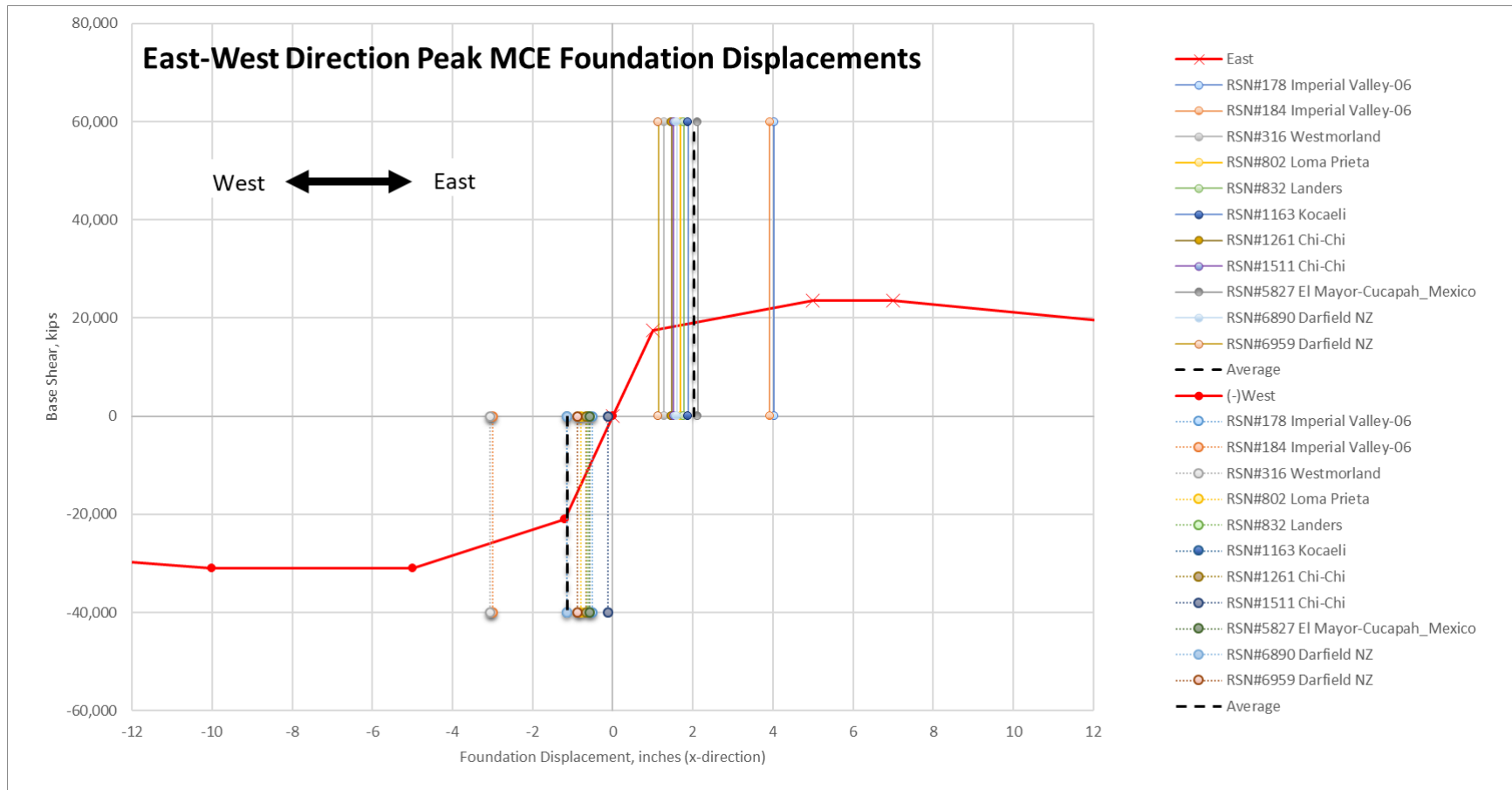


Figure 6-35 – East-West Peak Tower Foundation Displacements due to the MCE

7. ANALYTICAL MODEL: SAFE V16

7.1 SAFEV16 Model Description

For a complete model description, see Volume 2 Chapter 2.

7.2 Wind Loading

We determined the wind loading by using the reaction forces from the ETABS model. Section 2.2.1 describes the wind load procedure for the ETABS model. Since the vertical loads import feature of SAFE recognizes gravity (-Z) as positive, we reversed the vertical reaction forces from the ETABS model. All other forces have the same sign in both programs.

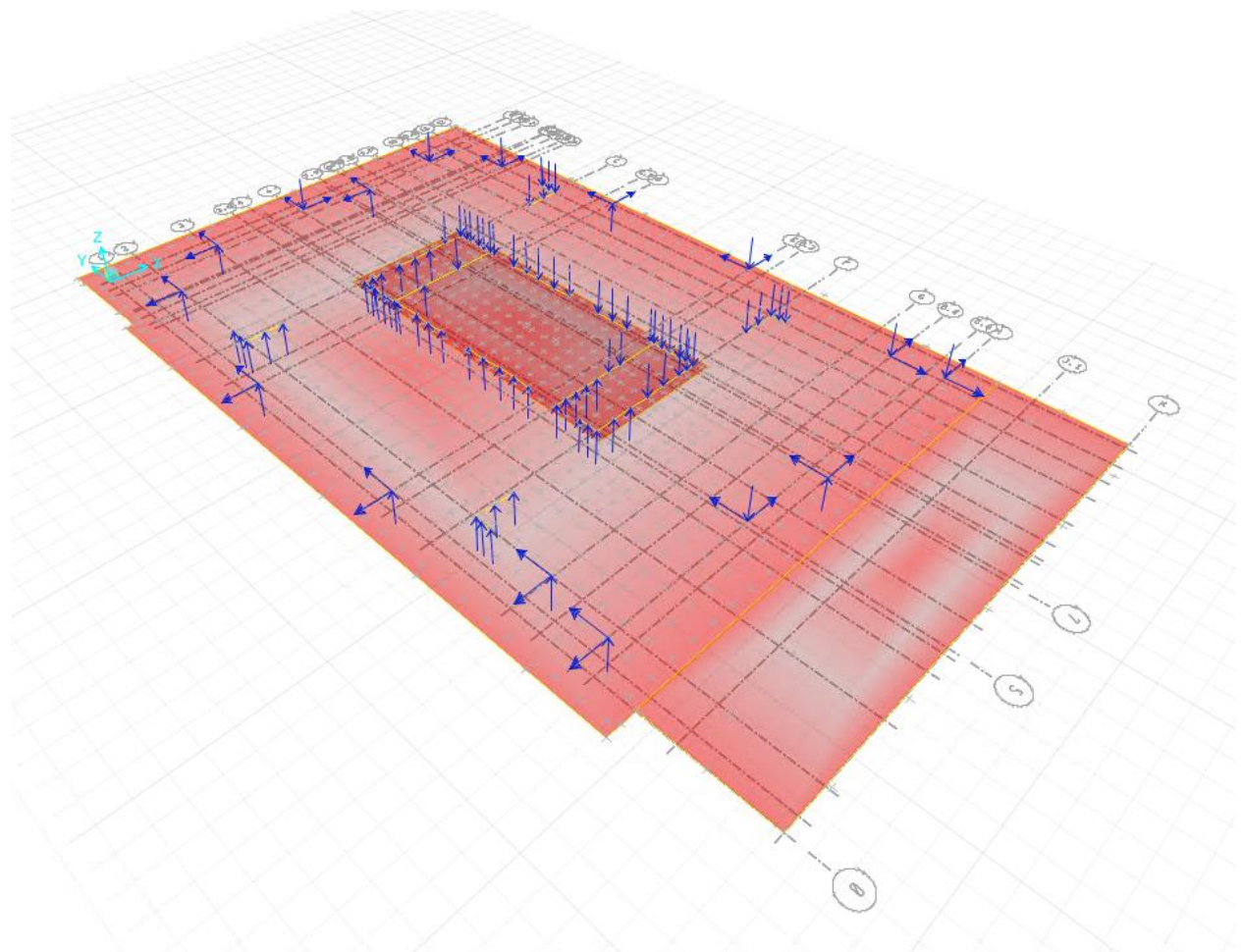


Figure 7-1: Wind Load Point Load Application in SAFE

7.3 Seismic Loading

We used results from modal response spectrum analysis (RSA) load cases following the procedures described in ASCE 7-10 Section 12.9. We input vertical support reactions from our ETABS analysis to the SAFE model of the mat foundation.

ASCE/SEI 7-10 Section 12.9.4.1 requires scaling design forces computed by RSA to 85% of the ELF base shear. We scaled the base shears as shown in the following calculations:

V.RSA.X =	31,028	kip	Base shear due to X-direction earthquake
MY.RSA.X =	7,687,526	kip	Overturning moment due to X-direction earthquake
V.RSA.Y =	28,252	kip-ft	Base shear due to Y-direction earthquake
MX.RSA.Y =	8,490,284	kip-ft	Overturning moment due to Y-direction earthquake
V.ELF.X =	8,876	kip	ASCE 7-10 Eq 12.8-1
0.85 * V.ELF.X =	7,545	kip	
Effective R =	V.RSA.X / (0.85 * V.ELF.X)		
=	4.11	<	7 (R factor from design calculations)
V.D.X =	7545	kip	Design base shear due to X-direction earthquake
MY.D.X =	1,869,226	kip-ft	Design overturning moment due to X-direction earthquake
V.ELF.Y =	8,876	kip	
0.85 * V.ELF.Y =	7,545	kip	
Effective R =	V.RSA.Y / (0.85 * V.ELF.Y)		
=	3.74	<	7 (R factor from design calculations)
V.D.Y =	7545	kip	Design base shear due to Y-direction earthquake
MX.D.Y =	2,267,288	kip-ft	Design overturning moment due to Y-direction earthquake

Rather than assume force directions, we used the distribution of joint reactions from ELF load cases and scaled them to match the design overturning moment for the entire building obtained from response spectrum analysis.

Three lateral systems in the tower transfer seismic force to the mat: (1) the core shear walls, (2) the outriggers, and (3) the perimeter moment frames. We used section cuts to obtain the total overturning moment resisted by each system for RSA and ELF loads. We divided the RSA section cut moments by the effective R factors calculated above. The sums of the scaled RSA

section cut moments in each direction are slightly less than the total design overturning moments, as depicted in Figure 7-2.

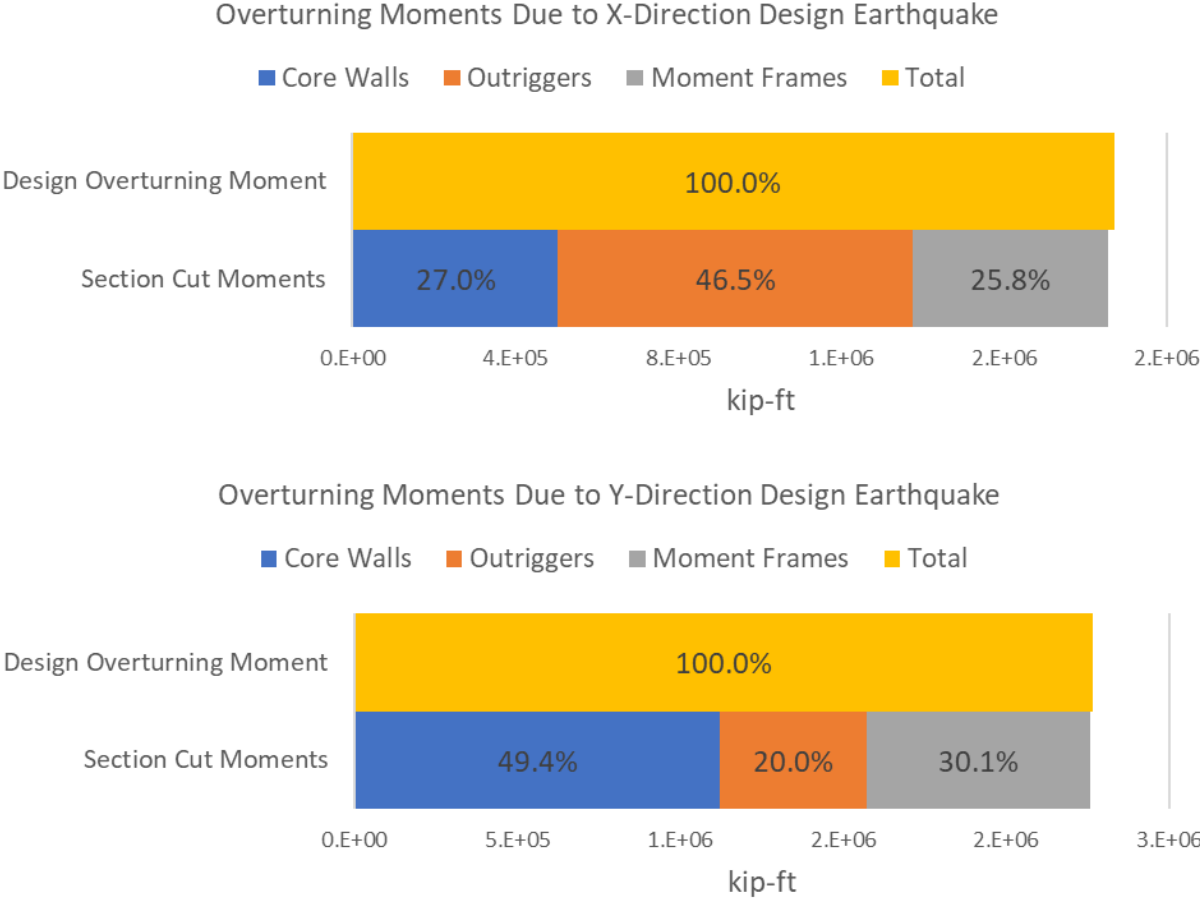


Figure 7-2: Response Spectrum Analysis Overturning Moments

In both directions, response spectrum section cut moments of the individual systems sum to about 99% of the Design Earthquake base overturning moment. We scaled the east-west and north-south section cut moments for all systems by a factor of 1.01 to correct for the summation of RSA results.

We used ETABS to compute six ELF load cases, considering lateral loading in the two orthogonal directions, each with no story mass eccentricity and with +/- 5% story mass eccentricity per ASCE/SEI 7-10 Section 12.8.4.2 for accidental torsion. Table 7-1 lists ELF and RSA section cut moments and associated scale factors. We applied the scale factors listed in

Table 7-1 to vertical joint reaction forces from the six ELF load cases. Figure 7-3 shows the X- and Y-direction scale factors for each joint.

We applied the six sets of scaled ELF vertical joint forces to the SAFE model as individual load patterns as well as point moments in both lateral directions. We considered combinations of seismic and gravity loads for both upward and downward seismic accelerations:

- 1.4 Dead + 1.0 Live + 1.0 Earthquake
- 0.7 Dead + 1.0 Earthquake

For both combinations of gravity and seismic loads, we also considered all possible 100% / 30% combinations of orthogonal seismic loads, including accidental eccentricity. The 32 seismic load cases we considered are listed in Table 7-2. We used an enveloping load combination to obtain maximum design strip demands due to the 32 seismic load cases. Within the combinations, we applied the omega factor to the seismic load patterns. We used an Omega factor of 2.5 based on Table 12.2-1 of ASCE 7-10.

Table 7-1 – ETABS Section Cut Moments

Lateral System	Earthquake Direction	ELF Moment (kip-ft)	Scaled RSA Moment (kip-ft)	Scale Factor
CORE	X (east-west)	901,285	504,305	0.56
OUTRIGGERS		2,171,913	869,884	0.40
MF		1,190,431	482,215	0.41
CORE	Y (north-south)	2,054,205	1,119,239	0.55
OUTRIGGERS		869,019	453,332	0.52
MF		1,278,546	683,303	0.53

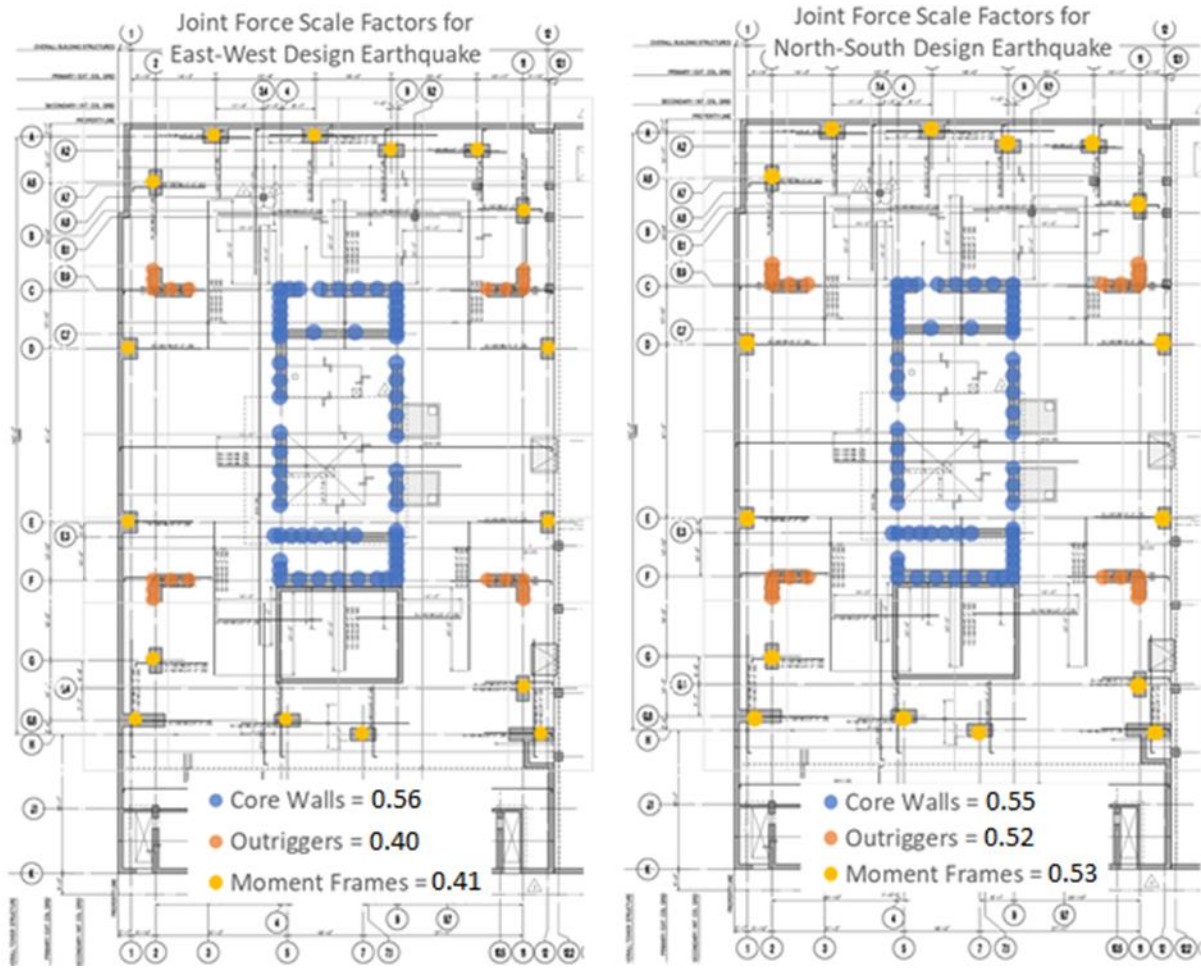


Figure 7-3: Scale Factors on ELF Vertical Joint Forces

Table 7-2 – List of Seismic Load Cases Applied to SAFE Model of the Mat

	SAFE Load Case Name
1	1.4D +L +100(X+ecc) +30Y
2	1.4D +L +100(X-ecc) +30Y
3	1.4D +L +100(X+ecc) -30Y
4	1.4D +L +100(X-ecc) -30Y
5	1.4D +L -100(X+ecc) +30Y
6	1.4D +L -100(X-ecc) +30Y
7	1.4D +L -100(X+ecc) -30Y
8	1.4D +L -100(X-ecc) -30Y
9	1.4D +L +30X +100(Y+ecc)
10	1.4D +L +30X +100(Y-ecc)
11	1.4D +L +30X -100(Y+ecc)
12	1.4D +L +30X -100(Y-ecc)
13	1.4D +L -30X +100(Y+ecc)
14	1.4D +L -30X +100(Y-ecc)
15	1.4D +L -30X -100(Y+ecc)
16	1.4D +L -30X -100(Y-ecc)
17	0.7D +100(X+ecc) +30Y
18	0.7D +100(X-ecc) +30Y
19	0.7D +100(X+ecc) -30Y
20	0.7D +100(X-ecc) -30Y
21	0.7D -100(X+ecc) +30Y
22	0.7D -100(X-ecc) +30Y
23	0.7D -100(X+ecc) -30Y
24	0.7D -100(X-ecc) -30Y
25	0.7D +30X +100(Y+ecc)
26	0.7D +30X +100(Y-ecc)
27	0.7D +30X -100(Y+ecc)
28	0.7D +30X -100(Y-ecc)
29	0.7D -30X +100(Y+ecc)
30	0.7D -30X +100(Y-ecc)
31	0.7D -30X -100(Y+ecc)
32	0.7D -30X -100(Y-ecc)

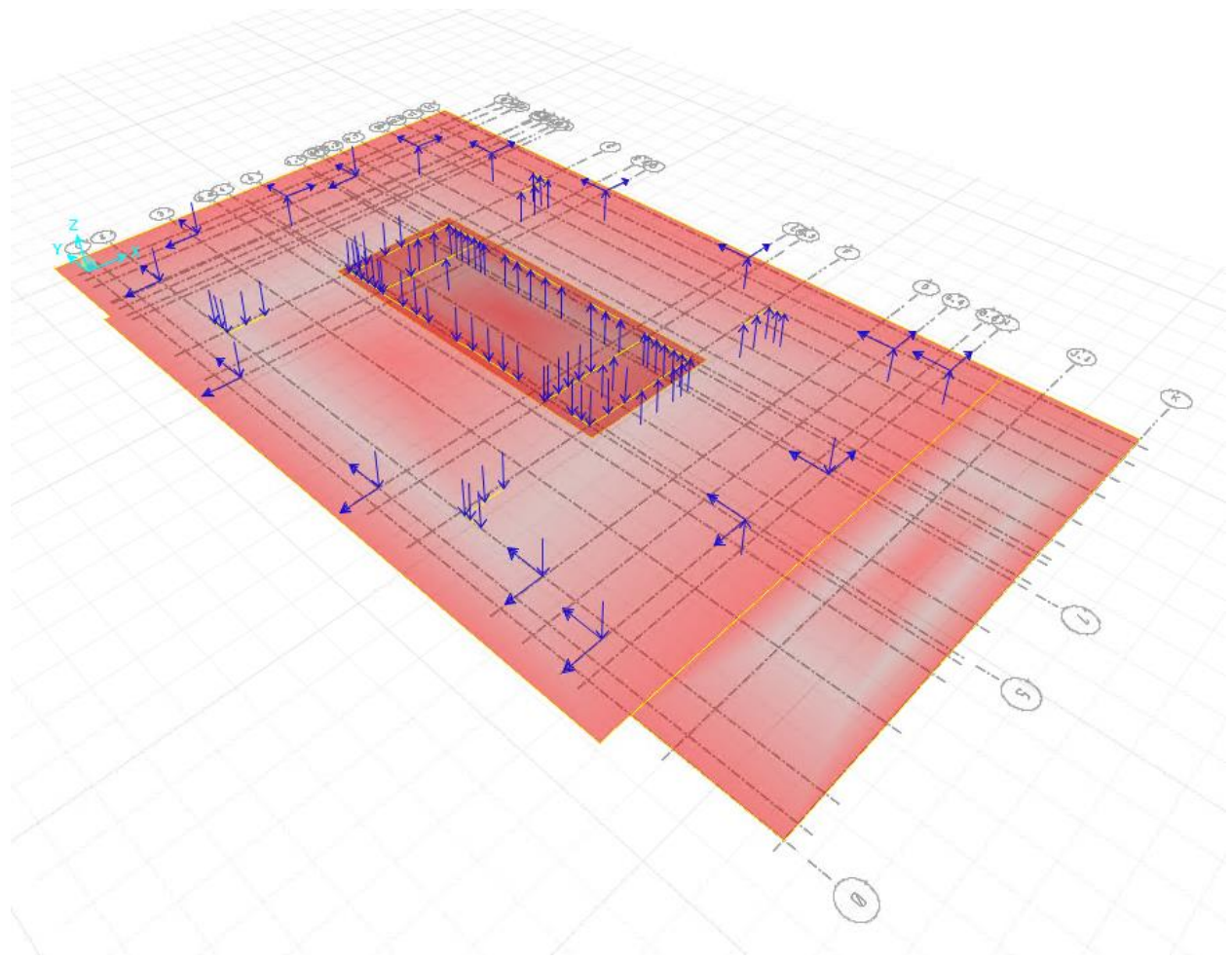


Figure 7-4: Seismic Load Point Load Application in SAFE

7.4 Analysis Results

7.5 Shear Calculations

 <p>SIMPSON GUMPERTZ & HEGER Engineering of Structures and Building Enclosures</p>	<p>SUBJECT: Mat Slab Shear Capacity</p>	<p>PROJECT NO: 140741.00</p>
		<p>DATE: 11/28/2018</p>
		<p>BY: SEB</p>
		<p>CHECKED BY: LH</p>

Title: Mat Slab Foundation One-Way Shear Capacity and Punching Shear

References: ACI 318-14, Design Calculations from Desimone (05/2005), Design Drawing Documentation DIP 22 (03/2006), Mat Slab Core Strength Tests (08/25/2006, 09/20/2006), RFI No. 210 (5/2/2006 5/3/2006) Webcor Builders/DeSimone Consulting Engineers.

<p>301 Mission 301 Mission San Francisco, CA 94105 Jobsite Office: 183 Fremont Street San Francisco, CA 94105</p>		<p>Project # 387 Tel: (415) 978-5700 Fax: (510) 476-3019</p>		<p>WEBCOR BUILDERS</p>	
<p>Submitted To Nic Rodrigues DeSimone Consulting Engineers, PLLC 160 Sansome Street, Suite 1600 San Francisco, CA 94104</p>			<p>Submitted By Spencer Sayles WEBCOR BUILDERS 183 Fremont Street San Francisco, CA 94105</p>		
<p>Subject Re-bar T-heads in Mat</p>		<p>Discipline Structural</p>		<p>Originator RFI Number</p>	
<p>Cc: Webcor Concrete Group</p>		<p>Contact Name: Greg Scott</p>		<p>Copies: PW</p>	
<p>Information Requested This RFI is to confirm the shear reinforcing (vertical #14 with T-heads) will not need to extend into or beyond the lower mat reinforcing. Due to congestion, the lower T-heads will be allowed to rest on the top layer of the bottom mat. Please respond as quickly as possible as fabrication is being held until this answer is confirmed. Thank you.</p>					
<p>Response Nicolas Rodrigues DeSimone 5-3-2006 Confirmed. T-heads can rest on the bottom mat of rebar.</p>					

Figure: RFI No. 210 stating as-built location of shear dowel reinforcement

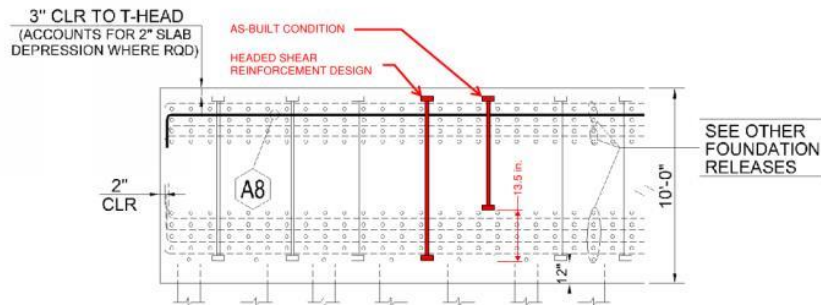


Figure: Illustration of as-built condition vs. design condition of shear dowel reinforcement

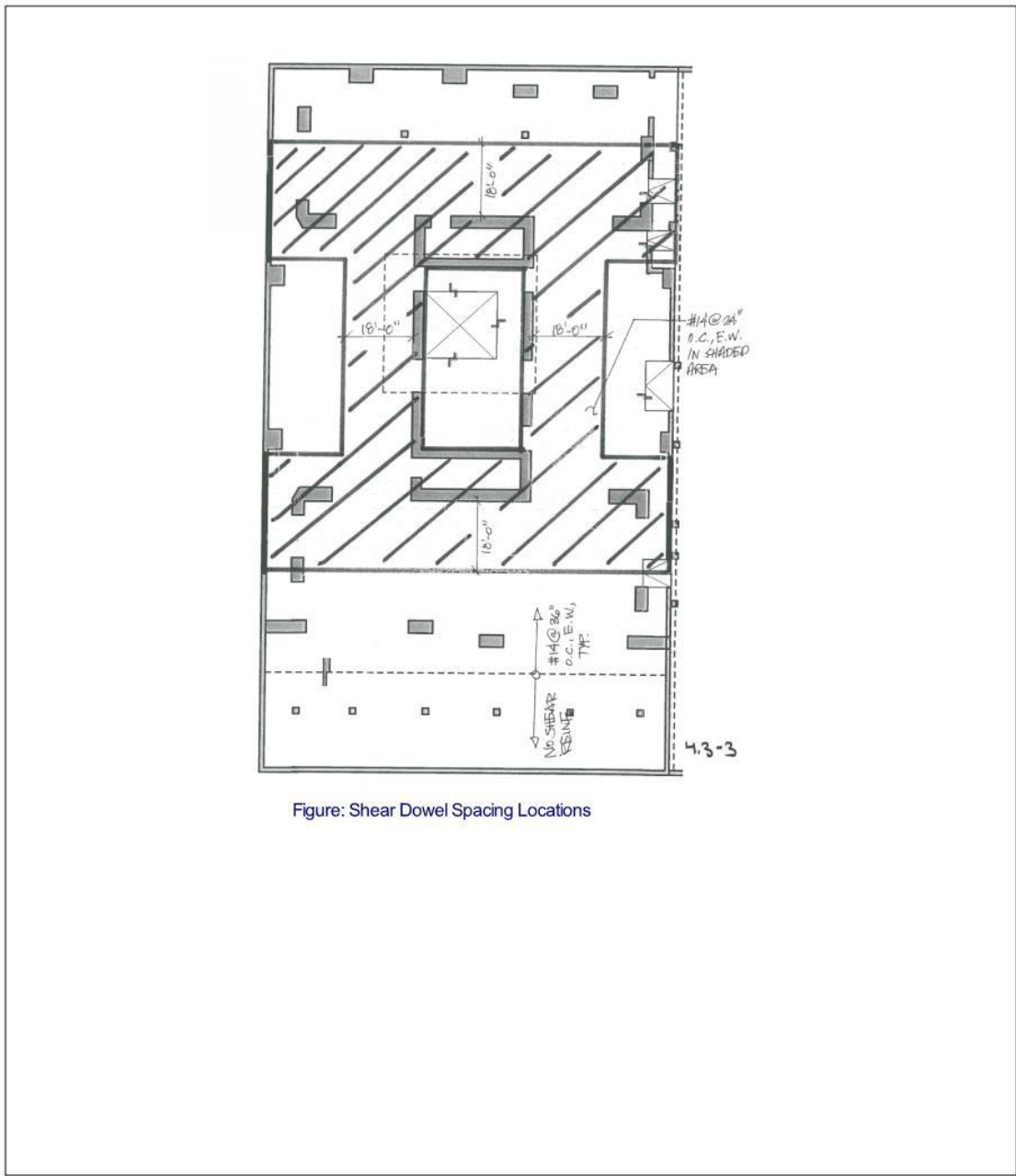
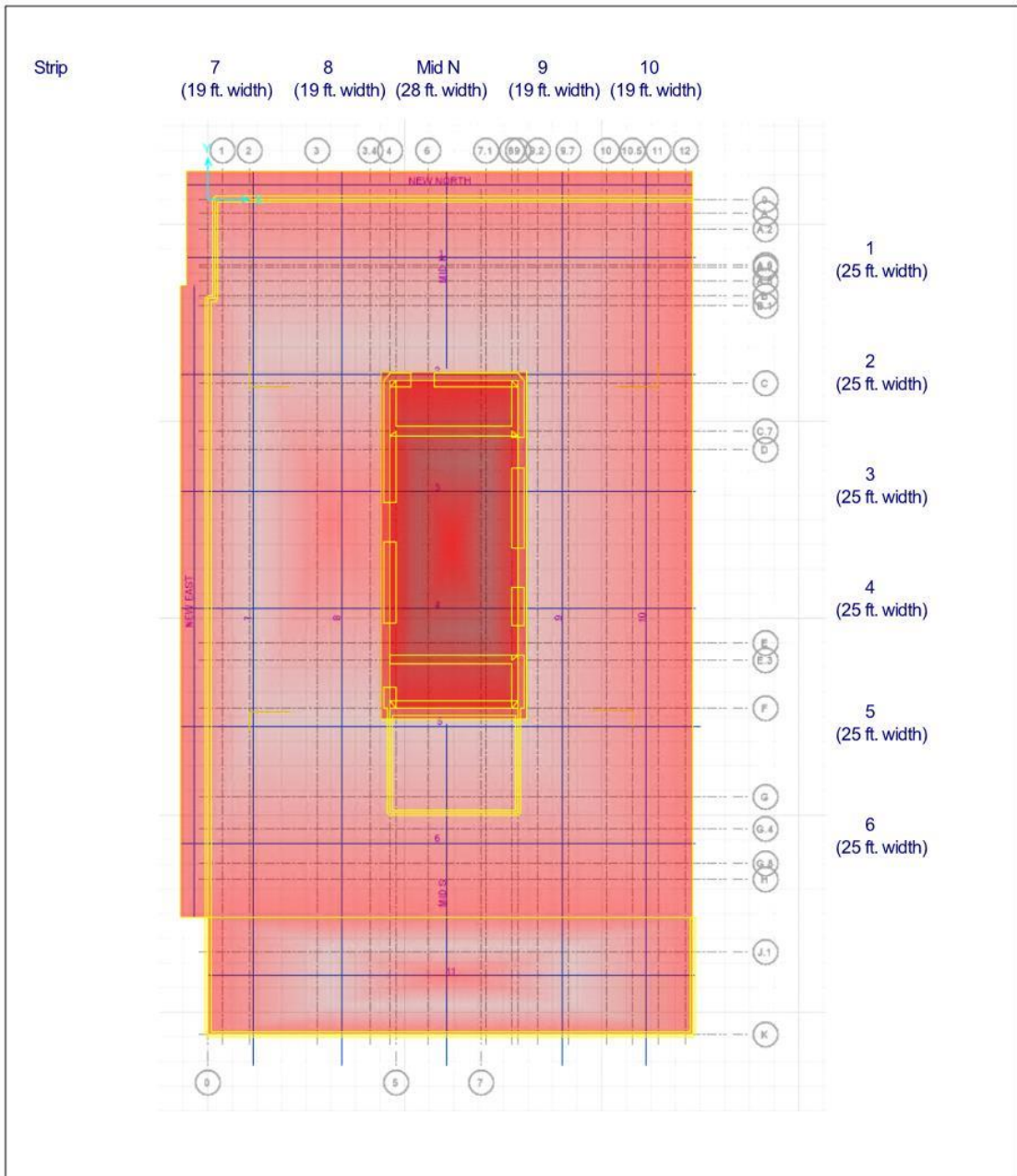


Figure: Shear Dowel Spacing Locations



Material Properties:

Strength reduction factor for shear	$\phi_v := 0.75$
Yield Strength of Reinforcing Steel	$F_y := 75\text{ksi}$
Strength of Concrete Estimated by ACI 301	$f'_c := 7155\text{psi}$
Diameter of #11 bar	$d_b := 1.41\text{in}$
Area of #11 bar	$a_b := 1.56\text{in}^2$
Diameter of #14 bar	$d_{b14} := 1.693\text{in}$
Area of #14 bar	$a_{b14} := 2.25\text{in}^2$
One-way Shear Capacity	
Strip width	$b_{19\text{ft}} := 19\text{ft}$
	$b_{25\text{ft}} := 25\text{ft}$
	$b_{28\text{ft}} := 28\text{ft}$
	$d := 120\text{in} - 12\text{in} - 1.41\text{in} \cdot 4 - 1\text{in} = 8.447\text{ft}$
Shear Strength from Concrete	$V_{c19} := 2\sqrt{f'_c \cdot \text{psi}} \cdot b_{19\text{ft}} \cdot d = 3.91 \times 10^3 \cdot \text{kip}$
	$V_{c25} := 2\sqrt{f'_c \cdot \text{psi}} \cdot b_{25\text{ft}} \cdot d = 5.144 \times 10^3 \cdot \text{kip}$
	$V_{c28} := 2\sqrt{f'_c \cdot \text{psi}} \cdot b_{28\text{ft}} \cdot d = 5.762 \times 10^3 \cdot \text{kip}$
	$d_s := d - 13.5\text{in} = 7.32\text{ft}$

Shear Reinforcement Area

$$A_{v36} := \frac{a_{b14}}{3\text{ft}} = 0.75 \cdot \frac{\text{in}^2}{\text{ft}}$$

$$A_{v24} := \frac{a_{b14}}{2\text{ft}} = 1.13 \cdot \frac{\text{in}^2}{\text{ft}}$$

$$V_{s36} := A_{v36} \cdot F_y \cdot \frac{d_s}{36\text{in}} = 137.3 \cdot \frac{\text{kip}}{\text{ft}}$$

$$V_{s24} := A_{v24} \cdot F_y \cdot \frac{d_s}{24\text{in}} = 308.9 \cdot \frac{\text{kip}}{\text{ft}}$$

$$\phi V_{n36_19\text{ft}} := (V_{c19} + V_{s36} \cdot b_{19\text{ft}}) \cdot \phi_v = 4.888 \times 10^3 \cdot \text{kip}$$

$$\phi V_{n36_25\text{ft}} := (V_{c25} + V_{s36} \cdot b_{25\text{ft}}) \cdot \phi_v = 6.432 \times 10^3 \cdot \text{kip}$$

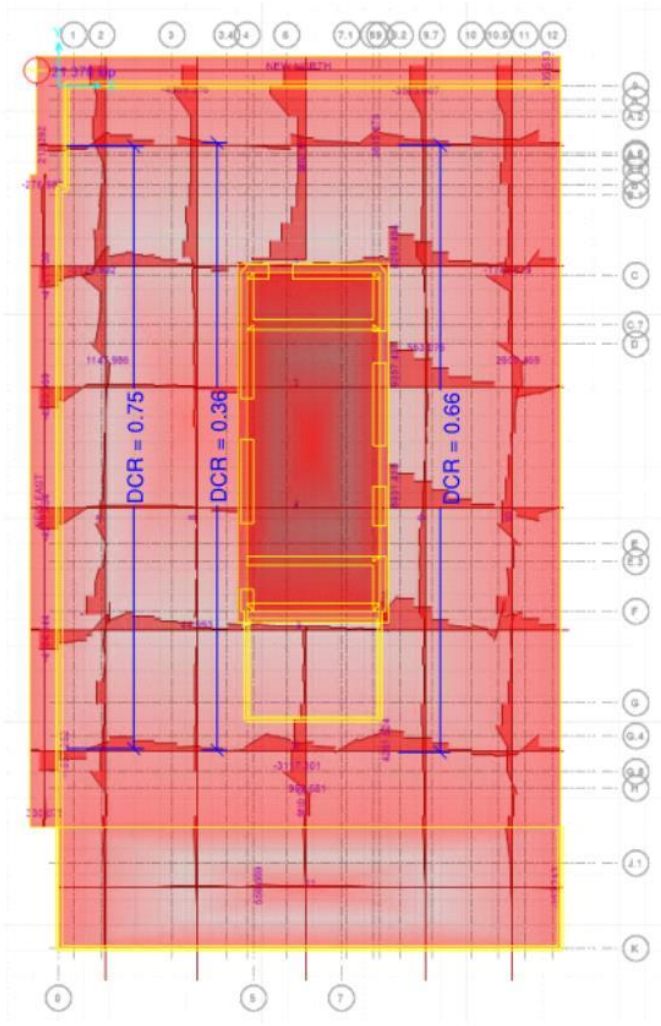
$$\phi V_{n36_28\text{ft}} := (V_{c28} + V_{s36} \cdot b_{28\text{ft}}) \cdot \phi_v = 7.204 \times 10^3 \cdot \text{kip}$$

$$\phi V_{n24_19\text{ft}} := (V_{c19} + V_{s24} \cdot b_{19\text{ft}}) \cdot \phi_v = 7.334 \times 10^3 \cdot \text{kip}$$

$$\phi V_{n24_25\text{ft}} := (V_{c25} + V_{s24} \cdot b_{25\text{ft}}) \cdot \phi_v = 9.65 \times 10^3 \cdot \text{kip}$$

$$\phi V_{n24_28\text{ft}} := (V_{c28} + V_{s24} \cdot b_{28\text{ft}}) \cdot \phi_v = 1.081 \times 10^4 \cdot \text{kip}$$

Seismic Envelope for Strips 1-6



Punching Shear Check

For shapes other than rectangular, β is taken to be the ratio of the longest overall dimension of the effective loaded area to the largest overall perpendicular dimension of the effective loaded area, as illustrated for an L-shaped reaction area in Fig. R22.6.5.2. The effective loaded area is that area totally enclosing the actual loaded area, for which the perimeter is a minimum.

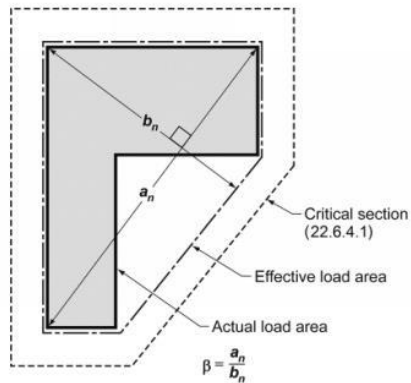


Fig. R22.6.5.2—Value of β for a nonrectangular loaded area.

Figure: ACI R22.6.5.2 Punching Shear

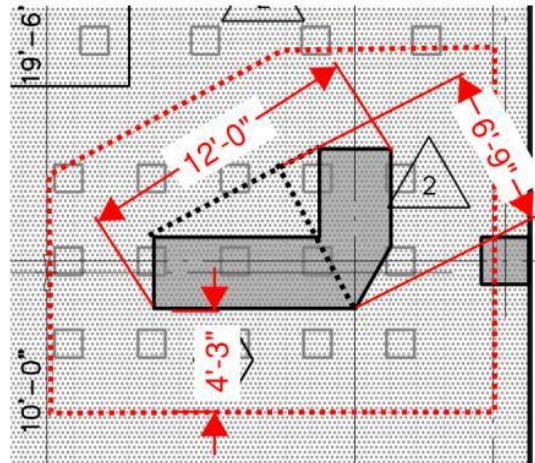


Figure: Outrigger dimension

$$d = 8.447 \text{ ft} \quad \frac{d}{2} = 4.223 \text{ ft}$$

$$a_n := 12 \text{ ft}$$

$$b_n := 6.75 \text{ ft}$$

Outrigger Dimension

$$b_o := 64.25 \text{ ft}$$

$$\lambda := 1.0$$

$$\alpha_s := 40 \quad (\text{Edge Column})$$

$$\phi_{vc} := 0.75$$

$$\beta := \frac{a_n}{b_n} = 1.778$$

ACI Shear Strength from Concrete - Table 22.6.5.2

$$V_{C_1} := 4 \cdot \lambda \cdot \sqrt{f_c \text{ psi}} \cdot b_o \cdot d = 2.644 \times 10^4 \cdot \text{kip}$$

$$V_{C_2} := \left(2 + \frac{4}{\beta} \right) \cdot \sqrt{f_c \text{ psi}} \cdot b_o \cdot d = 2.809 \times 10^7 \text{ lbf}$$

$$V_{C_3} := \left(2 + \frac{\alpha_s \cdot d}{b_o} \right) \cdot \sqrt{f_c \text{ psi}} \cdot b_o \cdot d = 4.798 \times 10^4 \cdot \text{kip}$$

For two-way members with shear reinforcement, v_c shall not exceed the following values from Table 22.6.6.1

$$v_{cLimit} := 3 \cdot \lambda \cdot \sqrt{f_c \text{ psi}} \cdot (b_o \cdot d) = 1.983 \times 10^4 \cdot \text{kip} \quad \text{ACI 22.6.6.1}$$

$$V_C := \min(V_{C_1}, V_{C_2}, V_{C_3}, v_{cLimit}) = 2 \times 10^4 \cdot \text{kip}$$

$$d_s = 7.322 \text{ ft}$$

Shear dowel reinf. area

$$a_{b14} = 2.25 \text{ in}^2$$

Shear area of steel with 2' spacing

$$A_v := \left(\frac{b_o}{2 \text{ ft}} \right) \cdot a_{b14} = 72.3 \cdot \text{in}^2$$

Shear strength from shear reinf.

$$v_s := \frac{A_v \cdot F_y}{2 \text{ ft}} \cdot d_s = 1.985 \times 10^4 \cdot \text{kip}$$

ACI Eq. 22.6.8.2

$$V_n := V_C + v_s = 3.968 \times 10^4 \text{ kip}$$

Maximum Shear Force from Seismic
Combination with Pile Jacking Load

$$V_u := 500 \frac{\text{kip}}{\text{ft}} \cdot 12 \text{ ft} = 6 \times 10^3 \text{ kip}$$

$$\text{DCR}(\phi_v \cdot V_n, V_u) = (0.202 \text{ "OK" })$$

7.6 Flexural Calculations

7.6.1 SAFE Model using ENGEO Pile Springs

For each load case presented in the sections above, SAFE calculates the moment demands along the defined strips in the east-west and north-south directions. The figures below present the demand-to-capacity checks between the demands calculated at discrete points along each strip with the calculated capacities. We used the ENGEO springs presented in Volume 2 in our SAFE model to produce the following results.

7.6.1.1 Wind Loading

7.6.1.1.1. Wind Demand to Capacity Ratios for Existing Condition

The results presented below include the maximum load envelope of the following wind load combinations:

$$\textit{Envelope 1: } 1.2 * D + L + W \textit{ and } 0.9 * D + W$$

DCR Legend

- DCR < 0.9
- DCR 0.9 TO 1.05
- DCR > 1.05

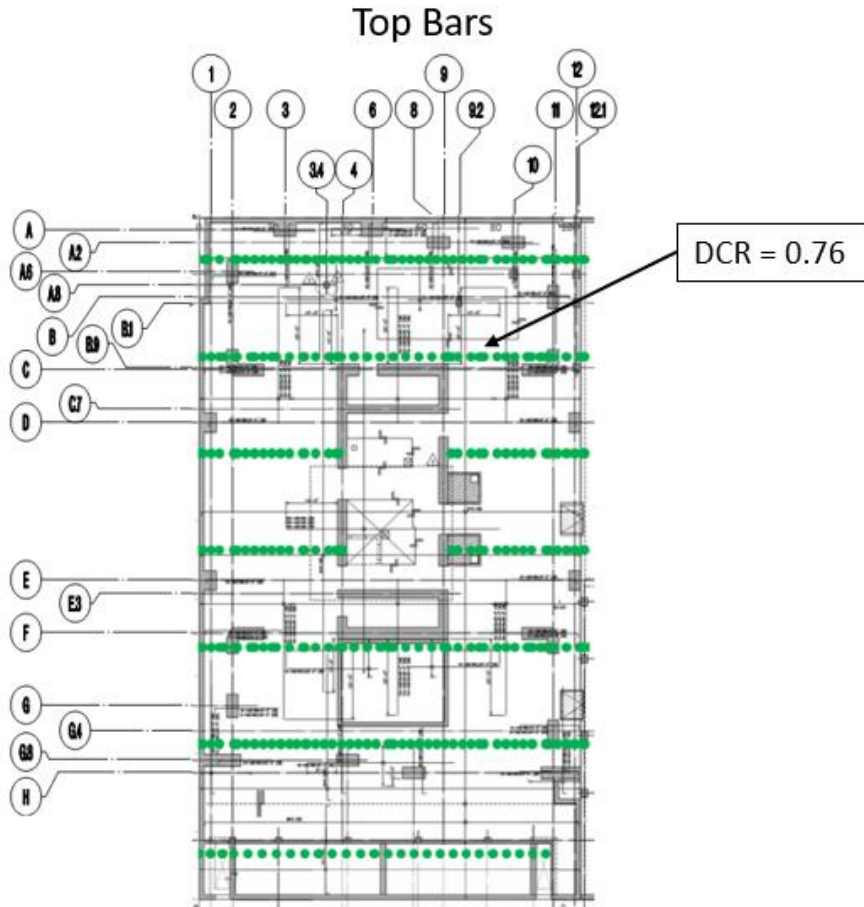


Figure 7-5: DCR Plot for East-West Top Reinforcement Design Strips for Wind Existing Condition

DCR Legend

- DCR < 0.9
- DCR 0.9 TO 1.05
- DCR > 1.05

Bottom Bars

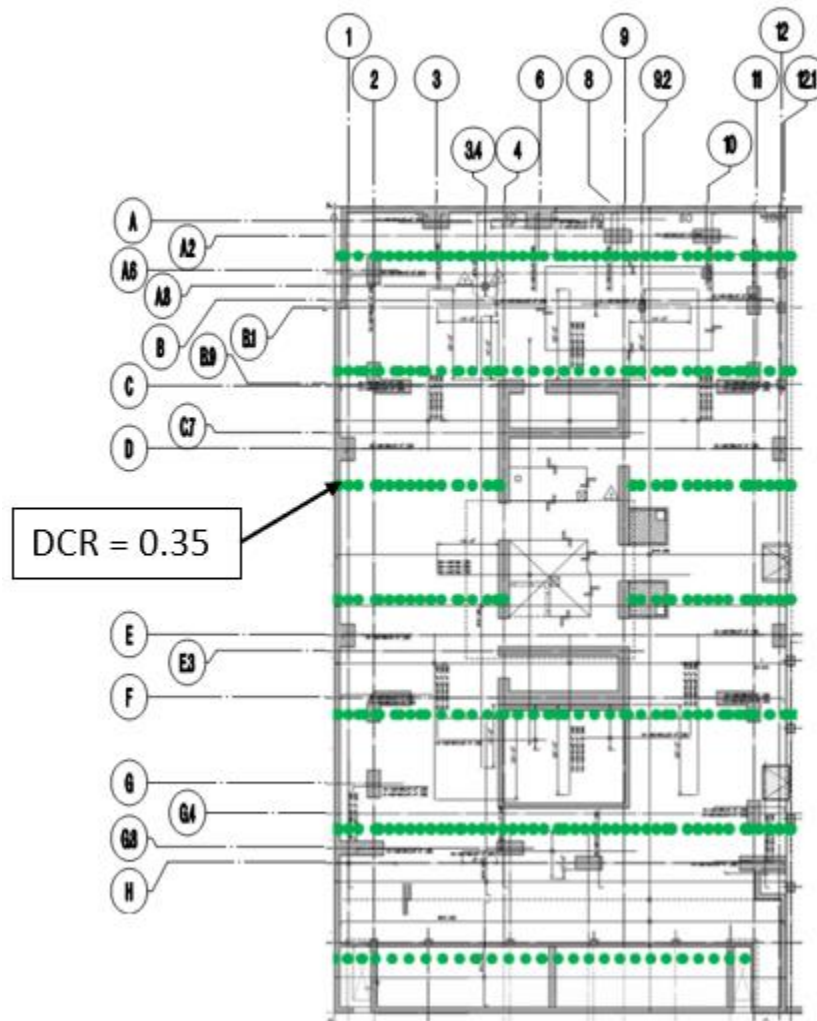


Figure 7-6: DCR Plot for East-West Bottom Reinforcement Design Strips for Wind Existing Condition

DCR Legend

- DCR < 0.9
- DCR 0.9 TO 1.05
- DCR > 1.05

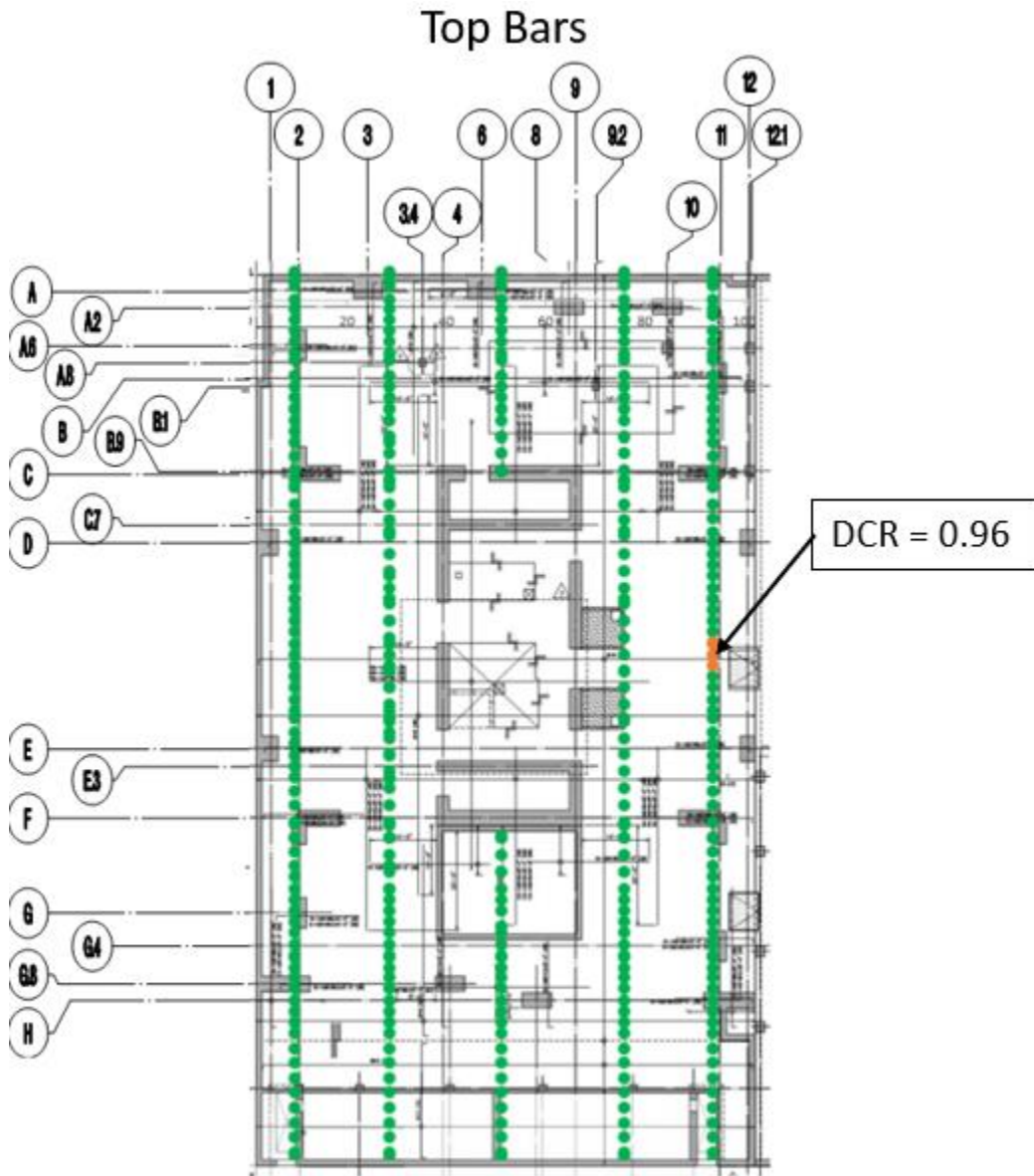


Figure 7-7: DCR Plot for North - South Top Reinforcement Design Strips for Wind Existing Condition

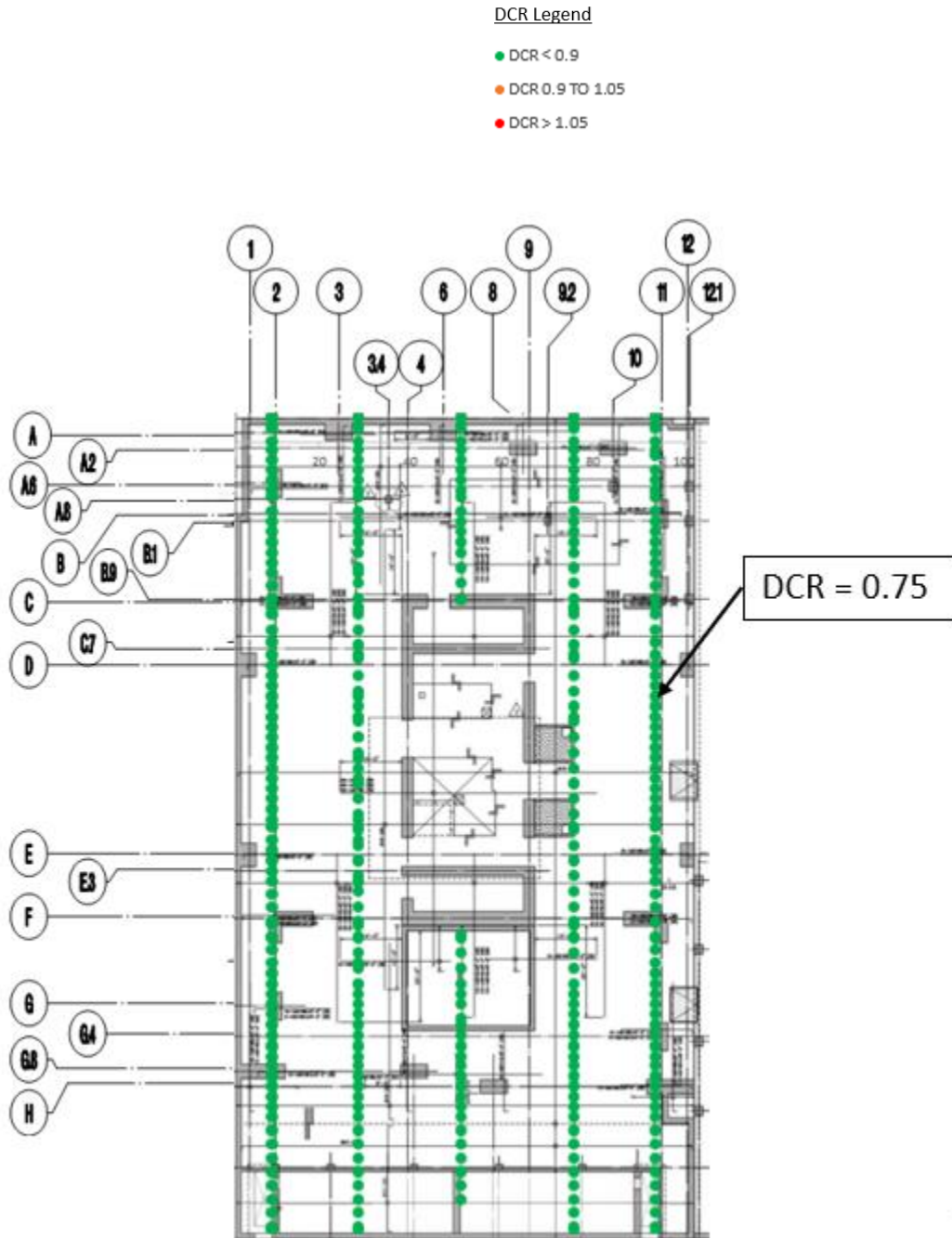


Figure 7-8: DCR Plot for North - South Bottom Reinforcement Design Strips for Wind Existing Condition

7.6.1.1.2. Wind Demand to Capacity Ratios for Retrofit Condition

The results presented below include the maximum load envelope of the following wind load combinations:

Envelope 1: $1.2 * D + L + W + \text{Jacking Load}$ and $0.9 * D + W + \text{Jacking Load}$

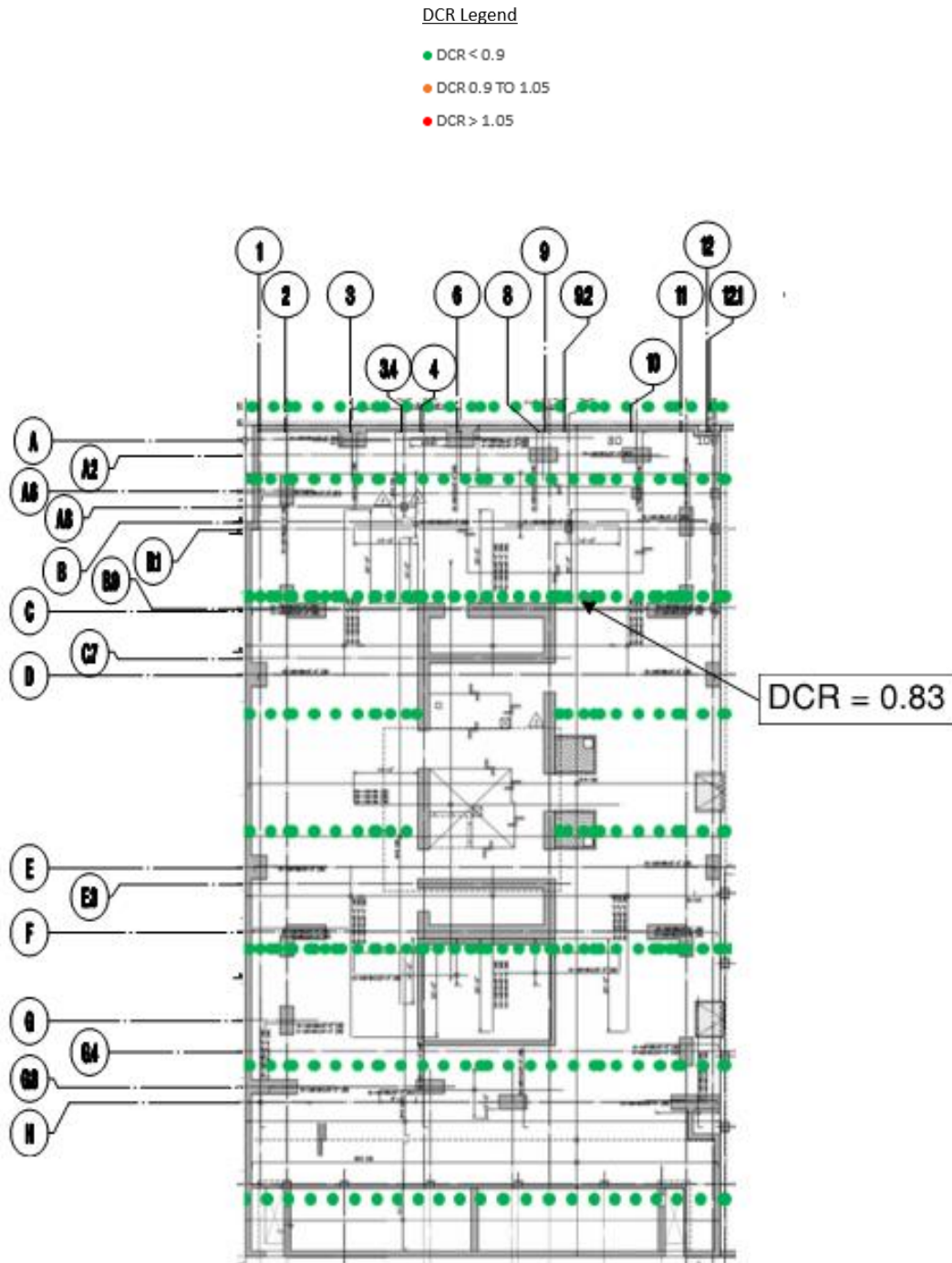


Figure 7-9: DCR Plot for East-West Top Reinforcement Design Strips for Wind + Jacking Load

DCR Legend

- DCR < 0.9
- DCR 0.9 TO 1.05
- DCR > 1.05

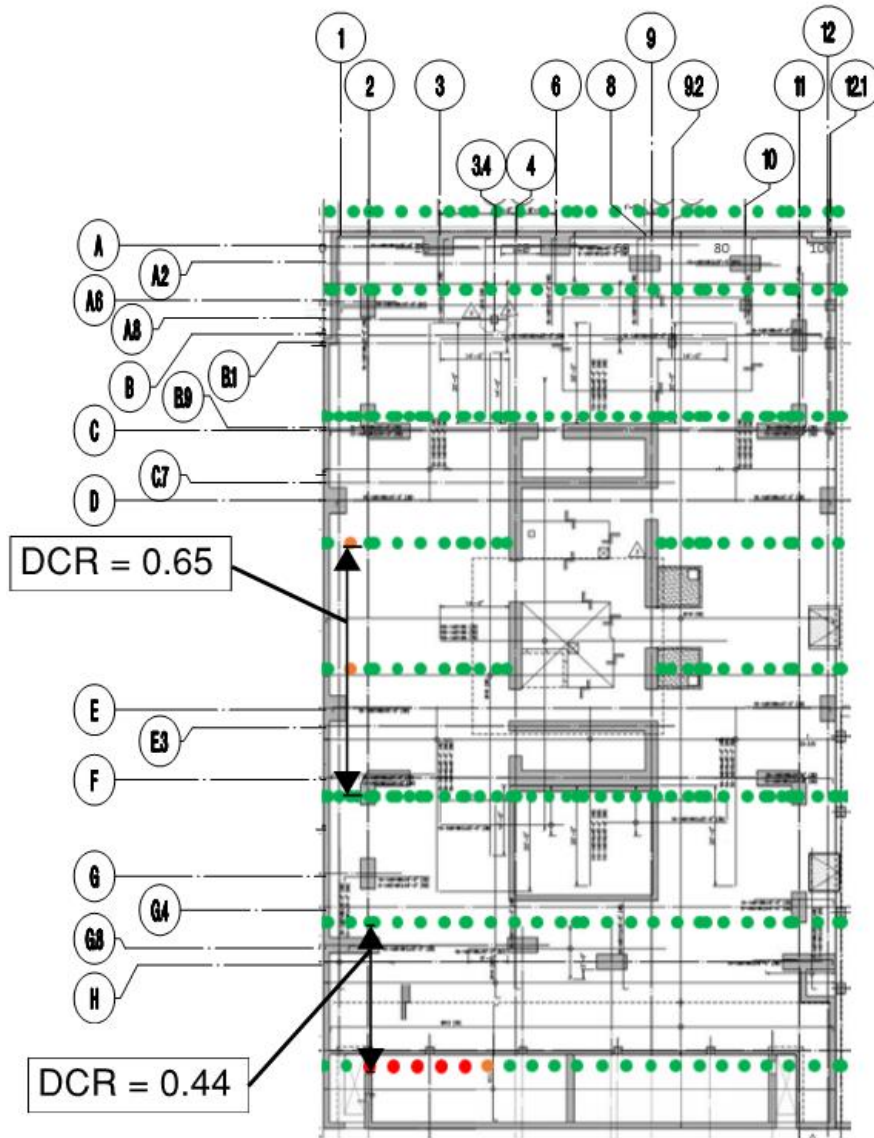


Figure 7-10: DCR Plot for East-West Bottom Reinforcement Design Strips for Wind + Jacking Load

DCR Legend

- DCR < 0.9
- DCR 0.9 TO 1.05
- DCR > 1.05

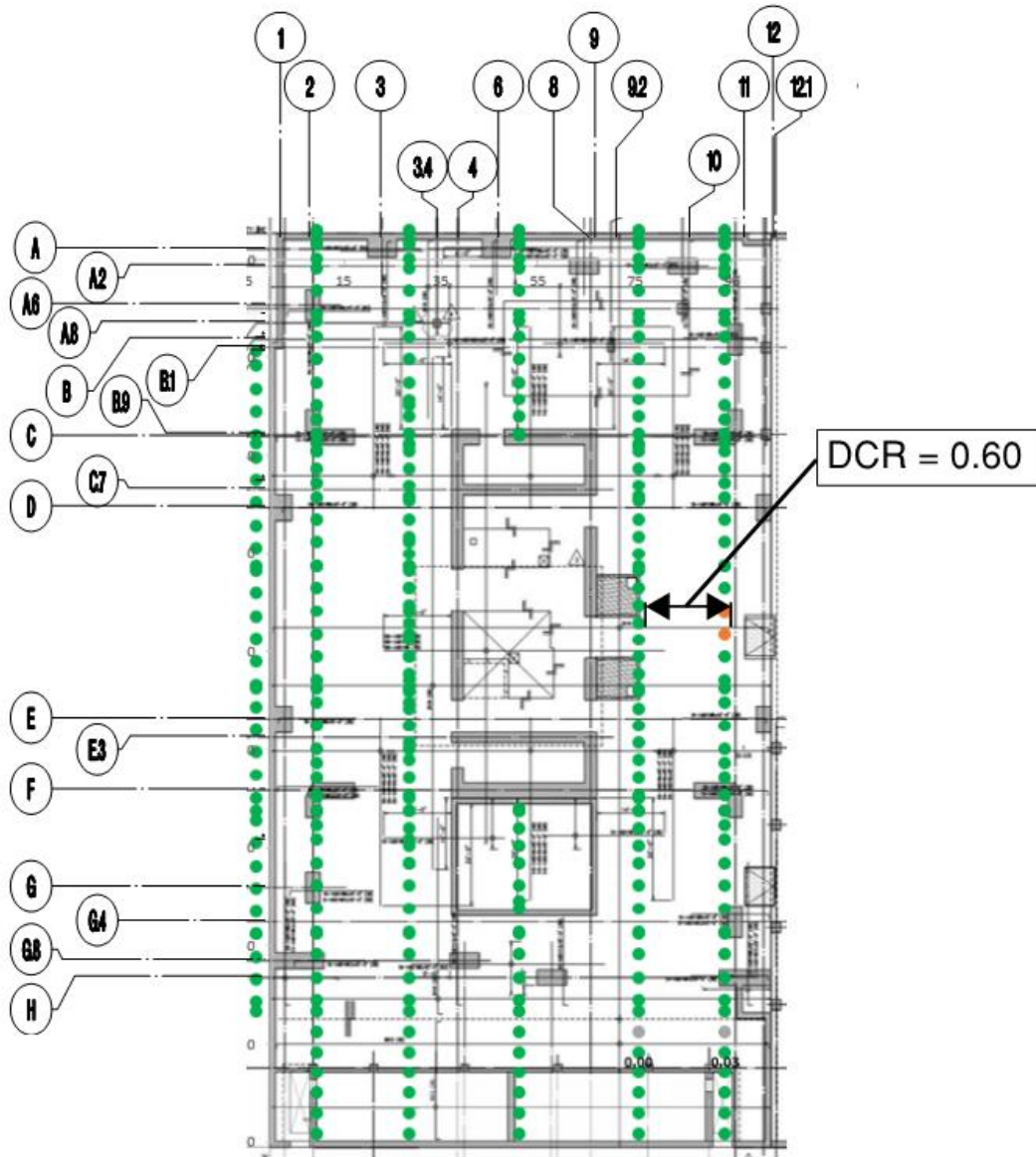


Figure 7-11: DCR Plot for North - South Top Reinforcement Design Strips for Wind + Jacking Load

DCR Legend

- DCR < 0.9
- DCR 0.9 TO 1.05
- DCR > 1.05

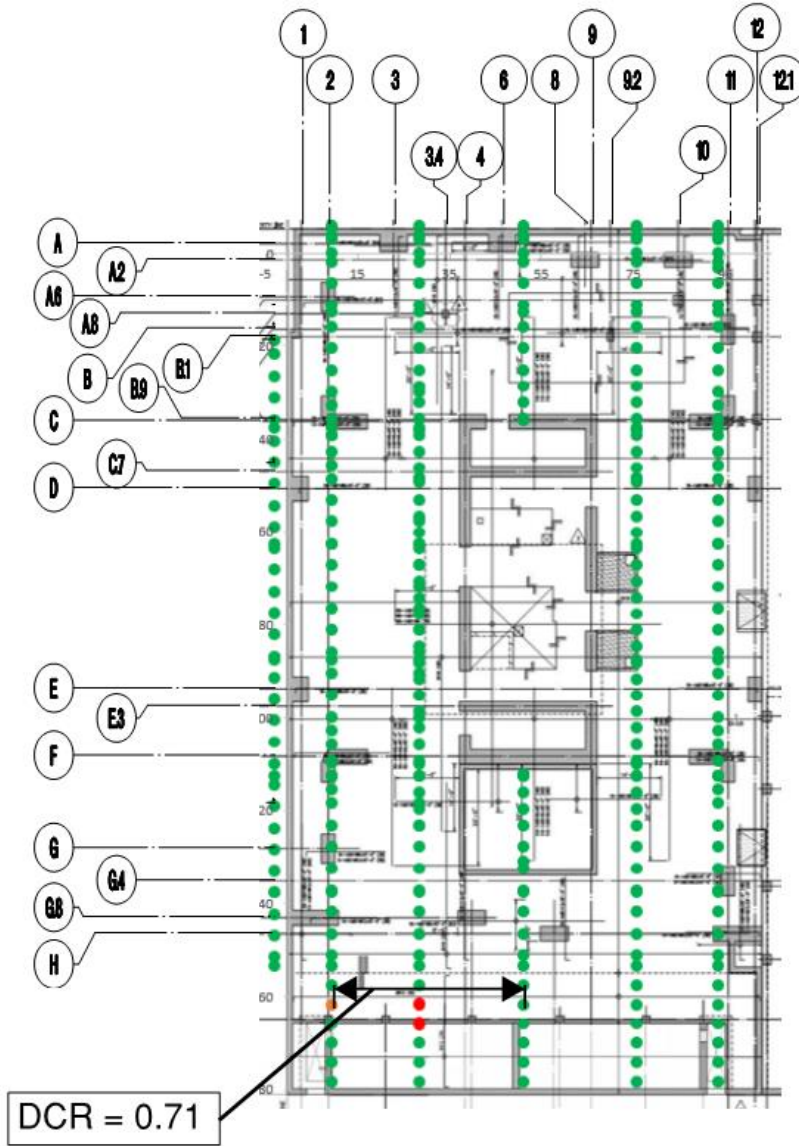


Figure 7-12: DCR Plot for North - South Bottom Reinforcement Design Strips for Wind + Jacking Load

7.6.1.2 Seismic Loading

7.6.1.2.1. Seismic Demand to Capacity Ratios for Existing Condition

The result figures below present the flexural demand to capacity ratio checks for the two load combinations listed below. The figures below highlight the locations of the maximum demand to capacity ratios.

*Envelope 1: $(1.4 * D) + L + E$ and $(0.7 * D) + E$*

DCR Legend

- DCR < 0.9
- DCR 0.9 TO 1.05
- DCR > 1.05

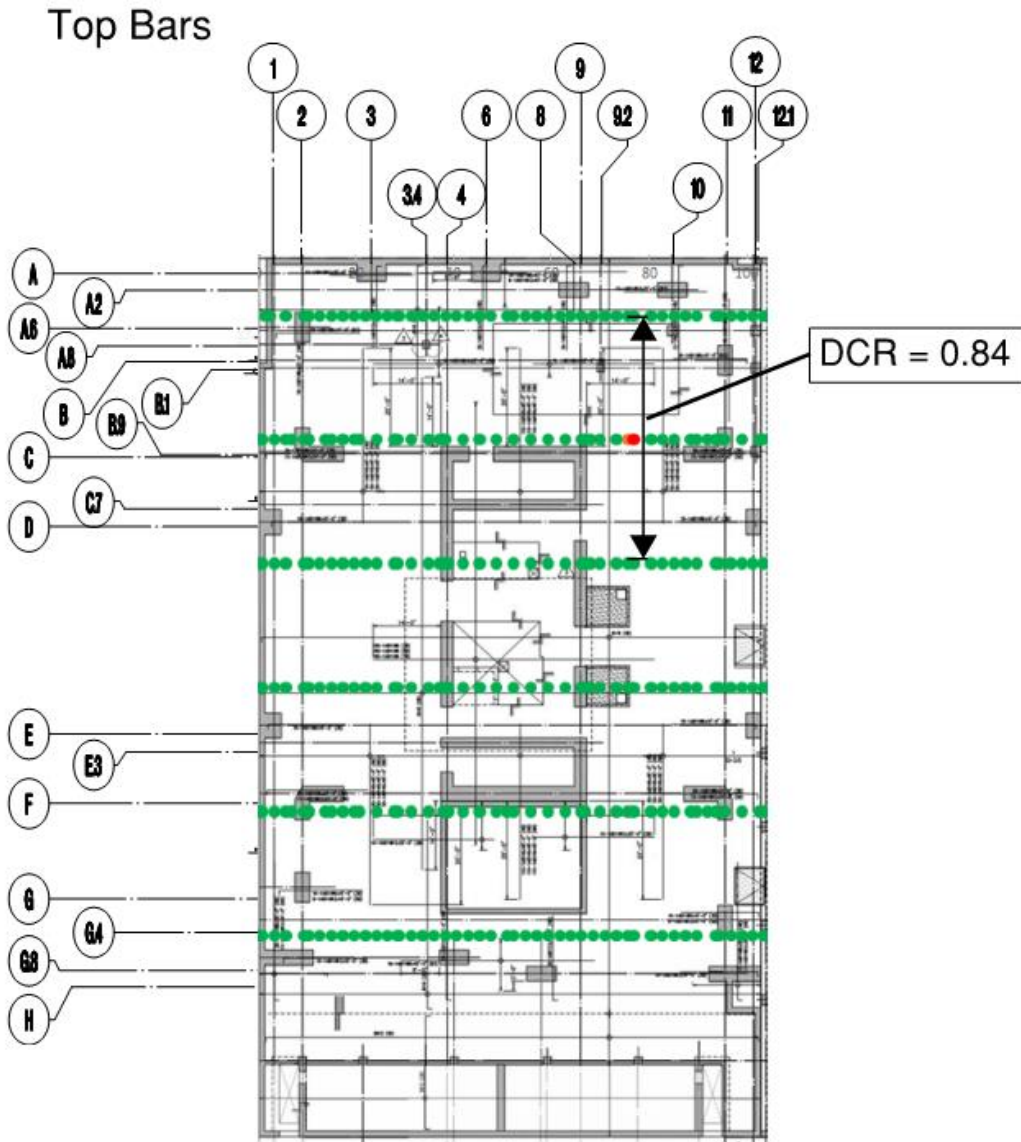


Figure 7-13: DCR Plot for East - West Top Reinforcement Design Strips for Seismic Existing Condition

DCR Legend

- DCR < 0.9
- DCR 0.9 TO 1.05
- DCR > 1.05

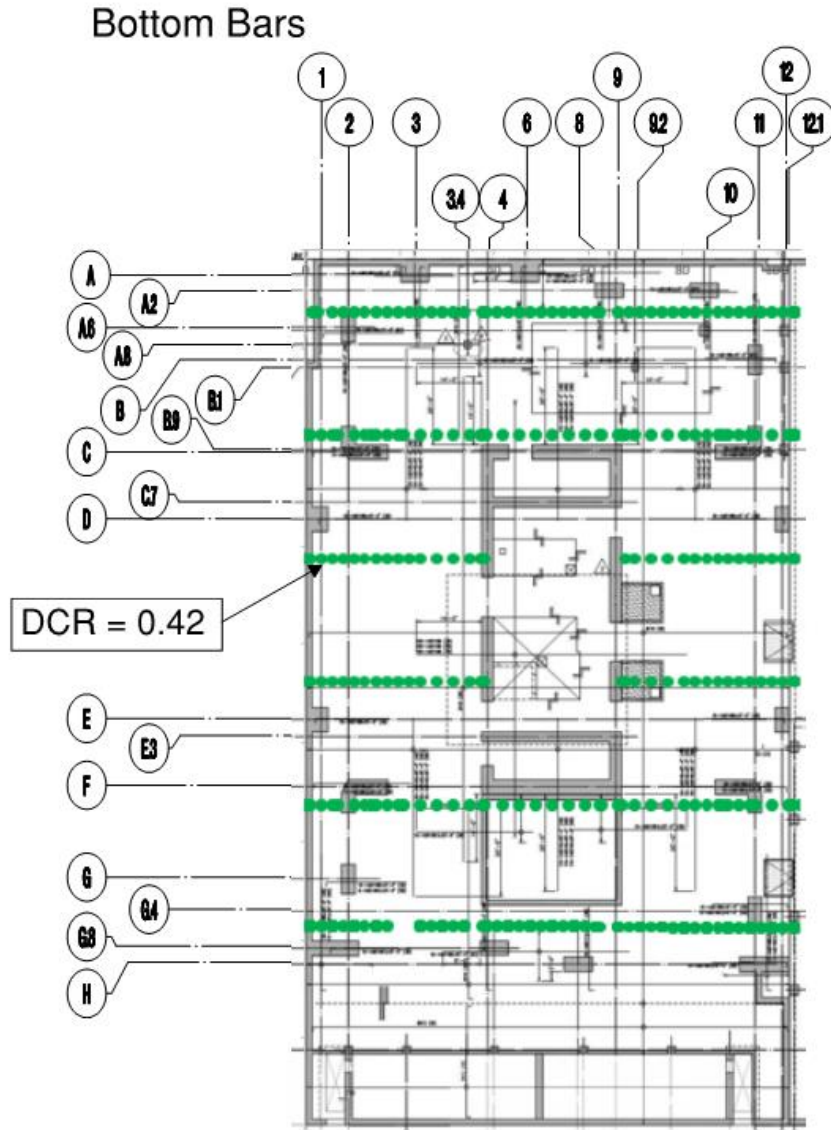


Figure 7-14: DCR Plot for East - West Bottom Reinforcement Design Strips for Seismic Existing Condition

DCR Legend

- DCR < 0.9
- DCR 0.9 TO 1.05
- DCR > 1.05

Top Bars

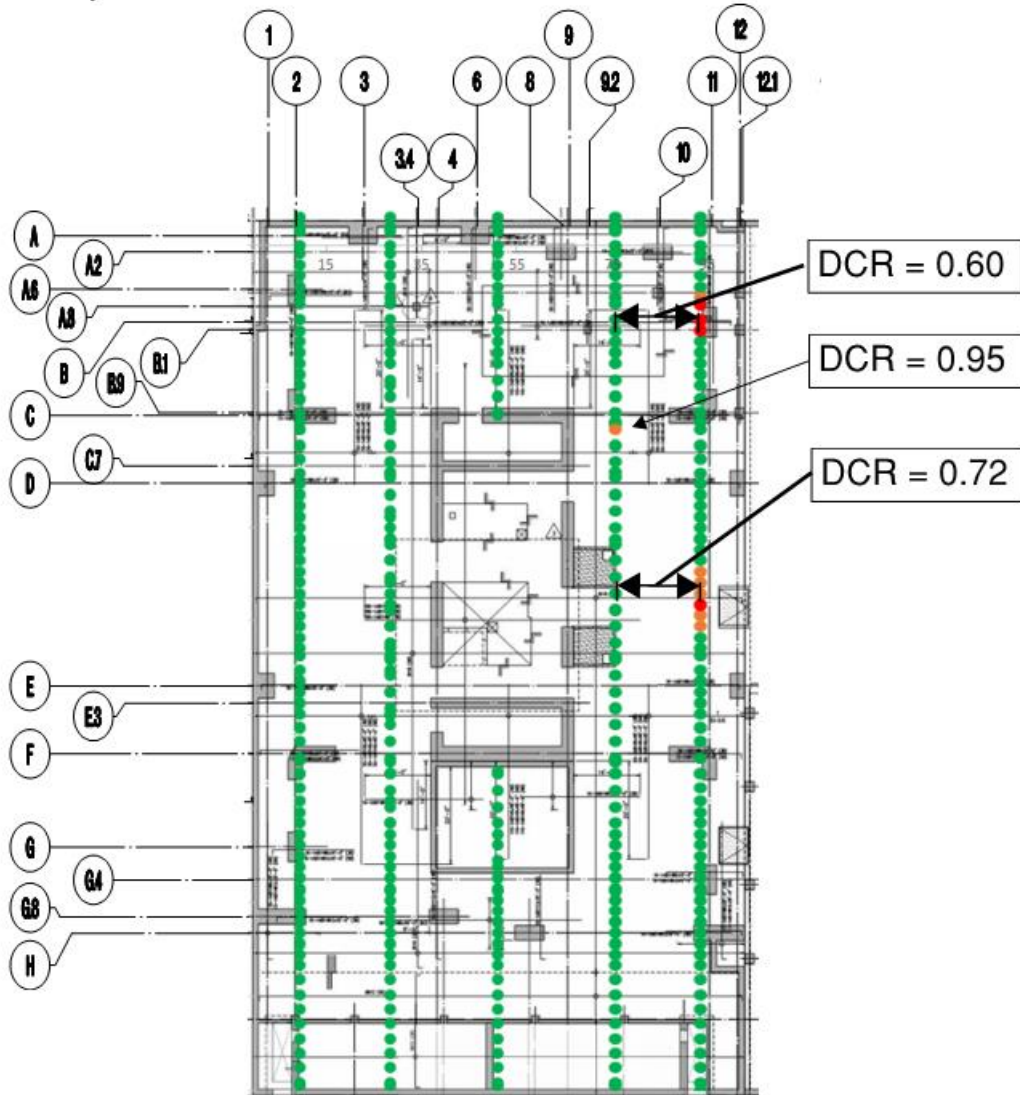


Figure 7-15: DCR Plot for North - South Top Reinforcement Design Strips for Seismic Existing Condition

DCR Legend

- DCR < 0.9
- DCR 0.9 TO 1.05
- DCR > 1.05

Bottom Bars

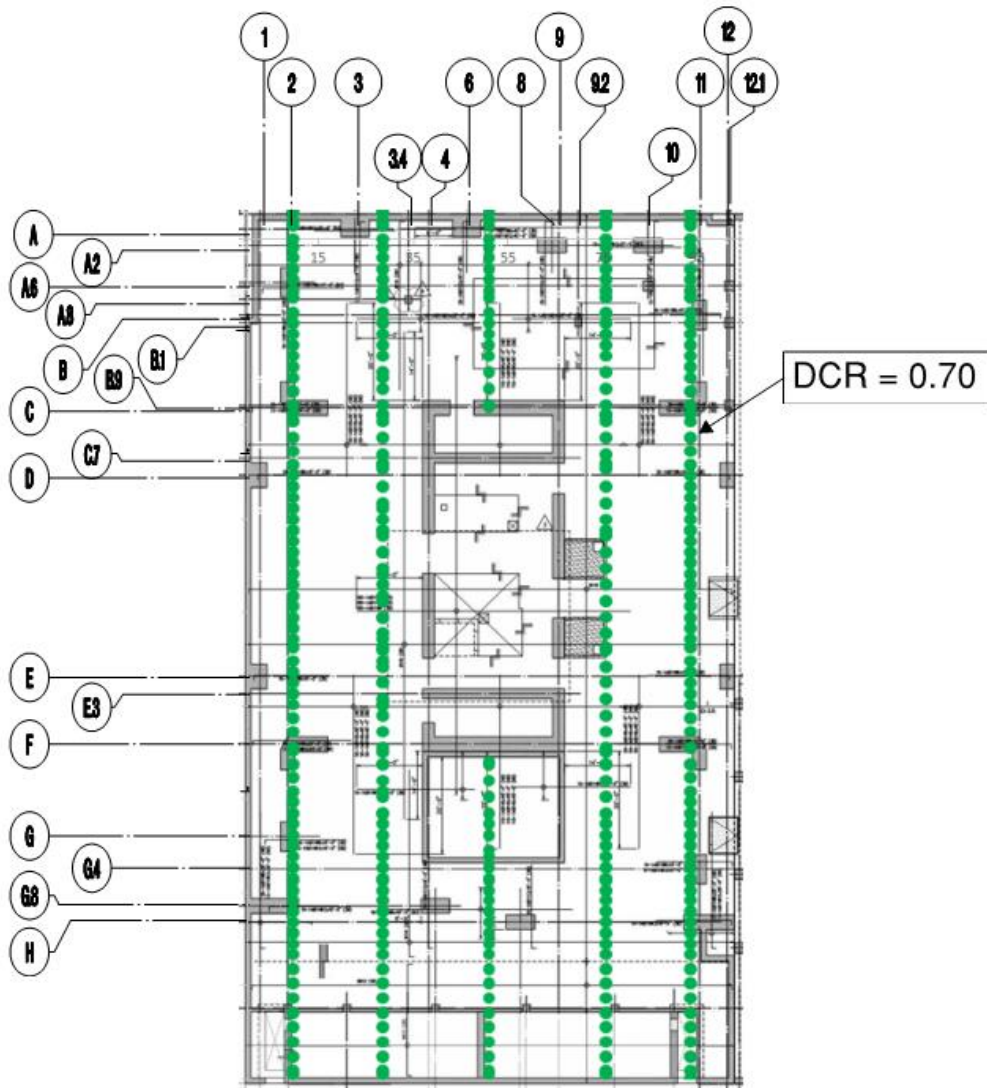


Figure 7-16: DCR Plot for North - South Bottom Reinforcement Design Strips for Seismic Existing Condition

7.6.1.2.2. Seismic Demand to Capacity Ratios for Retrofit Condition

The result figures below present the flexural design to capacity ratio checks for two envelopes listed below. The figures below highlight the locations of the maximum design to capacity ratios.

*Envelope 1: $(1.4 * D) + L + E + Jacking Loads$*

*Envelope 2: $(0.7 * D) + E + Jacking Loads$*

DCR Legend

- DCR < 0.9
- DCR 0.9 TO 1.05
- DCR > 1.05

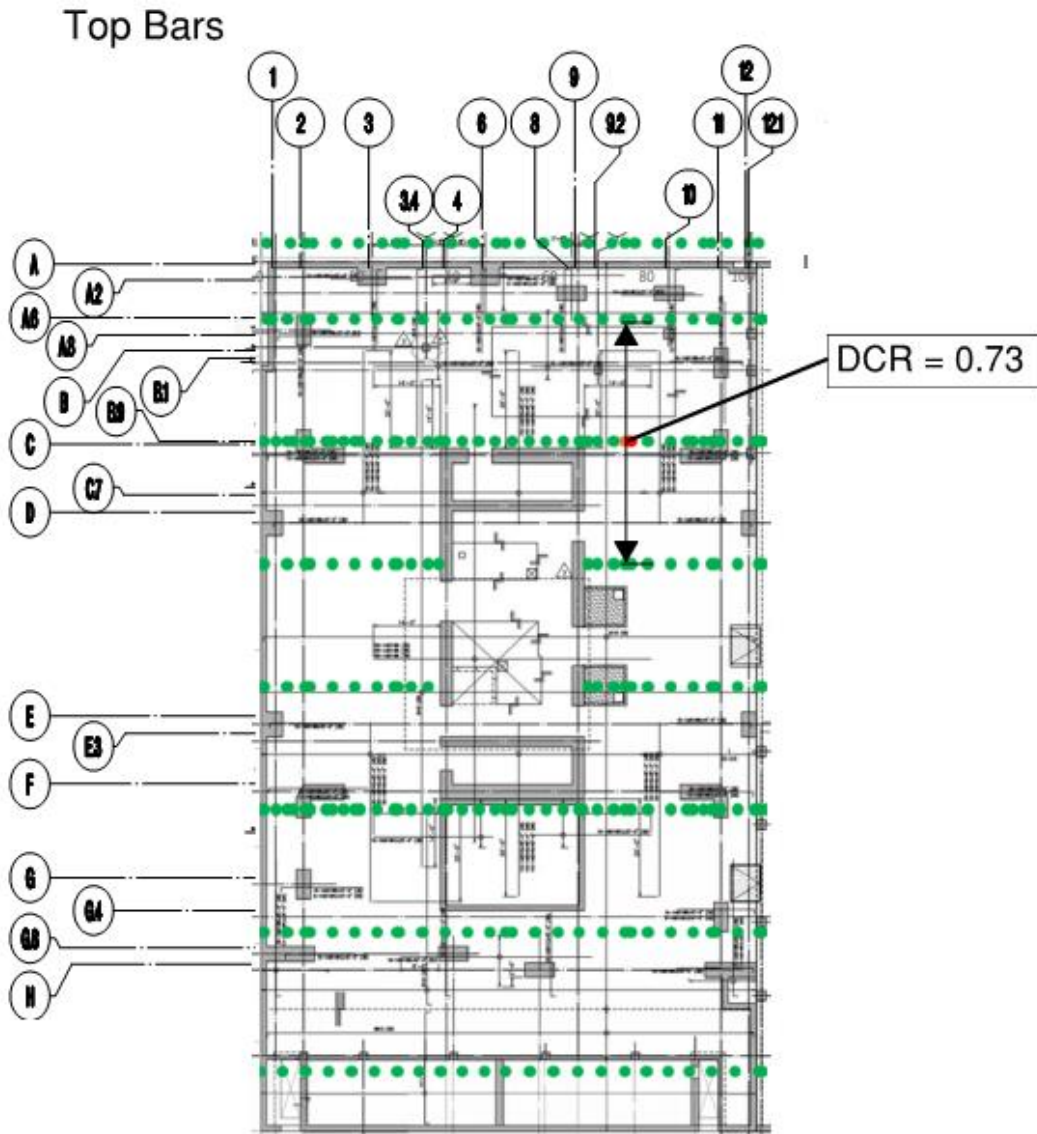


Figure 7-17: DCR Plot for East-West Top Reinforcement Design Strips for 1.4*D + L + E + Jacking Load

DCR Legend

- DCR < 0.9
- DCR 0.9 TO 1.05
- DCR > 1.05

Bottom Bars

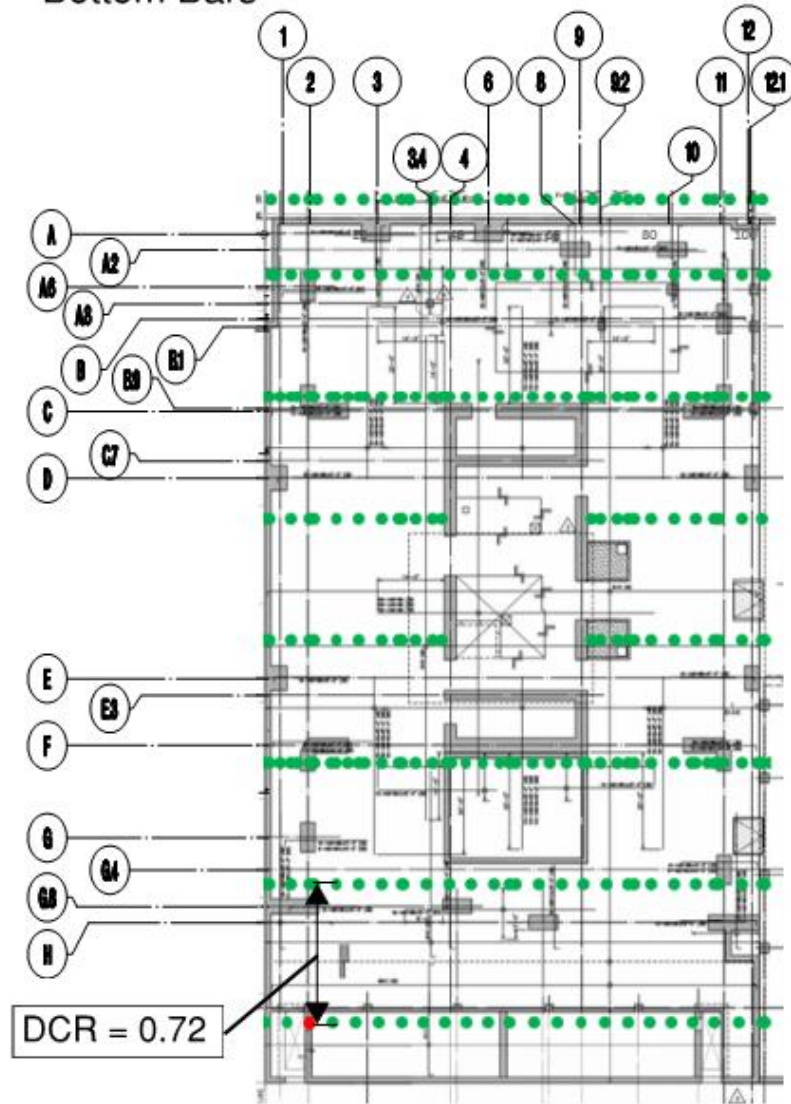


Figure 7-18: DCR Plot for East-West Bottom Reinforcement Design Strips for 1.4*D + L + E + Jacking Load

DCR Legend

- DCR < 0.9
- DCR 0.9 TO 1.05
- DCR > 1.05

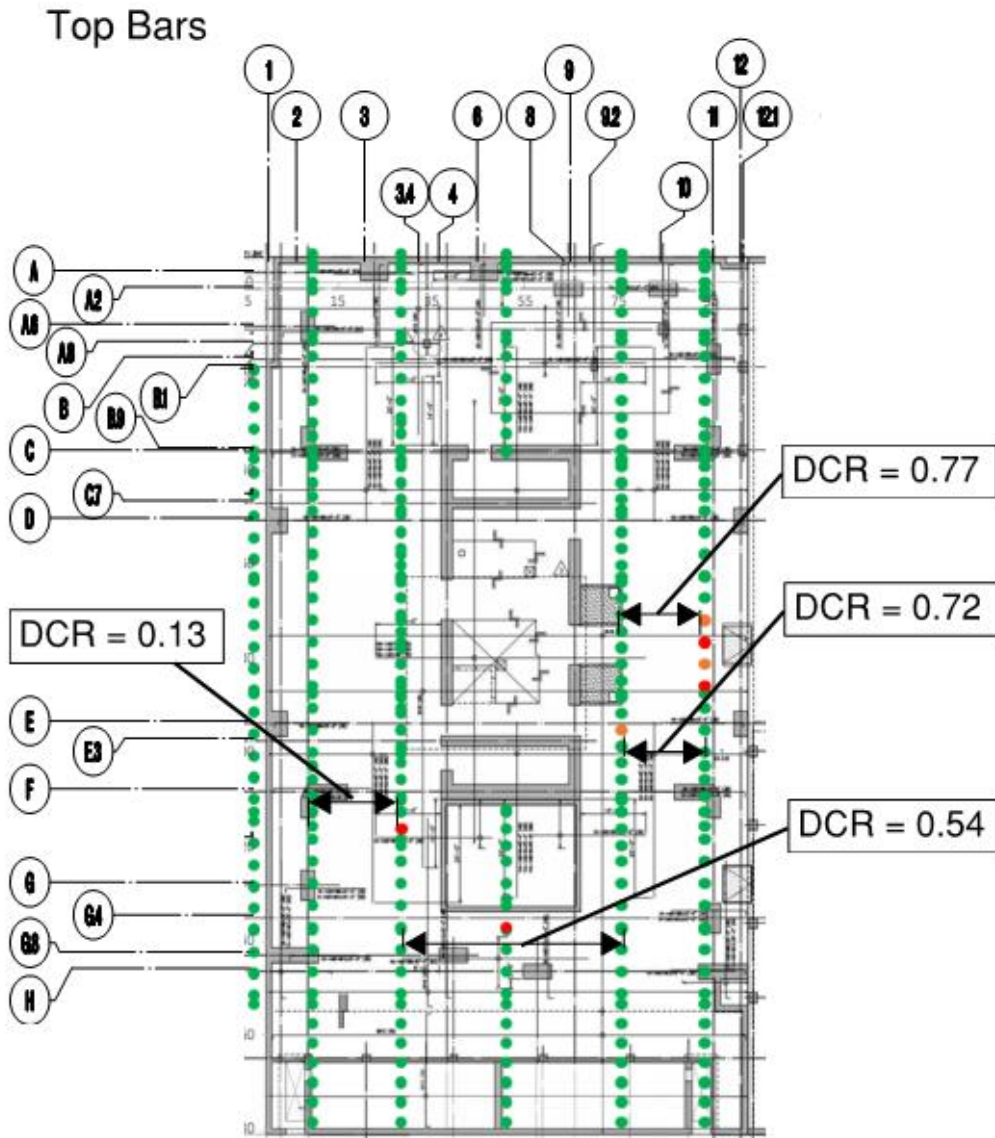


Figure 7-19: DCR Plot for North - South Top Reinforcement Design Strips
for $1.4 \cdot D + L + E + \text{Jacking Load}$

DCR Legend

- DCR < 0.9
- DCR 0.9 TO 1.05
- DCR > 1.05

Bottom Bars

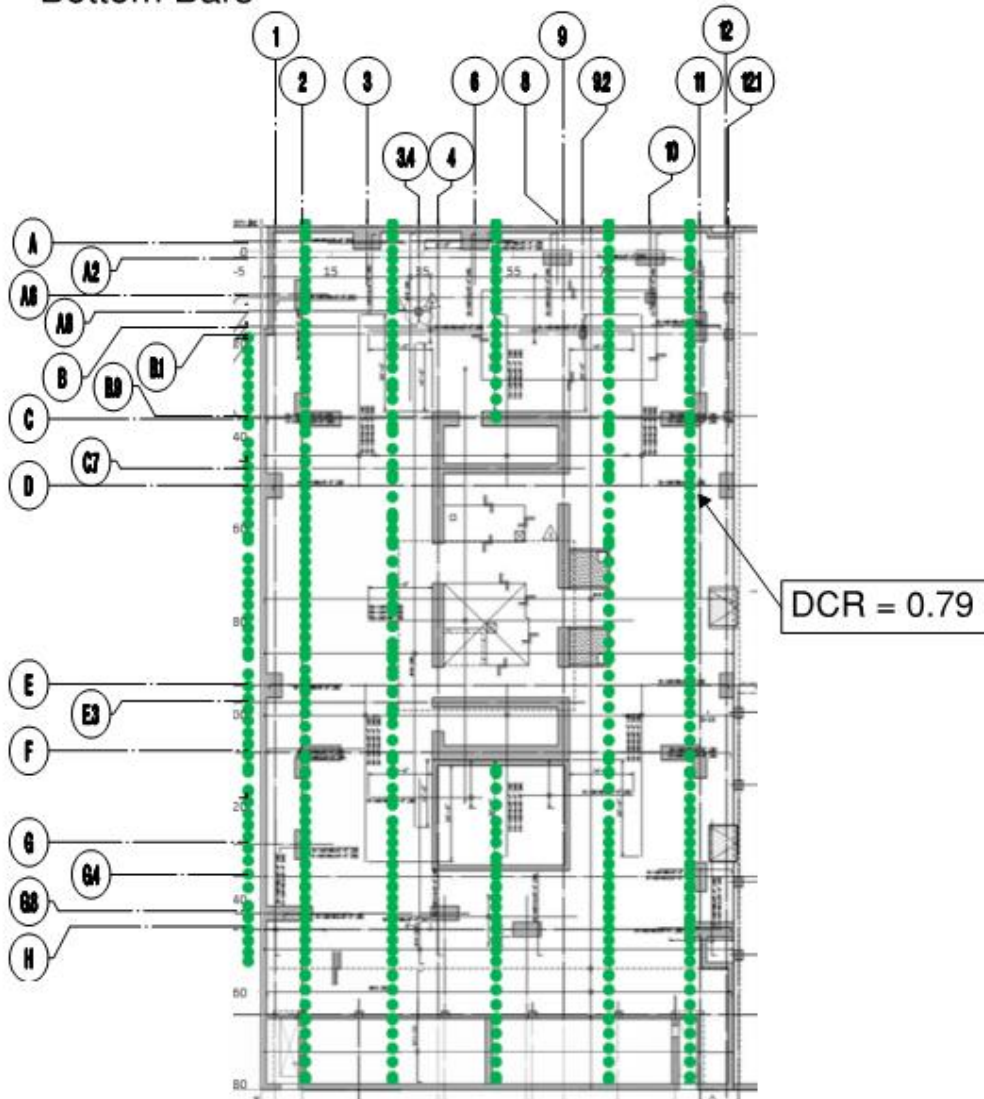
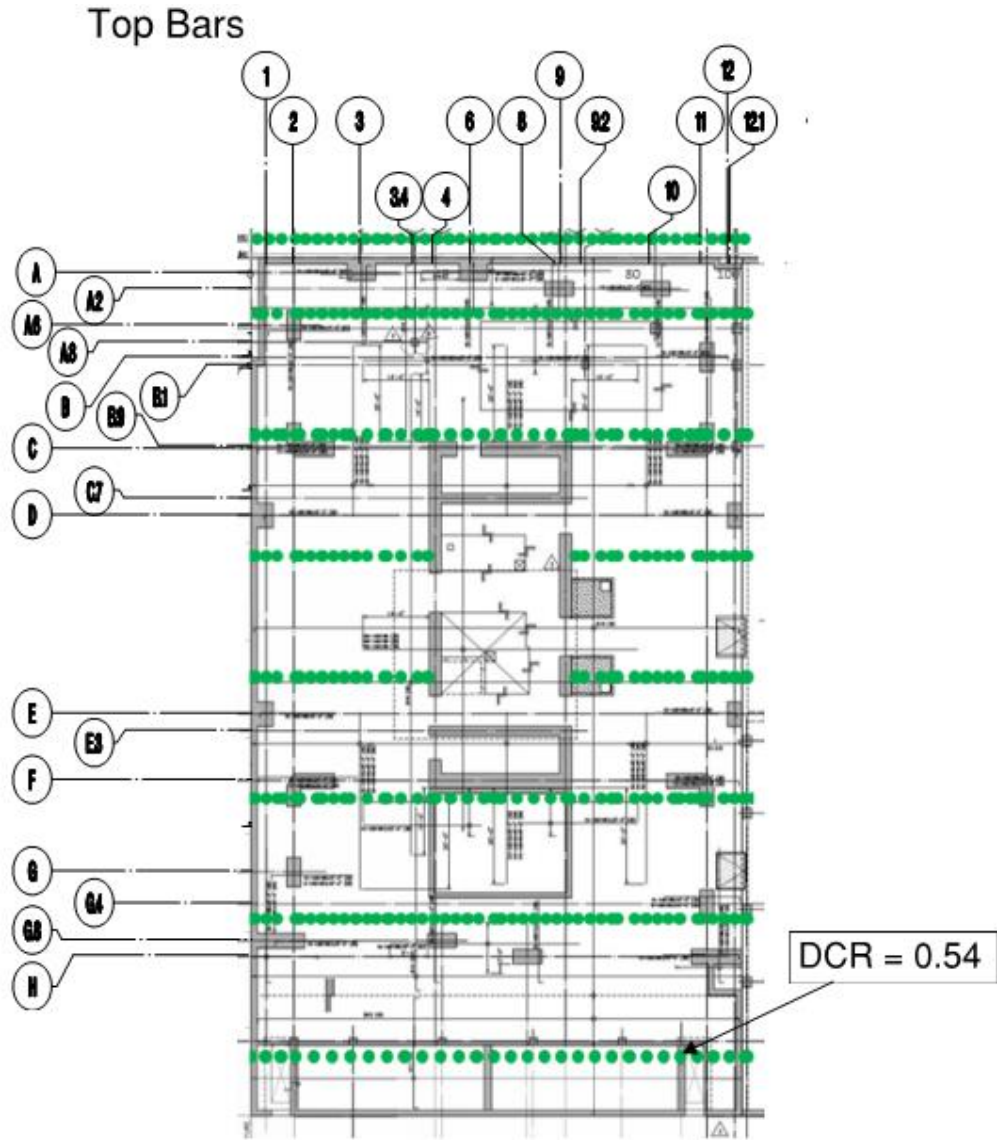


Figure 7-20: DCR Plot for North - South Bottom Reinforcement Design Strips for $1.4 \cdot D + L + E + \text{Jacking Load}$

DCR Legend

- DCR < 0.9
- DCR 0.9 TO 1.05
- DCR > 1.05



**Figure 7-21: DCR Plot for East - West Top Reinforcement Design Strips
for 0.7*D + E + Jacking Load**

DCR Legend

- DCR < 0.9
- DCR 0.9 TO 1.05
- DCR > 1.05

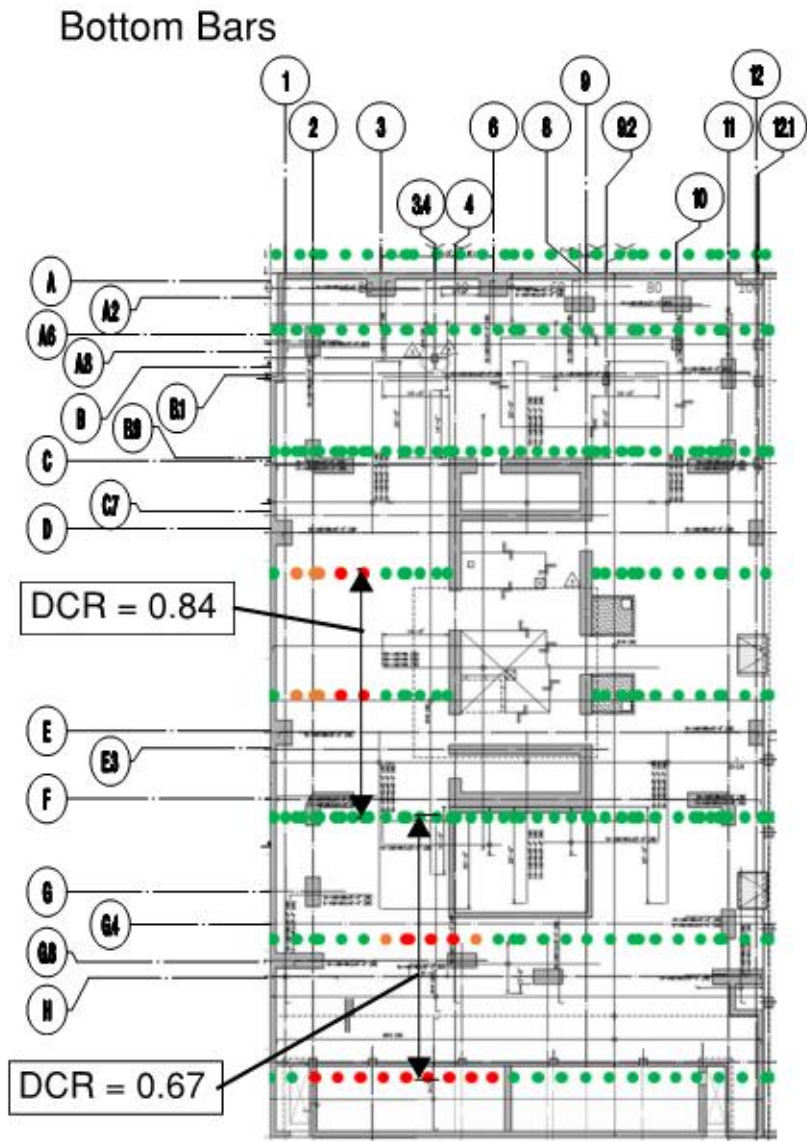


Figure 7-22: DCR Plot for East-West Bottom Reinforcement Design Strips for $0.7 \cdot D + E + \text{Jacking Load}$

DCR Legend

- DCR < 0.9
- DCR 0.9 TO 1.05
- DCR > 1.05

Top Bars

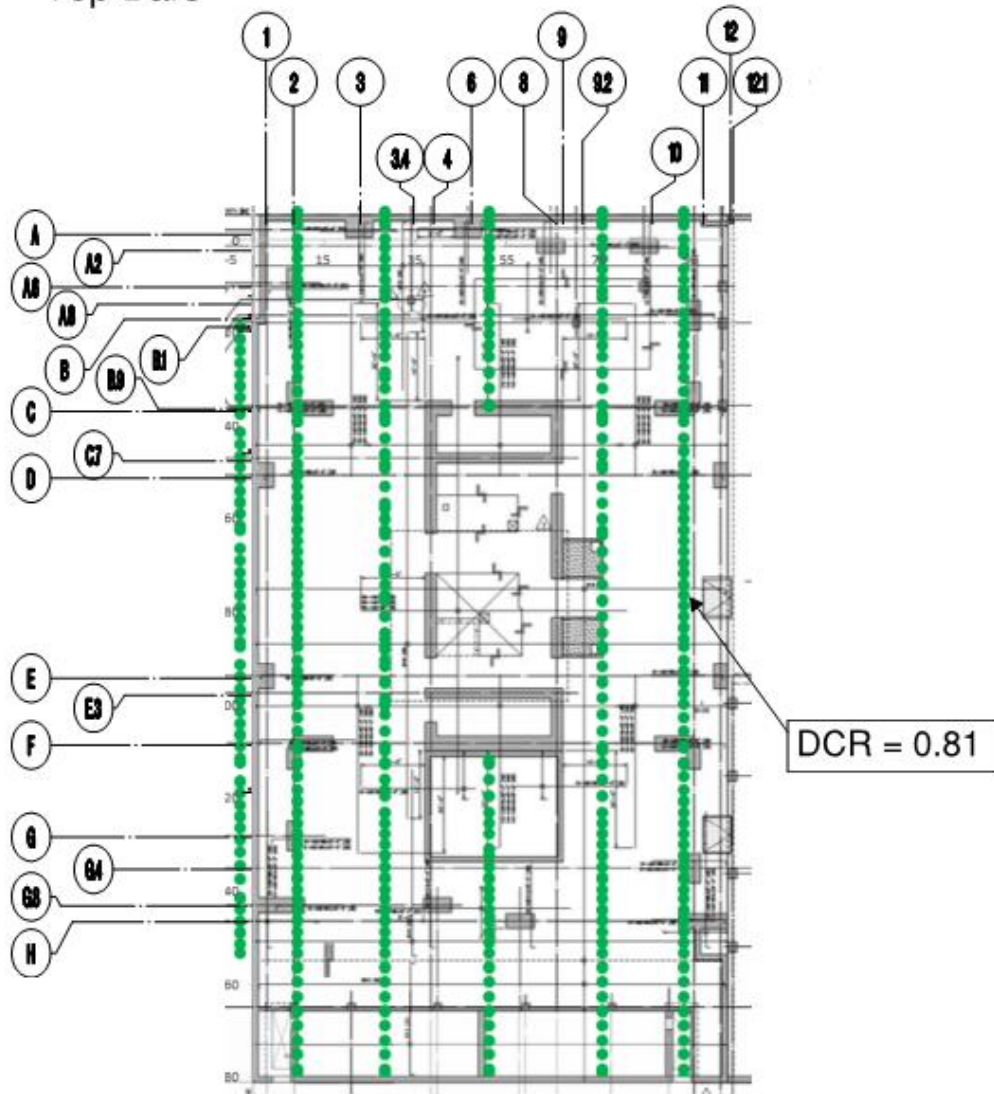
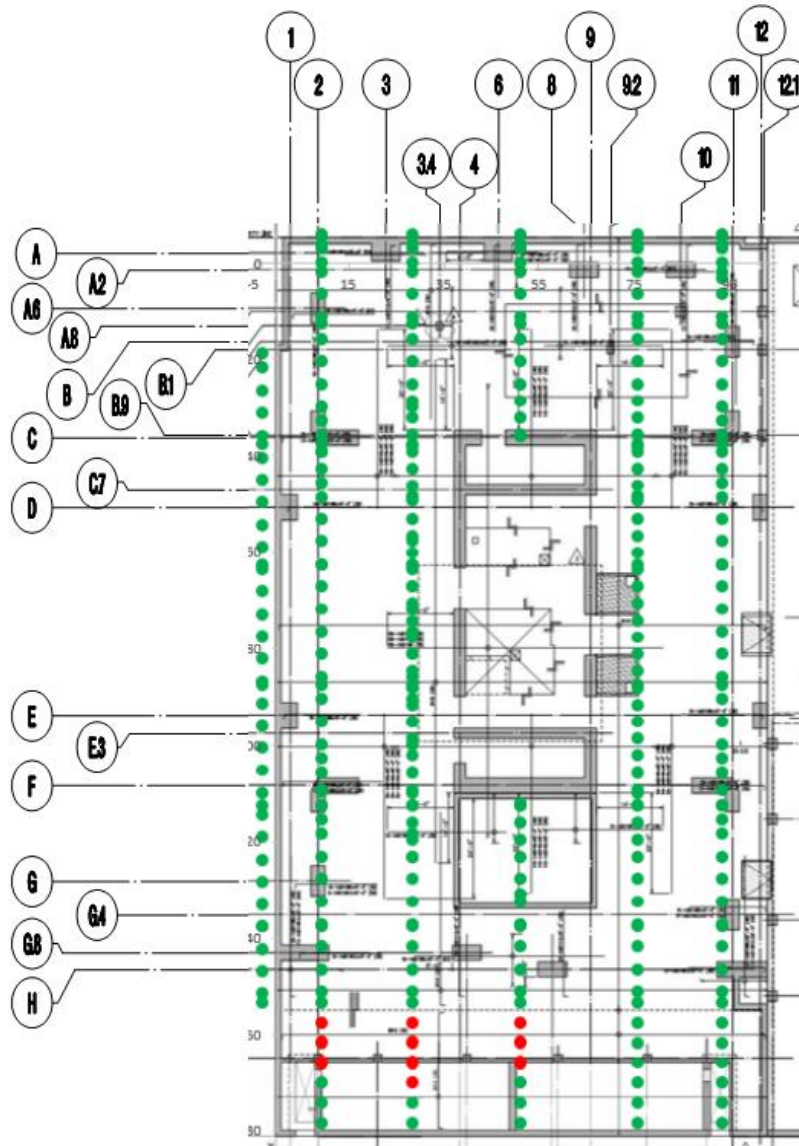


Figure 7-23: DCR Plot for North-South Top Reinforcement Design Strips for $0.7 \cdot D + E + \text{Jacking Load}$

DCR Legend

- DCR < 0.9
- DCR 0.9 TO 1.05
- DCR > 1.05



**Figure 7-24: DCR Plot for North-South Bottom Reinforcement
Design Strips for $0.7 \cdot D + E + \text{Jacking Load}$**

7.6.2 SAFE Model using Egan Team Pile Springs

Alternatively, we perform similar analyses with soil springs provided by John Egan Slate Geotechnical Consultants, Inc. and Shannon & Wilson, Inc. as presented in Volume 2.

7.6.2.1 Wind Loading

7.6.2.1.1. Wind Demand to Capacity Ratios for Existing Condition

The results presented below include the maximum load envelope of the following wind load combinations:

*Envelope 1: $1.2 * D + L + W$ and $0.9 * D + W$*

DCR Legend

- DCR < 0.9
- DCR 0.9 TO 1.05
- DCR > 1.05

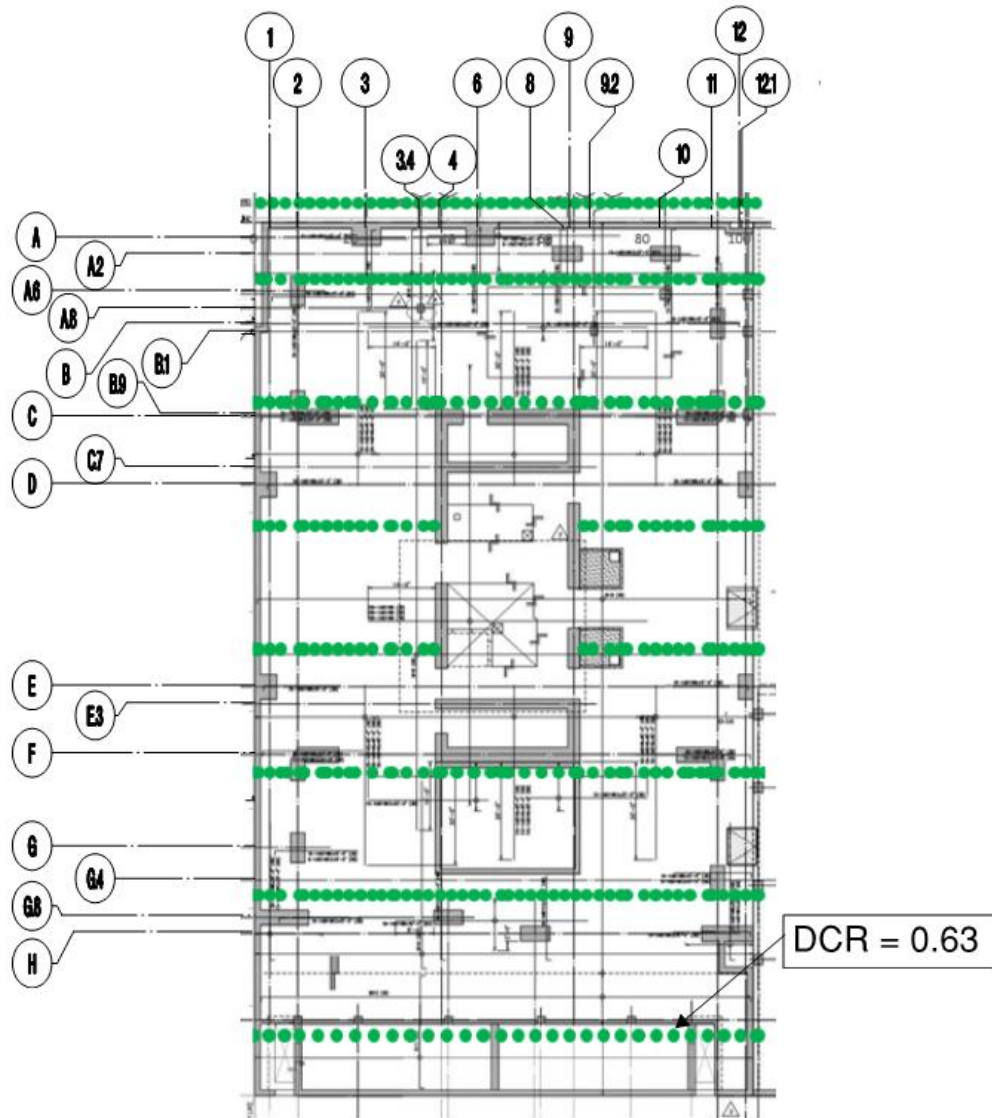


Figure 7-25: DCR Plot for East-West Top Reinforcement Design Strips for Wind Existing Condition

DCR Legend

- DCR < 0.9
- DCR 0.9 TO 1.05
- DCR > 1.05

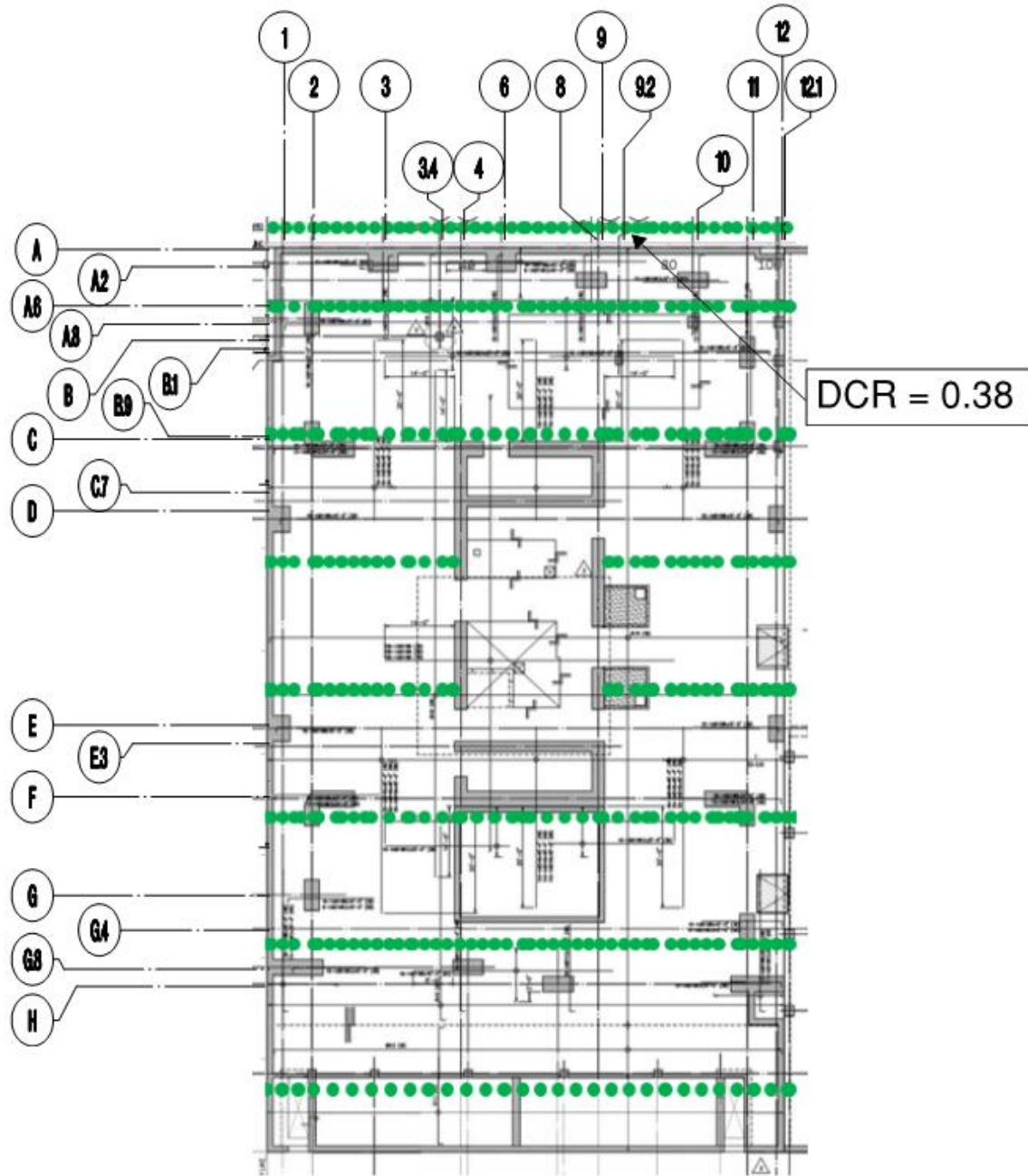


Figure 7-26: DCR Plot for East-West Bottom Reinforcement Design Strips for Wind Existing Condition

DCR Legend

- DCR < 0.9
- DCR 0.9 TO 1.05
- DCR > 1.05

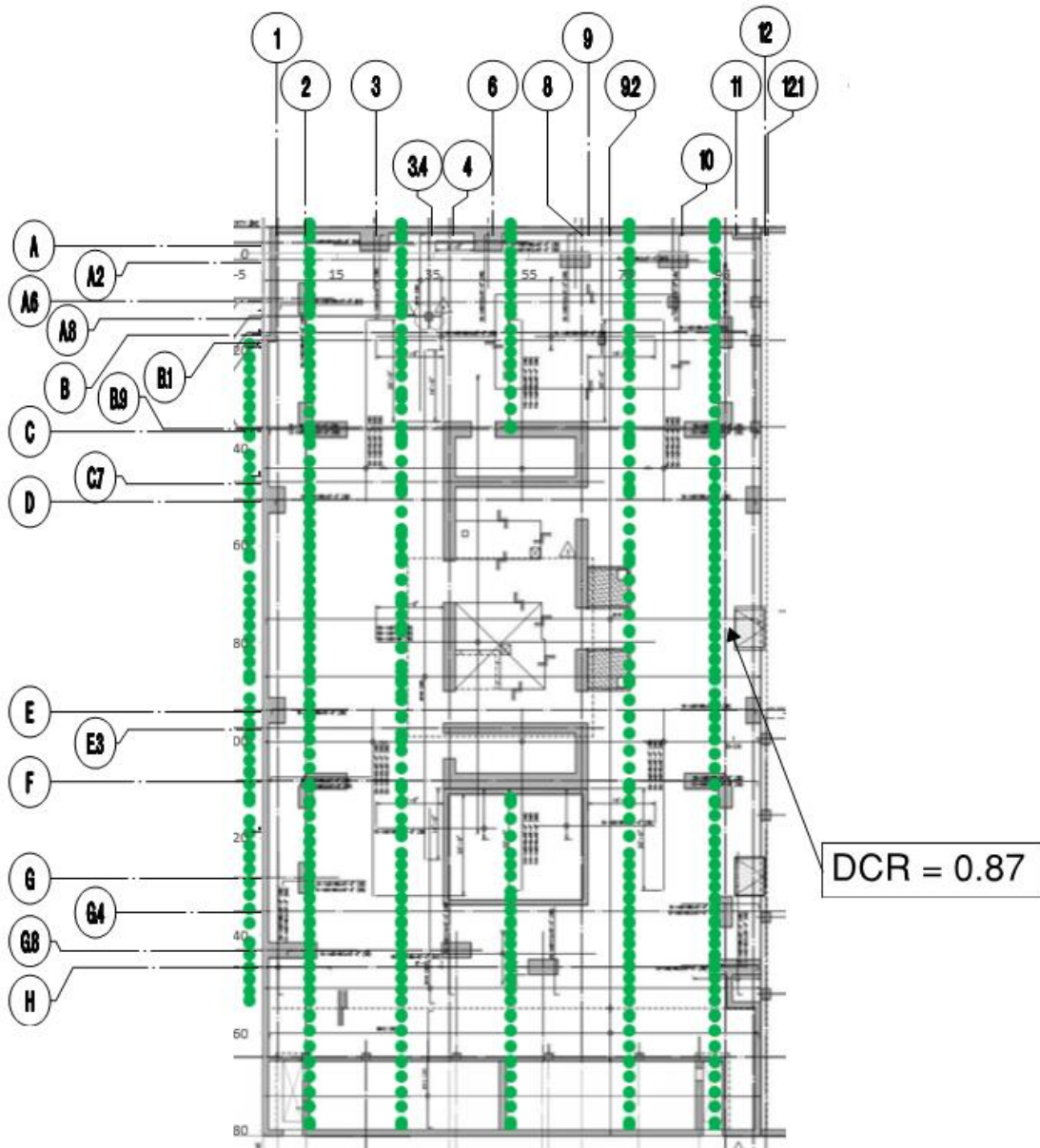


Figure 7-27: DCR Plot for North - South Top Reinforcement Design Strips for Wind Existing Condition

DCR Legend

- DCR < 0.9
- DCR 0.9 TO 1.05
- DCR > 1.05

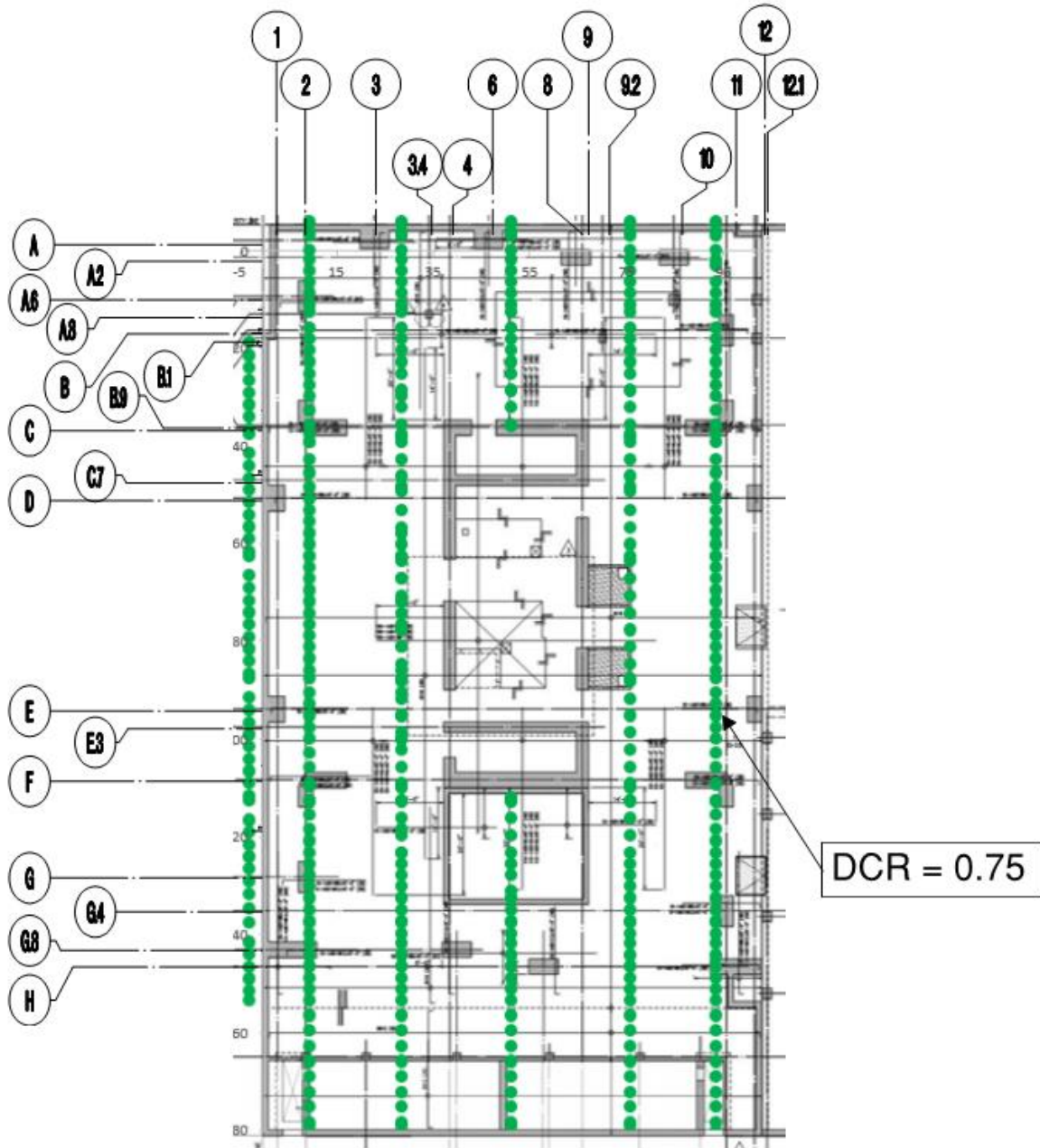


Figure 7-28: DCR Plot for North - South Bottom Reinforcement Design Strips for Wind Existing Condition

7.6.2.1.2. Wind Demand to Capacity Ratios for Retrofit Condition

The results presented below include the maximum load envelope of the following wind load combinations:

*Envelope 1: $1.2 * D + L + W + \text{Jacking Load}$ and $0.9 * D + W + \text{Jacking Load}$*

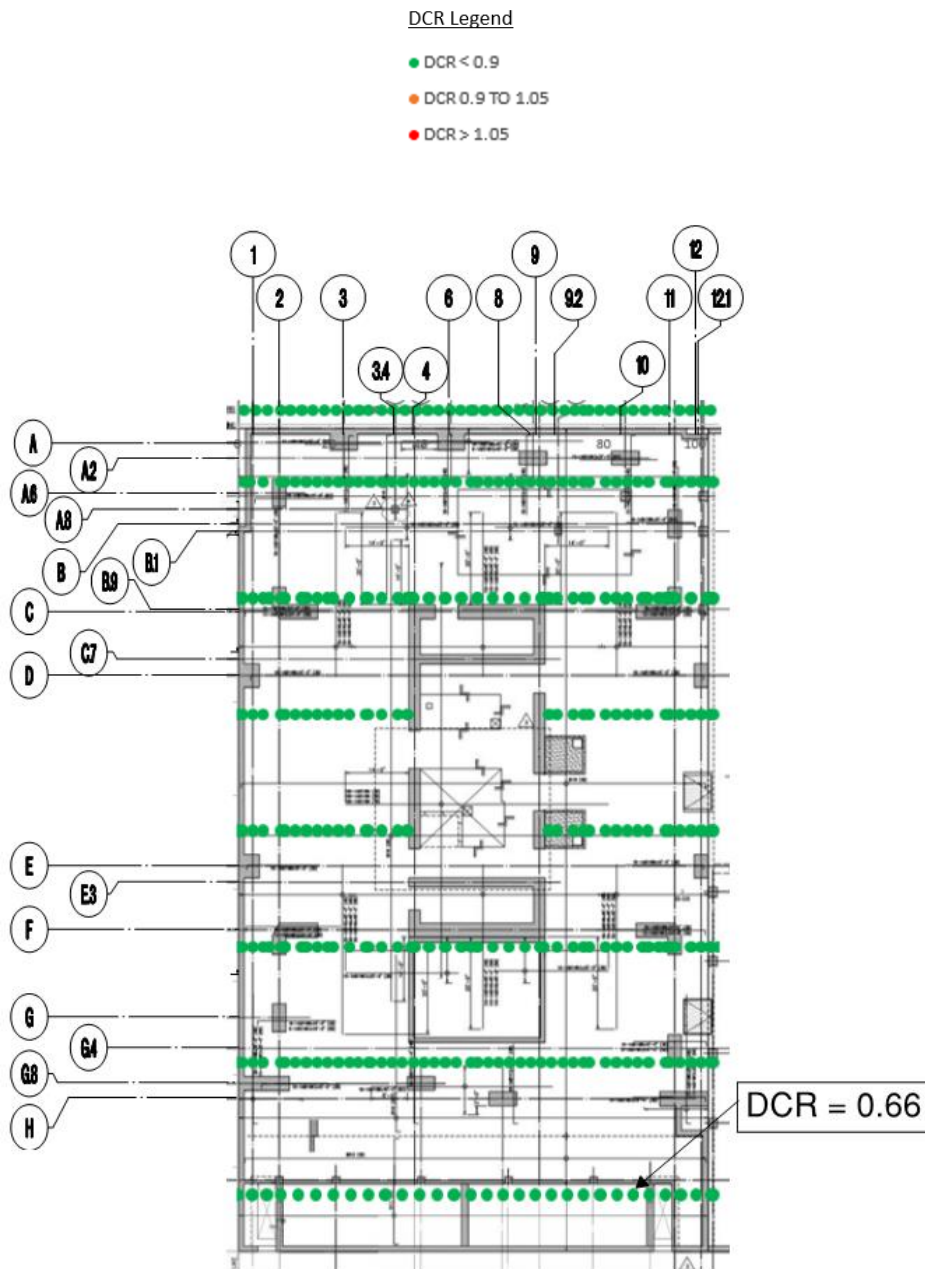
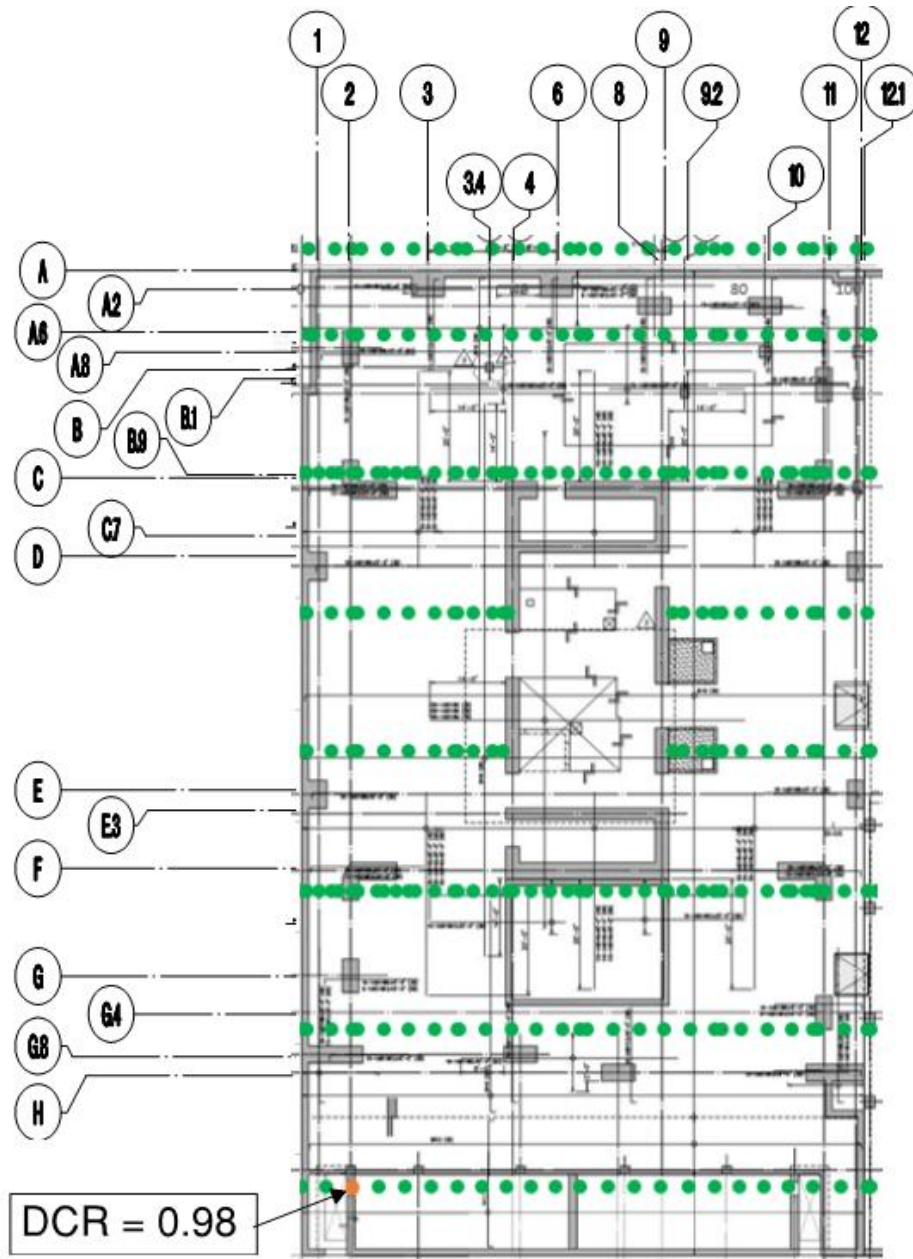


Figure 7-29: DCR Plot for East-West Top Reinforcement Design Strips for Wind + Jacking Load

DCR Legend

- DCR < 0.9
- DCR 0.9 TO 1.05
- DCR > 1.05



**Figure 7-30: DCR Plot for East-West Bottom Reinforcement Design Strips
for Wind + Jacking Load**

DCR Legend

- DCR < 0.9
- DCR 0.9 TO 1.05
- DCR > 1.05

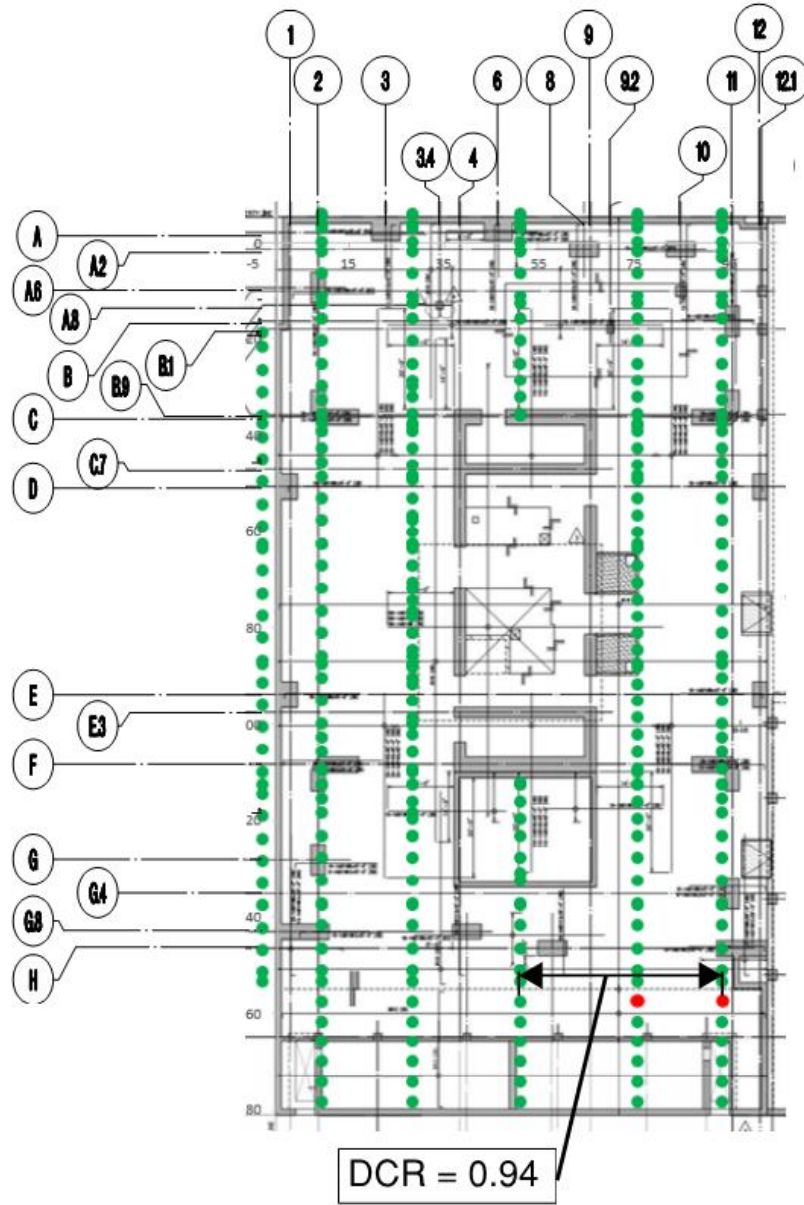


Figure 7-31: DCR Plot for North - South Top Reinforcement Design Strips for Wind + Jacking Load

DCR Legend

- DCR < 0.9
- DCR 0.9 TO 1.05
- DCR > 1.05

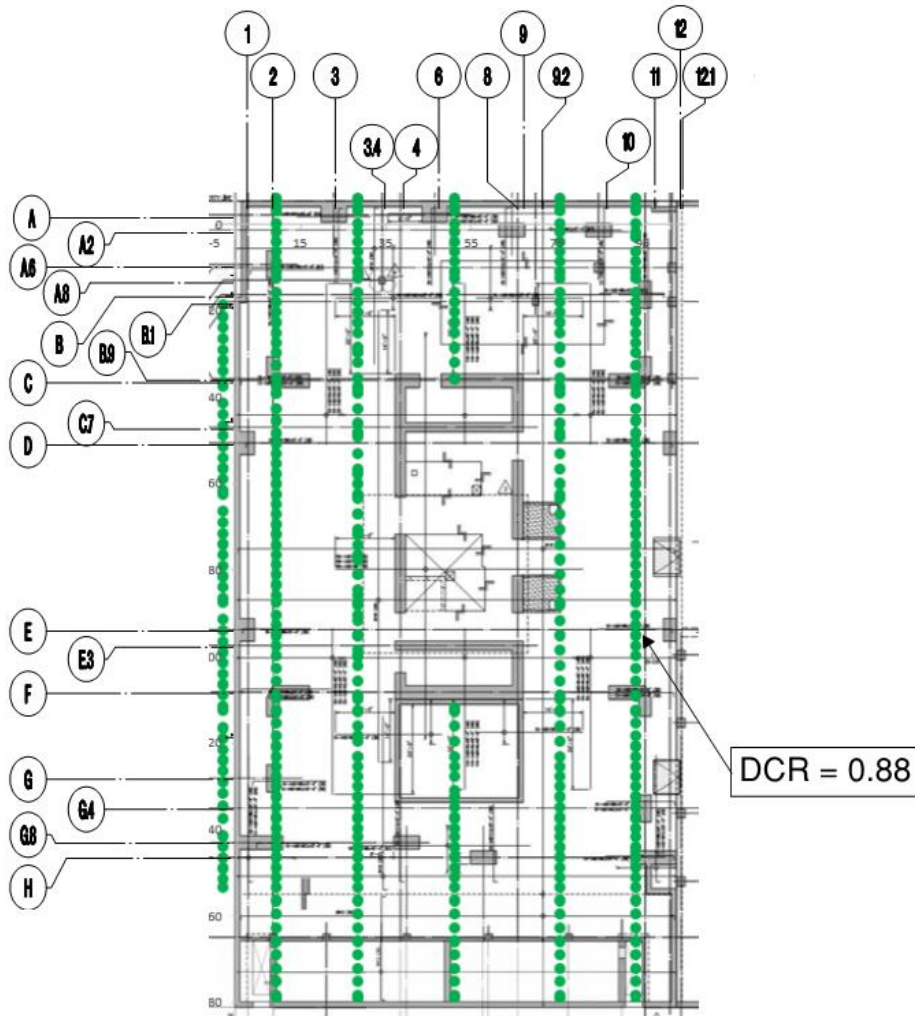


Figure 7-32: DCR Plot for North - South Bottom Reinforcement Design Strips for Wind + Jacking Load

7.6.2.2 Seismic Loading

7.6.2.2.1. Seismic Demand to Capacity Ratios for Existing Condition for Design Earthquake

The result figures below present the flexural design to capacity ratio checks for two envelopes listed below. The figures below highlight the locations of the maximum design to capacity ratios.

*Envelope 1: $(1.4 * D) + L + E$ and $(0.7 * D) + E$*

DCR Legend

- DCR < 0.9
- DCR 0.9 TO 1.05
- DCR > 1.05

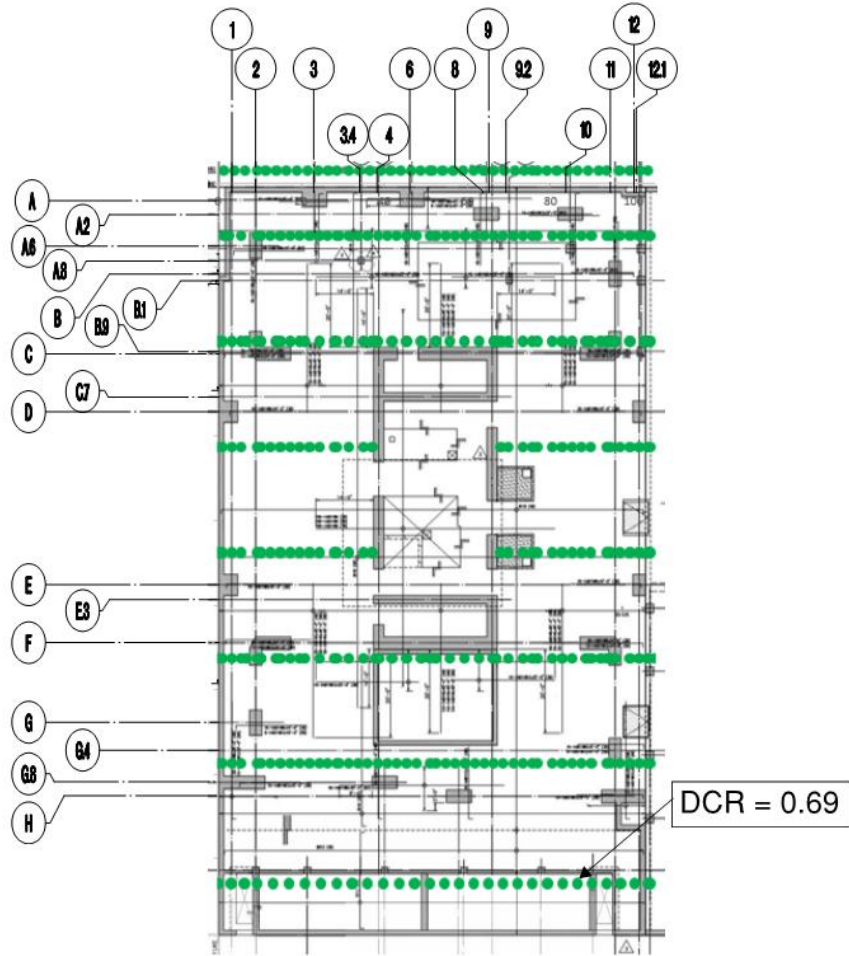
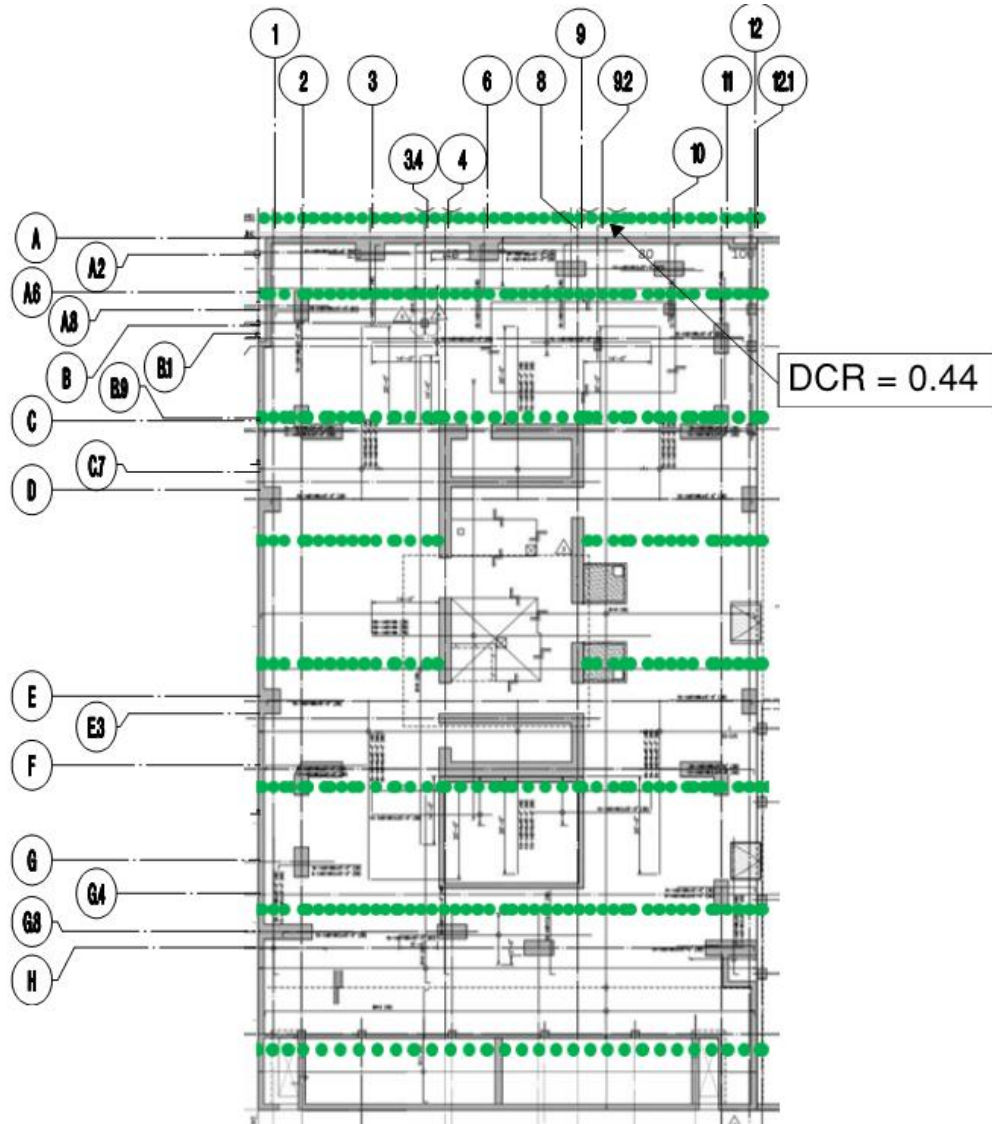


Figure 7-33: DCR Plot for East - West Top Reinforcement Design Strips for Seismic Existing Condition

DCR Legend

- DCR < 0.9
- DCR 0.9 TO 1.05
- DCR > 1.05



**Figure 7-34: DCR Plot for East - West Bottom Reinforcement Design Strips
for Seismic Existing Condition**

DCR Legend

- DCR < 0.9
- DCR 0.9 TO 1.05
- DCR > 1.05

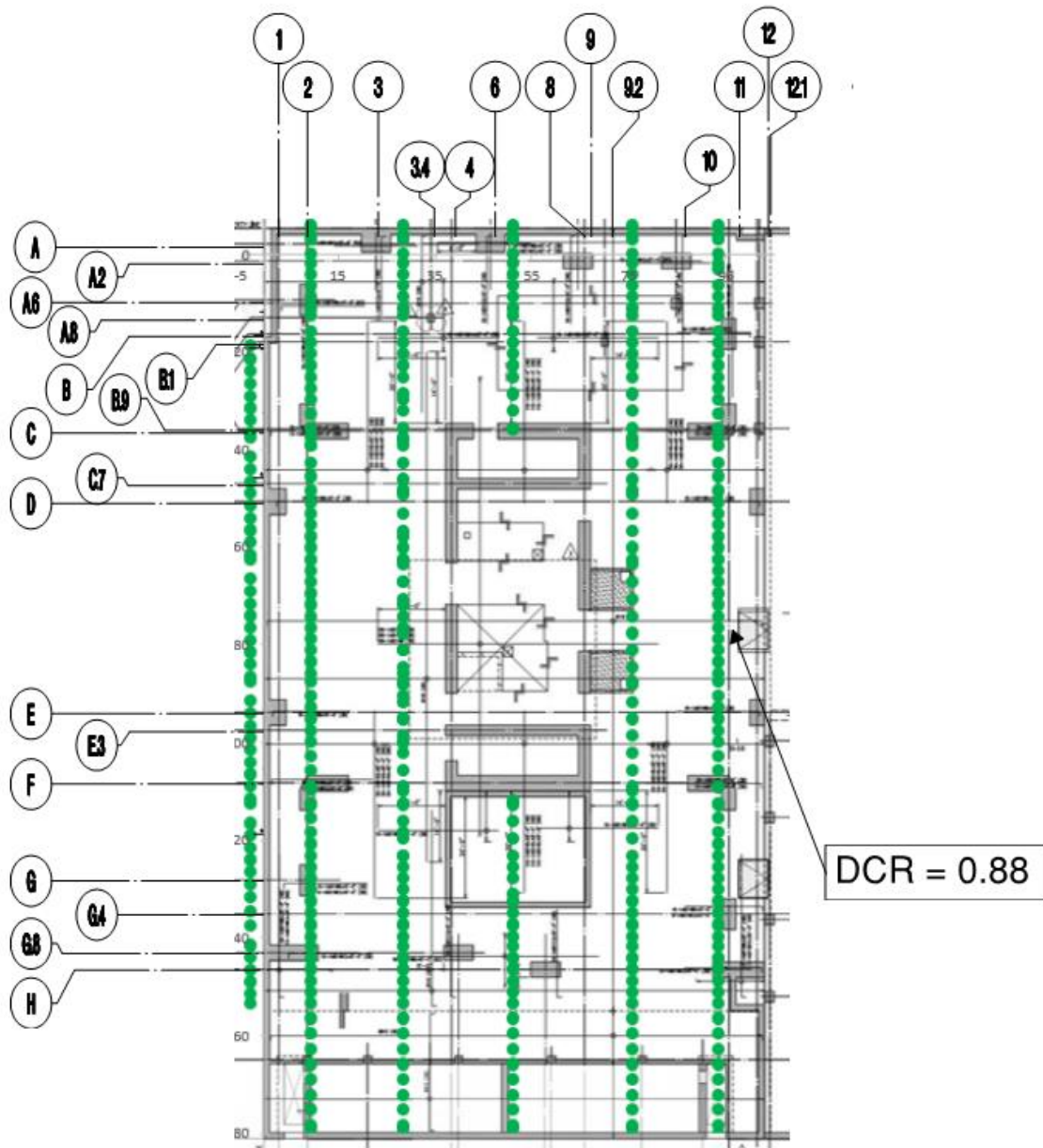


Figure 7-35: DCR Plot for North - South Top Reinforcement Design Strips for Seismic Existing Condition

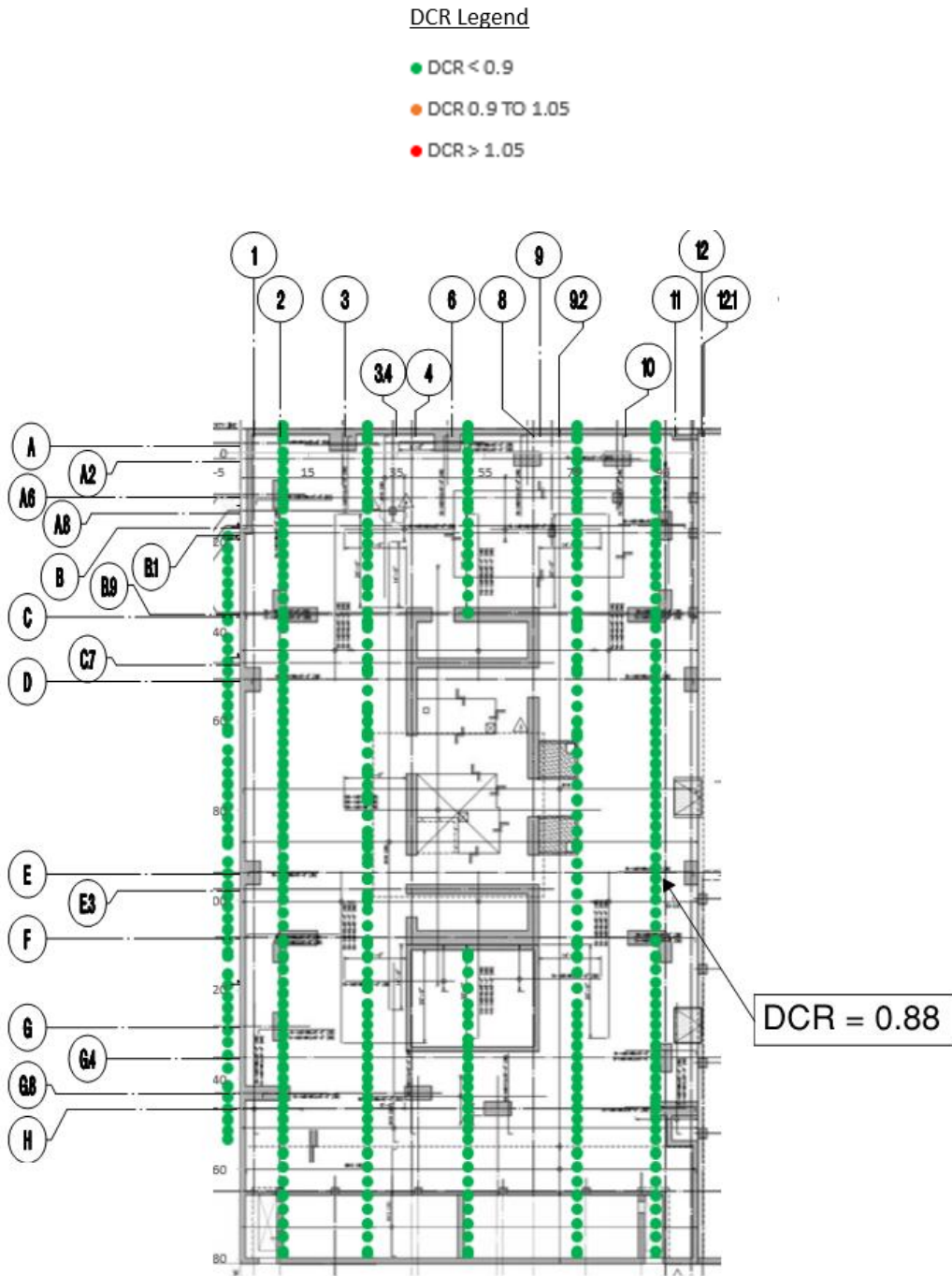


Figure 7-36: DCR Plot for North - South Bottom Reinforcement Design Strips for Seismic Existing Condition

7.6.2.2.2. Seismic Demand to Capacity Ratios for Retrofit Condition for Design Earthquake

The result figures below present the flexural demand to capacity ratio checks for the two load combinations listed below. The figures below highlight the locations of the maximum design to capacity ratios.

*Envelope 1: $(1.4 * D) + L + E + Jacking Loads$*

*Envelope 2: $(0.7 * D) + E + Jacking Loads$*

DCR Legend

- DCR < 0.9
- DCR 0.9 TO 1.05
- DCR > 1.05

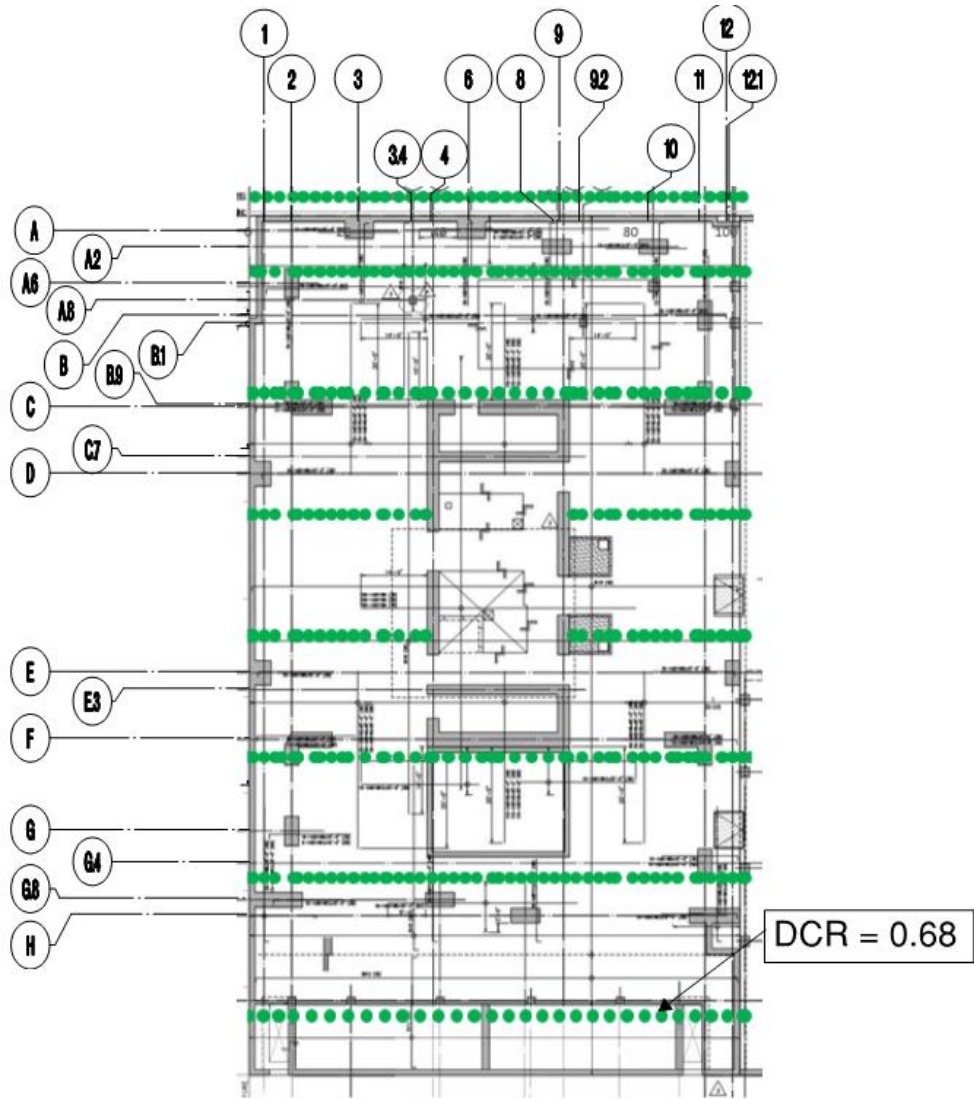
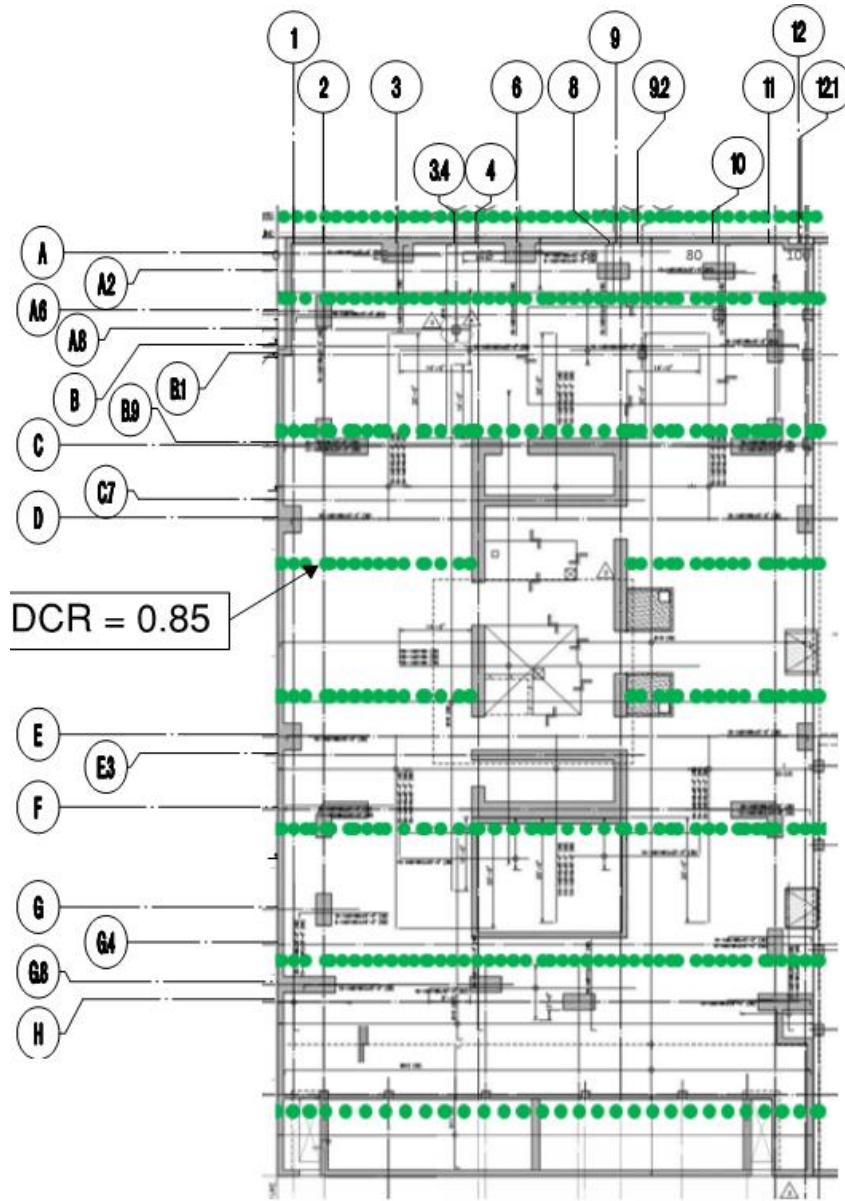


Figure 7-37: DCR Plot for East-West Top Reinforcement Design Strips for $1.4 \cdot D + L + E + \text{Jacking Load}$

DCR Legend

- DCR < 0.9
- DCR 0.9 TO 1.05
- DCR > 1.05



**Figure 7-38: DCR Plot for East-West Bottom Reinforcement
Design Strips for $1.4 \cdot D + L + E + \text{Jacking Load}$**

DCR Legend

- DCR < 0.9
- DCR 0.9 TO 1.05
- DCR > 1.05

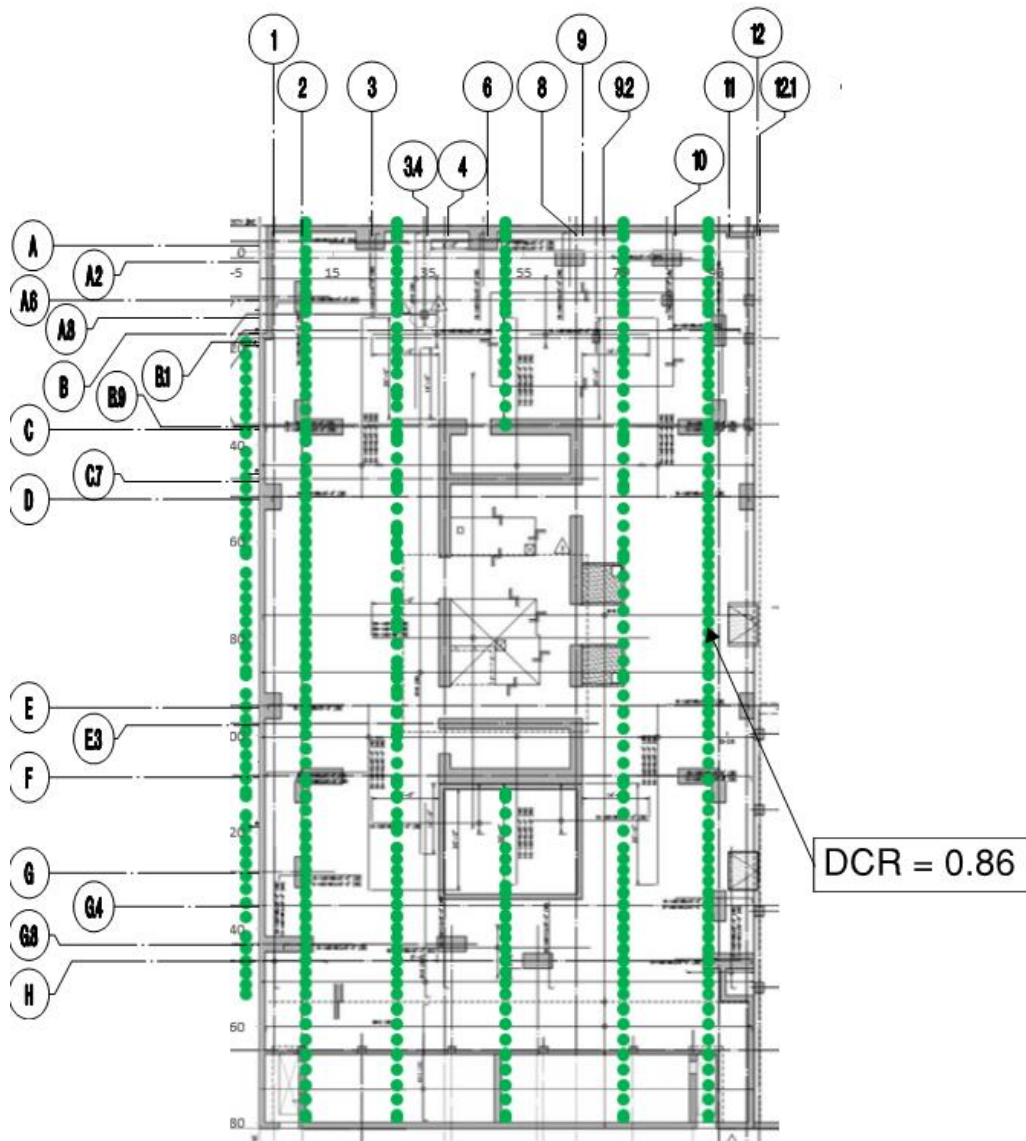


Figure 7-39: DCR Plot for North - South Top Reinforcement Design Strips
for $1.4 \cdot D + L + E + \text{Jacking Load}$

DCR Legend

- DCR < 0.9
- DCR 0.9 TO 1.05
- DCR > 1.05

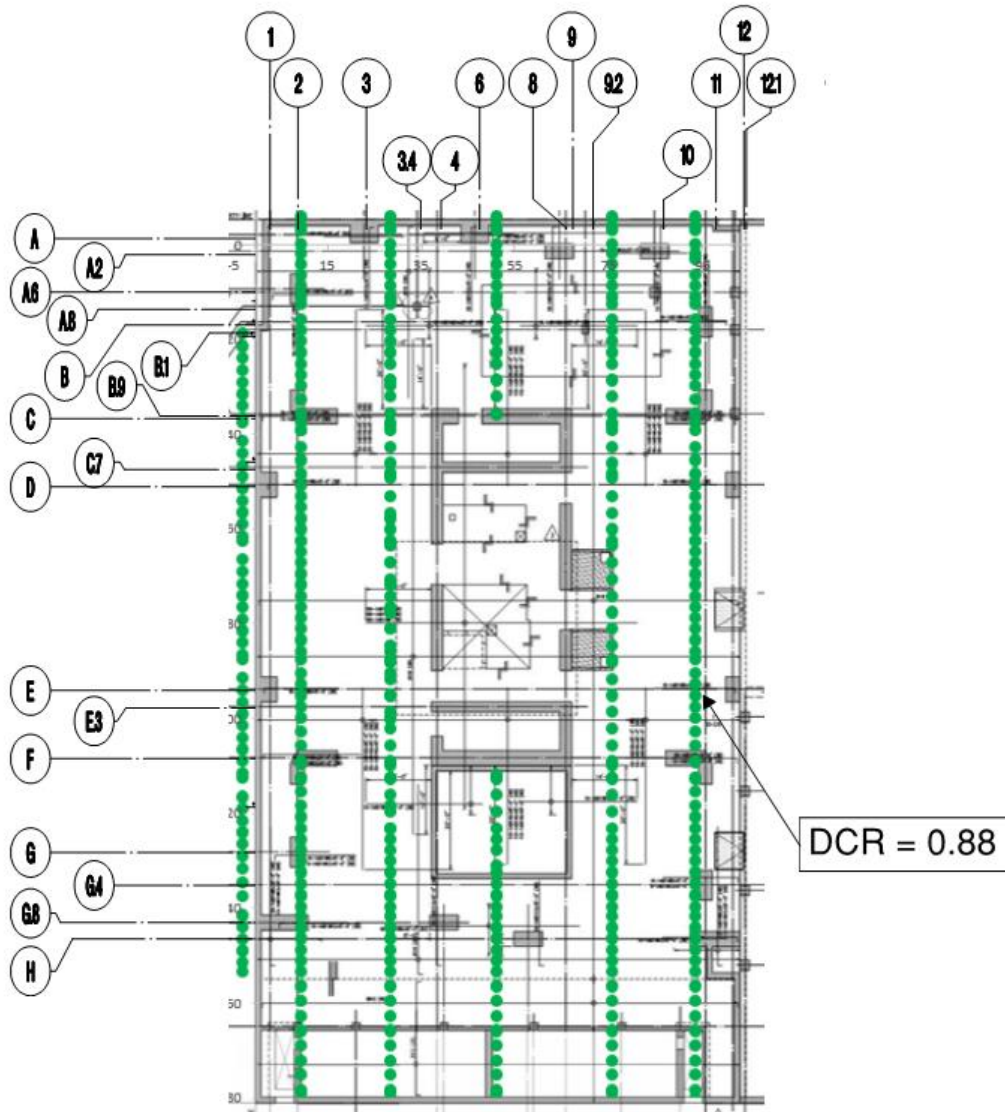
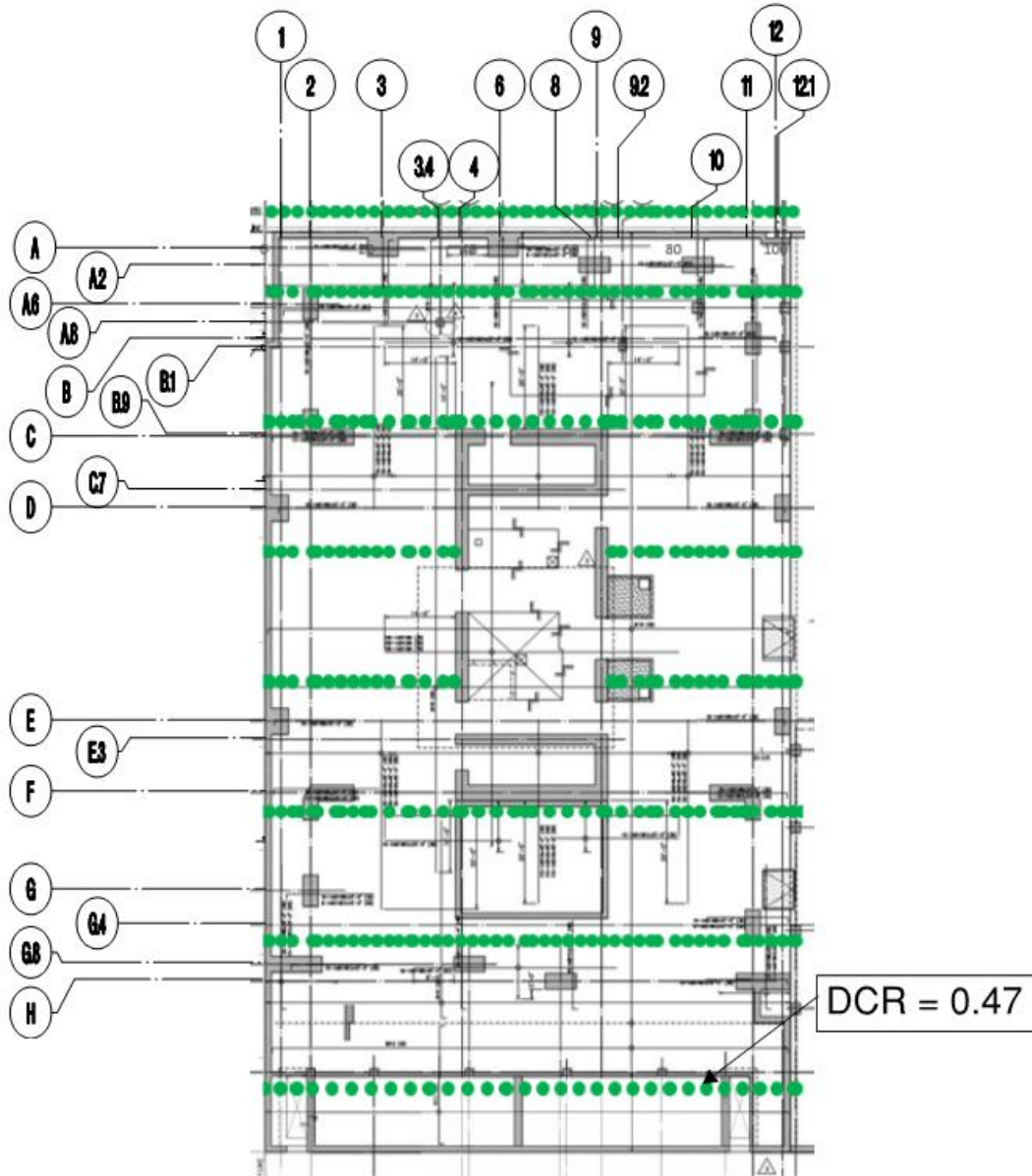


Figure 7-40: DCR Plot for North - South Bottom Reinforcement Design Strips for $1.4 \cdot D + L + E + \text{Jacking Load}$

DCR Legend

- DCR < 0.9
- DCR 0.9 TO 1.05
- DCR > 1.05



**Figure 7-41: DCR Plot for East - West Top Reinforcement Design Strips for
0.7*D + E + Jacking Load**

DCR Legend

- DCR < 0.9
- DCR 0.9 TO 1.05
- DCR > 1.05

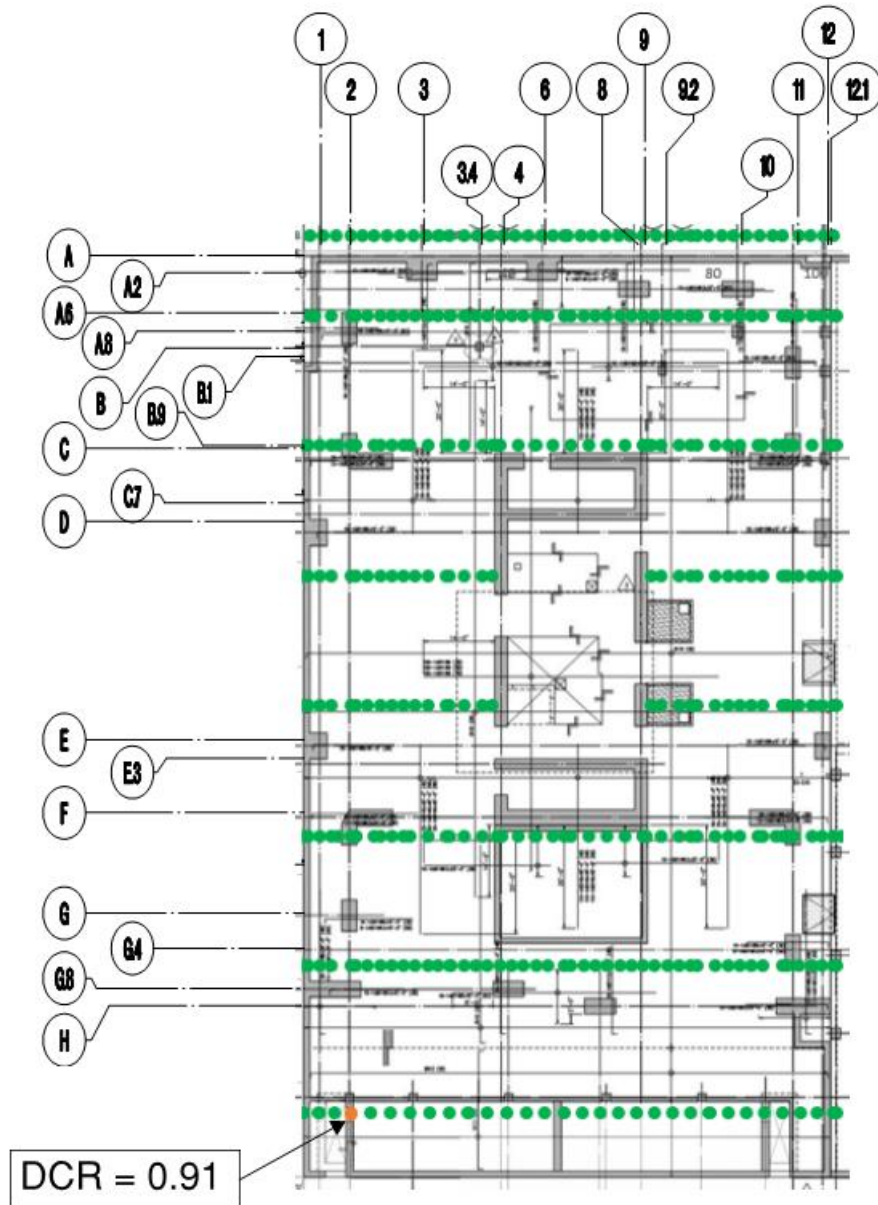
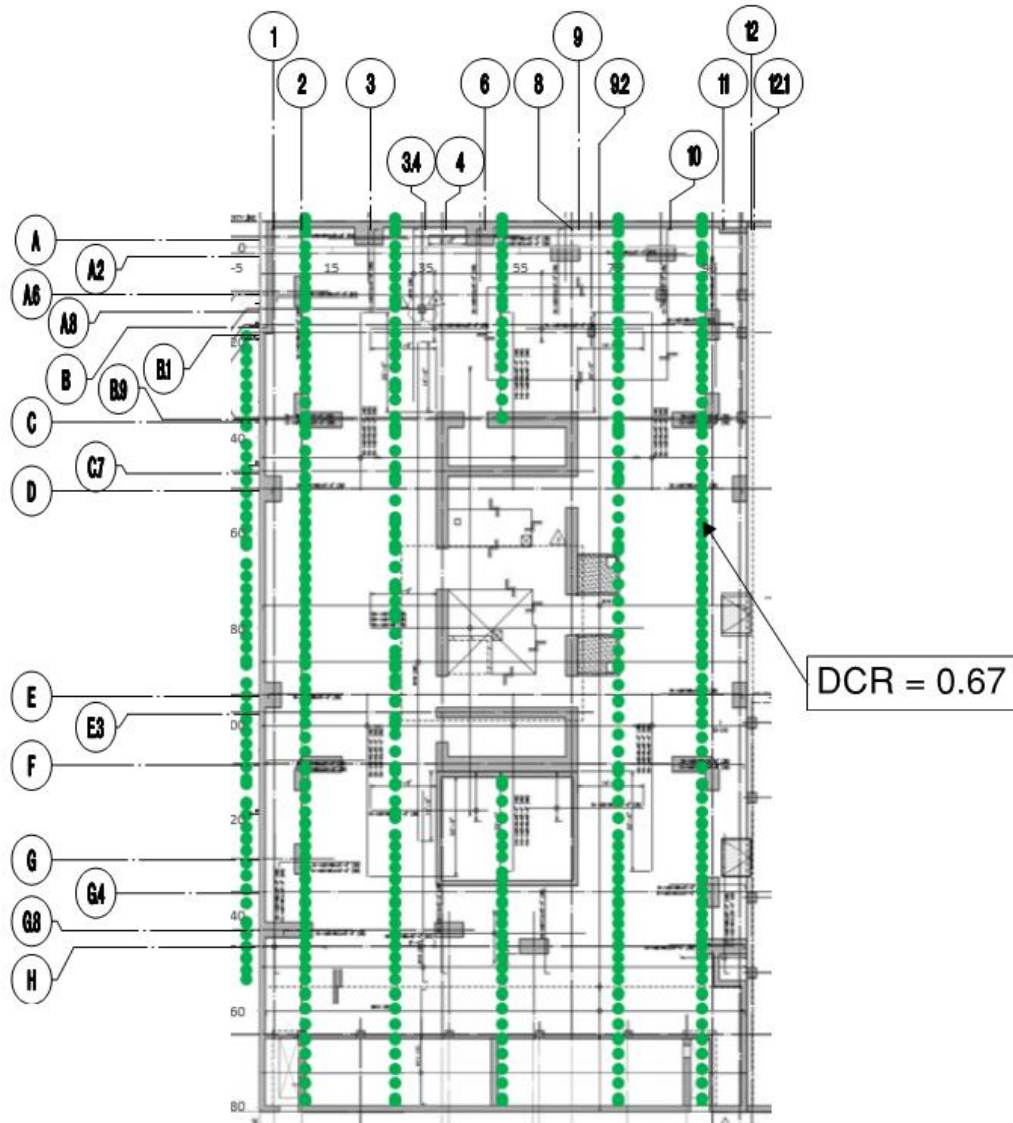


Figure 7-42: DCR Plot for East-West Bottom Reinforcement Design Strips for $0.7 \cdot D + E + \text{Jacking Load}$

DCR Legend

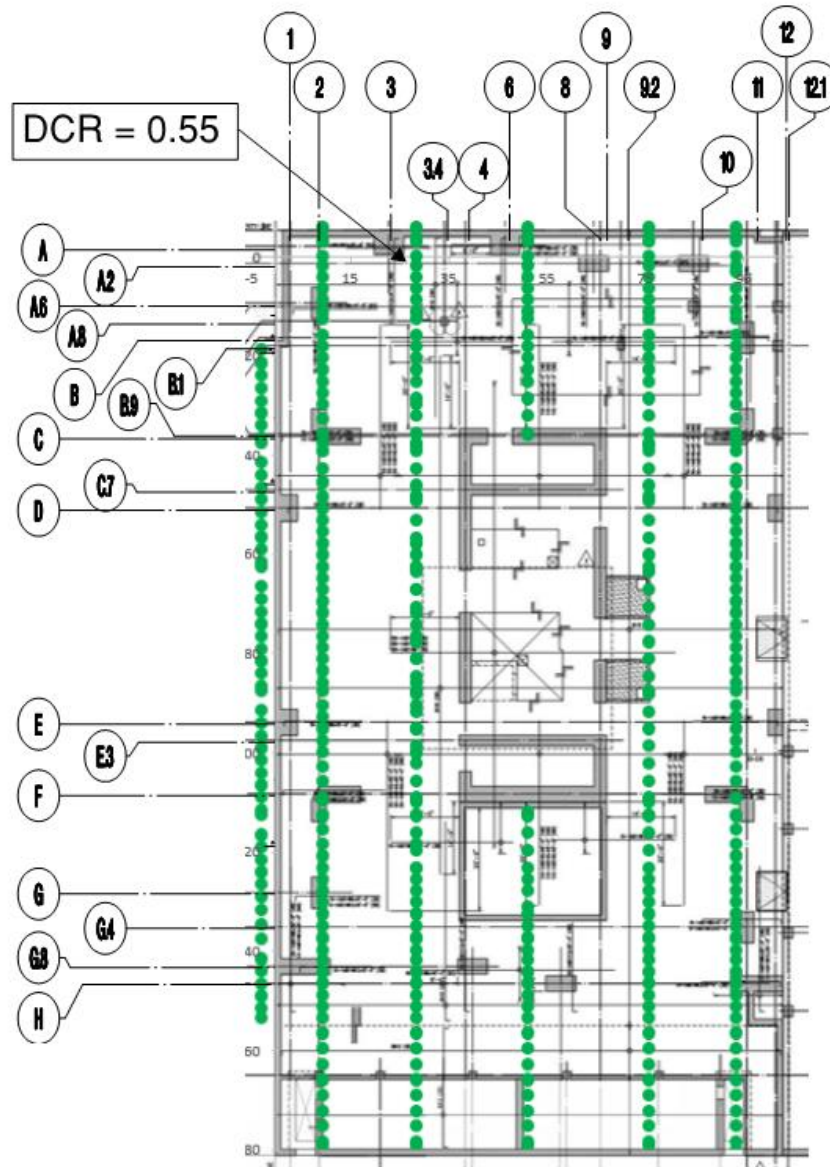
- DCR < 0.9
- DCR 0.9 TO 1.05
- DCR > 1.05



**Figure 7-43: DCR Plot for North-South Top Reinforcement Design Strips for
 $0.7 \cdot D + E + \text{Jacking Load}$**

DCR Legend

- DCR < 0.9
- DCR 0.9 TO 1.05
- DCR > 1.05



7.6.2.2.3. Seismic Demand to Capacity Ratios for Existing Condition for Design Earthquake with Omega

The result figures below present the flexural demand to capacity ratio checks for the envelope listed below. The figures below highlight the locations of the maximum design to capacity ratios.

*Envelope 1: $(1.4 * D) + L + E$ and $(0.7 * D) + E$*

DCR Legend

- DCR < 0.9
- DCR 0.9 TO 1.05
- DCR > 1.05

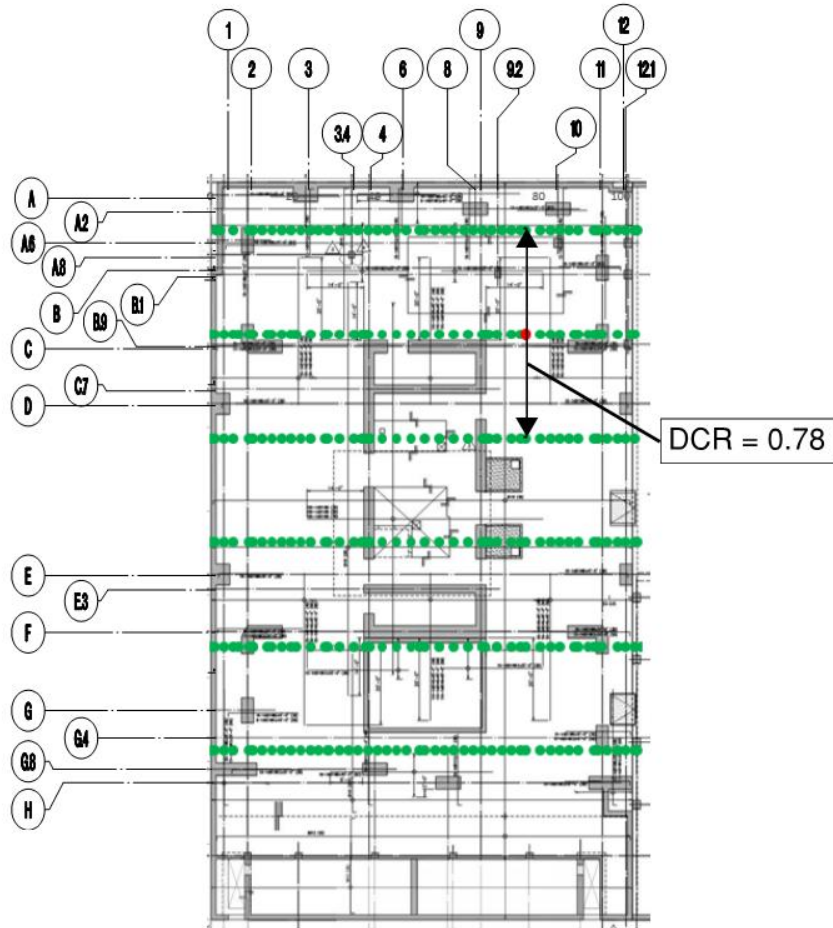


Figure 7-45: DCR Plot for East-West Top Reinforcement Design Strips for Earthquake Envelope

DCR Legend

- DCR < 0.9
- DCR 0.9 TO 1.05
- DCR > 1.05

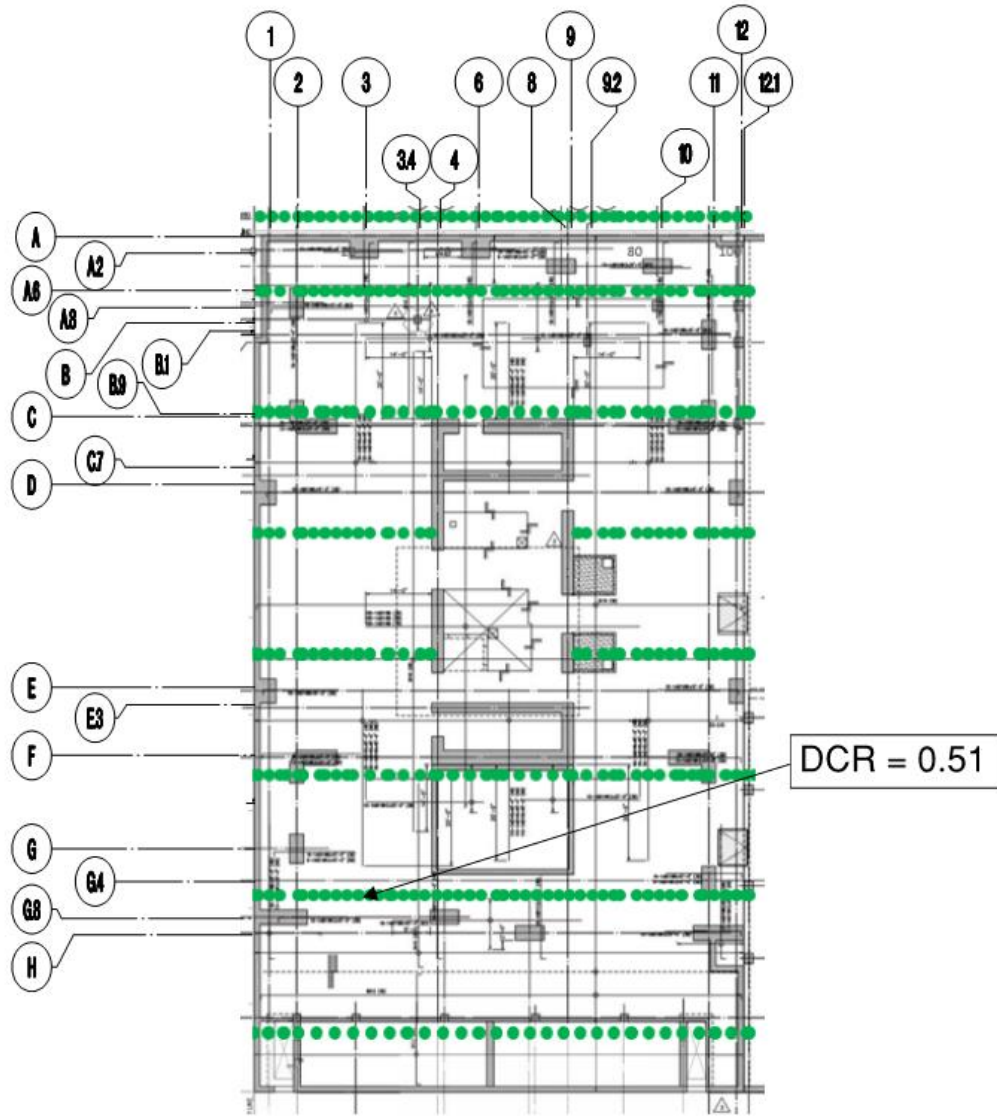


Figure 7-46: DCR Plot for East-West Bottom Reinforcement Design Strips for Earthquake Envelope

DCR Legend

- DCR < 0.9
- DCR 0.9 TO 1.05
- DCR > 1.05

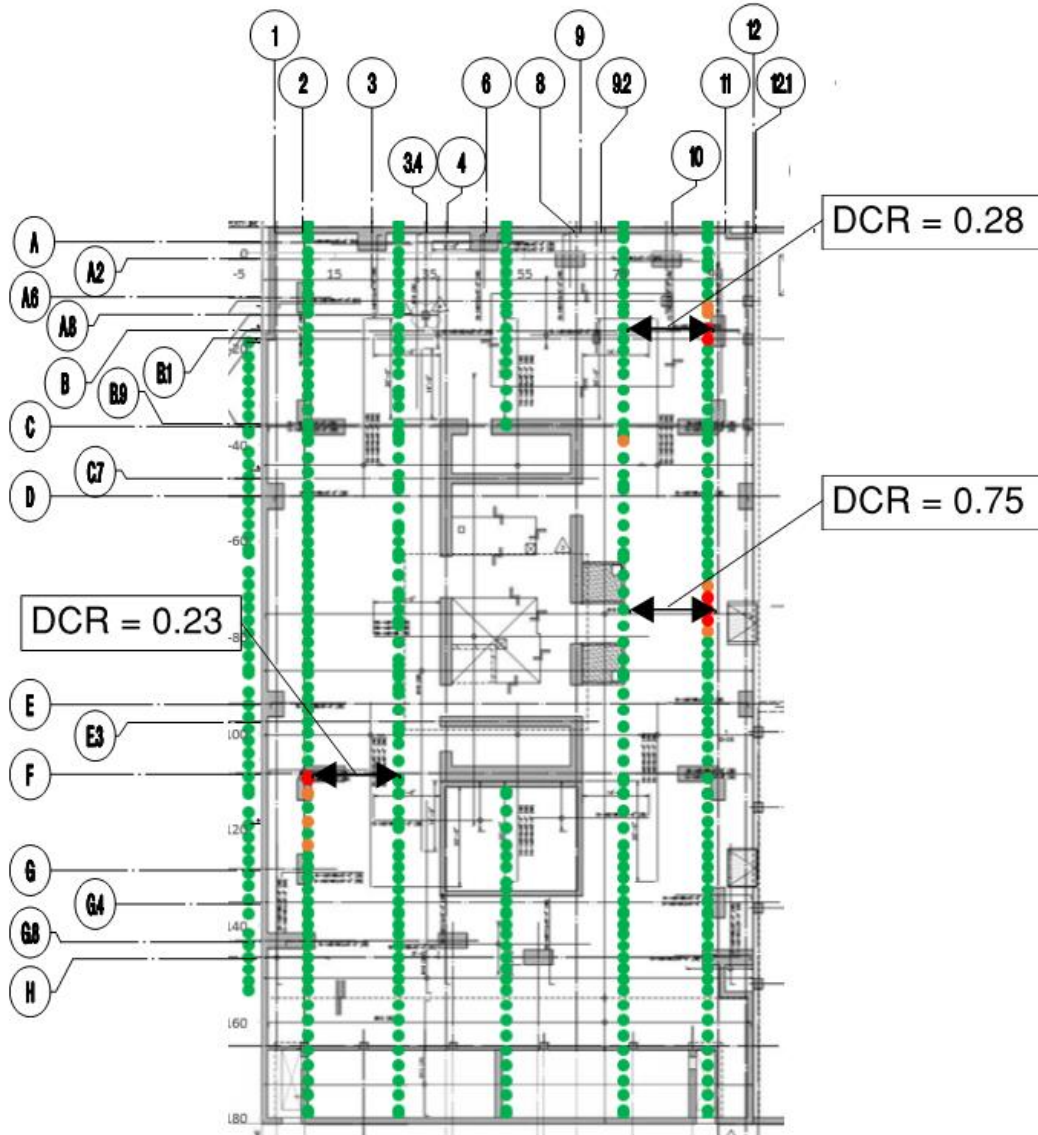


Figure 7-47: DCR Plot for North-South Top Reinforcement Design Strips for Earthquake Envelope

DCR Legend

- DCR < 0.9
- DCR 0.9 TO 1.05
- DCR > 1.05

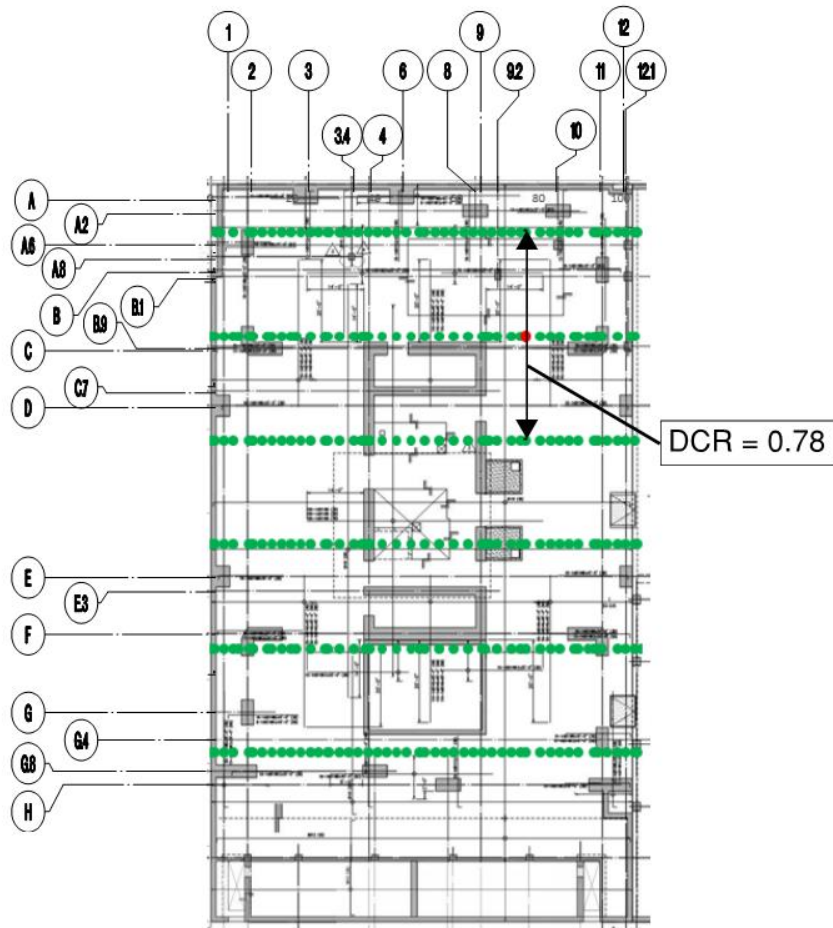


Figure 7-48: DCR Plot for North-South Bottom Reinforcement Design Strips for Earthquake Envelope

DCR Legend

- DCR < 0.9
- DCR 0.9 TO 1.05
- DCR > 1.05

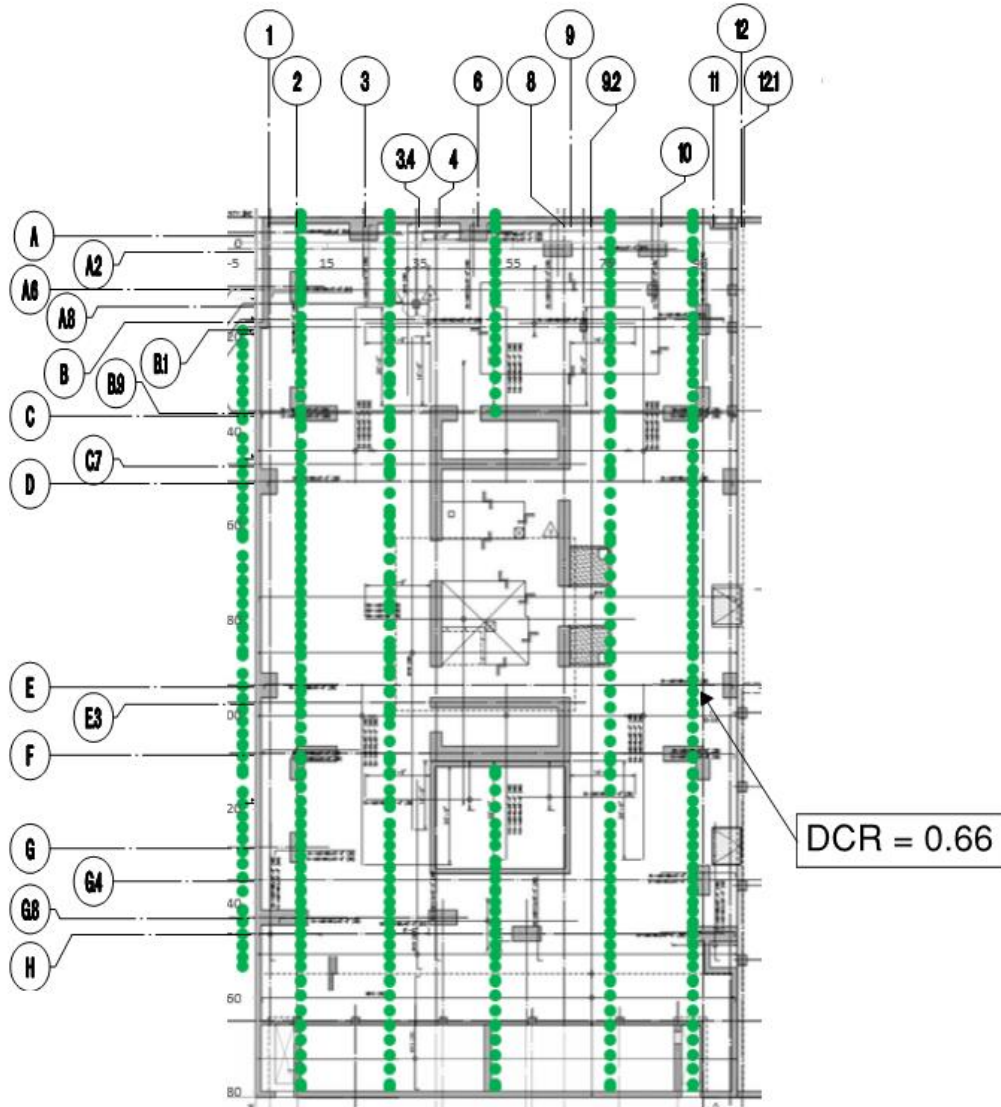


Figure 7-49: DCR Plot for North-South Bottom Reinforcement Design Strips for Earthquake Envelope

7.6.2.2.4. Seismic Demand to Capacity Ratios for Retrofit Condition for Design Earthquake with Omega

The result figures below present the flexural demand to capacity ratio checks for the two load combinations listed below. The figures below highlight the locations of the maximum design to capacity ratios.

*Envelope 1: $(1.4 * D) + L + E + Jacking Loads$*

*Envelope 2: $(0.7 * D) + E + Jacking Loads$*

DCR Legend

- DCR < 0.9
- DCR 0.9 TO 1.05
- DCR > 1.05

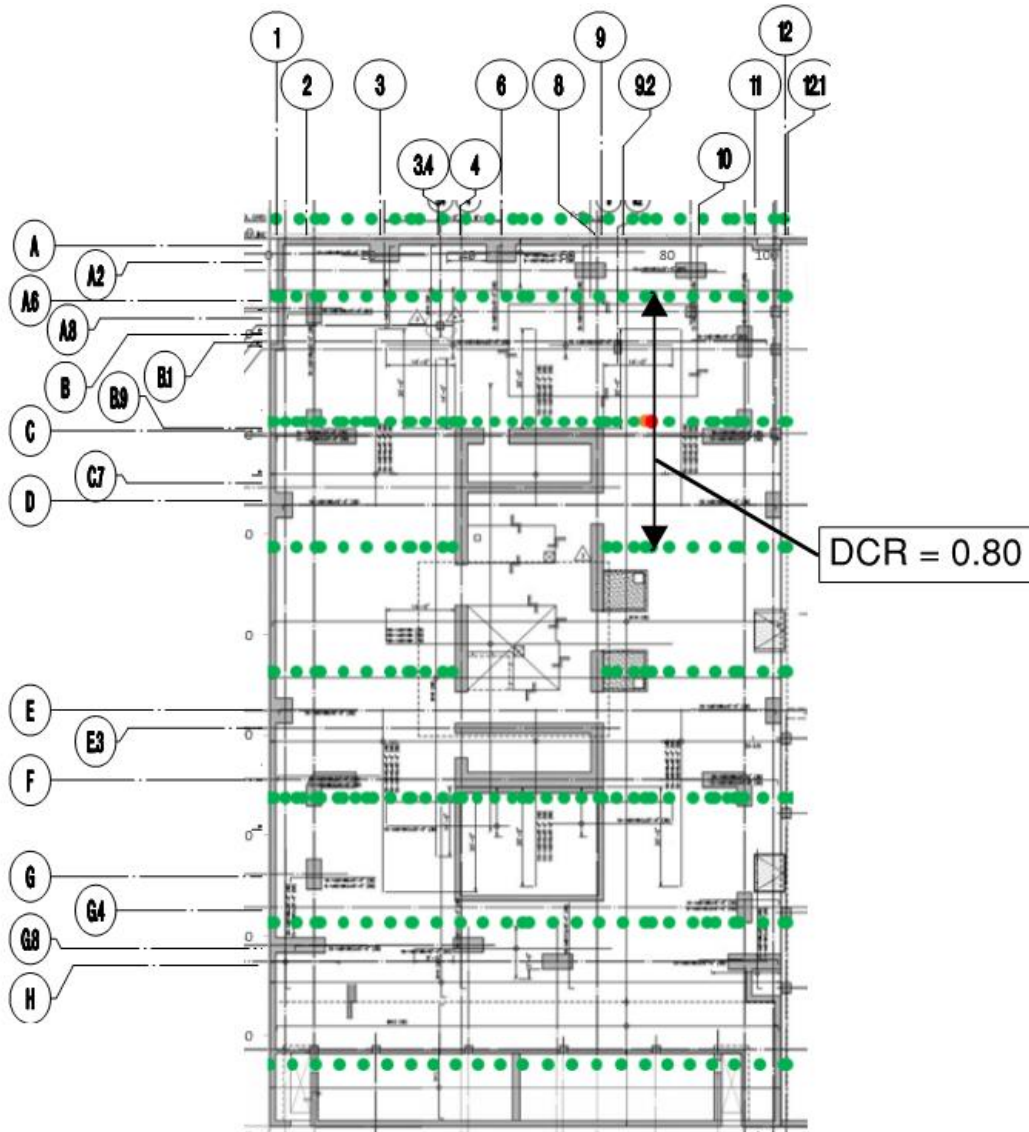


Figure 7-50: DCR Plot for East-West Top Reinforcement Design Strips for 1.4*D + E + Jacking Load Envelope

DCR Legend

- DCR < 0.9
- DCR 0.9 TO 1.05
- DCR > 1.05

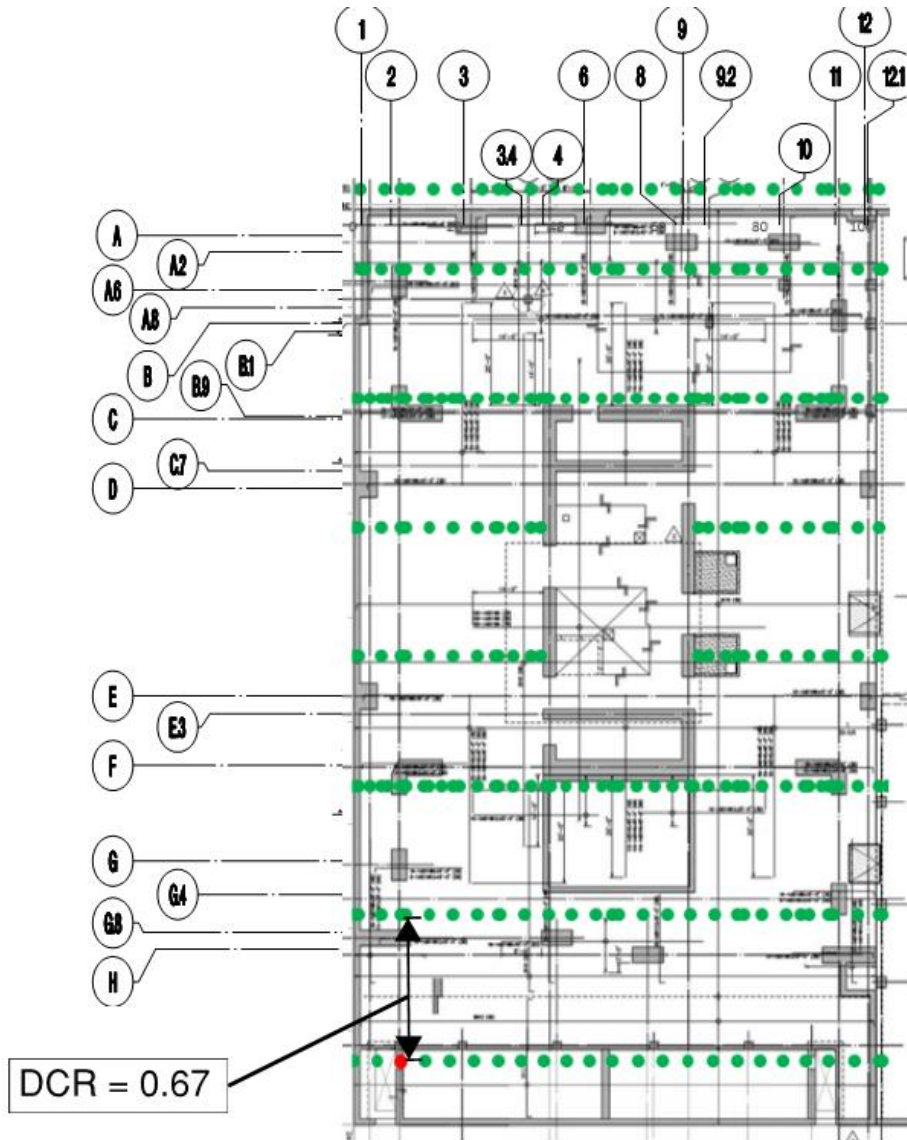


Figure 7-51: DCR Plot for East-West Bottom Reinforcement Design Strips for 1.4*D + E + Jacking Load Envelope

DCR Legend

- DCR < 0.9
- DCR 0.9 TO 1.05
- DCR > 1.05

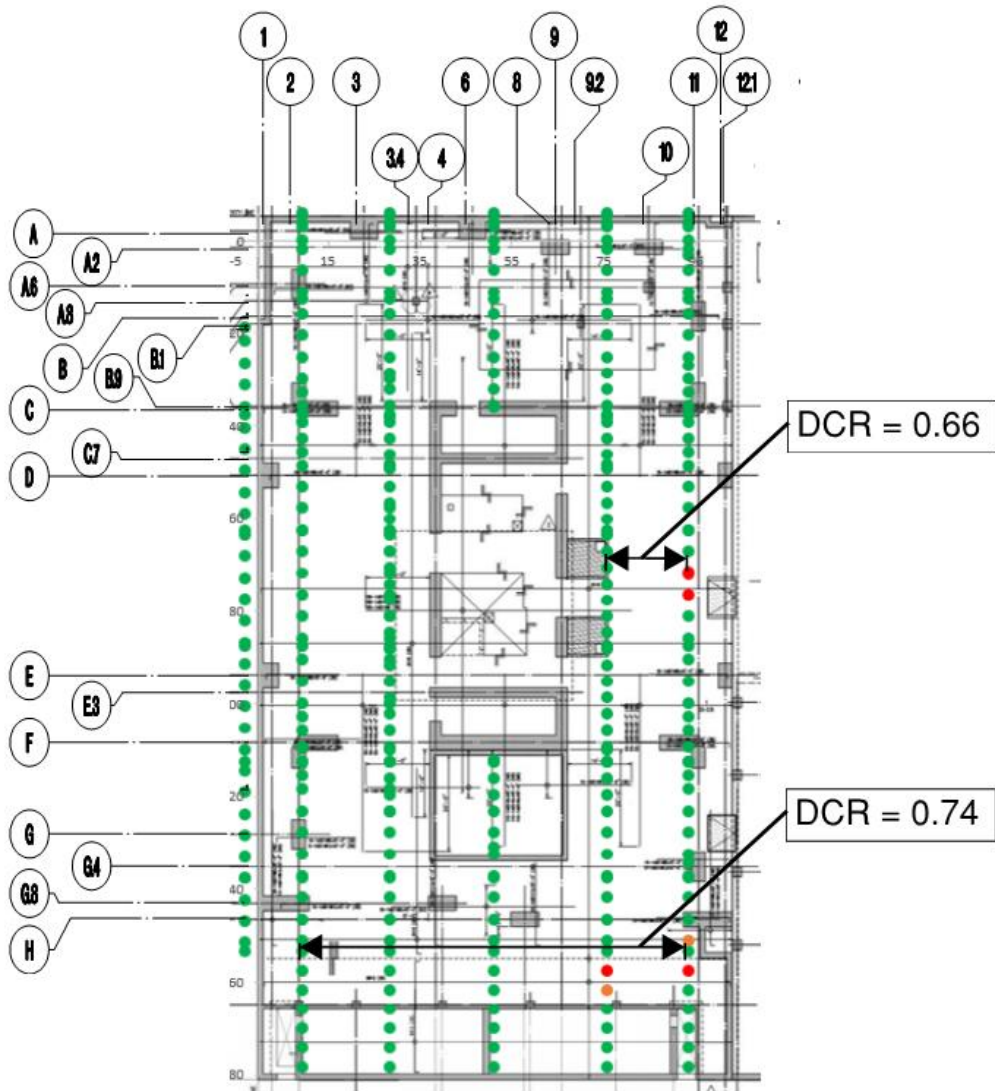


Figure 7-52: DCR Plot for North-South Top Reinforcement Design Strips for 1.4*D + E + Jacking Load Envelope

DCR Legend

- DCR < 0.9
- DCR 0.9 TO 1.05
- DCR > 1.05

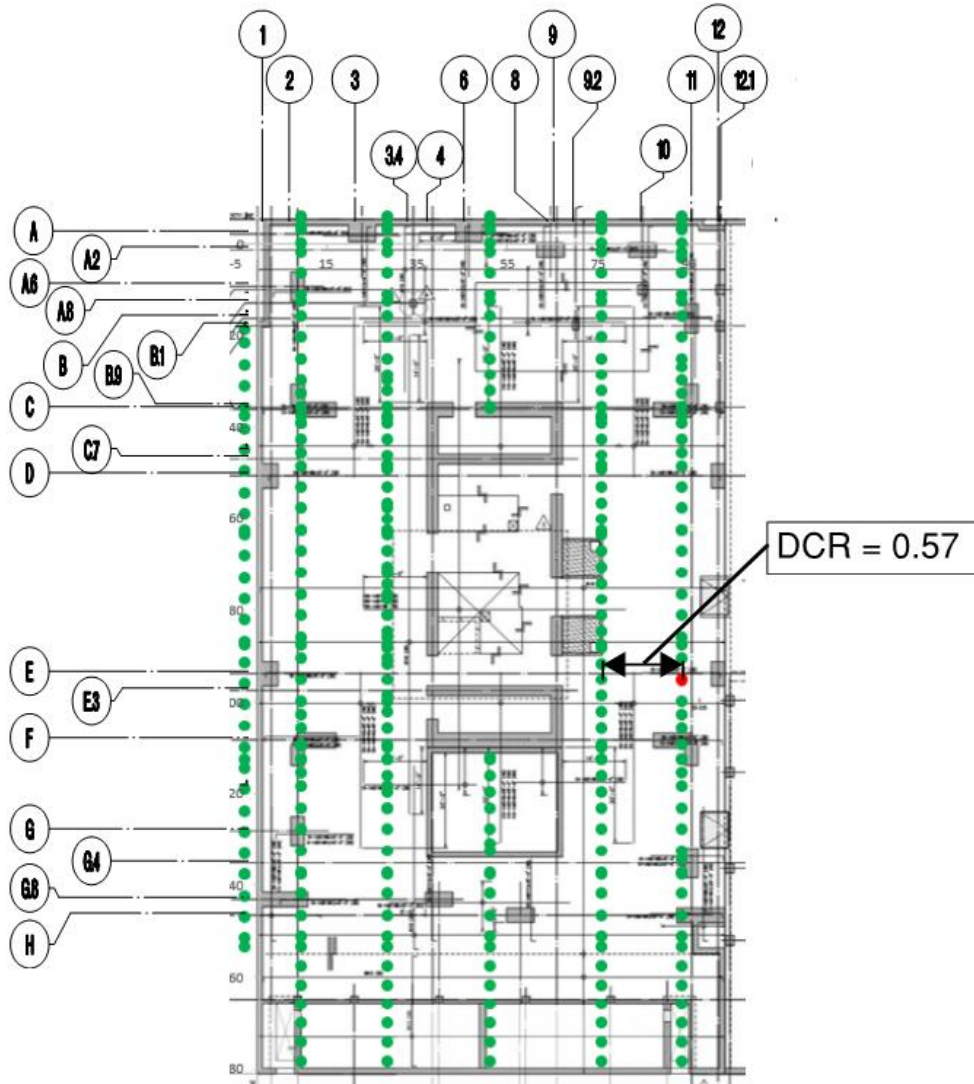


Figure 7-53: DCR Plot for North-South Bottom Reinforcement Design Strips for 1.4*D + E + Jacking Load Envelope

DCR Legend

- DCR < 0.9
- DCR 0.9 TO 1.05
- DCR > 1.05

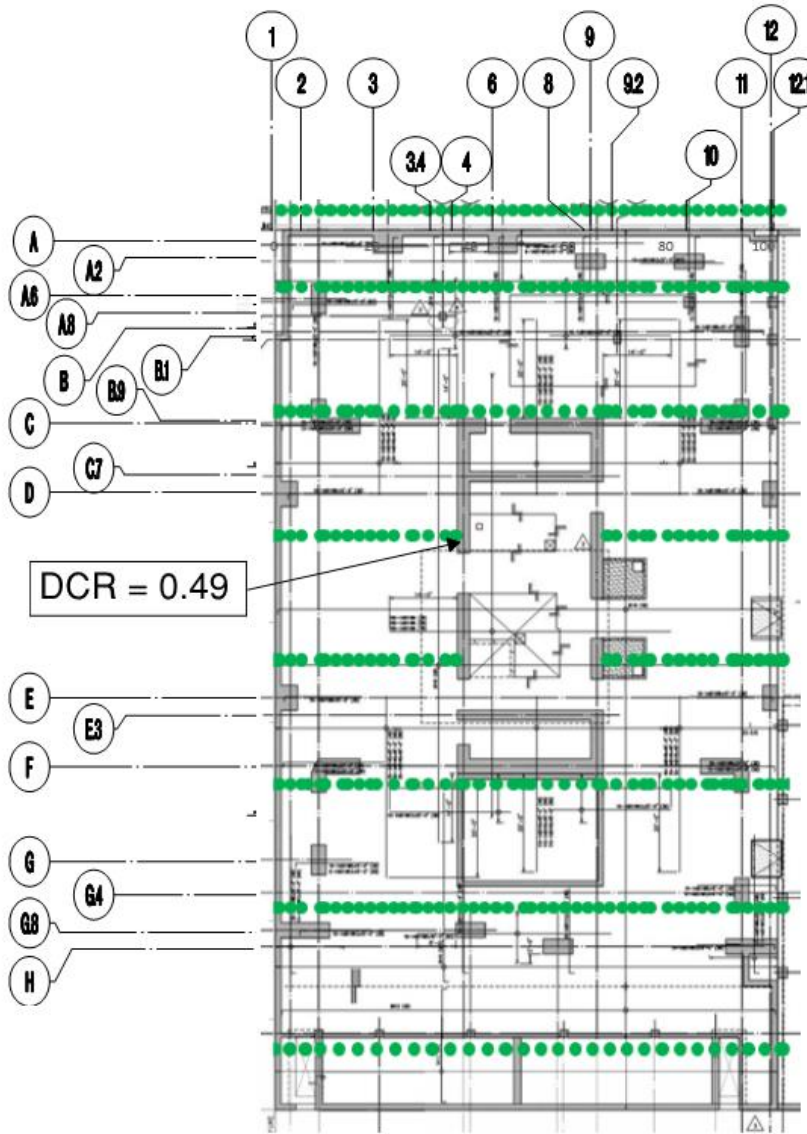


Figure 7-54: DCR Plot for East-West Top Reinforcement Design Strips for $0.7 * D + E + \text{Jacking Load Envelope}$

DCR Legend

- DCR < 0.9
- DCR 0.9 TO 1.05
- DCR > 1.05

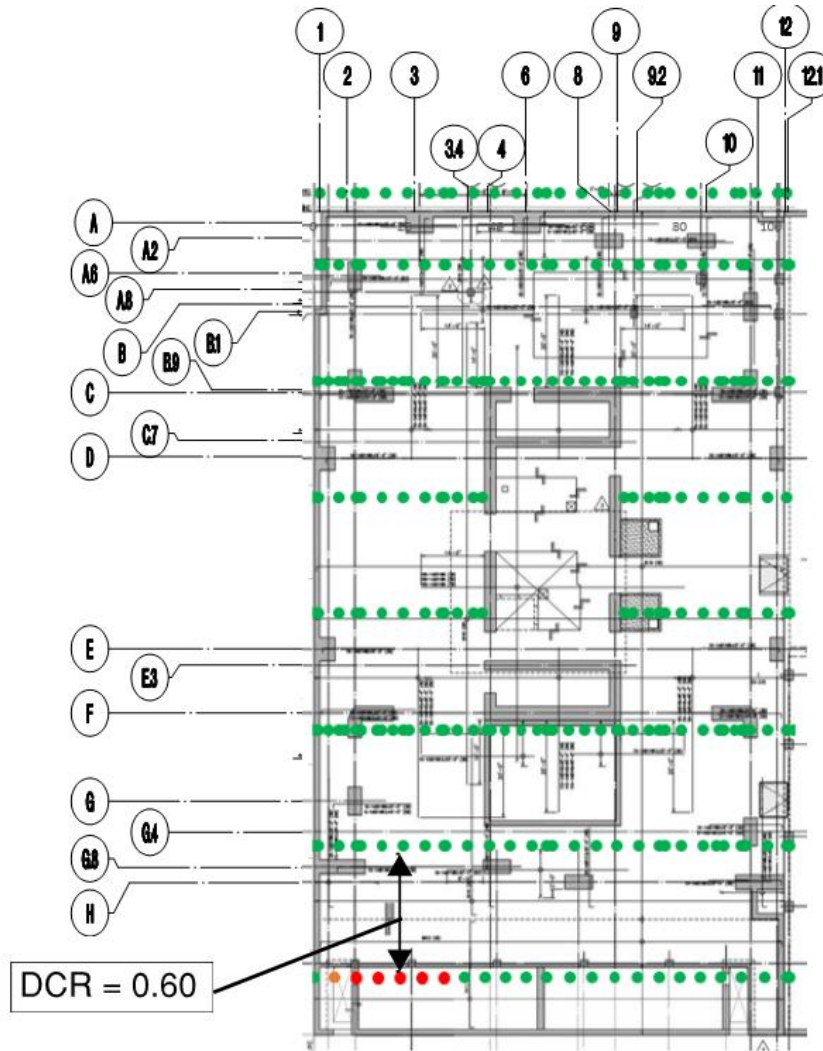


Figure 7-55: DCR Plot for East-West Bottom Reinforcement Design Strips for $0.7 \cdot D + E + \text{Jacking Load Envelope}$

DCR Legend

- DCR < 0.9
- DCR 0.9 TO 1.05
- DCR > 1.05

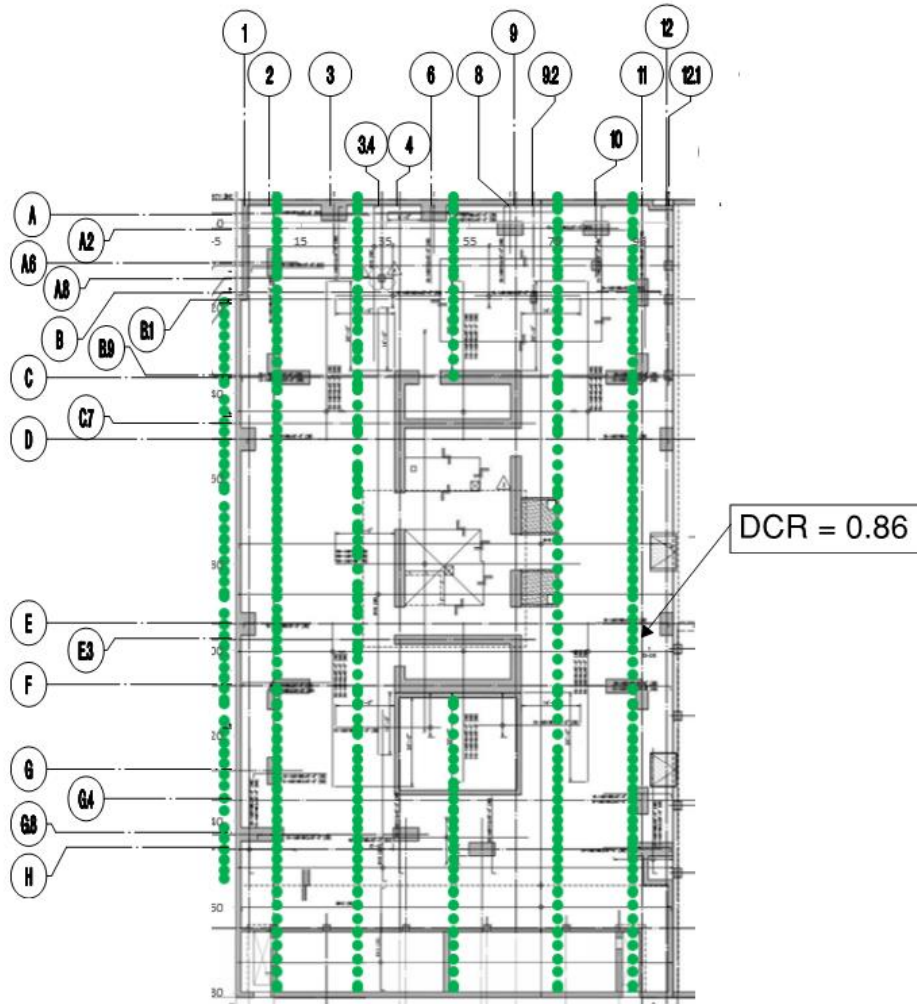
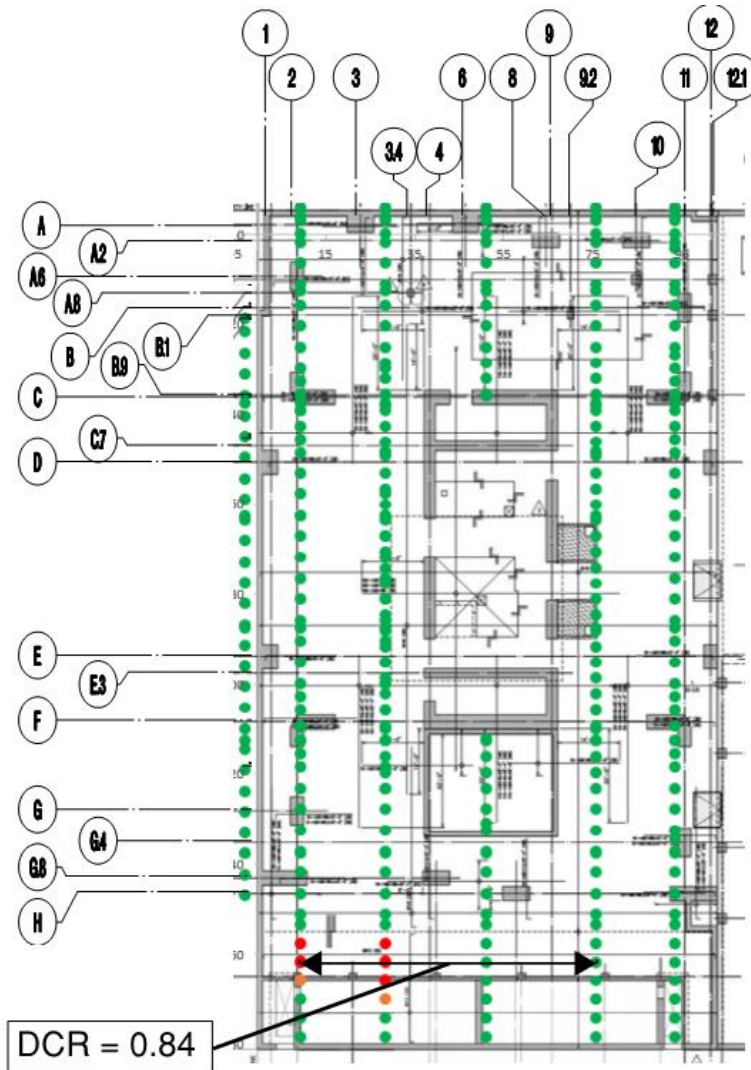


Figure 7-56: DCR Plot for North-South Top Reinforcement Design Strips for $0.7 \cdot D + E + \text{Jacking Load Envelope}$

DCR Legend

- DCR < 0.9
- DCR 0.9 TO 1.05
- DCR > 1.05



**Figure 7-57: DCR Plot for North-South Bottom Reinforcement
Design Strips for 0.7*D + E + Jacking Load Envelope**